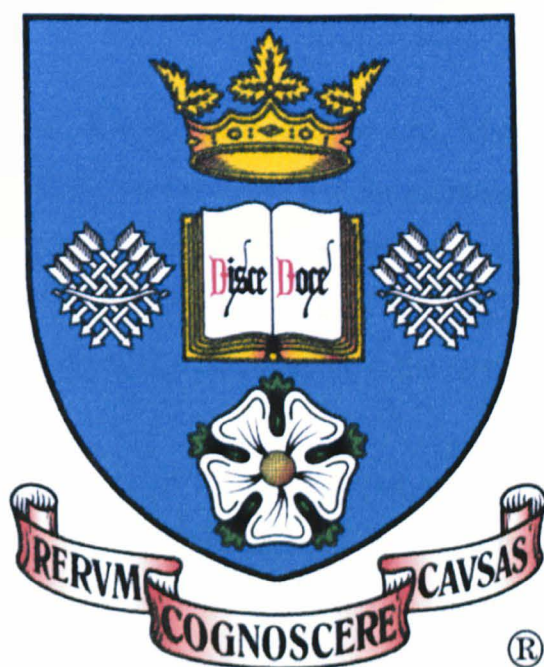# Automated Measurement of the Kinetics of Chemical Reactions in Ionic Liquids

Thesis Submitted for the Degree of Doctor of Philosophy (PhD)

Zhuo Chen

Department of Chemical and Process Engineering

The University of Sheffield

August 2006

Acknowledgements

The completion of this thesis relies on a great deal of support and help provided by many people.

To my supervisors, Prof. R.W.K. Allen and Dr J.M. MacInnes, my deepest gratitude for their invaluable guidance and support, and for granting me the opportunity to carry out this research. My special thanks are given to Dr. B. O'Sullivan, for his great help on the experimental work and questions about chemistry. Thanks also to Dr. B. Mark and Dr. P. Styring, for their advice and support in the research.

I would like to thank my family and friends who have supported me all the time. Special thanks are given to Mr.&Mrs. Amems, for their careful reading of the document. As my greatest source of strength and courage, I could not offer enough thanks to my dear parents and husband. Without their love and support, I would have never achieved what I have done today.

Finally, many thanks are given to all the people ever helped me during these years.

Abstract

This thesis has presented research work carried out searching for an automated measurement technique for the kinetics of chemical reactions in ionic liquids. The aim has been to develop a microchannel reactor system (MCR) to allow reaction kinetics measurement, involving mixing, reaction and sampling, in a single chip rapidly, automatically and accurately.

The difficulty of mixing ionic liquids on a microchannel system etched on a chip resulted from two problems; the high viscosity of the liquids together with the low diffusivity of reactant molecules within them, and the small feature size and hence low Reynolds number of flows in microchannels. In order to achieve a mixing time that is negligible compared to the reaction duration, special measures must be taken to accelerate the mixing process. As a result, different mixing schemes were discussed in the thesis, with CFD computations and experimental work. Comparisons were made between different types of mixers involving both their mixing uniformity and pressure drop. The conclusion drawn from the study has been that the folding network mixer was the most effective, and thus it was used in the reaction network of the MCR system.

The MCR system (Mark I) has been designed and constructed by selecting and assembling apparatus for the control of pressure, fluid flow, product sampling and analysis. A programme was developed to control the sequence and time scale of each operation, and models are developed for the determination of operating procedure and conditions. Furthermore, measurement techniques were developed for the determination of fluid flow, measurement of species composition and assessment of mixing performance. To assess the system performance, a series of tests have been carried out with a non-reacting solution system, and in addition, kinetics measurement in ionic liquids have been attempted. Drawbacks have been found in the apparatus' behaviour and control technique.

Further improvements have then been made on the design and operation of the system. Consequently, the Mark II design of the MCR system has been presented, of which a new reaction network was proposed and fabricated, and a set of modified procedures and conditions was presented. With the improved system performance and operating conditions, good repeatability of kinetics measurement has been achieved. The deviation of measurement of reaction kinetics with the MCR system (Mark II) was estimated to be within 5%.

CONTENTS

NOMENCLATURE

English Symbols

	Description	**Unit**
A	Area of channel's cross section	[m^2]
$[A]_0$	Initial concentration of reactant	[mol m^{-3}]
C	Species concentration	[mol m^{-3}]
C_0	Initial concentration of species	[mol m^{-3}]
C_m	Species concentration measured by HPLC	[mol m^{-3}]
C_r	Species concentration in the reaction chamber	[mol m^{-3}]
c	Changes of species concentration in chemical reaction	[mol m^{-3}]
$\mathcal{D}$	Diffusivity of fluid	[m^2 s^{-1}]
D	Diameter of cylinder pipe	[m]
DR	Dilution ratio in total of the sampling process	-
DR_E	Dilution ratio during sample ejection process	-
F_i	Force term of momentum equation	[kg m^{-2} s^{-2}]
f	Coefficient for pressure drop in microchannels	-
f_C	Capture fraction of sample loop in the MCR system	-
$f_{C,max,s}$	Simplified maximum capture fraction of sample loop in the model of sample capturing	-
H	Height of gap between two parallel plates	[m]
I	Light intensity	-
I_D	Light intensity of background image	-
k	Numbers of mixing elements	-

k_2	Rate coefficient of the second-order chemical reaction	[m^3 mol^{-1} s^{-1}]
k_σ	Number of mixing elements to achieve the required mixing uniformity σ_Y.	-
L	Channel length	[m]
$\bar{L}$	Distance that fluid passes through with time τ at the average flow rate	[m]
L_0	Effective length of the sample parabola in volume of V_S in the model of sample capturing	[m]
$\hat{L}_0$	Reference length	[m]
L_B	Effective distance that the back of the sample parabola travels in the flow passage in the model of sample capturing	[m]
L_F	Effective distance that the front of the sample parabola travels in the flow passage in the model of sample capturing	[m]
L_L	Effective length of circular section in volume of $(V_P + V_L)$ in the model of sample capturing	[m]
L_P	Effective length of circular section in volume of V_P in the model of sample capturing	[m]
L_e	Element length of FFM and FNM	[m]
L_{in}	Entrance length	[m]
L_{tip}	Distance that the front of the central fluid passes through with time τ	[m]
l	Mask width of wet-etched microchannel	[m]
m	Mass weight	[kg]
$\dot{m}$	Mass flow rate	[kg s^{-1}]
n	Number of streams in microchannel	-
P_m	Pressure applied on the diluent reservoir	[Pa]
P_r	Pressure applied on reactants can catalyst reservoirs	[Pa]
p	Pressure	[Pa]
Δp	Press drop	[Pa]

Q	Volume flow rate	$[\text{m}^3 \text{ s}^{-1}]$
Q_0	Flow rate of species i in the feeding passage connected to reservoir k.	$[\text{m}^3 \text{ s}^{-1}]$
Q_D	Volume flow rate of diluent	$[\text{m}^3 \text{ s}^{-1}]$
Q_I	Volume flow rate of stream ejected from the reaction chamber	$[\text{m}^3 \text{ s}^{-1}]$
Q_r	Volume flow rate in the reaction chamber	$[\text{m}^3 \text{ s}^{-1}]$
Q_t	Total volume flow rate of fluid flow in the sample loop	$[\text{m}^3 \text{ s}^{-1}]$
R	Channel depth	$[\text{m}]$
R_0	Reference radius of circular section in the model of sample capturing	$[\text{m}]$
r_k	Change rate of species k in chemical reaction	$[\text{kg m}^{-3} \text{ s}^{-1}]$
S_g	Space between slanted ridges of FM	$[\text{m}]$
Δs	Segment length of a channel	$[\text{m}]$
T	Temperature	$[°\text{C}]$
t	Time	$[\text{s}]$
$t_{1/2}$	Half-life of chemical reaction	$[\text{s}]$
u	Velocity	$[\text{m s}^{-1}]$
u, v, w	Velocity components	$[\text{m s}^{-1}]$
u_{DEV}	Velocity of fully developed flow	$[\text{m s}^{-1}]$
$u_{L_{in}}$	Definition velocity of entrance length	$[\text{m s}^{-1}]$
V	Average velocity	$[\text{m s}^{-1}]$
V_C	Volume of sample V_S captured by the sample loop in the reaction kinetics measurement	$[\text{m}^3]$
V_D	Volume of diluent accumulated during the ejection time	$[\text{m}^3]$
V_E	Volume of sample ejected from the reaction chamber in the reaction kinetics measurement	$[\text{m}^3]$

V_{EC}	Volume of sample V_E captured by the sample loop in the reaction kinetics measurement	$[m^3]$
V_L	Volume of sample loop in MCR system	$[m^3]$
V_O	Volume of flow passage leading from the sample loop to the outlet in the MCR system	$[m^3]$
V_P	Volume of flow passage between the dilution mixer and the sample loop in the MCR system	$[m^3]$
V_S	Volume of sample diluted through the dilution mixer in the reaction kinetics measurement	$[m^3]$
$V_{reactor}$	Volume of the reaction chamber	$[m^3]$
V_{valid}	Valid sample ejected from the reaction chamber	$[m^3]$
W	Channel width	$[m]$
W_D	Diffusion distance	$[m]$
x_i, x_j	Coordinates component	-
x, y, z	Cartesian coordinates component	-
Y	Mass fraction	-
Y_k	Mass fraction of species k	-

Greek Symbols

	Description	Unit
α	Constant in exponential decay fitting law for FNM	-
β	Element pressure drop coefficient of FFM and FNM.	-
δ	Offset between glass layers	$[m]$
δ_x	Channel length needed for completely diffusive mixing	$[m]$
ε	Pressure fraction in viscosity measurement	-
η	Distortion rate of glass over a span in with of W	-

μ	Dynamic viscosity	[kg m^{-1} s^{-1}]
ν	Kinematic viscosity	[m^2 s^{-1}]
θ	Oblique angle of the slanted ridges in SHM and FM	[°]
ρ	Density	[kg m^{-3}]
σ_Y	Relative standard deviation of mixture's uniformity	-
σ_{Y_0}	Constant in exponential decay fitting law for FNM	-
τ	Time	[s]
τ_D	Time for diffusion mixing	[s]
τ_E	Ejection time of reaction kinetics measurement	[s]
τ_F	Flushing time of reaction kinetics measurement	[s]
τ_L	Loop opening time of reaction kinetics measurement	[s]
τ_P	Pressure build-up time of reaction kinetics measurement	[s]
τ_R	Reaction time of reaction kinetics measurement	[s]
τ_S	Sample delay time of reaction kinetics measurement	[s]
τ_W	Diffusion time cross channel width	[s]
τ_e	Time to flow through one mixing element	[s]
τ_σ	Mixing time to achieve the required mixing uniformity σ_Y.	[s]
ζ	Constant in exponential decay fitting law for FNM	-

Dimensionless Numbers

Parameter	Description
Pe	Peclet number
Re	Reynolds number
Re$_C$	Critical Reynolds number for laminar flow transforming into Turbulent flow

Sc   Schmidt number

Subscripts

Description

0   Reference variable

C Parameter of glass capillary in viscosity measurement

D Diluent in MCR system

i Parameter (concentration and volume flow rate) of species i

max   Maximum value of parameter

P Parameter (concentration) of the pyrene

T Parameter of transferring tubing in viscosity measurement

g Parameter of ridges in microchannel

σ Parameter to achieve the desired σ_γ

Superscripts

Description

k Species reservoirs

*   Non-dimensional variable

Chapter 1

INTRODUCTION

1.1 ORIGIN OF RESEARCH

Aiming to combine for the first time the enabling technologies of ionic liquids and microreactors, the research presented here originated from the need for rapid and accurate measurement of reaction kinetics in ionic liquids and the advantages of microreactors such as low hold-up, fast response and precise control.

Since their emergence as alternative battery electrolytes a few decades ago, ionic liquids have attracted much attention. This interest stems from factors such as the unique solubility to a wide range of molecules, tuneable properties, unmeasurably low vapour pressures and the capability of being repeatedly used and recycled. Ionic liquids are thus regarded as environmentally benign solvents and have an appeal to most chemists and chemical engineers (Wilkes 2002). However, to be widely used in the chemical industry, detailed studies of ionic liquids are still needed, especially on how they will influence reactions kinetics as solvents. There are vast numbers of ionic liquids available due to their customized properties, and they can be used in combinations with a range of temperatures, reaction times and stoichiometries (Seddon 2002). The study thus addresses a crucial problem, that is, how to accurately measure the reaction kinetics thus to optimise the multi-variable system offered by ionic liquids as designer solvents in a time as short as possible.

Conventionally, there are two ways to determine the kinetics of chemical reactions. These are the real-time analysis and the quenching methods (Atkins and De Paula 2002). In a real-time analysis, the analysis of species composition is carried out when the reaction is progressing. For example, in the flow method, a typical method of real-time analysis, the reactants are firstly fully mixed in a chamber, and then the mixed solutions are pushed to flow through a tube, in which the species compositions are measured at different positions. As the solution is fully mixed before it flows through the tube, the reaction time after mixing is equivalent to the distance of the measured position away from the chamber. One advantage of the real-time technique is that it allows kinetics measurement in a time scale of milliseconds to second. However, in order to achieve a study of reaction in so short time, a rapid mixing in the big sample volume necessary for fast flow must be guaranteed.

The other conventional approach to kinetics measurement is the quenching method. Here the reaction is to be stopped or quenched after the reaction has proceeded for a certain time. The advantage of this method is that the composition of samples can be analysed at leisure and reaction intermediates may be detected. More importantly, the analysis can be made by slow processes such as mass spectrometry and chromatography. Thus rapid spectroscopic data gathering will not be needed as in the real-time analysis. Therefore, this technique is more often carried out manually.

Comparing the two conventional approaches to kinetics measurement, the real-time analysis seems less practical for the study of reactions in ionic liquids, because supply of ionic liquids is limited by their preparation to small amounts at the lab scale. Moreover, as the viscosities of ionic liquids are 30 to 200 times those of water, it will be more difficult to obtain a fast flow with the usual pressure conditions for the spectroscopic measurement of species compositions. However, as quenching methods are usually carried out manually, especially when carrying out analysis of

compositions with separate chromatography and mass spectrometry, it is not suitable for the need of kinetics study of ionic liquids either, because their vast varieties make the task too tedious and thus impossibly time-consuming for manual operations.

Microreactors, however, open up new possibilities for this tedious task. Due to their small dimensions and high mass and heat transfer rates, microreactors are able to provide precise control over mixing process and temperatures with fast responses and low hold up (Haswell and Watts 2003). Hence, large quantities of data can be produced in a short time. More importantly, only small amount of reagents will be involved in each analysis, which makes them especially attractive for the study of ionic liquids that are normally supplied in small amounts, partly because their purity is easily affected during handling and storage. As microreactors meet well the requirement for kinetics study of reactions in ionic liquids, the topic of the research presented was identified as designing and constructing a microchannel reactor system, to achieve measurements of the reaction kinetics in ionic liquids rapidly, automatically and accurately.

The main challenges to the research resulted from the mixing of ionic liquids on-chip and the automation of the kinetics measurements. Since microfluidic flow is characterised by low Reynolds numbers, the mixing process in microchannels purely depends on molecular diffusion (MacInnes and Allen 2005). However, for ionic liquids, high viscosities and low diffusivities make the process even harder, as their Peclet numbers are in the order of magnitude of 10^5. For example, if no special action is taken, the time to achieve complete mixing of ionic liquids in a channel in width of 100µm can be unacceptably long as hours. Therefore, to make kinetics measurements with a microreactor system, improvements must be made on the species mixing, in order to make the reaction start and stop in a negligibly short time. Automatic control over the whole system is the other difficulty of the research. Several processes were

included in a time sequence for the whole system and the time scale of each part was of great importance. To achieve reliable and accurate measurement with the microreactor system, proper procedures and conditions must be determined, on the basis of detailed understanding of the processes in the whole system.

In detail, the objectives for the research include:

- To propose a proper scheme for the mixing of ionic liquids in microchannels

- To design and fabricate a reaction network that is capable of carrying out mixing and reaction on-chip

- To design and construct a microchannel reactor system, with which all the processes needed for kinetics measurement can be automatically performed, such as feeding, reaction, sampling and chemical analysis.

- To develop necessary models for understanding of processes and determination of operating conditions.

- To test and evaluate the performance of device, as well as to determine operating method and parameters for each process.

- To carry out one chemical reaction in an ionic liquid and measure its kinetics with the developed MCR system.

1.2 STRUCTURE OF THESIS

There are all together nine chapters to present the work carried out for the research.

Chapter 2 provides background knowledge on the subjects involved in the research, in which reviews of the literature are carried out in both the fields of microreactor technology and ionic liquids. In this chapter, introductions are first made on the definition of microreactors, their advantages, fabrication technologies and their applications having evolved over last two decades. This is then followed by

discussions of mixers, in which the prevailing passive mixers are classified into four categories, and the feature and principle of each type mixer are clearly illustrated. To prepare basic knowledge about the reaction media, a simple introduction is also made to ionic liquids, on their histories, properties and applications.

Chapter 3 provides a theoretical basis for the thesis. Discussions in this chapter include the theory of fully developed laminar flow, governing equations for study of pressure-driven flow, and the network analysis model that is often used for prediction and control of fluid flows in microchannels. Moreover, as the fully developed flow theory is applied for the entire channel length in the network analysis, CFD computations of entrance effect are also introduced and the results are discussed, in order to assess the error of pressures prediction resulting from the assumptions.

Details of species mixing in microchannels are discussed in Chapter 4. By characterizing the mixing process in microchannel with parameters such as the Peclet number and diffusion time, the development of mixing schemes along the whole research period is introduced. Comparisons are also made for four types mixers with parameters of mixing uniformity and pressure drop. As a result, the folding network mixer is selected for the design of the microchannel reactor system, due to its better performance over other candidates.

The design and construction of the whole microchannel reactor system is presented in Chapter 5. Here discussion is carried on the selections of all apparatus used in the MCR system, such as pressure controllers, solenoid valves and the switching/injection valves for automatic HPLC analysis. Meanwhile, control of the system including programme and model are described in this part.

In Chapter 6, the principles and procedures of the measurement techniques that are necessary for the kinetics measurement are clarified. These techniques, employed in the experiments, involve determination of fluid flow, measurement of species composition and assessment of mixing performance.

Chapter 7 presents an evaluation of performance of the prototype device. By carrying out tests on each part, mixing performance, valve behaviour and sampling method are studied one by one. Drawbacks are then found in the overall system. These include insufficient mixing elements, misalignment in chip structure and poor repeatability of valve operation. As a result, approaches are proposed to achieve results that are as good as possible with the developed system. The measures taken for the improvement are introduced in detail, both theoretically and experimentally. At the end of the chapter, results for the measurement of reaction kinetics in ionic liquids are presented. The reaction order and reaction rate are determined from the raw experimental data.

Regarding the drawbacks found in experiments, further improvements are made on the MCR system in Chapter 8. The work includes the redesign of mixers and changes of sampling method. As a final output, the Mark II design of the MCR system is presented, and a set of appropriate operating conditions is determined to gain a good control over the system. Measurements of reaction kinetics are carried out, of which good repeatability of data is achieved. The deviation of the kinetics measurement with Mark II MCR system is estimated less than 5%.

Chapter 9 is the conclusion, in which all the work of the research is summarised. In addition, recommendations are made for further work in the future.

Chapter 2

LITERATURE REVIEW

2.1 INTRODUCTION

By surveying the relevant literature in the fields of chemical engineering and chemistry, this chapter aims to put the research of "automated measurement of the kinetics of chemical reactions in ionic liquids" into context. It begins with a review of the development of micro-reactor technologies and applications, and proceeds with a specific description of micro-mixers that are very important in achieving the aims of the research. It ends with an introduction to ionic liquids, showing their importance and providing the background knowledge of their use as reaction media. This review of previous research in the fields of microreactors and ionic liquids demonstrates the need for new research and detailed study necessary to widen the application of ionic liquids in practice. Conventional methods of kinetics measurement are not suitable as they are tedious and time-consuming. Microreactors meet the requirement well with their fast response and precise control of the process.

2.2 MICROREACTORS

In the last two decades, micro-system technology has opened up completely new possibilities for chemical processing and biotechnology. Powerful micro-electromechanical systems (MEMS) technology has been developed, enabling

7

engineers to fabricate micro devices with characteristic dimensions in the order of micrometers (Ehrfeld and Lehr 1995). The essential features of MEMS, miniaturization of mechanical, electrical, optical, thermal and fluidic components have contributed to inventions, including the development of micro-reactors and ink-jet printer heads (Ehrfeld 1996). The success of the micro total analysis system (μTAS) is a good example of a mature extension of the MEMS technology to chemistry and biology. Also the merging of the μTAS techniques with micro-reaction technology has led to microreactors being used for studies of high throughput screening studies of reaction kinetics and mechanisms, as well as on-line monitoring of production systems (Jensen 1999, 2001).

The origins of research on micro-fluidic devices can be traced back to the end of 1970s. The first micro-systems were developed in 1979, including a gas chromatograph at Stanford University (Terry et al. 1979) and simultaneously ink-jet printer nozzles at IBM (Peterson 1979). However, the follow-up was quite modest in the following ten years, until a micro-capillary electrophoresis device was fabricated at the Ciba Geigy laboratory in Switzerland in 1990 (Manz et al. 1990). Since then, research on micro-reactors has become a hot topic and attracted more and more attentions from chemical and biochemical engineers. With the commercial advantages of micro-reactors being acknowledged and the systems becoming increasingly more complex, a more detailed study of micro-devices, both theoretically and experimentally, becomes important and necessary.

2.2.1 Concept of Microreactors

The term "microreactor" has actually been used for a long time. In traditional reaction engineering, it meant a laboratory tubular reactor for the purpose of testing catalyst performance (Benson and Ponton 1993; Jensen 2001). However, with the widening use

of micro-fabrication technology, this word today is increasingly used to designate chemical systems with feature sizes in the microns to hundreds of micron range and with reaction components integrated with sensors and actuators. Hence, synonyms like "micro-engineered" or "micro-structured" reactor have been suggested and considered more appropriate in respect of distinguishing the modern microreactor from its traditional meaning (Gavriilidis et al. 2002).

The concept of a microreactor was first put forward by Wegeng, as "components and systems that exploit engineered structures, surface features or dimensions that are typically measured in terms of microns (one millionth of a metre) to hundreds or thousands of microns, and that may include microelectronic components as an integral part of the system" (Wegeng et al. 1996). It is quite clear that this definition mainly emphasized the size of the microreactor and constrained it to be in the μm range.

Then Ehrfeld proposed a concept that is mostly accepted nowadays. As he pointed out, the microreactor should not be characterized only by its dimensions, but should also reflect the complexities of the system. The microreactor in his definition is therefore not only a reaction unit, but also an integrated system consisting of subsystems or unit operations, such as micro mixing, micro heat exchange, micro pumping and micro valves (Ehrfeld 1998). Later, the Haswell group outlined the concept more generally as "a series of inter-connecting channels (10-300microns in diameter) formed in a planar surface in which small quantities of reagents are manipulated" (Haswell et al. 2001)

2.2.2 Advantages of Microreactors

Characterized by small dimensions and highly integrated technology, the microreactor exhibits many advantages over conventional scale chemistry (Gavriilidis et al. 2002; Haswell and Watts 2003; Jensen 1999, 2001).

- Microreactors provide new prospects for chemical reactions.

  The decrease in the dimensions confers on microreactors the property of larger surface to volume ratios, compared to conventional chemical reactors. As a result, the heat transfer rate in microreactors is much higher than the macro-heat exchanger by an order of magnitude and the mixing of species is faster (Knight *et al.* 1998). The efficient heat and mass transfer in the microreactors then allows reactions under more aggressive conditions to be performed and even optimised by better conditions. For example, unwanted side reactions could be eliminated by good control of the local temperature and/or concentration gradients associated with microreactors. More importantly, some reactions that have been regarded as too difficult to be carried out in conventional equipment are now possible in microreactors. For example, the use of elemental fluorine in organic synthesis is problematic because of the difficulties associated with the safe handling of gaseous fluorine. In addition, fluorination reactions are generally extremely exothermic and it is difficult to control the temperature of such reactions when performed on a large scale (Haswell and Watts 2003). The microreactors then have considerable attraction for use in such potentially hazardous processes since the small amount of chemicals involved together with the heat and mass transfer properties of the microreactor can overcome the safety issue. As a result, it is reported that Chambers and Spink developed a microreactor from a block of nickel to carry out the direct fluorination of aromatic compounds (Chambers and Spink 1999).

- The small scale of the microreactor reduces the danger of system failures. As only small quantities of materials are loaded and the microreactor system is enclosed, in the event of a runaway process, the release of toxic and hazardous chemicals will be less harmful and the contamination will be easier to stop. In addition, with

integrated sensors and control units, the failed reactor can be isolated and replaced without interrupting the production of other parallel units. The inherent safety characteristics of microreactors suggest that hazardous materials can be synthesised as required at the point of use, thus avoiding problems in the process of storage and shipping (Hendershot 2000; Lerou *et al.* 1996).

- The replication capacity of microreactors provides great flexibility for manufacturing of real chemical systems.

Being able to be scaled-out rather than scaled-up, microreactors enable the development process to be changed into designing and optimising a single reactor performance in the laboratory, then building up the system by simple replication and parallelization. This feature not only saves both time and capital by bypassing the pilot plant scale, but also enables production to respond more quickly to demand changes, since the capacity can be adjusted through adding or removing units from the parallel network. Moreover, as all parameters for the full-scale production are kept exactly the same as they are optimised in the laboratory, high level control and good performance are guaranteed in the application.

## 2.2.3 Fabrication Technologies for Microreactors

Fabrication methods for microreactors build, in part, on advances in micro-electromechanical systems (Wise 1998). A number of materials such as silicon, glass, quartz, metals and some polymers have been used to construct microreactors. Glass and certain polymers are found particularly useful because of their physical properties and chemical inertness. Aiming at manufacturing more complex and ingenious microreactors with higher reliability and precision while with lower cost, a range of fabrication methods have also been explored (Madou 2002; Ziaie et al. 2004).

Photolithography and etching techniques

Photolithography and etching are the most well developed methods of all micro-fabrication techniques. They are widely used for silicon and glass substrates because of the simplicity of the method coupled with the versatility of the devices (McCreedy 2000). The generic procedure is as illustrated in Figure 2-1.
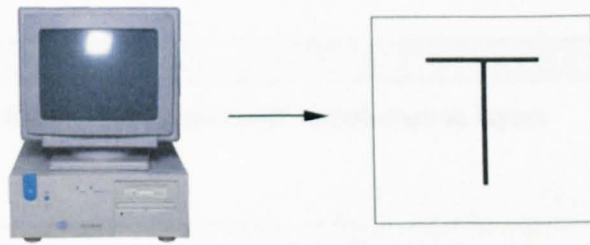
Step 1: Drawing and printing a pattern
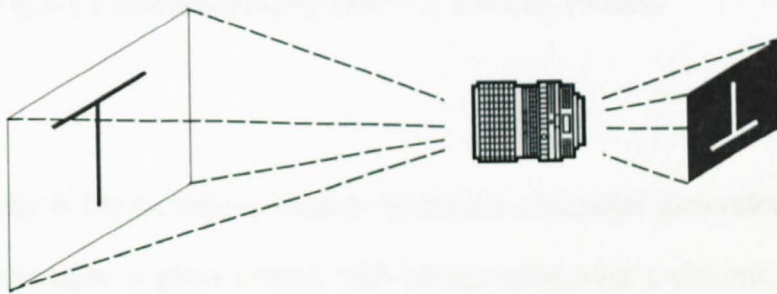
Step 2: Taking picture to produce a negative
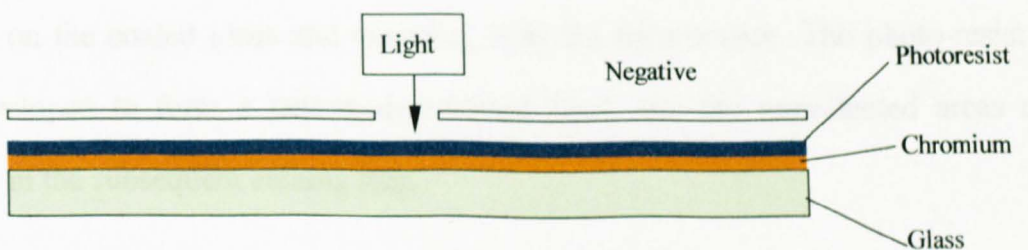
Step 3: Transferring the negative pattern to coated glass to form a mask

Step 4: Removal of photo-resist

Step 5: Removal of exposed chromium

Step 6: HF etching of the glass

Step 7: Removal of Photo-resist and chromium layers
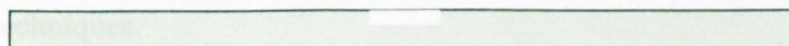
Step 8: Bonding with a piece of glass at the top of the channel

Fig.2-1 Photolithography and Wet Etching Process

Photolithography is the technique used to transfer a computer-generated pattern onto a substrate, for example, a glass coated with photo-resist over a chromium layer. In the procedure, a negative is first produced by photography from the pattern designed and printed with a computer. Then, the pattern is transferred to the substrate by fixing the negative on the coated glass and exposing it to the light source. The photo-resist is later developed to form a patterned-protected layer and the unprotected areas are removed in the subsequent etching step.

Etching techniques fall into two categories as "wet" and "dry". According to the selectivity and directionality, wet etching can be further divided into isotropic etching and anisotropic etching. The wet etchants are by and large isotropic in reactivity and show superior material selectivity as compared to the dry technique. Etching at the

same rate in all directions (isotropic) results in round corners in the geometry. This means that it is difficult to achieve high precision with wet etching and the minimum feature that can be made is limited to >3μm. The three most important anisotropic etchants are potassium hydroxide (KOH), ethylene diamine pyrochatechol (EDP), and tetramethyl ammonium hydroxide (TMAH). Anisotropic etching attacks silicon along preferred crystallographic directions and gives higher precision. However, the etching rate is low, and more importantly it is possible only for monocrystalline structures. A large variety of metals and stainless steels can be structured through isotropic wet etching techniques.

Dry etching has several advantages, compared to the wet etching techniques. It allows a smaller undercut and higher anisotropicity, resulting in good pattern transfer for accurately etching at small dimensions. However, the selectivity of dry etching is lower than for wet methods. The basic methods of dry etching include High-Pressure Plasma Etching, Reactive Ion Etching (RIE) and Ion Milling. Of the three methods, ion milling is a purely physical process, which utilizes accelerated inert ions, striking perpendicular to the surface, to remove unwanted material. High-pressure plasma etching is a chemical reaction process, using species that are highly reactive with the materials to be etched. RIE etching, is a combination of physical and chemical processes, in which the reactive species react with the material only when the surfaces are "activated" by the collision of incident ions from the plasma (Lang 1996).

LIGA

The acronym LIGA comes from the German name for lithography, microelectroplating and micromoulding processes (German: Lithographie, Galvanoformung, Abformung). It is based on the principle of transferring a given pattern from a mask into an extremely thick layer of a radiation sensitive polymer (resist) by means of a micro-lithography process or by well-defined deflection of radiation. In this method, X-rays

are used to perform photolithography on the thick resist to produce a three-dimensional structure. After development and removal of the resist, a complementary metal structure is generated from the resist master by means of electroplating. The metal structure then serves as a mould insert for the subsequent replication processes such as injection moulding, reaction injection moulding or embossing (Thornell and Johansson 1998). The use of highly coherent X-rays provides the typical advantages of LIGA technology, such as the high precision, large aspect ratios up to 1000, high surface quality, and the wide variety of materials available for electroplating and moulding including metals, alloys, ceramics, and polymers. But as the X-rays are produced by synchrotrons, it is expensive and this has resulted in the development of a LIGA-like process using UV-photolithography and thicker layers of resist (Loechel 2000).

Laser-LIGA is a variant of the LIGA technique. It employs an excimer laser for the ablation of the resist followed by injection moulding or hot embossing (Banks 2005; Ehrfeld *et al.* 1999). The interesting point of the excimer laser is that it does not remove materials by burning or vaporising, so material adjacent to the area machined will not be melted or distorted by the heat effects. This characteristic enables this Laser-LIGA technique to shape the materials laterally as well as depth-wise. Also as a direct-writing process, Laser-LIGA is suitable for rapid prototyping.

Soft lithography

Based on the old techniques of moulding and embossing, "soft lithography" uses soft materials for the fabrication of microstructures. The typical material used in this method is the poly-dimethly-siloxane (PDMS), also known as silicone rubber. With a mould made by any hard micro-machining technique like photolithography and etching, the designed pattern is transferred to the PDMS by either moulding or embossing (McCreedy 2001; Xia and Whitesides 1998a,1998b). The processes of micro-moulding and hot embossing are illustrated respectively in Figure 2-2 and

Figure 2-3 (Ziaie et al. 2004). The PDMS is inexpensive, biocompatible and has excellent sealing properties, so it is very suitable for micro-fluidics (Whitesides and Stroock 2001). Meanwhile, as it can be easily bonded to itself, the usage of the PDMS makes it possible to fabricate multi-layer structures.
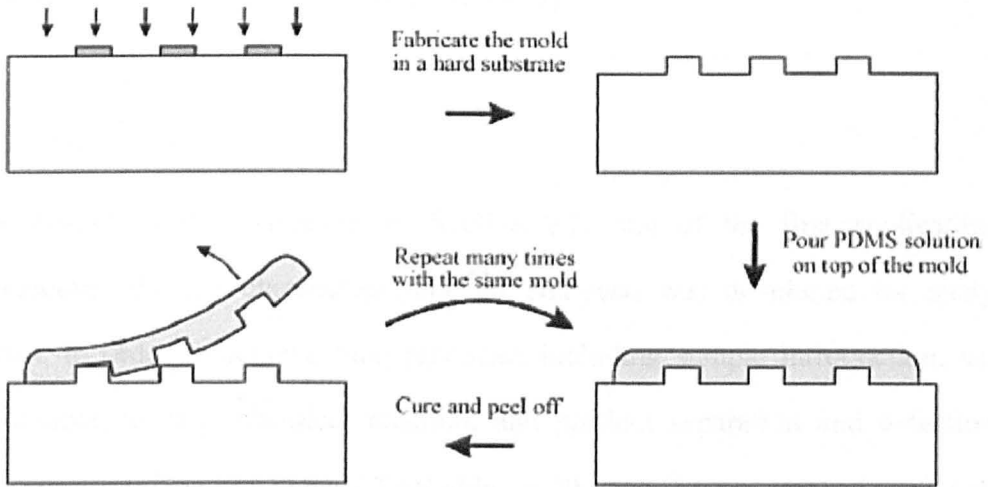

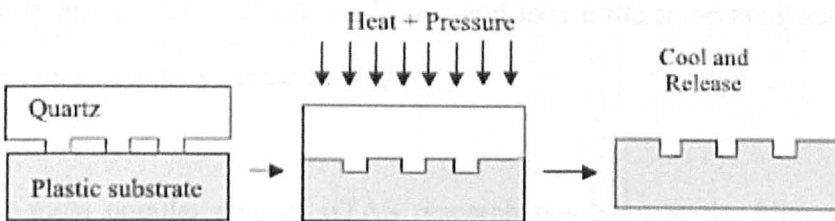**Fig.2-2 Micro-moulding Process (Ziaie et al. 2004)**

Fig.2-3 Hot Embossing Process (Ziaie et al. 2004)

2.2.4 Applications of Microreactors

Due to the advantages associated with their small dimensions and the fact that they are fabricated for highly integrated technology, microreactors are increasingly being used in many applications, and the demand for such micro-devices is still rapidly rising. For example, the biochip market was $400M in the year 2000 and was expected to increase by a factor of five by 2005 (Stone and Kim 2001)

1. Chemical analysis

As mentioned in the beginning of Section 2.2, one of the first applications of microreactors, the gas chromatographic air analyser, was developed for analytical purposes. In order to achieve this, processes including sample introduction, sample pre-treatment, mixing, chemical reaction, and product separation and detection are incorporated into one complete μ-TAS chip, as illustrated in many devices developed (Erickson and Li 2004). The miniaturization of analytical systems is of benefit for improving reliability, decreasing analysis time, reducing sample size and reagent consumption. For example, the microfluidic sample-sequencing unit designed for composition analysis makes it possible to operate a large number of tests simultaneously and under identical conditions and to use the same analyser to process samples from many sources (Tesar *et al.* 2004).

To date, the most popular area of μTAS research has been in the biomedical field, particular in the analysis of DNA and proteins and has resulted in the release of commercial devices (Fletcher et al. 2002; Watts and Haswell 2003). For example, a chip-based sensor array composed of individually addressable agarose micro-beads was developed and demonstrated for the rapid detection of DNA oligonucleotides (Ali *et al.* 2003). In this design, DNA capture probes containing micro-beads were selectively arranged in micro-machined cavities localized on silicon wafers. The

micro-cavities possess trans-wafer openings, which allow for both fluid flow through the microreactors/analysis chambers and optical access to the chemically sensitive micro-beads. Collectively, these features allow the identification and quantitation of target DNA analytes to occur in nearly real time using fluorescence changes that accompany binding of the target sample. The unique three dimensional micro-environment within the agarose bead and the micro-fluidic capabilities of the chip structure afford a fully integrated package that fosters rapid analyses of solutions containing complex mixtures of DNA oligomers.

2. High throughput screening

Applications for high throughput screening make full use of the advantages of microreactors such as efficient heat and mass transfer, quick response, defined flow characteristics and large surface to volume ratios. Small reactors are already used for the testing of process chemicals. Chemical detection is usually the rate-limiting step in most techniques since detailed product information must be obtained by sequential screening. However, with the advantages of μTAS and micro-fabrication techniques, the micro-chemical system consisting of the integrated micro-fluidic circuits, sensors, controls and reaction components could totally replace the conventional macroscopic test systems, thus requiring less space, fewer utilities and produce less waste. Moreover, the small dimensions of the microreactor and the laminar flow that are usually used in microchannels, makes it feasible to fully characterize the heat and mass transfer process, hence to extract the kinetic parameters (Charpentier 2005).

In a similar way to μTAS, the high-throughput screening applications still attract a great deal of attention from the biochemical field, since a microreactor would be the preferred reaction device for many biochemical reactions (Boberge et al. 2005). The limits of high cost of reagents and safety concerns for conventional bench-scale

experimentation have thus been effectively eliminated in microreactors because of their small volumes and inherent safety characteristics. However, the related challenge comes from the need to define the conditions for the translation of the results from micro-systems to the conventional lab and then industrial scale. For instance, a miniature gas-liquid bioreactor was designed as a fermenter, which is mechanically agitated and aerated with a micro-fabricated bladed turbine impeller to imitate the flow conditions created in conventional mechanically stirred reactors. Micro-fabricated fibre optic probes were used for *in situ* measurement of process parameters such as dissolved oxygen, pH and temperatures. However, before the micro-reactor was used to obtain the volumetric oxygen transfer data under different operating conditions, results had to be compared with data obtained from parallel experiments of large-scale fermentation to calibrate its performance as a fermenter (Lamping *et al.* 2003).

The application of microreactors for high-throughput screening purpose in chemistry and chemical engineering mainly focuses on work with catalysts. For example, an approach has been proposed as a new concept for high throughput screening of catalysts, which includes a combination of pulse injections of the catalysts and the substrate, a static micro-mixer mounted in a dynamic micro-activity test unit, and a tubular stainless steel capillary reactor. In this microreactor unit, the catalyst library was subsequently screened for two test reactions, a liquid-liquid isomerization of allylic alcohols and a gas-liquid asymmetric hydrogenation. The results then led to the selection of the best catalyst showing activity towards a large class of allylic alcohols (De Bellefon *et al.* 2000). Other research includes different work on the parallel quantitative screening of selectivity of catalysts, of which most are in gas-phase and gas-liquid reactions (Cong *et al.* 1999; Liu *et al.* 2000b; Mills and Nicole 2004; Potyrailo *et al.* 2003; Zech *et al.* 2005). To provide the basis of the rapid screening of catalysts with microreactors, work has also been done to compare the performance of individual micro-channels and a large number of parallel channels. The outcome

model is then able to provide a quick, though rough, estimation of how the difference in channels would affect the performance of the microreactors (Delsman *et al.* 2005).

The fast identification of substances and the screening of large number of samples allow the use of combinatorial methods in chemical reaction development (Gavriilidis *et al.* 2002). Meanwhile, the small size of the sample also calls for improvement of the detection sensitivity. Optical methods have been most commonly applied, which allow on-site detection of chemical composition. Detection methods developed and applied in past years include spectroscopic methods and electrochemical techniques (Chabinyc *et al.* 2001; Keoschkerjan *et al.* 2004; Potyrailo *et al.* 2003; Schwarz and Hauser 2001; Senkan *et al.* 1999).

3. Access to new chemistry and process development

Microreactors have become important tools for the access to new chemistry because of their ability to accommodate reaction regimes and conditions not accessible for conventional equipment. As an example that has been mentioned before, Jenson and his co-workers have demonstrated the direct fluorination of aromatic compounds in a microreactor, a process that is too difficult to perform on a conventional scale because of the highly exothermic nature of the process. Using ten equivalents of fluorine in methanol (the solvent), the authors reported 80% conversion to give the mono-fluorinated toluenes at room temperature (Haswell and Watts 2003). Even earlier, microreactors have been reported with a cross-flow heat exchanger and a Pt/Al_2O_3 catalyst to carry out catalytic oxidation of hydrogen. An explosive mixture with volumetric concentration of oxygen and hydrogen up to 50% was operated safely and complete conversion of hydrogen to water was succeeded (Janicke et al. 2000).

The properties of fast mixing and good control of temperatures and residence times also make microreactors attractive for process development. Due to their small

dimensions, process characteristics and operating conditions can be tested quickly with low consumption of chemicals. The results then can be used for the design of conventional reactors or be optimised for standard processes (Pennemann et al. 2004). For instance, BASF developed, in collaboration with IMM, a microreactor for the synthesis of vitamin precursors. In conventional equipment, it is difficult to study and optimise this process because the reaction is highly exothermic and also by-products are formed quickly. However, in the microreactor with a reaction channel $900\mu m$ deep and $60\mu m$ wide, surrounded by cooling channels, a maximum yield of 95% with by-products reduced by 50% was obtained because conditions of short residence time, isothermal operation and fast quenching can be achieved. This is not possible in existing laboratory equipment (Worz et al. 2002). More recently, microreactors have attracted lots of attention from the field of micro-fuel processing. Several groups are working on development of metal- silicon- and ceramic- based microreactor components of a portable fuel processor for *in situ* methanol reformation (Hu *et al.* 2003; Pattekar and Kothare 2004; Tanaka *et al.* 2004). As a highly endothermic process, the methanol reformation process confronts the research with a challenge of heat management within the unit, since endothermic and exothermic components need to be coupled and heat losses to be minimized to achieve high heat efficiency (Shah *et al.* 2005).

4. Distributed and mobile processing

The inherent safety characteristics and the scale-up capabilities of microreactors enable distributed production of chemicals at the point of use and adjustment of production capacity to meet varying demands. This application is especially suitable for processes with high risks and costs concerning transport and storage of hazardous chemicals. The first proposal for distributed manufacturing with miniaturized plants was presented in 1993, referred to as miniplants (Benson and Ponton 1993), followed by research work

demonstrating the feasibility of safe operation of hazardous reactions in microreactors, e.g. the synthesis of methyl isocyanate from methylformamide and oxygen at high temperature (Lerou et al. 1996). The more recent example is that Wiles et al demonstrated the use of silyl enol ethers in the aldol reaction within a microreactor. A conversion of 70% was observed in 20 minutes, what is a dramatic decrease compared to the traditional batch reactions where high yields could be obtained only when the reaction time was extended to up to 24 hours. Moreover, the air sensitive immediate was produced *in situ* within a sealed microreactor and had a life time of a few seconds before it was further reacted (Watts and Haswell 2005). This example well illustrates that with the capability of production at point of use, microreactors provide opportunities to exploit highly reactive and/or unstable chemicals in synthetic reactions.

5.   Extraterrestrial processing

Utilization of microreactors in extraterrestrial processing is very promising. The lightweight and compact structure of microreactors meet well the requirement of space technology with high performance per unit mass. Research has been conducted at the Pacific Northwest National Laboratory (PNNL), involving the design of a micro-chemical plant in which carbon dioxide from the Martian environment can be converted with stored hydrogen into propellants and oxygen for the return trip, so that the required mass can be reduced when the airship is launched from the earth. NASA plans to launch such micro-chemical plant to Mars in 2011, followed by a human mission in 2013. But a significant challenge to the extraterrestrial chemical plant is the energy management, which means the microreactor systems must be able to operate efficiently and reliably for a long time, as required by their utilization in the outer space (Gavriilidis *et al.* 2002).

2.3 MIXING OF SPECIES IN MICRORACTORS

As described above, microreactors and microreactor systems are becoming increasingly popular for applications across all chemical and biochemical engineering. The development of micro-fabrication techniques allows not only inexpensive large-scale production of micro-devices from replication moulds, but also the high integration of active elements such as micro-pumps and micro-valves on the chip. But no matter how advanced the system and technologies are, micro-mixers are a crucial part in the micro-reactor, due to their importance in providing a uniform mixture for the chemical reaction or analysis.

The difficulty of rapid mixing comes from the fact that the fluid flow at the microscopic scale is restricted to the laminar regime, typically with a Reynolds number usually less than 1. In addition, the sizes of microchannels are too small to allow incorporation of conventional mixing mechanisms. The mixing of species in microchannels constrained by the low Reynolds number mainly relies on molecular diffusion. Diffusive mixing in laminar flow is very slow, especially in liquid phases, since the diffusivities in gases exceed those in liquid by several orders of magnitude. To achieve complete mixing purely by diffusion, long channel lengths will be needed. However, channel length is usually limited by factors such as the chip size and high pressure-drop and thus high requirements on the system controls. More importantly, long channel length means a long residence in the mixer. Since chemical reactions occur while species mix, the reaction rate must be different from that in the well-mixed reagents and it varies as the fluid flows through the micro-mixer. As it is hard to separate the mixing time from the total reaction duration, the variation of reaction rate associated with the mixing process results in errors in the counting of reaction time and thus the reaction rate. For example, if the residence time in the micro-mixer is 100ms, the resulting error in the reaction rate will then be 1% when the reaction duration is 10s,

reaction duration is 10s, which increases to 10% when the reaction time reduces to 1s. Hence the channel length and thus the residence time in the micro-mixer must be limited within an acceptable range. This is particularly crucial for the study of reaction kinetics, especially when the reaction time is short. Therefore different schemes have been developed to enhance the mixing process in microchannels, aiming at producing homogeneous mixtures within the length scale compatible with the chip design.
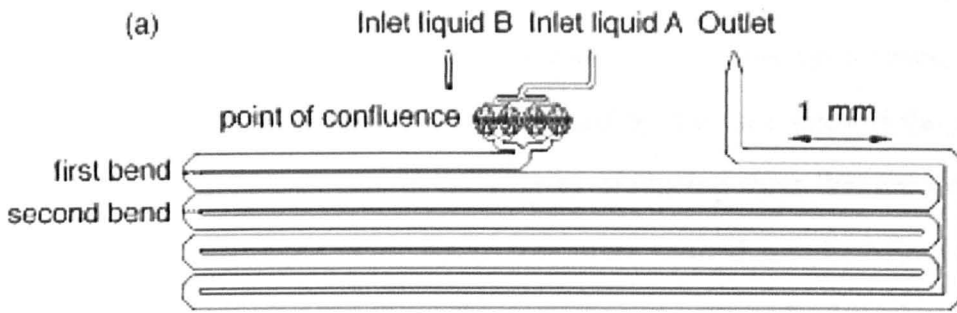
Most micro-mixers can be classified as either active or passive (Oddy 2001). Active mixers accelerate the mixing process by moving parts or externally applied force. Different methods have been demonstrated with the assistance of externally forced mass transport ranging from miniature stirrers (Lu et al. 2002), magneto hydrodynamic pumping (Bau et al. 2001), to ultrasonic waves (Rife et al. 2000; Yang et al. 2000). For example, a mixing chamber was designed, in which the fluid was effectively stirred by using micro-fabricated valves and phase-change liquid micro-pumps (Oddy 2001); and a strategy was also explored to enhance the mixing in microchannel by forming and controlling nano-scale, submerged fluid jets (Hardt *et al.* 2005). Although active mixers are effective, they are often difficult to fabricate. Additionally, the electrical fields and heat generated by the active control of these mixers may cause damage to the samples especially during biochemical processes. Nowadays, active mixers are mostly used for silicon substrates.

As the more common scheme, passive mixers typically use the channel geometry to increase the interfacial area between the liquids to be mixed. Therefore, they are also referred to as static mixers. According to their principle, passive mixers are being further categorized into different types (Aubin *et al.* 2005; Wang *et al.* 2002). Adopting the division proposed by MacInnes and Allen (2005), the micro-mixers discussed in the thesis are put into four categories as follows.
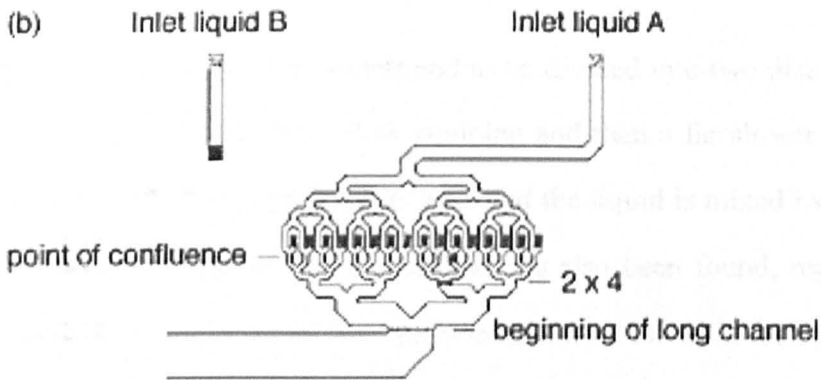
1. Simple channel micro-mixer (SCM)

The simple channel mixers are the most basic among all four types of the micro-mixers. Using "T" and "Y" shape channels to bring two or more streams together, the fluid streams flow parallel to each other in the main channel, so that the mixing process purely depends on molecular diffusion. The channel then has to be fabricated as narrow and serpentine as possible in order to reduce the diffusion distance and give enough mixing time. Therefore the mixers are normally characterized by small channel width, such as tens of microns, and long channel length. As a result, a very large pressure drop is usually required to achieve a reasonable flow rate. Examples of this are the so-called series-mixing device (Jacobson et al. 1999), which was used for the dilution of samples by an array of T-intersections, and the winding channel, which relies on the chaotic advection created by the helical flows induced in a simple meandering channel to accelerate the mixing process (Baier *et al.* 2005).

The other "interdigitated" type of the SCM was proposed by Bessoth *et al.* (1999). As shown in Figure 2-4, with a series of T-junctions, the two original fluid steams are divided into a number of sub-streams, interdigitated and collected into the same long channel. The diffusion distance between two streams is then decreased, exponentially proportional to the layer to divide the fluid stream. The attractiveness of this kind of mixer is that the rapid mixing does not depend on the flow rate, hence will not ask for extra demand on the pressure drop. However, the geometric dimensions to produce striations of species that are small enough for rapid mixing require high accuracy from the fabrication technology. Any defect in the geometry will cause non-uniformity in the interdigitation streams, and thus produce a globally non-uniform mixture, as illustrated by MacInnes and Allen (2005)

(a)   Inlet liquid B   Inlet liquid A   Outlet

point of confluence

first bend

second bend

1 mm

(a) Schematic of the mixer

(b)   Inlet liquid B   Inlet liquid A

point of confluence

2 x 4

beginning of long channel

(b) Detail of the interdigitation part

Fig. 2-4 Interdigitated SCM (Bessoth et al. 1999)

2. Alternating flow micro-mixer (AFM)

The principle of the alternating flow micro-mixer is trying to increase the diffusion interfaces between streams by forcing one fluid into another. In this mixer, the flow of liquids to be mixed is switched at a junction, hence slugs are formed due to the fluid deformation associated with strain rate in pressure-driven flow, and so the different solutions are mixed.

There are two typical ways to produce alternating flow in the mixer. One is to form slugs via periodically injecting two or more streams into a main channel, by which the interfaces between fluids are vertical. Furthermore, as the slug geometries, i.e. the thickness and the space in between, are determined by the flow rates of the injected streams, the diffusion distance can be reduced by producing slugs that are small and close to each other (MacInnes et al. 2005). The other method is pulsed-flow mixing. By introducing time pulsed cross-flows from one or more perpendicular inlets into the main channel, pulsed-flow mixing aims at enhancing the mixing process by periodically distorting the interface between species (Glasgow and Aubry 2003).

The mixing process in the AFM has been found to be divided into two distinct stages: first a rapid mixing of outer liquid by flow straining and then a far slower process in the core of the flow where strain rate falls to zero and the liquid is mixed by diffusion, as shown in Figure 2-5. Furthermore, a weakness has also been found, regardless of the injection method, that is, a lateral non-uniformity can be found in the solution and it remains for the channel width diffusion time scale (MacInnes et al. 2005).
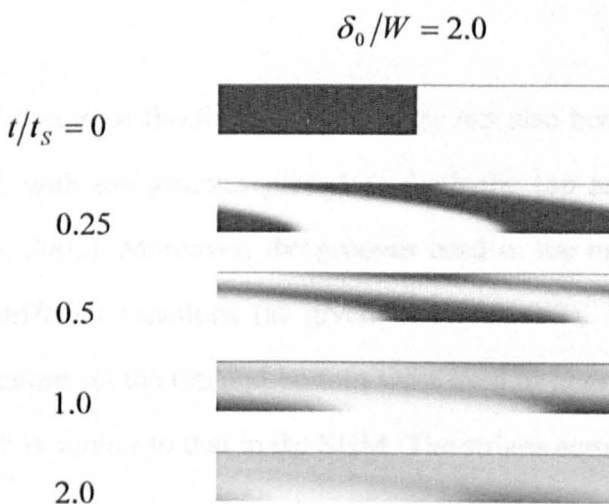
$$\delta_0/W = 2.0$$

$t/t_s = 0$

0.25

0.5

1.0

2.0

Fig. 2-5 Sequence of Mixing in AFM (MacInnes et al. 2005)

3. Folding flow micro-mixer (FFM)

The folding flow micro-mixer takes advantages of rapid stretching and folding of fluid flow associated with pressure-driven chaotic advection. Transverse flows are generated in the mixers by employing either patterned surface (Johnson et al. 2002; Stroock et al. 2002a) or twisted geometries (Bertsch *et al.* 2001; Jen *et al.* 2003; Liu *et al.* 2000a). The fluid is then rotated and folded under the effect of the transverse flow created by the geometry, hence diffusion distance is reduced and the interfaces between species are increased.

A well-known design of the folding fluid micro-mixer was presented by the Strook group at Harvard University, which was also referred to as the staggered herringbone mixer (SHM). Consisting of a straight channel with some V-shaped ridges placed on the bottom wall, the mixer includes several mixing cycles. In each cycle, the ridges are arranged zigzagging to the left in the first half cycle, then to the right in the next half cycle. By varying the shape of the grooves on the bottom, transverse flows are produced, subjecting the volume of fluid to a repeated sequence of rotation and extension (as shown in Figure 2-6) (Stroock et al. 2002b; Stroock and Whitesides 2003).

An improved design of the folding fluid mixer has also been put forward recently by Howell *et al*, with the grooves placed on both the top and bottom of the channel (Howell *et al.* 2005). Moreover, the grooves used in the mixer were in two kinds of patterns for different functions (as given in Figure 2-7). The chevrons, pointing in opposite directions on the top and bottom were used to generate a pair of vortices side by side, which is similar to that in the SHM. The stripes across the channel width at the angle of 45° were to create the pair of vertically stacked vortices. As a result, the design of the mixer not only increases the driving force in the lateral direction, but also

only on the bottom. Even in its early stage, the mixer shows a mixing process over a shorter channel length than the SHM. However, a high demand for precision of fabrication emerges as the geometry becomes more complicated.
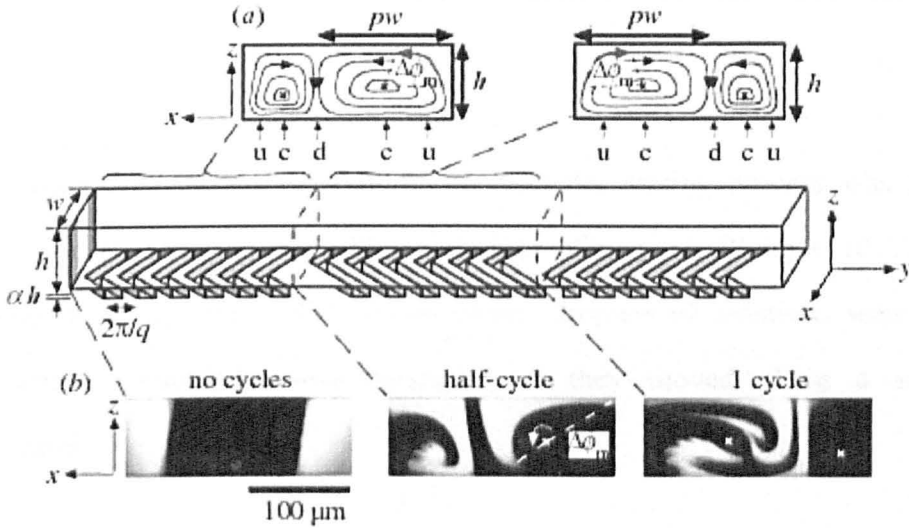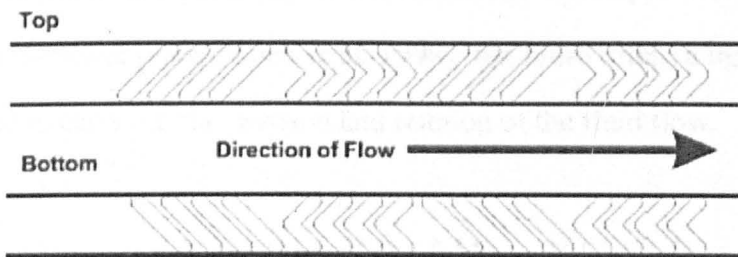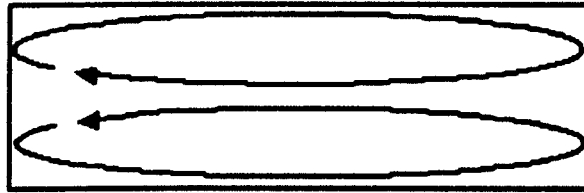

Fig.2-6 Staggered Herringbone Mixer (SHM) (Stroock and Whitesides 2003)

a. Schematic layout of the channel

b. Vortices generated by chevrons

c. Vortices generated by stripes

Fig.2-7 FFM with Grooves on Both Top and Bottom (Howell *et al.* 2005)

Another interesting design reported to improve the mixing process was to create chaotic advection in slugs of multiple solutions of reagents (Song *et al.* 2003). By introducing a second immiscible liquid phase, droplets of solutions were formed, within which recirculation was produced as they moved along a serpentine microchannel.

4. Folding network micro-mixer (FNM)

Mixing processes in folding network micro-mixers are improved by repeated split and stack of fluid streams. The geometry of the mixer can be simple with all the patterns projected onto the same plane (Koch et al. 1998); but more often, a three-dimensional network is used to carry out the division and reunion of the fluid flow.

Figure 2-8 illustrates several structures of the folding network mixer, of which (a) is reported by MacInnes and Allen (2005) and (b) by Chen and Meiners (2004) respectively. For these two designs, the mixers consist of a number of elements. In each mixing element, fluids are split, turned and reunited, hence the thickness of the species striation is halved and the interfaces doubled. Therefore, by repeating the splitting and reuniting the flow, diffusion distances reduce exponentially and the surface areas expand rapidly. Another design of the FNM is proposed by Lee and Lee (2005) (Figure2-8 (c)). Using the same principle, the splitting and reuniting of fluid

streams was carried out by guiding walls and expanding walls arranged in the channel. Comparatively, the structure is even more complicated than the two introduced above.

The drawback of the folding network mixer is again the difficulty of manufacture. Due to the complexity of the structure, it needs multi-layer fabrication technology, which makes it less attractive, especially for electro-kinetic systems where one- or two-layer structures are normal. However, with the development of micro-fabrication technology, this is no longer a big issue. Commercial manufacturers such as Micronit [R] (the Netherlands) have emerged, who can fabricate complex micro-channel networks within acceptable tolerances.
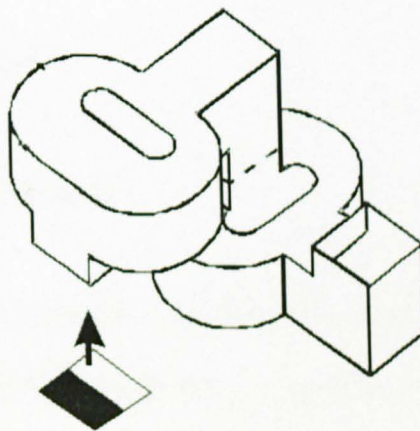
(a) MacInnes and Allen's design (2005)

(b) Chen and Meiners's design (2004)
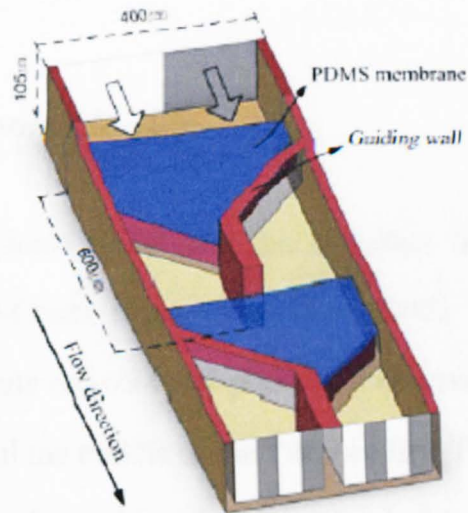
(c) Lee and Lee's design (2005)

Fig.2-8 Examples of FNMs

2.4 IONIC LIQUIDS

2.4.1 What are Ionic Liquids

Formed only by ions, "ionic liquids" are defined as salts with melting points below 100-150°C (Visser et al. 2000), so that they are liquids at low temperatures. It is quite important to note that they are not a solution of ions in water, instead, they are the mixture of organic and inorganic ions, as their name suggested.

There are many synonyms for ionic liquids in the literature, among which, "Molten salts" is the most common one, particularly in early publications. Since molten salts normally exist at much higher temperatures typically over 600°C, ionic liquids are also practically accepted as "room temperature molten salts" or "ambient temperature molten salts". But they are different and it is not just a matter of degree. In fact, molten salts tend to be highly corrosive and viscous, whereas ionic liquids are generally more stable and much easier to be handled.

2.4.2 History of Ionic Liquids

The first documented ionic liquid was the so-called "red-oil" in the 19th century formed during Friedel-Crafts reactions (Wilkes 2002). In the prototypical Friedel-Crafts reaction, a separate red-coloured phase was observed. However, its composition remained unknown until the middle of the 19th century. The structure of the liquid was later proposed to be the heptachlorodialuminate salt for AlCl3-catalysed reactions, as shown in Figure 2-9. The red ionic liquid and more complicated variations were later patented (CAS Registry Number: 78041-07-03), but no major industrial use was ever found (Wilkes 2002).

The first ionic liquid with a melting point of 12°C, [EtNH$_3$][NO$_3$], was discovered in 1914 (Sugden and Wilkins 1929; Welton 1999). But no further interest developed until Wier (Wier and Hurley 1948), who worked on electro-deposition of aluminium in some AlCl$_3$-based molten salts, discovered that the 1-ethylpyridinium cations and a mixture of halides (mainly the bromide) and chloroaluminate(III) anions could produce room-temperature ionic liquids.

The modern era of ionic liquids started since the late 1970s, and it is marked by the simultaneous collaborative discovery and development of the 1-butylpyridinium chloride-aluminium chloride mixture (BPC-AlCl$_3$) by the groups at Colorado State University and the Air Force Academy(Gale et al. 1978; Nardi et al. 1978). This all-chloride system was an improvement on the mixed bromide-chloride ionic liquids of Wier and Hurley. However, as the melting point of the equimolar composition is 40°C, the BPC-AlCl$_3$ ionic liquid is not, strictly, a room-temperature ionic liquid at the composition that has the highest conductivity (Wilkes 2002).

Since 1979, Wilkes and Hussey had worked to find an alternative chloride salt that would make a chloroaluminate ionic liquid with low melting point but a cation that would be more difficult to reduce (Wilkes 2002). What they finally found was that an ionic liquid was formed, with a freezing point below room temperature, for all compositions of $AlCl_3$ ranging from 0.33 to 0.67M when the 1-ethyl-3-methylimidazolium chloride ([emim]Cl) was mixed with aluminium chlorides. After measuring the properties of ionic liquids made from a series of dialkylimidazolium chlorides with different lengths of alkyl substituents, the ionic liquids containing the 1-ethyl-3-methylimidazolium cation, were found to represent the best compromise between easy synthesis and good physical, chemical and electrochemical properties (Wilkes et al. 1982).

These chloroaluminate(III) ionic liquids are generally referred to as the first generation ionic liquids. The main disadvantage of these ionic liquids is that they are reactive with water and a product of the reaction is the corrosive HCl. This feature of chloroaluminates requires that they must normally be handled in a glove box, with exclusion of moisture. However, it doesn't affect the use of the chloroaluminate ionic liquids in high-energy batteries, which are sealed from atmospheric conditions.
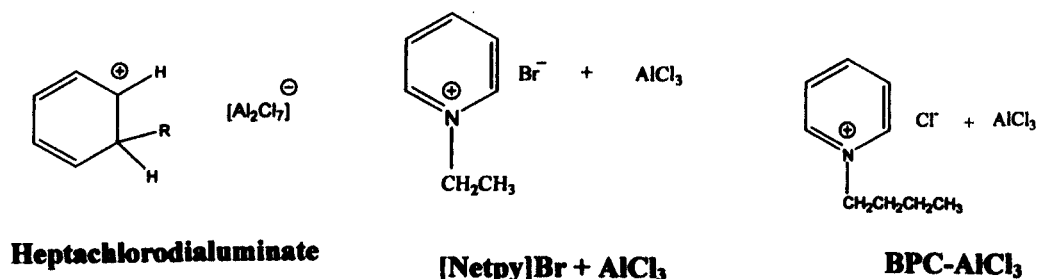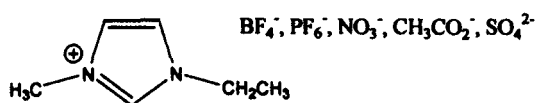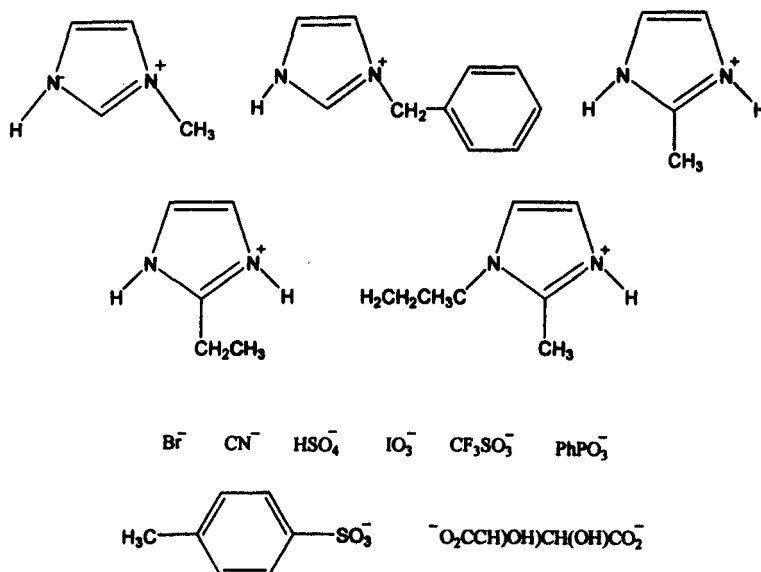

Fig.2-9 Examples of First Generation Ionic Liquids (Wilkes 2002)

Another significant step was taken in 1992 when Wilkes and Zaworotko (Wilkes and Zaworotko 1992) prepared and characterised salts with dialkylimidazolium cations, but with water-stable anions. Using tetrafluoroborate, hexafluoraphosphate, nitrate, sulphate and acetate salts, the first air and water stable ionic liquids were made by metathesis reactions of the dialkylimidazolium halide with the appropriate silver salt. Further extension of the catalogue of water stable ionic liquids was made by Fuller, from traditional dialkylimidazolium cations to a series of mono and trialkylimidazoliums, as well as series of larger anions (Fuller and Carlin 1994; Fuller et al. 1994). These air and water stable ionic liquids are referred to as the second generation ionic liquids.

Traditional water-stable ionic liquids (Wilkes 2002)

Fuller's extension of cations and anions (Fuller and Carlin 1994; Wilkes 2002)

Fig.2-10 Examples of Second Generation Ionic Liquids

2.4.3 Properties of Ionic Liquids

Consisting of a bulky cation and a smaller inorganic ion, ionic liquids are usually colourless viscous liquids with densities about 1400-1800 kg/m^3, viscosities ranging from 0.03 to 0.200 Pa·s, but very low diffusivities in the order of magnitude of 10^{-11}-10^{-12} m^2/s, compared to the water diffusivity in order of 10^{-9} m^2/s.

Ionic liquids are environmentally benign solvents because they are non-volatile and have no measurable vapour pressure. In addition, they are non-flammable. (Bradley 1999). As they do not release any vapour to the atmosphere through evaporation, ionic liquids can be used in high-vacuum systems. They can also be easily contained and recycled in the chemical plants so that the waste production in some processes is dramatically reduced (Holbery and Seddon 1999).

Ionic liquids are excellent solvents, capable of dissolving a wide range of organic and inorganic materials, and can bring the unusual combinations of reagents into the same phase (Welton 1999). For example, the chloroaluminate-based ionic liquids, which can dissolve up to 50% benzene (by volume) (Renner 2001), have been used in the extraction of kerogen, an insoluble organic material that cannot be extracted with normal sulphuric and nitric acid but only with hydrofluoric acid (Freemantle 1998). During investigations by chromatographic techniques (Coddens et al. 1986; Pomaville and Poole 1988; Poole et al. 1989), it was generally found that when considered as polar phases, the solvent properties of ionic liquids are largely determined by the ability of the salt to act as a hydrogen-bond donor and/or acceptor and the degree of localization of the charge on the anions, and this property may act differently in acidic and basic liquids (Koel 2000). The lipophilicity of the ionic liquids was found to increase with the length of the alkyl chain substituents on both cations and anions (Furton and Morales 1991; Shetty *et al.* 1987). Also, the influence of hydrogen

bonding can be diminished by fluorinating the ionic liquids (Pomaville and Poole 1990). Therefore, ionic liquids can be prepared ranging from hydrophobic to hydrophilic as well as from water-sensitive to air-stable (Seddon 1999).

In addition, ionic liquids are usually composed of poorly coordinating ions, so they can provide a highly polar non-coordinating environment (Welton 1999). Unlike either the polar solvents such as acetonitrile that usually coordinate to the metal centre of catalysts thus blocking the active site, or the non-polar non-coordinating solvents like hexane that cannot dissolve the catalysts, this unique feature provides the possibility of biphasic reactions, in which the catalyst is dissolved in the ionic liquid, however the ionic liquid is immiscible with the reagents and products (Bates *et al.* 2002; Cull *et al.* 2000). Therefore, it becomes easy to recover the products and reuse the solvent and catalyst.

But the most attractive characteristic of ionic liquids is their tuneable properties, for which they are also referred to as "designer solvents" (Freemantle 1998). According to their structures, ionic liquids come into two main categories: the simple salts (made of single anion and cation) and the binary ionic liquids (salts where an equilibrium is involved). The properties of both types greatly depend upon the chemical structures. For instance, the change of cations generally has a profound effect on the physical properties such as melting point, density and viscosity, while changes of anions will dramatically affect the chemical behaviour and stability of the ionic liquids (Seddon 2002). Hence ionic liquids can be customised by changing the nature of the anion and cation to suit the requirement of a particular process (Earle and Seddon 2000).

One typical example of the tuneable properties of ionic liquids is the melting point. The melting points of simple ionic liquids are usually a function of the length of alkyl chain. For example, if the ethyl group is exchanged for a generic linear alkyl function,

R (where $R = C_n H_{2n+1}; n \in I[1,18]$), a series of cations is then generated, so the properties of the ionic liquids change. Figure 2-11 illustrates the significant variation in melting points by this simple change for [Rmim][PF$_6$] and [Rmim][BF$_4$] (Holbery and Seddon 1999).

But for binary ionic liquids, such as mixtures of aluminium(III) chloride and 1,3-dialkylimidazolium chloride, the melting point behaviour is more complicated as a result of the presence of several different ionic species. It depends upon the mole fraction of the aluminium(III) chloride and 1,3-dialkylimidazolium chloride present(Hussey et al. 1986), as given in Figure 2-12 (Fannin et al. 1984). By carefully selecting the cation and anion and hence changing the melting points, the liquid range of ionic liquids can then be expanded enormously over a range as wide as 300°C (from −100°C to 200°C), in comparison with other common solvents, e.g. 100°C (from 0°C to 100°C) for water and 44°C (from −77.7°C to −33.3°C) for ammonia (Seddon 1997).
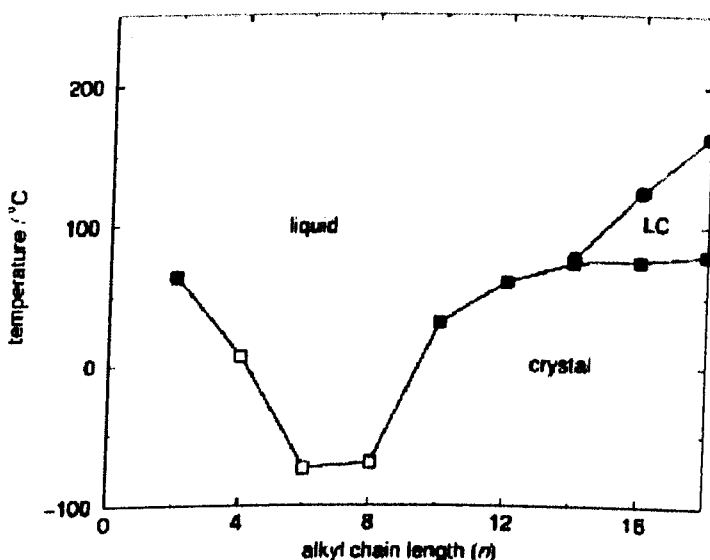
a) Melting point phase diagram of [Rmim][PF$_6$] as a function of alkyl chain length n
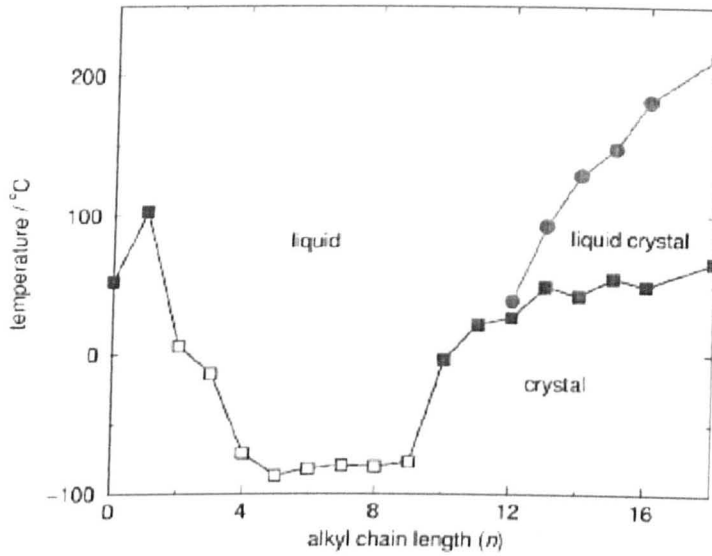
b) Melting point phase diagram of [Rmim][BF₄] as a function of alkyl chain length *n*

Fig.2-11 Melting Point Phase Diagram of Simple Ionic Liquid

(Holbery and Seddon 1999)

(showing the melting transitions from crystalline (closed square) and glassy (open square) materials and the clearing transition (closed circle) of the liquid crystalline (LC) terms.
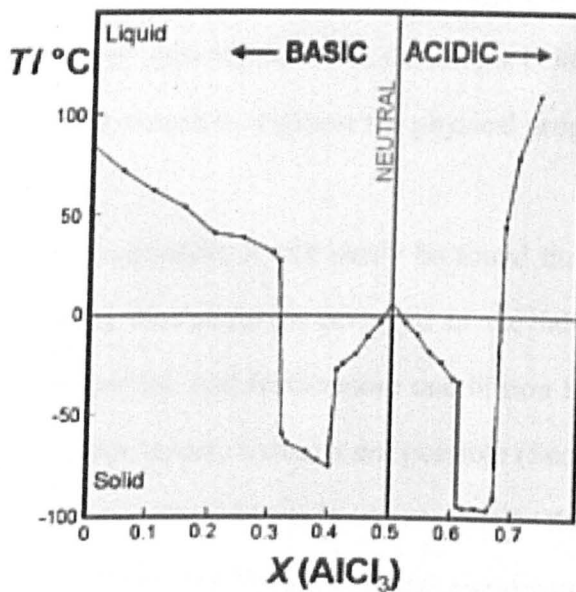

Fig.2-12 Experimental Phase Diagram for [emim]Cl-AlCl3 System (Fannin et al. 1984)

The miscibility with water changes with the structure as well. It has been proved that both the anion and cation group of ionic liquids have an effect on the miscibility (Swatloski et al. 2002). For instance, [Rmim][BF$_4$] (1-alkyl-3-methylimidazolium tetrafluoroborate) is miscible with water at 25°C when the alkyl chain length is less than 6, while at or above 6 carbon atoms, they form a separate phase when mixed with water (Earle and Seddon 2000; Swatloski et al. 2002). Moreover, [bmim][PF$_6$] is immiscible with water, whilst, [bmim][BF$_4$] is water-soluble (Davis and Fox 2003). This behaviour can be of substantial benefit when carrying out solvent extraction or production separation, as the solubility of the ionic liquids can be adjusted as required.

Just like their solubility, both physical and chemical properties of ionic liquids can be tailored, by either modifying the chain length of the alkyl substituents in the cation or by using different anions. Therefore, for every chemical reaction of interest, it is possible to generate an ionic liquid as the solvent to suit the required combination of reactivity, solubility, viscosity etc. The ions that constitute ionic liquids have been said to resemble colours on an artist's palette (as shown in Figure 2-13), which may then be used to create a vast range of ionic liquids, with the anions being chosen to control the chemistry, the cations being chosen to engineer the physical properties (Seddon 2002).

With a small amount of imagination, it will easily be found that there are as many as one million simple systems that could be prepared in the laboratory with different physical and chemical properties, and furthermore one billion binary combinations of these and one trillion possible ternary systems are possible (Seddon 2002). In contrast with the limited range of molecular solvents in use nowadays, the adjustable properties provide ionic liquids with flexibility of function and significant advantages for their industrial application in green chemistry.
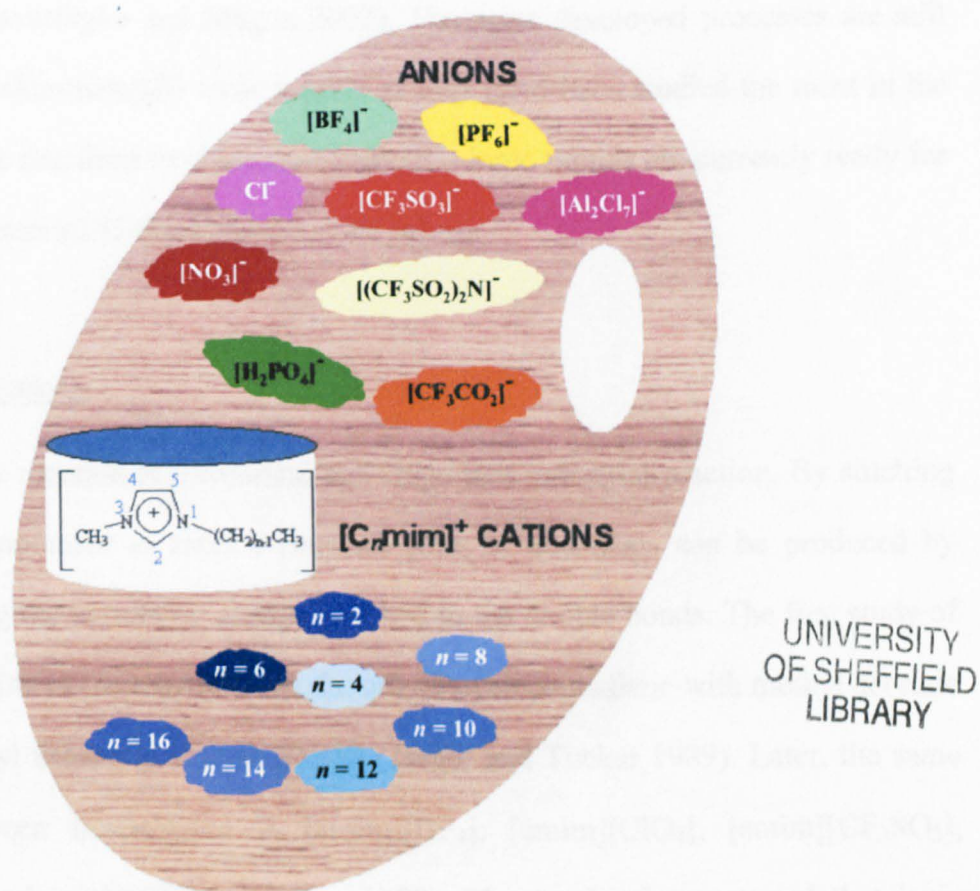
ANIONS

$[BF_4]^-$

$[PF_6]^-$

Cl^- $[CF_3SO_3]^-$ $[Al_2Cl_7]^-$

$[NO_3]^-$ $[(CF_3SO_2)_2N]^-$

$[H_2PO_4]^-$ $[CF_3CO_2]^-$

$[C_nmim]^+$ **CATIONS**

$n = 2$

$n = 6$ $n = 4$ $n = 8$

$n = 16$ $n = 10$

$n = 14$ $n = 12$

Fig.2-13 The Artist's Palette of Anions and Cations (Torres 2001)

2.4.4 Applications of Ionic Liquids

Although the application of tetraalkylammonium salts of $[SnCl_3]^-$ and $[GeCl_3]^-$ anions as catalytic solvents with dissolved $PtCl_2$ for the hydrogenation, isomerization, hydroformylation and carboalkoxylation of olefins was reported as early as 1972 (Parshall 1972), it is not until the late 1990s that ionic liquids have been considered and studied as candidate clean solvents.

A wide range of reactions has been undertaken using ionic liquids as solvents in the laboratory, including Diels-Alder reactions, Heck coupling reactions, hydrogenation

and hydroformylation of olefins, Friedel-Crafts alkylation and acylation reactions and so on (Olivier-Bourbigou and Magna 2002). The most developed processes are still based on chloroaluminate(III) ionic liquids as they have been studied the most in the past years. Some reactions in chloroaluminate(III) ionic liquids are currently ready for industry (e.g. Dimersol/Difasol process, vide infra).
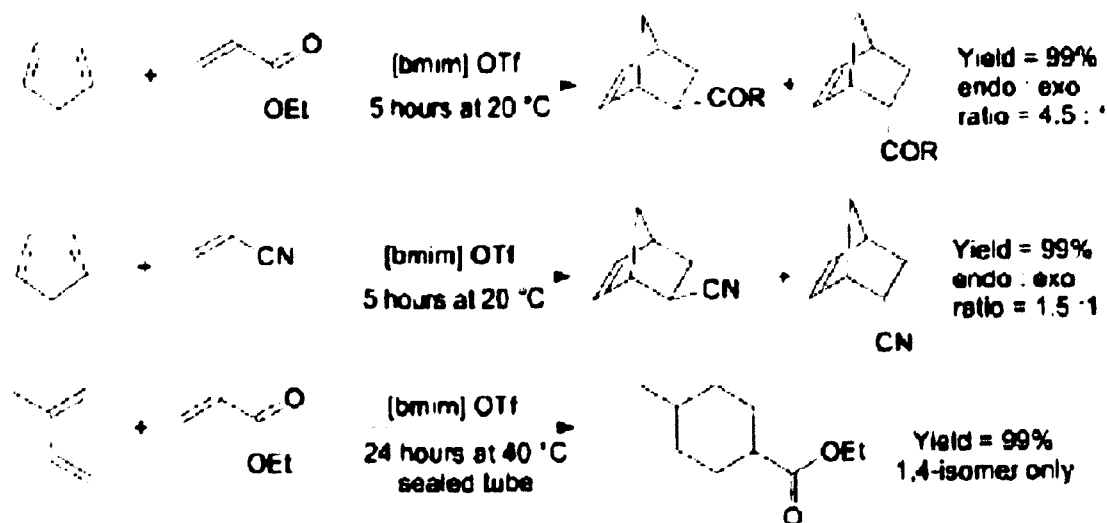
Diels-Alder reactions

The Diels-Alder reaction is a common and important industrial reaction. By stitching two carbon compounds to form a ring, all sorts of chemicals can be produced by simply changing the peripheral groups attached to the double bonds. The first study of using ionic liquids in the reaction was the one of cyclopentadiene with methyl acrylate and methyl vinyl ketone in [EtNH$_3$][NO$_3$] (Jaeger and Tucker 1989). Later, the same reaction has been investigated in [emim][BF$_4$], [emim][ClO$_4$], [emim][CF$_3$SO$_3$], [emim][NO$_3$] and [emim][PF$_6$] (Welton 1999). The results demonstrated that ionic liquids are effective solvents for Diels-Alder reactions (Earle et al. 1999; Fischer et al. 1999) and significant enhancement could be found in both yields and selectivity (as shown in Figure 2-14), over the results with conventional solvents. Also, using ionic liquids made the separation of products easier and the reaction less sensitive to impurities such as water (Bradley 1999).

Heck reactions

Heck reactions are widely used in the pharmaceutical and fine chemical industry. They involve the formation of a new C-C bond in aromatic and vinylic systems. Alkylammonium and phosphonium ionic liquids have been used as solvent with dichloro-bis (triphenylphosphine) palladium(II) and palladium(II) acetate as the catalyst precursors (Kaufmann et al. 1996). By using ionic liquids, no excess of PPh3 is required (as in conventional solvents) for the purpose of stabilising the palladium

catalyst. The products can be removed from the solution by distillation and high

conversion rates are also observed (Holbery and Seddon 1999).

Fig. 2-14 Application of Ionic Liquids in Diels-Alder Reaction

(Holbery and Seddon 1999)

Hydrogenation and hydroformylation reactions

Hydrogenation of olefins catalysed by transition metal complexes has been reported

using rhodium- (Suarez et al. 1996), ruthenium- and cobalt-containing catalysts

(Suarez et al. 1997) dissolved in ionic liquids. The reaction rates have been found to be

up to five times higher than the comparable reactions in propanone or analogous

biphasic aqueous-organic systems. For example, pentene has been hydrogenated using

rhodium catalyst [Rh(norbornadiene)(PPh$_3$)$_2$][PF$_6$] in ionic liquids containing [BF$_4$]$^-$,

[PF$_6$]$^-$, [SbF$_6$]$^-$, and [CuCl$_2$]$^-$ anions, and the best result obtained came from the [SbF$_6$]$^-$

ionic liquid.

Hydroformylation of pent-1-ene has been investigated with rhodium catalysts in

[bmim][PF$_6$], showing high catalytic activity, and again the products separate as a

second organic phase. But it was also noted that small part of the catalysts leached into the organic phase (Fuller et al. 1997). Sulphonated triphenylphosphine derivatives were also used as the phosphine, however, this led to the reduction in the reaction rate (Chauvin et al. 1995; Chauvin et al. 1999).

Friedel-Crafts chemistry

Friedel-Crafts acylation and alkylation are of great commercial importance. Typically, these reactions are carried out in an inert solvent with suspended or dissolved aluminium (III) chloride as a catalyst and the process may take six hours and go only to 80% completion to give a mixture of isomeric products. However, with ionic liquids, the results are quite different. Both alkylation and acylation reactions have been investigated under Friedel-Crafts conditions using chloroaluminate(III) ionic liquids as solvents and catalysts (Boon et al. 1987; Earle et al. 1998). Reaction rates are much greater with total reagent conversion, and often with surprising specificity to a single product.

For example, benzene can be alkylated with chloromethane in an acidic ionic liquid, giving a mixture of mono- to hexa- substituted products. In this case, the ionic liquid solvent/catalyst activates the reaction and the alkylation can be carried out at a temperature as low as -20°C. The products are easily separated, as the solubility is low in the ionic liquid. Hydrogensulphate and tetrakis(hydrogensulphato)borate ionic liquid have also been used as additives to sulphuric acid in the Friedel-Crafts alkylation of benzene with 1-decene. The result showed that a low amounts of ionic liquid additive results in a dramatic improvement of product yield (Wasserscheid et al. 2002). Friedel-Crafts acylation of benzene can be promoted by acidic chloroaluminate ionic liquids (Boon et al. 1986). The products of these reactions show high selectivities to a single isomer, for example, toluene, chlorobenzene and anisole are acylated in the

4-position with 98% specificity. However, the greatest problem of Friedel-Crafts acylation still exists when reactions are carried out in ionic liquids, that is, the misnamed "catalytic" process is in fact stoicheometric, which consumes 1 mole of $AlCl_3$ per mole of reactant (Holbery and Seddon 1999).

The Dimersol/Difasol process

The Dimersol process is an important process for the industrial dimerisation of alkenes, typically propene and butenes, to the more valuable branched hexenes and octenes. The long-chain olefins produced in the dimerisation process are usually hydroformylated to alcohols for use in the manufacture of plasticisers. Developed by the IFP (the Institut Français du Pétrole), the dimerisation process is commonly operated solvent-free with an active catalyst (a cationic nickel complex of the general form $[LNiCH_2R'][AlCl_4]$ in which $L=PR_3$). But the catalyst has been found to be soluble in aromatic and halogenated hydrocarbon solvents and be more active in solution. The major problem for the process is the separation of products from the catalyst, and this leads to increased operational costs and environmental impact. Chauvin and co-workers found that the chloroaluminate ionic liquids would be a good solvent for the nickel catalyst. By using a ternary ionic liquid system $[bmim]Cl^-AlCl_3^-$ $EtAlCl_2$, it is possible to form an active catalyst system and more importantly, stabilize the catalyst (Chauvin et al. 1990). The Dimersol reaction can then be performed with the ionic liquid catalyst as a two-phase liquid-liquid process at atmospheric pressure at $-15\sim5°C$ (Einloft et al. 1996). The products are not soluble in the ionic liquids and form a second layer that is a less dense phase and can be easily separated. The catalyst remains selectively dissolved in the ionic liquid, which permits simple extraction of products. The key benefits from using the ionic liquid solvent are the higher activity of catalyst than that ever found in both solvent-free and conventional solvent systems, the better selectivity to desirable dimers, and the efficient recycling of the liquid catalyst

process (Holbery and Seddon 1999). The Difasol system can be retro-fitted into existing Dimersol plants, improving yields while lowering catalyst consumptions and associated cost.

Ionic liquids are also used in other aspects, such as (Freemantle 1998):

- *Reprocessing nuclear waste:* the British Nuclear Fuels(BNFL) is carrying out extensive research into dissolving the spent nuclear fuels in ionic liquids, by adding an oxidant to the ionic liquids, thus transforming the insoluble uranium(IV) and plutonium(IV) into uranium(VI) and plutonium(VI) respectively.

- *Dissolution of heavy oil:* it is found that the ionic liquids can break down the high molecular weight hydrocarbon fraction, producing a solution of oil that is much less viscous therefore more easily to be transported by the pipelines; and the ionic liquids can be recovered and reused after the reaction.

- *Cleaning of contaminated natural gas:* H_2S and CO_2 are usually removed from the contaminated natural gas (sour gas) by an aqueous solution of amine. Problems associated with the traditional methods are the uptake of water and loss of amine into the gas stream. With the advantage of the unmeasurable vapour pressure, new ionic liquids, referred as *task-specific ionic liquids (TSIL)*, have been proposed and studied to capture CO_2 from the sour gas (Bates *et al.* 2002).

However, there are also some problems for the wider application of ionic liquids, one of which is the issue of cost. It is estimated that every gram of ionic liquid currently costs about £5 more than a common organic solvent. This cost could be expected to be reduced by as much as 90%, depending on the compositions of the liquid as well as its production (Renner 2001).

The biggest problem for the application of ionic liquids is still related to the environment. Although ionic liquids themselves are considered as environmentally benign solvents, they are mostly made from volatile organic compounds (VOCs). Moreover they are recycled or cleaned by washing with water or VOCs. The potential pollution that might be caused during the process of preparing and recycling ionic liquids has come to the attention of chemists. Besides, the most recent research on ionic liquids reveals that they may have toxic effects in the aquatic environment and cause a detrimental effects on fish depending on their chemical structure (Pretti et al. 2006). As most ionic liquids are water soluble, this will become a significant concern for their wider application.

2.5 CONCLUSION

As reviewed above, the literature reveals that the customizing properties of ionic liquids make them appealing for use as solvents in chemical reactions. But before wide application takes place, the greatest concern of most chemists is how the ionic liquids as solvents will influence the reaction kinetics. Hence detailed information is required on the effect of using ionic liquids in different chemical reactions and to study parameters such as reaction rate, conversion and yield. This is in fact very difficult work. The vast diversity of ionic liquids, in combination with a range of reaction conditions such as temperatures, residence times and stoichiometries leads to the dilemma of how accurately to measure and thus to optimise the multi-variable system in the shortest possible time. Conventional technology is obviously not suitable for this aim because it is not only a tedious but also an impossibly time consuming task for manual operation. However, micro-reactors meet well the requirement for the study of effect of ionic liquids on reaction kinetics and allow the production of large quantities of data in short time. Therefore, the need for the project has been established, that is, to design a microreactor or a microreactor system for the kinetic study of chemical

reactions using ionic liquids as solvents. In addition to the previously reported applications in the study of chemical processes and screening of catalysts mostly in the bio-chemical field, the approach seems promising to achieve the goal of measuring the reaction kinetics in ionic liquids rapidly, automatically and accurately, to enable a much wider industrial application of them as a replacement for VOC solvents.

To measure the kinetics of chemical reactions with microreactors, the mixing process is of high importance. It involves not only producing well-mixed reactants for the reaction, but also quenching the reaction by mixing the reaction mixture with diluent. Since the reaction occurs or stops concomitantly with the mixing process, it is quite hard to distinguish the actual reaction period from the total residence time that the fluid flows through the micro-mixer and microreactor. Therefore, the more rapid and effective the mixing process is, the less the error between the above two time scales becomes. In other words, the rapidity of the mixing of the species determines the accuracy of the measurement of the reaction time, and thus that of the reaction rate. This is of particular importance when the reaction time (or the residence time of the reactants in the microreactors) approaches zero.

As the result, the tasks of the research "Automated measurement of the kinetics of chemical reactions in ionic liquids" lie in two aspects.

One is the mixing of ionic liquids on the chip. Since ionic liquids are much more viscous than normal aqueous solutions (for example, the viscosity of Emim[NTf$_2$] is about 40 times that of water at ambient temperature) and since their diffusivities can be as low as $1/100$ of that of water, the fluid flow of ionic liquids is limited within very low Reynolds number regime, and the diffusion between molecules becomes much slower. As a consequence, the mixing process in ionic liquids is even more difficult than in more usual liquid phases. Therefore, in order to achieve efficient and effective

mixing results, finding and designing an appropriate micro-mixer is of high priority in the research.

The other is the automation of the measurement process. In order to achieve a fast response of the system, the time scale of each operation in the measurement aims to be controlled in the order of milliseconds. This is not possible using manual method. However, with the help of computer control and fast response microchannel reactors, this not only becomes possible, but also can be carried out at high accuracy. Hence, the second target of the research is to design and assemble a microreactor system, which can make the chemical reaction occur on-chip, sample the reaction product and analyse the reaction sample automatically. Of course, it must also include the development of proper controls over the whole system in order to achieve good performance of the system.

Chapter 3

PRESSURE-DRIVEN FLOW IN MICROCHANNELS

3.1 INTRODUCTION

To design a microreactor system for the automated kinetics measurement of chemical reactions in ionic liquids, CFD computation and microchannel network analysis have been used as the main approaches. Of these two methods, CFD computations help to understand the fluid flow and mixing process in microchannels, and hence to design the geometric structure of the microreactor, whilst microchannel network analysis helps to decide the operating parameters of the system. The equations involved include the flow equations and species equations used in CFD computations, as well equation groups for the network analysis. To solve the equations, some assumptions have to be made to simplify the problem. The most important one is that the fluid flow of interest in the microchannels is in developed laminar flow regime. As a result, only steady flow equations are involved in the CFD computations, and the developed flow theory is applied through the entire length of the uniform segment of the channel network. This is no doubt a simplification, and it would definitely result in some errors. Later CFD computations, however, show that the error depends on the Reynolds number of the fluid flow. At a low Reynolds number, typically when $Re \leq 10$, the error is negligible because the entrance effect in the microchannels is minor due to the small characteristic dimensions compared to the channel length. However, when the

Reynolds number becomes higher, the entrance effect must be taken into account, and corrections must be made in order to reduce the errors.

As the theoretical basis of the thesis, this chapter gives the equations used in the CFD computations and the microchannel network analysis. But prior to the introduction of the equations, the theory of developed pressure-driven flow will be first described. Based on the assumption that the developed flow theory is applied to the entire channel, equations that govern the fluid flow and species mixing are then put forward, starting from their general forms, and then reduced and normalised to non-dimensional forms. Detailed introduction is also made to the analysis method for control and modelling of fluid flow in the channel network. At the end of the chapter, the relation of Reynolds number to the entrance effect is discussed, combining with computational results in different Reynolds number regimes, and formula to calculate the pressure drop of fluid flow in microchannels is obtained by solving the momentum equation based on the restriction to low Reynolds number.

3.2 DEVELOPED FLOW THEORY

The term "developed flow" applied to laminar flow means a steady state in which the velocity becomes purely axial ($u = u(y, z)$) and the flow profile does not change along the flow direction (White 2006).

For any flow in a passage of an arbitrary but constant shape, it takes some time for the flow to develop fully. The length of this time depends on the flow pattern, or in other words, the Reynolds number. The process by which the fluid flow reaches steady state is usually called the developing process, and the distance that the fluid passes during the process is called the entrance length.

A good example used to illustrate the developing process of laminar flow is that in a cylindrical pipe, as given Figure 3-1. It is well known that the major characteristic of developed Poiseuille flow is its parabolic velocity distribution. However, as shown in the figure, when fluid enters the pipe, it does not immediately achieve the typical parabolic velocity profile along the diameter. Instead, a thin boundary layer is formed near the wall. In the boundary layer, the fluid flow is retarded and the velocity drops quickly to zero at the solid boundary. As the fluid flows, the boundary layer grows in depth along the flow direction. When the boundary layer finally meets and the core disappears at the stream centre, the steady state of fluid flow is established. More importantly, the flow pattern remains the same downstream unless changes occur in either the geometry of the passage or in the flow conditions. The fluid flow in this steady state is called "fully developed flow".
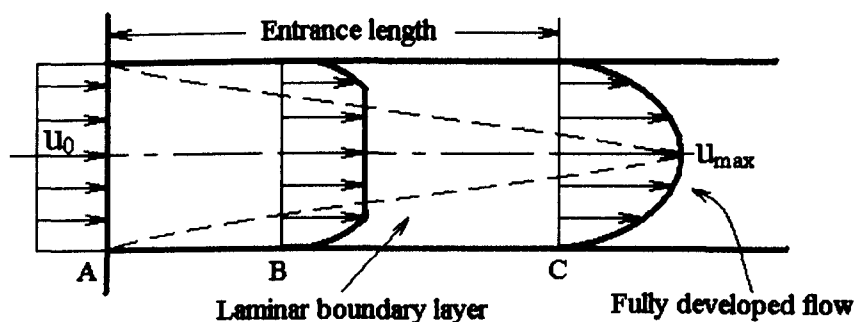
Fig.3-1 Development of Laminar Flow in a Cylindrical Pipe (White 2006)

The "fully developed flow " is an important state for the study of fluid flow, because it makes things much simpler. This is particularly remarkable under the conditions of fully developed laminar flow. Since the developed laminar flow is characterised by zero transverse components of velocity and uniform gradient of pressure in the x direction, i.e.

$$v = w = 0 \text{ and } p = f(x) \tag{3-1}$$

not only can the time dependent terms be crossed out from the governing equations due to the unchanged flow pattern, but also equations can be greatly reduced thus analytical solutions can possibly be obtained. Therefore, as detailed information about the developing process in microchannels is of no particular interest to the current research, attention has been mainly focused on developed laminar flow in the microreactor, in order to simplify the problem.

One thing that needs to be noted is that, in theory, the fully developed state of fluid flow can be reached only after an infinite distance. But in practice, the "entrance length" is artificially defined, and the flow is considered close enough to the fully developed state after the "entrance length". A convenient definition for this practical entrance length, L_{in}, is the distance from the inlet along the flow passage to the point where the velocity at the centreline is equal to 0.99 times its fully developed value (Shah and London 1978), i.e.:

$$u_{L_{in}} = 0.99 u_{Dev} \qquad\qquad (3\text{-}2)$$

3.3 GOVERNING EQUATIONS OF PRESSURE-DRIVEN FLOW

The equations presented here for pressure-driven flow include the flow equations and the species equations. These equations form the basis for the CFD computations to understand and predict the mass transfer and mixing process in microchannels.

3.3.1 Flow Equations

The equations governing the fluid flow include the momentum equation and the continuity equation.

As the motion of fluid flow obeys Newton's second law, the general form of the momentum equation in fluid mechanics is:

$$\frac{D\rho u}{Dt} = -\nabla p + \nabla \cdot (\mu \nabla u) + F \qquad (3\text{-}3)$$

in which the variable F_i in the equation is the force term that enables the introduction of either gravity or electric fields into the equation. The density and viscosity in the momentum equation are normally treated as uniform, but they can also be solved from the species and energy equation if required. As the only variable left unknown, the pressure is then constrained by the continuity equation as:

$$\frac{\partial \rho}{\partial t} + \nabla \cdot (\rho u) = 0 \qquad (3\text{-}4)$$

These equations can then be reduced under different conditions. Specifically, the reductions made in the current research on the governing equations of fluid flow include:

1) The time dependent terms can be neglected because only steady state fluid flow is of interest in the research.

2) The force term is also left out as no external force is applied on the fluid system.

3) In some cases, the density is regarded as uniform. As there are often two fluids, the reagents and the diluent, involved in the flow system, the assumption of constant density has to be made according to the flow situations conceived. For the reagent solutions, since chemicals are dissolved at low concentration in the same solvent, the densities of solutions greatly depends on that of the solvent, hence this reduction results in an excellent approximation. For the reagents mixing with the diluent, density difference must be taken into account until the two fluids are well mixed. Once the

complete mixing is achieved, the assumption of uniform density will be appropriate again, thus giving a good simplification.

Based on the reduction described above, the governing equations used in the research are:

Continuity: $\nabla \cdot u = 0$ (3-5)

Momentum: $\rho u \cdot \nabla u = -\nabla p + \mu \nabla^2 u$ (3-6)

3.3.2 Species Equations

The general form of transport equation for species k including chemical reaction is:

$$\frac{\partial \rho Y_k}{\partial t} + u \cdot \nabla(\rho Y_k) = \nabla \cdot (\rho \mathcal{D} \nabla Y_k) + r_k \qquad (3-7)$$

in which, the change rate of species k along a streamline is equal to the combined rate of molecular diffusion and reaction.

Similarly, simplifications have also been made according to the conditions of interest of the research. Firstly, the density and diffusivity are again considered uniform in the fluid except for those cases where the detailed mixing process of reagents and diluent is occasionally studied. Secondly, the chemical reaction term is ignored because no reaction is involved in species mixing situations. Hence, the species equation has been reduced in the form of Eq.(3-8), in which the diffusivity becomes the key factor in the mass transfer process of species k in the fully developed fluid flow.

$$u \cdot \nabla Y_k = \mathcal{D} \nabla^2 Y_k \qquad (3-8)$$

3.3.3 Non-dimensional Form of Governing Equations

The non-dimensional forms of flow and species equations are important for both CFD computation and results analysis, because the characters of the equations have been clarified by normalising all variables to be of order unity. Thus information about the flow and mixing process of interest in microchannels becomes more straightforward and clear.

The normalisation of variables usually uses the reference scale ρ_0, u_0, and $\hat{L}_0$ for density, velocity and length in flow equations, and Y_k for mass fraction of species k in species equations. Then non-dimensional variables are defined as:

$$\rho^* = \frac{\rho}{\rho_0}, \mu^* = \frac{\mu}{\mu_0}, \ x^* = \frac{x}{\hat{L}_0}, \ u^* = \frac{u}{u_0}, \ p^* = \frac{p}{\rho_0 u_0^2}, \ Y_k^* = \frac{Y_k}{Y_0} \qquad (3\text{-}9)$$

In terms of these non-dimensional variables, the equations for fully developed flow can be reduced to:

Continuity: $\nabla \cdot u^* = 0$ \qquad\qquad\qquad\qquad\qquad\qquad\qquad\qquad (3-10)

Momentum: $u^* \cdot \nabla u^* = -\nabla p^* + \frac{1}{Re} \nabla^2 u^*$ \qquad\qquad\qquad (3-11)

Species: $u^* \cdot \nabla Y_k^* = \frac{1}{Re\,Sc} \nabla^2 Y_k^*$ \qquad\qquad\qquad\qquad (3-12)

Two dimensionless parameters then emerge during the process of normalisation. The Reynolds number, arising from the momentum equation (as defined in (3-13)), is the primary parameter that controls the flow pattern, while the Schmidt number from the species equation relates the viscous diffusion with the molecular diffusion, as defined in (3-14).

$$Re = \frac{\rho_0 u_0 \hat{L}_0}{\mu_0} \qquad (3\text{-}13)$$

$$Sc = \frac{\mu_0}{\rho_0 \mathcal{D}_0} \qquad (3\text{-}14)$$

But more often, another dimensionless parameter is used in describing the mixing process in flows, namely the Peclet number. As the product of Re and Sc (see (3-15)), the Peclet number represents the molecular diffusion of species in relation to the fluid convection.

$$Pe = Re\,Sc = \frac{u_0 \hat{L}_0}{\mathcal{D}_0} \qquad (3\text{-}15)$$

The other non-dimensional form of the momentum equation is given in (3-16), in which the pressure is normalised by the viscous stress scale as in (3-17):

$$Re\,u^* \cdot \nabla u^* = -\nabla p^* + \nabla^2 u^* \qquad (3\text{-}16)$$

$$p^* = \frac{p}{\mu u_0 / \hat{L}_0} \qquad (3\text{-}17)$$

The above form is more usual at low Reynolds number as it highlights the diminishing of convection term in the equation, therefore equation (3-16) can be further simplified when $Re \rightarrow 0$ as:

$$\nabla p^* = \nabla^2 u^* \qquad (3\text{-}18)$$

Comparatively, Eq (3-11) is used more often in the CFD computations because it is the default form implemented in the computer code, whilst Eq.(3-18) is more convenient for obtaining an analytical solution for some simple cases. By applying the boundary condition that the velocity and the flux of species at the wall are zero, together with

appropriately selected inlet and outlet conditions for the domain of interest, the fluid flow and mixing process in microchannels are then numerically solved via Equation (3-10) to (3-12).

3.4 EQUATIONS FOR CHANNEL NETWORK ANALYSIS

A network of microchannels can be treated following the techniques used for electrical resistance circuits. This method has been proved an effective tool in designing the experimental rig and determining the operating conditions of flows in microchannels.

The channel network in this method is regarded as a collection of interconnected channel segments (as shown in Figure 3-2). Both channel geometries, i.e. the channel width and depth and fluid properties like density and viscosity are approximated to be uniform in each segment. In addition, two continuity constraints are introduced for each junction and loop in the network, namely:

1) The net mass flow at each junction of the network must be zero, which is called the junction continuity.

2) Pressure changes around any closed loop of the network must sum to zero, known as the loop continuity.

Based on these constraints, two groups of equations can be developed: one is for the mass continuity at each junction, and the other is for the pressure change in each independent loop. Then the equations for all junctions and loops describe the channel network.

For example, for a flow network as illustrated in Figure 3-2, which includes five segments and two junctions, all the equations will be:

a) Equations of junction continuity:

Junction C:

$$Q_1 + Q_2 - Q_3 = 0 \qquad\qquad (3\text{-}19)$$

Junction E:

$$Q_3 + Q_4 - Q_5 = 0 \qquad\qquad (3\text{-}20)$$

b) Equations of loop continuity:

Loop A to F:

$$\Delta p_1 + \Delta p_3 + \Delta p_5 = p_F - p_A \qquad\qquad (3\text{-}21)$$

Loop B to F:

$$\Delta p_2 + \Delta p_3 + \Delta p_5 = p_F - p_B \qquad\qquad (3\text{-}22)$$

Loop D to F:

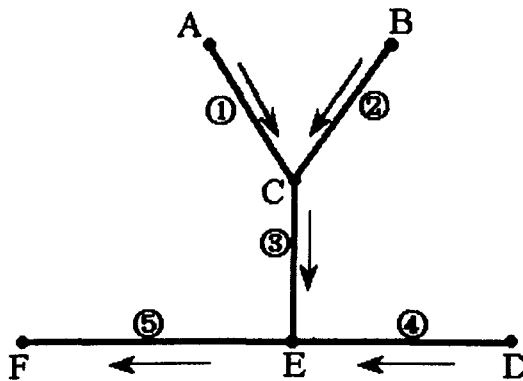$$\Delta p_4 + \Delta p_5 = p_F - p_D \qquad\qquad (3\text{-}23)$$

Fig.3-2 Schematic of Channel Network

These five equations can be solved only for five unknowns. However there are altogether ten variables existing in the equations, that is, five volume flow rates and five pressure drops are for each segment. Hence some other constraints are needed to solve the equations. These constraints are then the relation of pressure drop and

volume flow rate for developed flow in each segment, which can be solved from Eq.(3-6) by making further simplifications.

3.5 PRESSURE DROP OF FLUID FLOW IN MICROCHANNELS

The pressure drop along the flow passage can be solved from the momentum equation, by making further simplifications based on developed flow theory. However, as the fluid flow in the developing process is different from that of the developed stage, the simplifications will result in errors, and the errors will depend on the flow conditions. In cases where a big difference exists between the real situation and the assumption, corrections must be made to reduce the inaccuracy of the results based on the simplifications.

3.5.1 Entrance Length/Bend Length and Reynolds Number

As indicated in Section 3.2, the fluid flow will experience a developing process before it reaches the steady state. This process is referred to as the "entrance effect" when fluid enters the flow passage, and an "entrance length" is used to describe the distance along the flow passage that the fluid flow needs to be fully developed. But actually there also exists a similar process when the flow direction is suddenly changed, during which the fluid flow develops from the chaotic into a steady pattern. For convenience in the following discussions, the process occurring around a bend is to be referred to as the "bend effect", and similarly a "bend length" will be used to describe the distance that the fluid flow takes to be fully developed again in such a situation.

Then, before the pressure drop along microchannels is solved from the momentum equation by making simplifications based on the developed flow theory, studies have been made on how these two developing processes change with Reynolds number, in order to assess the error of applying the developed flow theory throughout the microchannel, as well as to judge the situations as to whether corrections are needed on the pressure drop which is solved from the simplified momentum equation on the basis of the developed flow theory.

CFD computations have been carried out for both the cases of fluid entering the channel and flowing along a 90° bend. By dividing the fluid into flow two categories, i.e., $Re \leq 10$ and $10 < Re \leq Re_C$, computations have been made for each case at $Re = 10$ and $Re = 100$ respectively.

Figure 3-3 gives the geometries used for the CFD computation as well as their dimensions. One thing that needs to be noted is that the dimensions have been normalised by the mask width of the wet etched channel ($l = 1.0$ in Fig.3-4 (a)), in order to better represent a series of channel geometries rather than one. Moreover, the geometry of the microchannel discussed here are what is used in the chip design thereinafter.
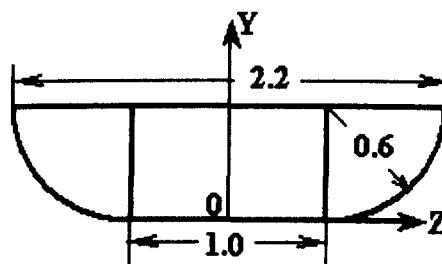
(a) Normalised dimension of channel cross-section in CFD computation
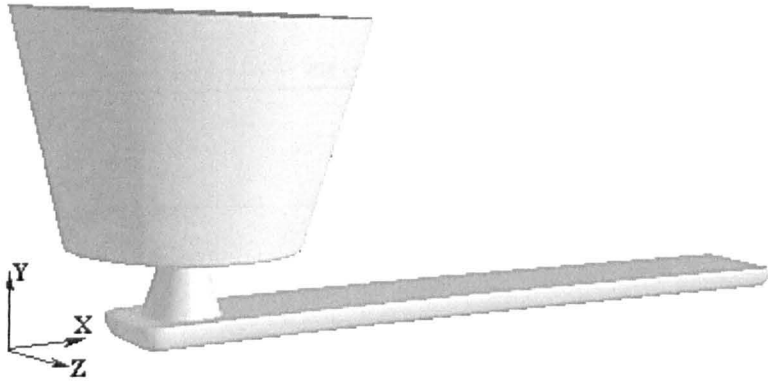
(b) Computational geometry for study of entrance effect
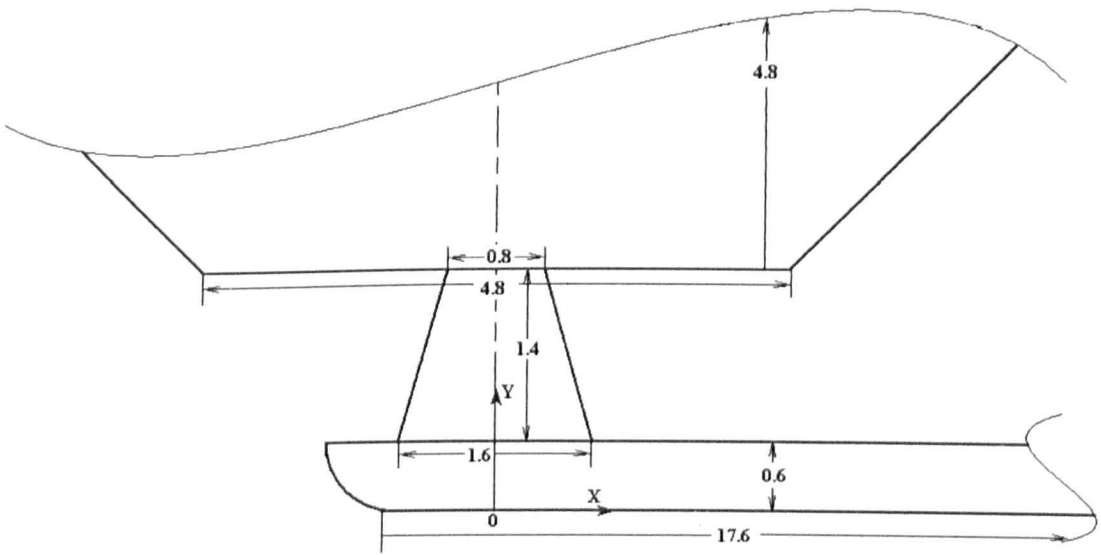
(c) Geometry dimensions for study of entrance effect
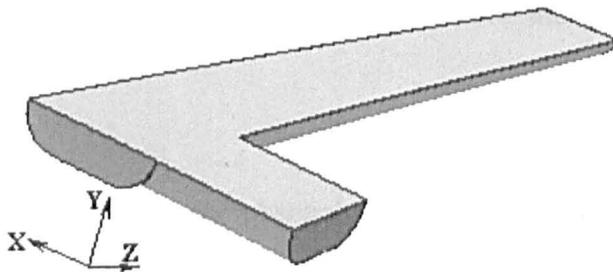
**(d) Computational geometry for study of bend effect**
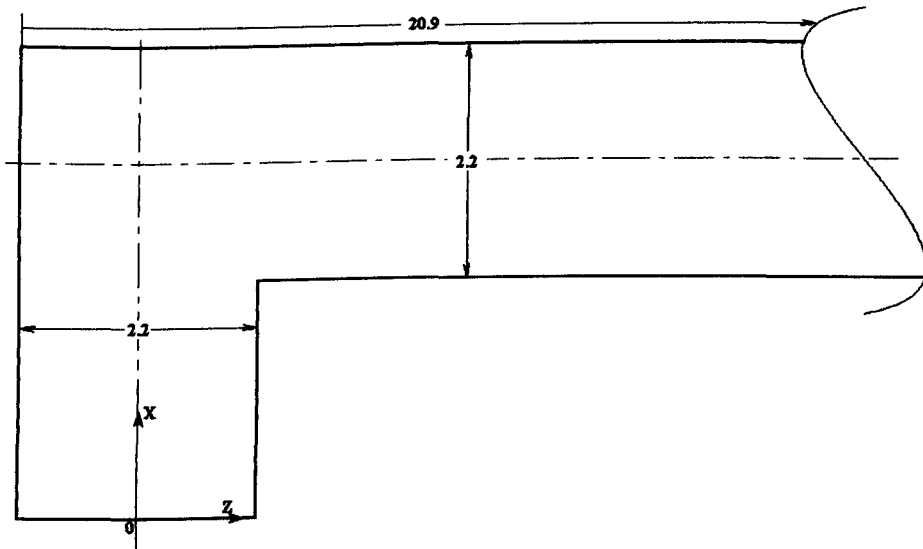
(e) Geometry dimensions for study of bend effect

**Fig.3-3 Geometries and Dimension for CFD Study of Entrance and Bend Effects**

When plotting the results of two cases at different Reynolds numbers, the pressure has been found to exhibit different changes along the flow directions, as illustrated in Figure 3-4. For example, when the Reynolds number is low (Re = 10), as given in Fig.3-4 (a) and (b), for both the cases of fluid entering the channel and flowing around the bend, the pressure drops a little bit faster at the beginning, then falls at the same rate until the end of the channel. When Reynolds number increases to 100, the same trend can be also found in both cases (Fig.3-4 (c) and (d)). However, the changing rate of pressure along the beginning of the channel is much faster than that at low Reynolds number, and the distance it takes for the pressure to fall into the steady changing rate is longer as well.

This behaviour of pressure along the channel is considered to be associated with the developing process of fluid flow. Since the flow pattern within either the entrance length or the bend length is different from that in the steady state, parameters such as
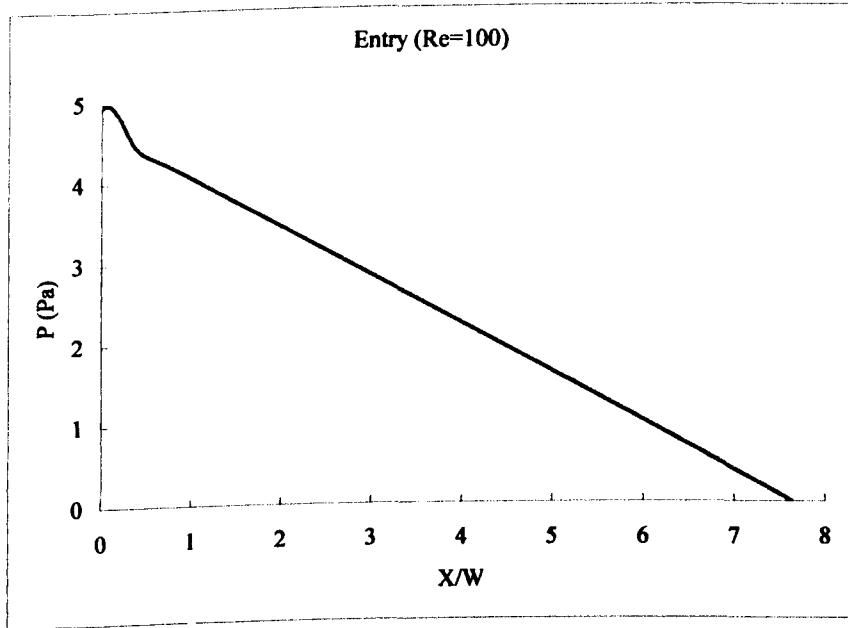
pressure will no doubt change in a rate different from that in the fully developed flow. Moreover, the developing process, thus the entrance length and the bend length seem to increase with the Reynolds number.
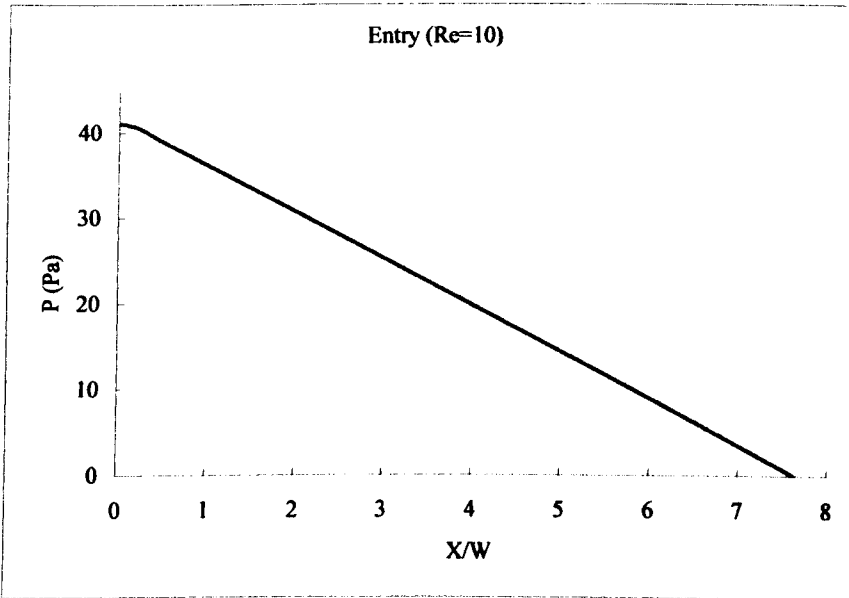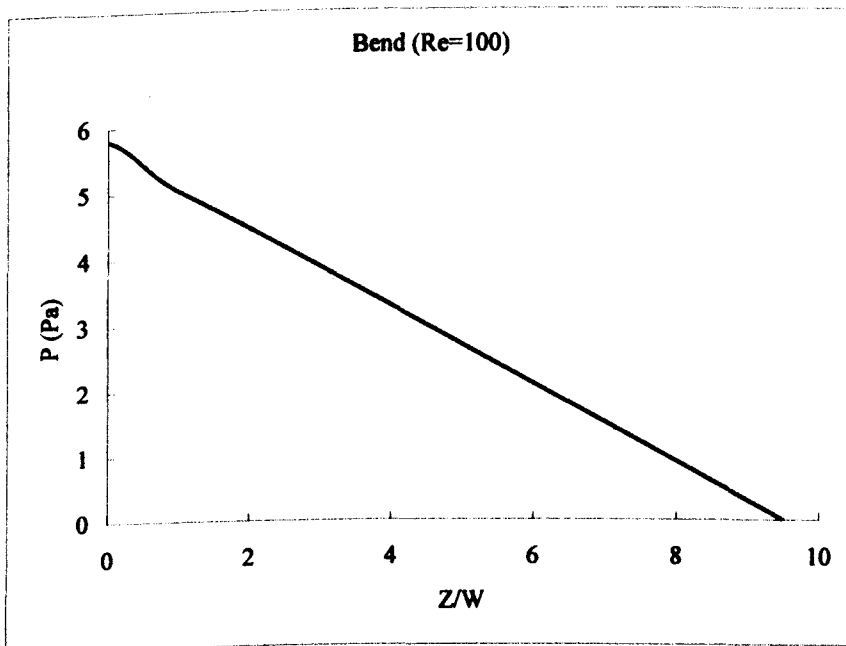

(a)
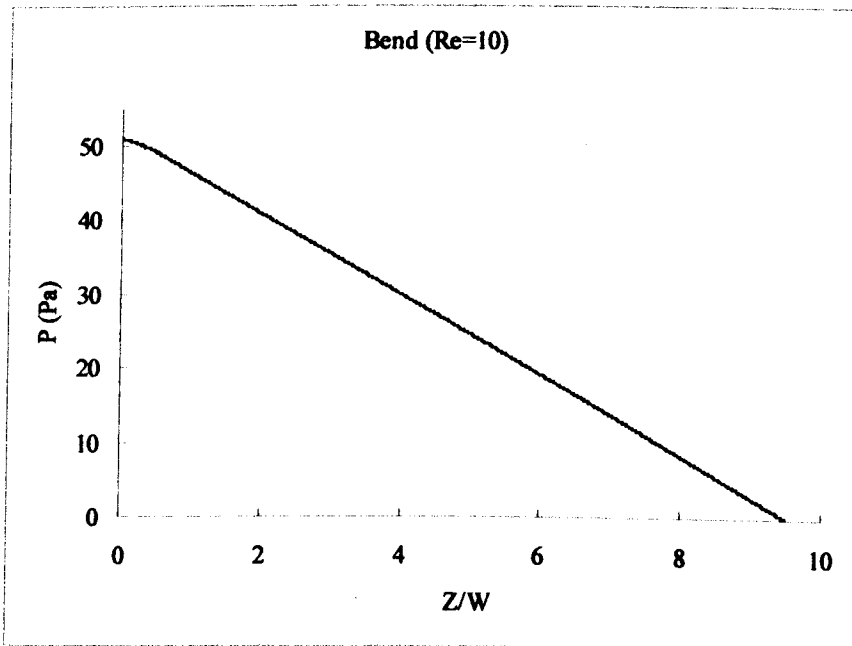
(b)

(c)

(d)

**Figure 3-4 Pressure Drop of Fluid Entering a Channel and**
Turning around a Bend in Microchannel

This point is important because it means when the pressure drop in relation to flow rate in microchannels is solved by the simplification of applying the fully developed flow theory throughout the entire channel, errors will be definitely caused and will be bigger for high Reynolds number flow than in the cases of low Reynolds numbers. Therefore, to remedy the result properly and in time, entrance length and bend length must be worked out for different Reynolds number, so that the errors associated with the simplification made in the microchannel can be assessed and judgements can be made as to whether results need to be corrected.

In the research, the entrance length and bend length are worked out based on the definition given in Section 3.2. Since according to Eq. (3-2), the end of the developing process of fluid flow, which is also the end of the entrance length, is where the velocity at the centreline is equal to 0.99 times its fully developed value, a velocity profile of developed flow is needed as the reference in the study of both the entrance effect and the bend effect. Hence, the velocity at the horizontally central face of the channel has been plotted across the channel width at different positions along the flow direction. By comparing the velocity plots, an unchanged velocity profile can be found at some distance downstream and it is then regarded as the pattern of the fully developed flow. Meanwhile, as the plotting position moves from the beginning of the flow downstream, a point can be determined, which is the first one that the relative deviation between its velocity and the corresponding data point in the reference pattern is less than 1%. Consequently, the distance of the point away from the inlet (the centre of the bend) is the so-called entrance length (the bend length).

Figure 3-5 gives the velocity profile plotted at different positions along the flow direction, by which the reference pattern and the entrance length/bend length have been determined in the way described above (details given in Table 3-1).
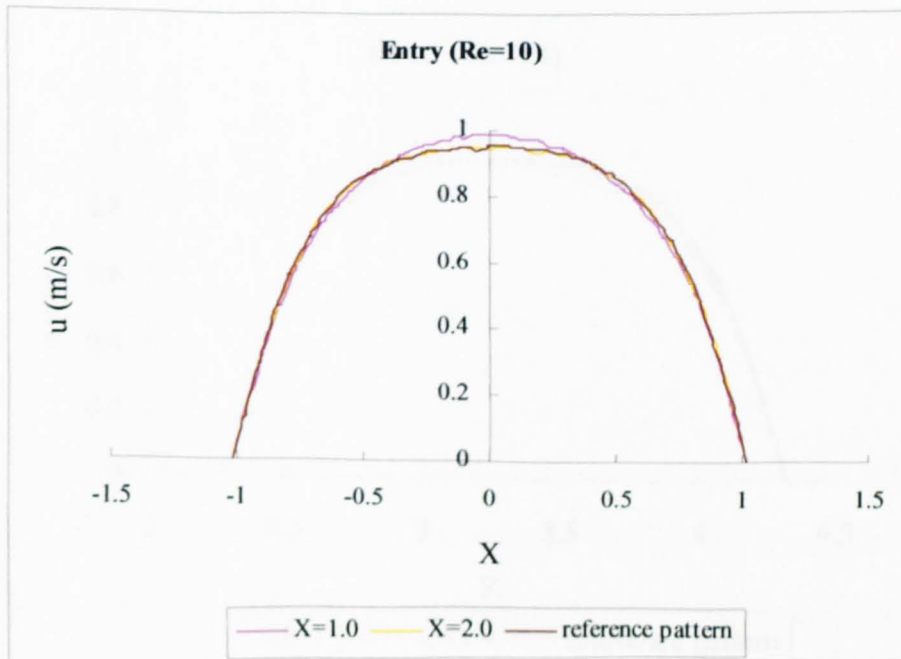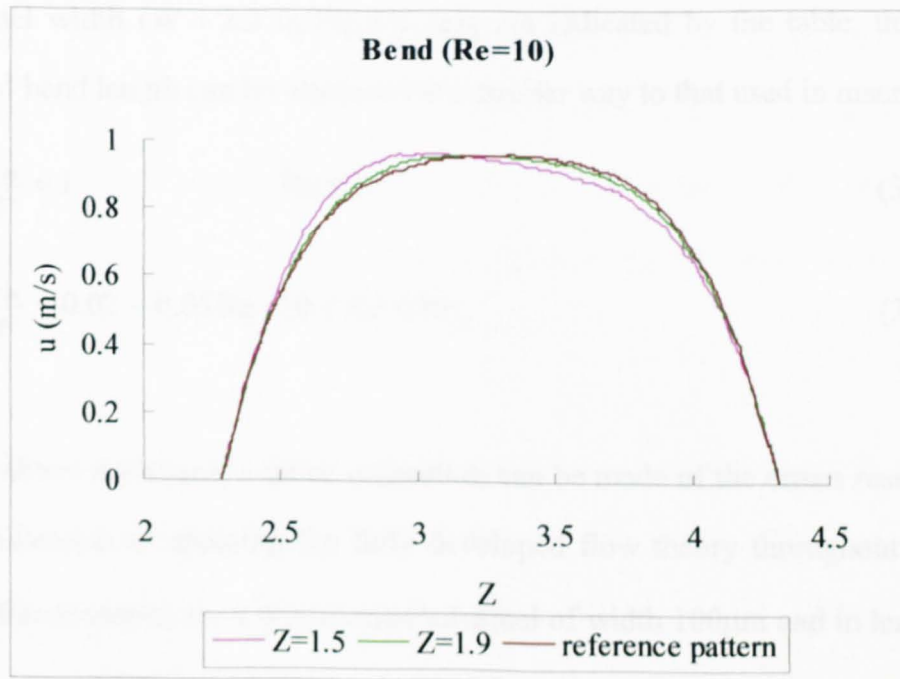
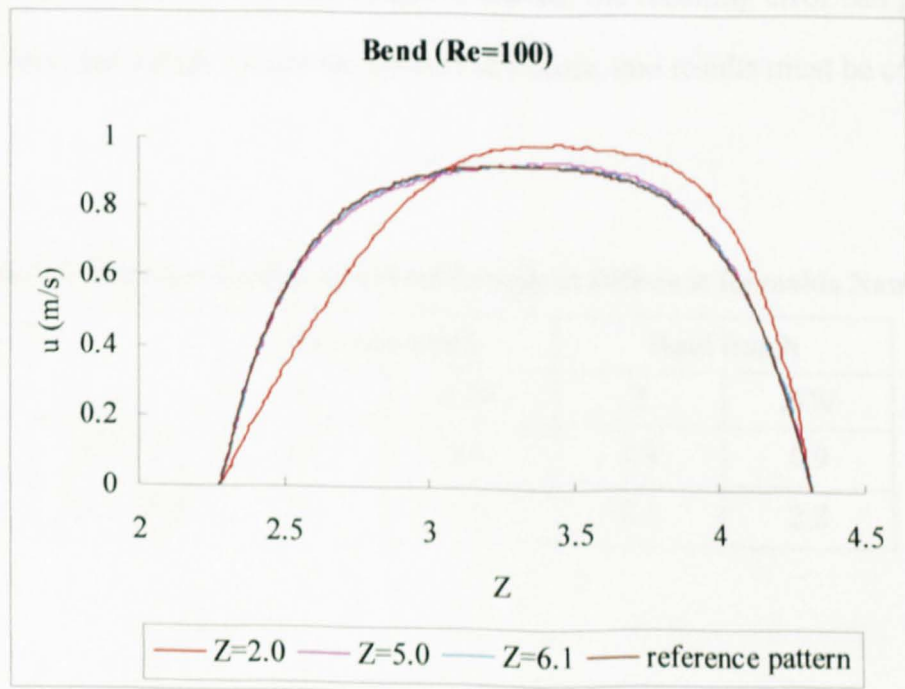**(a) Velocity profile for fluid entering channel at Re=10**
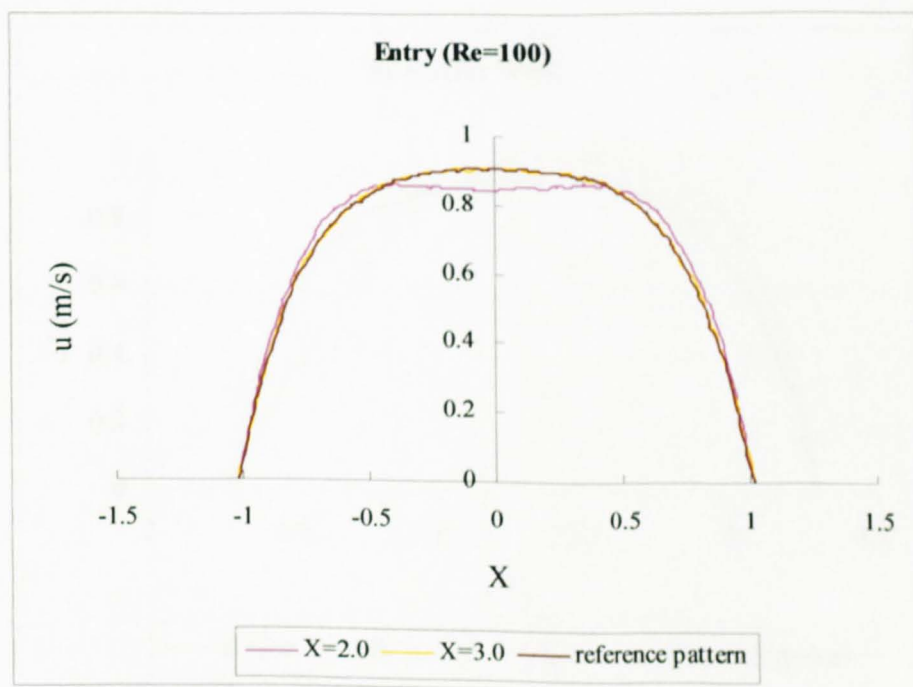
(b) Velocity profile for fluid entering channel at Re=100

(c) Velocity profile for fluid turning round a bend at Re=10

(d) Velocity profile for fluid turning round a bend at Re=100

Figure 3-5 Velocity Profile Plotted to Determine the Entrance Length and Bend Length

Table 3-1 also gives the value of both entrance length and bend length normalised by the channel width ($W = 2.2$ in Fig.3-4 (a)). As indicated by the table, the entrance length and bend length can be estimated in a similar way to that used in macro scale as:

$$\frac{L_{in}}{W} \approx 1 \qquad\qquad \text{Re} \leq 10 \qquad\qquad (3\text{-}24)$$

$$\frac{L_{in}}{W} \approx 0.02 \sim 0.05\,\text{Re} \quad 10 < \text{Re} \leq \text{Re}_C \qquad\qquad (3\text{-}25)$$

With the above equations, a quick estimation can be made of the errors resulting from the simplification of applying the fully developed flow theory throughout the whole channel. For example, for a typical microchannel of width 100μm and in length of, for instance, 1cm which is 100 times of channel width, the resulted in error will be no more than 1% when $\text{Re} \leq 10$, thus can be considered as negligible. But the error increases when Reynolds number becomes larger or the channel is shorter, e.g., when Re reaches 100 whilst the channel length is halved, the resulting error can get as high as 6%. In this case, errors cannot be ignored any more, and results must be corrected.

Table 3-1 Entrance Length and Bend Length at Different Reynolds Numbers

	Entrance length		Bend length	
	X	X/W	Z	Z/W
Re = 10	2.0	0.9	1.9	0.9
Re = 100	3.0	1.4	6.1	2.8

3.5.2 Pressure Drop of Fluid Flow in Microchannels

Since fluid flow in microchannels is characterised by its low Reynolds number (usually $\text{Re} \leq 10$, and in some cases in an extremely low regime as $\text{Re} \rightarrow 0$), entrance effect/bend effect can be ignored because of the negligible errors. In these situations, fully developed flow is assumed right from the beginning and applied throughout the entire channel. As a result, the momentum equation can be further reduced and the pressure drop along the microchannel can be solved.

As the developed flow is characterised by zero transverse components of velocity and uniform gradient of pressure in the x direction, i.e.: $v = w = 0$ and $p = f(x)$ (see Eq.(3-1)), Eq.(3-6) can be further reduced to the form:

$$\frac{dp}{dx} = \mu \frac{d^2 u}{dy^2} \qquad (3\text{-}26)$$

The well-known analytical solutions of Equation (3-26) have been obtained for flow between two parallel plates and in the cylindrical pipe respectively as:

$$\text{Parallel plates:} u = \frac{1}{\mu}\frac{dp}{dx}\left(\frac{y^2}{2} - \frac{Hy}{2}\right); \qquad -\frac{dp}{dx} = 12\frac{\mu V}{H^2}$$

$$\text{Cylindrical pipe:} \ u = \frac{D^2}{4\mu}\frac{dp}{dx}\left(\frac{r^2}{D^2} - \frac{1}{4}\right); \qquad -\frac{dp}{dx} = 32\frac{\mu V}{D^2} \qquad (3\text{-}27)$$

in which H is the height of the gap between two parallel plates, and D is the diameter of the pipe.

As the fluid flow in a microchannel (setting in the coordinates as in Figure 3-6) may be considered to be equivalent to a flow intervening that between parallel plates and in the pipe, it is supposed that the relation of pressure drop along the microchannel would obey the rule as:

$$-\frac{dp}{dx} = f\frac{\mu V}{R^2} \qquad \text{with } V = \frac{Q}{A} \qquad\qquad (3\text{-}28)$$

in which, Q is the volume flow rate and A is the area of the channel's cross-section. The friction coefficient f is a dimensional function only of the aspect ratio of the channel's cross-section.
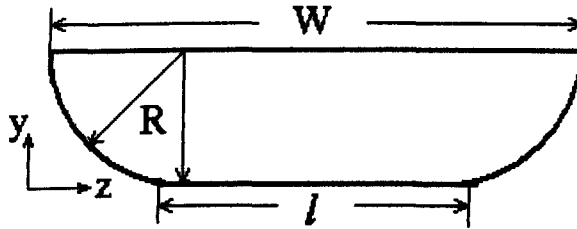
Fig.3-6 Schematic of Cross-section of a Wet Etched Microchannel

A series of CFD computations have then been carried out on various values of the ratio of l/R. The results not only prove that the supposed linear relation of pressure drop in microchannels is right, but also produce the value of f for some shapes of microchannels (results are given in Table 3-2). In order to check the results, values of f have also been compared with some analytical solutions. As a typical example, for the channel with a semi-circular cross-section in which $l/R = 0$, the error between the computed value and the exact solution of f is only 0.01%, as published by MacInnes *et al.* (2003)

Since the pressure gradient is uniform in the x direction, formula (3-28) can also be expressed in the terms of the distance along the flow direction, Δs, as:

$$\Delta p = f\frac{\mu V}{R^2}\Delta s \qquad\qquad (3\text{-}29)$$

Table 3-2 f as a Function of Aspect Ratio of Channel Section

l/R	Computed f ($\pm 0.1\%$)	f (Exact)
0	21.13	21.115
0.2	19.59	
0.4	18.47	
0.8	16.96	
1.6	15.38	
3.2	14.05	
6.4	13.15	
12.8	12.61	
25.6	12.31	
∞	12.00	12

Formula (3-29) is quite important, and suitable for flows in microchannels when the Reynolds number is low ($\text{Re} \leq 10$) so that entrance effect can be neglected. In this situation, Eq. (3-29) can be rewritten as:

$$Q = \frac{A_i R_i^2}{f_i \mu_i} \frac{\Delta p_i}{\Delta s_i} \qquad (3\text{-}30)$$

Hence the volume flow rate is expressed in terms of the geometric parameters and the pressure drop along the microchannels. Applying the equation in each segment i of the channel network as shown in Figure 3-2, another five equations can be established. Therefore with equation (3-19) to (3-23), the simultaneous equations for channel network analysis can be solved with known pressure conditions at four ports A, B, D and E.

It must be noticed that Eq.(3-29) is only appropriate for fluid flow at low Reynolds numbers ($\text{Re} \leq 10$) and in microchannels with reasonable length ($W/L \leq 5\%$). For situation when short channel length is used ($W/L > 5\%$), the equation may not be

quite suitable since the flow is still in the developing process and the assumption made for Eq.(3-29) is not satisfied. And for high Reynolds number flow, the situation is more complicated because f then becomes a function of both channel geometry and fluid flow ($f = f(\text{Re}, l/R)$). Hence, in these cases, entrance/bend effects must be taken into accounts. Usually, CFD computations and experimental measurements need to be carried out to correct the relation between the pressure drop and flow rate, and thus the channel network analysis equations can be solved.

Chapter 4

DEVELOPMENT OF MIXING SCHEMES

IN MICROCHANNELS

4.1 INTRODUCTION

Mixing of species in microchannels is important in a variety of applications, particularly for producing homogeneous solutions of reagents for chemical reactions. However, it has also proved to be a bottleneck in the development of compact and effective microreactors or microreactor systems. The difficulty of rapid mixing in microfluidic systems comes from two aspects: the small dimensions of the geometry and the fluid flow at low Reynolds number. As the generation of turbulence in the dimension below the millimetre length scale requires flow rates that are impractical under common conditions, the techniques normally used in macro devices are not applicable in microchannels. Meanwhile, because the fluid flow is limited to Reynolds numbers of order unity or even lower, it is not only laminar, but also dominated by a lack of the inertia that is important in the promotion of mixing. Diffusion thus becomes increasingly important as the size of microchannels reduces. However, this is a slow process. For example, the time required for diffusion from one side of a $100\mu m$ channel to the other side is around 10s in normal aqueous solution like water, but it can increase to hours for large molecules in dense solutions. Therefore an effective mixer is of great importance in a microchannel reactor system that has the purpose of measuring reaction kinetics. Several kinds of designs of micro-mixers have been

reported in the literature, and they can be divided into four types (see Chapter 2): the simple channel mixer (SCF), the alternating flow mixer (AFM), the folding fluid mixer (FFM) and the folding network mixer (FNM).

In this chapter, the results from three of the mixer types that have been tested are presented. They are the folding flow mixer, a flapjack mixer and a folding network mixer. Their performance will be compared from the aspects of both the mixing uniformity achieved and the pressure drop required. A choice is then made as to design of the experimental device to be used for the kinetics measurement.

4.2 CHARACTERIZATION OF MIXING FLUIDS IN MICROCHANNELS

Mixing of species in microchannels is important process for the kinetics measurement of chemical reactions so that reaction can start and be stopped at exactly known times. However, the mixing process in microchannels has also been proved to be a bottleneck in the development of compact and effective microreactors as well as microreactor systems. Hence, many efforts have been focused on the study of mixing approaches in microchannels.

4.2.1 Mixing of Fluid in Microchannels

Since the species mixing in microchannel mainly depends on the molecular diffusion, the Peclet number emerges as an important parameter for further discussion of the mixing process in microchannels. In definition, the Peclet number is the ratio of the mass transfer caused by fluid convection to that by molecular diffusion, i.e.:

$$Pe = \frac{VW}{\mathcal{D}} \qquad (4\text{-}1)$$

The average velocity V ($V = \dfrac{Q}{A}$, in which Q is the volume flow rate and A is the area of the channel's cross section.) and the channel width W are normally used as reference velocity and length scale in the calculation of the parameter.

The equilibration time needed for the pure diffusion process across the channel width, τ_W, scales quadratically with the channel width, W:

$$\tau_W = \frac{W^2}{\mathcal{D}} \qquad\qquad (4\text{-}2)$$

Hence, for two miscible fluid streams flowing side-by-side, the channel length, δ_x, needed for complete diffusive mixing across the channel cross-section is:

$$\delta_x = V\tau_W = \mathrm{Pe}\,W \qquad\qquad (4\text{-}3)$$

A high Peclet number means a strong convective motion of fluid relatively to the diffusive mixing. But for fluid flow in microchannels, the high value of Pe results more often from the low diffusivities of the species, because the Reynolds number is very low and the developed flow is characterised as zero transverse flow. Furthermore, as indicated in Eq. (4-3), a high Peclet number also means that long channel length and hence an unacceptably long residence time is required if good mixing is wished to be achieved by diffusion.

Then one may argue that a high Peclet number may result from strong fluid flow as well such as turbulent flow, and the turbulence will be of great help to the mixing process. But in fact, it is very difficult to create turbulent flow in a microchannel even though it is not totally impossible. The problem mainly comes from the pressure applied to the system. For example, to produce a turbulent flow for a 100µm channel that is in a length of 1cm or so, a pressure supply of 10bar is needed for normal aqueous liquids. For the ionic liquids used as solvents in the current research, of which

the viscosity is at least 20 times greater, the pressure required may be over 100bar. The high demand on the pressure supply makes turbulent flow an impossible option for mixing of fluids in microchannels, especially for ionic liquids.

But mixing depending on the pure diffusion process is notoriously slow and consequently two problems arise. On the one hand, the channel length needed for uniform mixing is too long to be practical. For instance, given the channel width of 100μm, the channel length required for a complete diffusive mixing will be 10cm at $Pe = 10^3$ and 10m at $Pe = 10^5$. These values are obviously too high to be applied in a real microchannel. On the other hand, the diffusion time is also incredibly long. For example, it takes 10s to well mix usual aqueous solutions like water with diffusivity in the order of magnitude of 10^{-9}. However, this time can increase up to a quarter of an hour for solution of large molecules such as ionic liquids, in which the diffusivities are 100 times less than water. In this case, if a reaction goes in only 5 minutes or even shorter, it is impossible to homogenize the system in time. Thus measuring the reaction kinetics will not be feasible. Therefore some measures must be taken to improve the mixing process. Referring back to Formula (4-2), one can easily find that the most effective way to decrease the diffusion time will be to decrease the channel width W. But as an alternative, it sounds more practical to introduce several streams of fluid interdigitated into the channel (as illustrated in Figure 4-1), so that the diffusion distances between species W_D decreases, and diffusion time τ_D reduces in the way of:
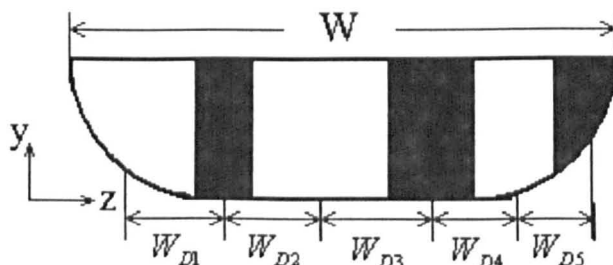
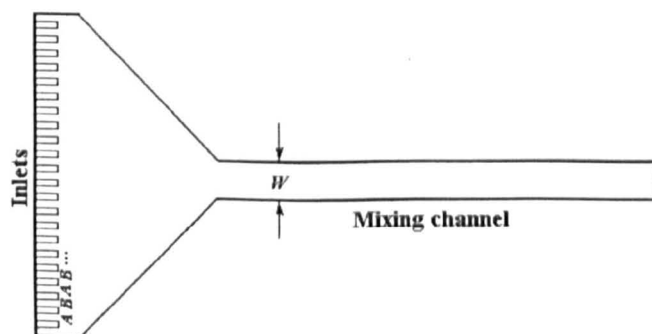$$\tau_D = \frac{W_D{}^2}{D} \qquad\qquad (4\text{-}4)$$

Fig.4-1 Schematic Diagram of W and W_D

## 4.2.2 Different Approaches to Mixing Fluids in Microchannels

As introduced in Section 2.3, the available micro-mixers can be put into four categories as: simple channel mixer (SCM), alternating flow mixer (AFM), folding flow mixer (FFM) and folding network mixer (FMM), as illustrated in Figure 4-2.
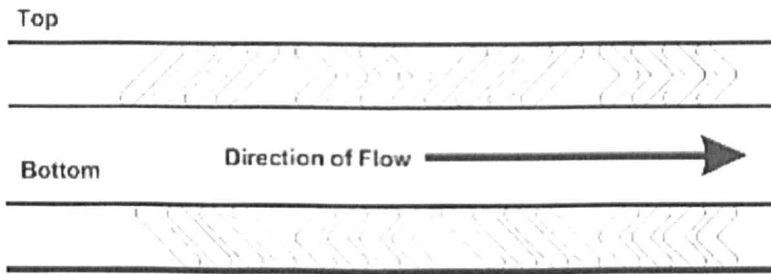

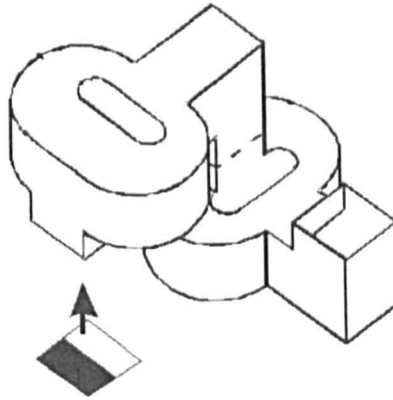**(a) Simple channel mixer (SCM) (Hardt *et al.* 2005)**
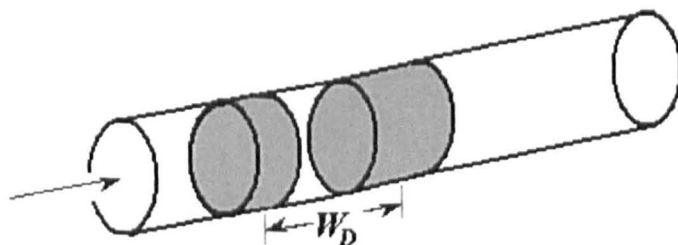
(b) Alternating flow mixer (AFM) (MacInnes and Allen 2005)
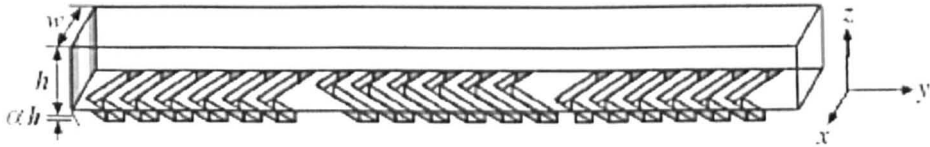
(c) Folding flow mixer (FFM) (Stroock *et al.* 2002b)

Top

Bottom   Direction of Flow

(d) Folding flow mixer (FFM) (Howell *et al.* 2005)

(e) Folding network mixer (FNM) (MacInnes and Allen 2005)

Fig.4-2 Schematic Diagram of Micro-mixers

The simple channel mixers (SCM) aim to achieve rapid mixing with basic "T" or "Y" shape channels. The diffusion distance in this kind of channels is then reduced in two

ways. One is to adopt extremely small dimensions, using the channel width as the diffusion distance. The other is to bring large number of fluid streams through different inlets into a narrow mixing channel, thus the diffusion distance between species W_D is the channel width W over the numbers of streams n guided into the system, i.e., $W_D = W/n$ (as illustrated in Figure 4-2 (a)).

The alternating flow mixer (AFM) uses the fluid deformation associated with the strain rate in pressure-driven flow to form slugs, thus interfaces between species increases with the numbers and the diffusion distances W_D decreases with the sizes of slugs inside the channel (Fig4-2 (b)). As mentioned in Section 2.3, its mixing process is characterized by a rapid mixing in the outer layer, followed by a far slower process in the core due to the strain rate distributed in the flow. As a consequence, a lateral non-uniformity can be found in the solution and it remains for the channel width diffusion time scale (MacInnes *et al.* 2005).

The folding flow mixer (FFM) intends to improve the mixing process by creating recirculation flow inside the channel. By placing ridges on the upper or the lower wall or even both of the channel, fluid is then "stirred" and folded when it is driven over the pattern surface under an applied pressure gradient. Hence the species interfaces increase and the diffusion distance greatly reduces. Typical examples include the staggered herring arrangement of grooves introduced by Stroock et al (Stroock *et al.* 2002a) (Figure 4-2 (c)), and the improved design of Howell et al which adopts chevrons and stripes and puts ridges on both top and bottom walls (Howell *et al.* 2005) (Figure 4-2 (d)).

The folding network mixer (FNM) consists of a numbers of mixing elements. In each element, the fluid is split and recombined, thus the diffusion distance is halved and the

species interface doubled. But what makes the mixer especially appealing is that it allows a multi-lamination of fluids to be achieved in the microchannels under moderate pressure and without severe fabrication constraints. Only a few kinds of designs of FNM have been ever reported. As a typical representative, Figure 4-2 (e) illustrates the one proposed by MacInnes and Allen (2005), which is a three-layer microchannel network.

4.3 DEVELOPMENT OF THE MICRO-MIXER

The challenge of mixing species in microchannels for this research in particular stems from the extraordinary properties of the ionic liquids. Having been proved to be excellent solvents for most chemicals, ionic liquids however possess high viscosities that are normally above 0.03 Pa·s, with low diffusivities, about two orders of magnitude smaller than water. In addition, for kinetics measurement, it is necessary to deliver and mix the ionic liquids through the mixer in a reasonably short time. These two factors consequently result in very high Peclet numbers and the mixing process becomes more difficult because the inertial effect is weaker whereas diffusion is even slower. Therefore, an effective mixer is of greater importance in a microreactor system designed for the measurement of reaction kinetics in ionic liquids, in which rapid mixing is needed in order to determine the start of reaction time correctly and precisely.

The research began with a quest for a satisfactory scheme to perform rapid mixing in microchannels. Several designs were tried and analysed, mainly by CFD computation, with dimensions as given in Table 4-1. No matter what kind of topology was adopted in the design, the aims were all to reduce the diffusion distance as well as enlarge the interfacial area between species streams.

Table 4-1 Dimension of Mixers for CFD Computation

Dimensions (mm)		SHM	FMRS	DGFM
Channel	L	2.136 (cycle)	0.5 (cycle)	0.5 (cycle)
	W	0.2	0.2	0.2
	R	0.07	0.07	0.07
Ridges	W_g	0.05	0.05	0.05
	R_g	003	0.03	0.03
	S_g	0.05	0.05	0.05
	θ	45°	45°	45°
	Number per cycle	20	-	-

4.3.1 Folding Flow Mixer

Just as its name implies, the principle of the folding flow mixer is to use the channel geometry to create transverse flow, thus achieving the rotation and folding of the fluid volume in the microchannel. A good example of this kind of mixer is the staggered herringbone mixer (SHM). Put forward by Stroock et al (2002b), it has been discussed quite a lot and reported as an effective mixer under a wide range of Pe numbers as $Pe = 10^3 \sim 10^5$ (Stroock *et al.* 2002b). Hence, an initial study started from the CFD computation of mixing of ionic liquids in SHM.

The major design feature of the SHM mixer is the additional ridges put on the bottom of the straight channel. As illustrated in Figure 4-3, the geometry for the CFD computation consists of a straight main channel and two 45° oblique ridges intersecting at a right angle that is in the shape of herringbone. Put on the bottom of the

main channel, the herringbone of the mixer is arranged in different ways in two half parts of each cycle of the mixer. In the first half cycle, the two intersecting ridges cross at the position of 1/3 channel width to one side wall of the channel; while in the next half part, their vertices switch to the opposite side, but the same distance away from the wall. For details of the geometry of each part, please refer to Table 4-1.
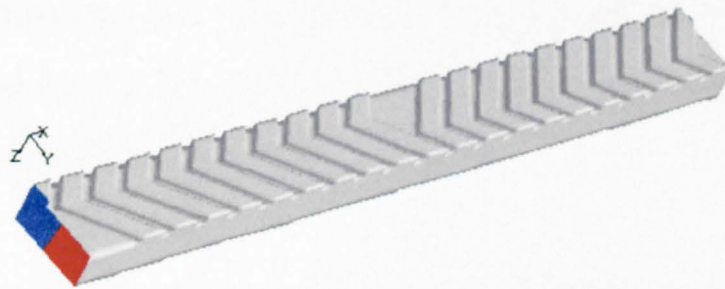
(a) 3D Geometry of SHM (Seen from bottom)
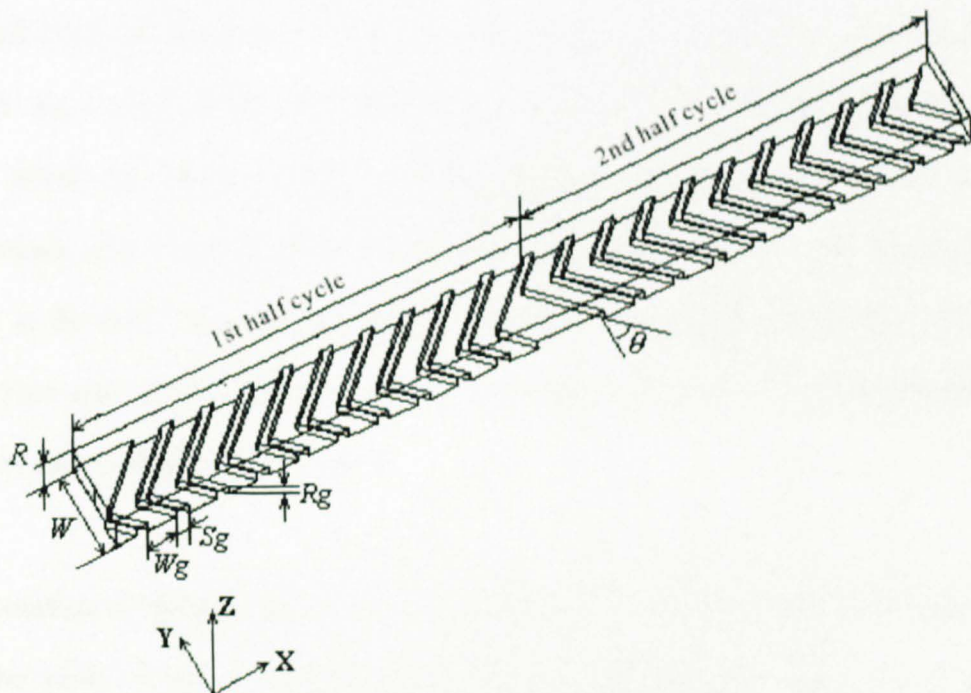
(b) 3D Wire frame of SHM Structure

Fig.4-3 Geometry of SHM for CFD Computation

The computation was made with the CFD commercial package Fluent 6.0 in two steps. Firstly, a mixing cycle as shown in Figure 4-3 was used for the computation of the fluid flow, in which the developed flow profile was generated with periodic boundary conditions. Then the geometry was rebuilt, by extending the geometry to twice the channel width downstream in order to prevent the reslts at the outlet surface of the cycle from being affected by the outlet boundary conditions of the computational domain. The velocity profile produced in the first step was imported as the inlet boundary conditions for the first cycle. The results at the outlet of each cycle are then transferred as the inlet of the next one. By this means, a long channel length is thus avoided and size of grid file is reduced.

Figure 4-4 illustrates the vectors of the transverse velocity in the SHM, which is exported from the CFD computation. Though two circulations are found over the cross section of both half cycles, the patterns vary with the arrangement of the ridges. In the first half cycle, as the chevron lies closer to the right sidewall, more fluid is guided to the left. As a result, a big circulation is formed in the left side and a small one in the right. When the chevron shifts to the opposite side in the next half cycle, the circulations also switch their positions, with the big one in the right while the small one is in the left. The patterns are then repeated by arranging the ridges in the same way cycle after cycle. Hence the fluid volume is subjected to a repeated sequence of rotation and stretching in the SHM.

Computation of species has also been carried out. But due to the computation intensity and the limit of the computer, only a coarse grid was ever used in an attempt to understand the mixing process in the SHM. Reagent A (red) and B (blue) were fed side by side with equal areas at the inlet. It was found that the interface between two species was rotated to the left in the first half cycle then to the right in the second half due to the fluid motion generated in the patterned geometry. But more important, the

species interface was found to be keeping almost straight in the upper part, while the lower part was oscillating along the bottom of the channel (as given in Figure 4-5). The reason for the results may come from two aspects. First, the ridges at the bottom of the channels are shallow, so that the transverse flow created was not strong enough to push the liquid further and cause movement of the upper interface. Second, the length for each half cycle was not long enough; therefore the fluid volume could not be fully rotated to fold the interface. In comparing the two, the first reason seems more likely to be the main factor responsible for the results given in the figure.
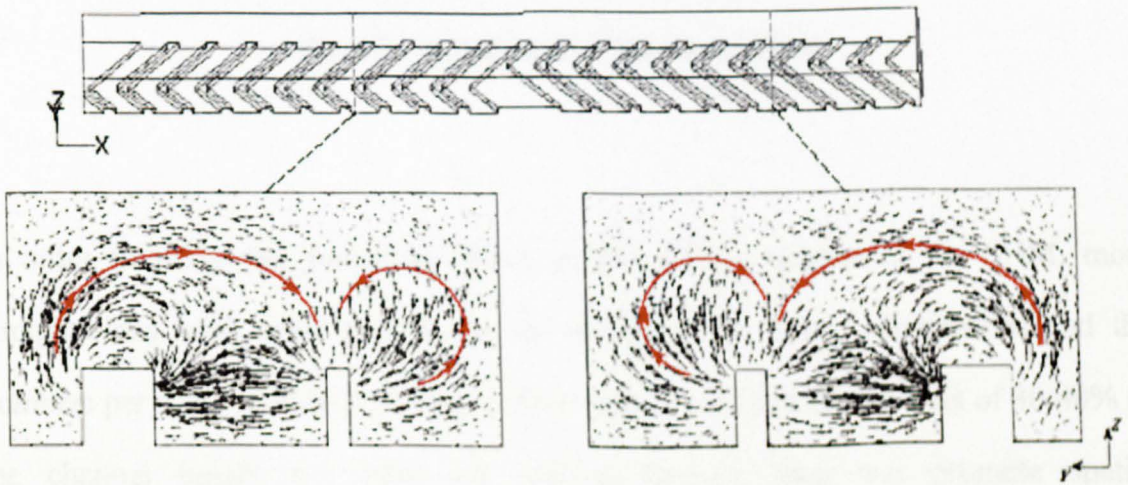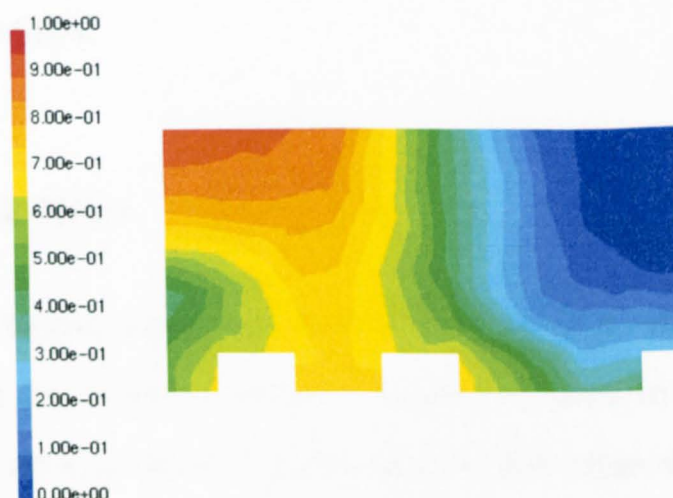

Fig. 4-4 Vectors of Transverse Flow in SHM
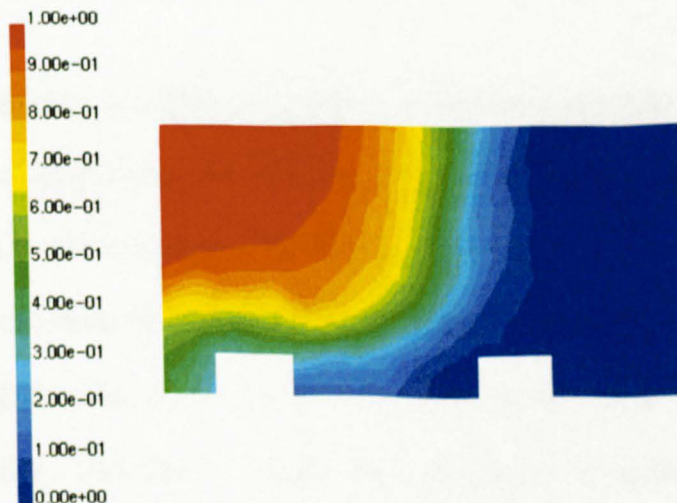
(a) Result at the end of 1ˢᵗ half cycle of SHM

(b) Result at the end of 2nd half cycle of SHM

Fig.4-5 Computation of Species in SHM

In order to study the geometric effect on the mixing quality of the SHM, more computations have been carried out, by changing the ridges' dimensions and the numbers per cycle (Aubin et al. 2005). The result shows that deep ridges of 30-40% of the channel height are good for mixing because they can promote spatial homogenisation. However, too wide ridges and more than 20 ridges per cycle do not show too much help in the mixing, as they increase the dead zone over the cross section and the pressure drop along the mixer.

Although the staggered herringbone mixer is effective at creating chaotic flow inside the channel, thus improving the mixing process, the channel length to achieve a complete mixing is still excessive. The diffusion distance after 1cm in the mixer is still around 10μm, according to Aubin's results, and the diffusion time for solvents like ionic liquids, will then be about 10s. This is obviously too much for the measurement of reaction kinetics. Therefore a longer channel length is needed, associated with a higher pressure-drop across the mixer and a larger size of the chip dimension. As an

alternative, another mixing scheme must be designed and studied based on the advantages of the SHM.

4.3.2 Flapjack Mixer

The idea of the flapjack mixer (FM) evolved from that of the staggered herringbone mixer. Its design aims to take advantage of the effective geometry of the rotating fluid volume of SHM but to avoid the long channel required to reduce the diffusion distance. As a result, the mixing process is carried out in two steps in the flapjack mixer, namely, the flipping and squashing of the species interface. Figure 4-6 gives the schematic diagram of the mixer.

The design of the flapjack mixer includes two parts: the rotation section and the mixing section. The rotation section, as its name indicates, is used to rotate the fluid volume, ideally by 90° thus changing the species interface from vertical at the inlet into the horizontal as expected. For this purpose, the slanted ridges borrowed from the SHM are arranged at the same oblique angle along the channel, to stir the volume of fluid in the channel. As a result, the transverse flow in the cross section created in such geometry follows the same direction so that the flipping of the interface can occur in a short channel length. The mixing section of the mixer is a shallow channel in the shape of a pancake. Being one millimetre wide and only a few microns deep, the mixing section squashes and stretches the fluid over the cross section. The surface boundary between species is greatly enlarged in the mixing section. More importantly, when the two streams of fluid are introduced into the mixing section in the form of one layer on top of the other (as shown in Fig.4-6), the diffusion distance can be reduced to half the depth of the shallow pan, therefore the diffusion for complete mixing of species like ionic liquids can be achieved at the scale of hundreds of milliseconds, for example, when the gap is only 2 microns.
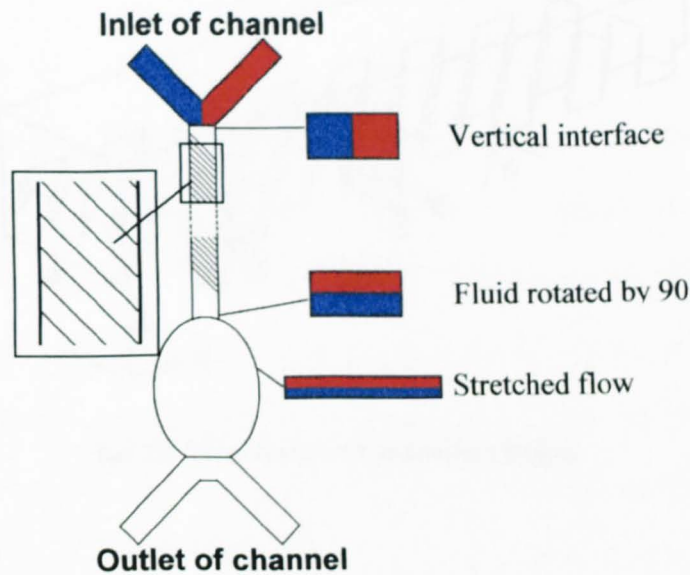
Inlet of channel

Vertical interface

Fluid rotated by 90

Stretched flow

**Outlet of channel**

Fig.4-6 Schematic of Flapjack Mixer

The idea of the flapjack mixer looked promising. However some drawbacks in respect of two functional parts of the geometry were found later in CFD computations as well as in the fabrication process.

4.3.2.1 Flipping the interface

CFD computation was carried out on the rotation section of the flapjack mixer (referred to as FMRS in Table 4-1) in order to understand the flipping process of the species interface in the rotation section. The procedure and method used to deal with boundary conditions in the computation of the SHM were applied the same way here to solve the momentum and species equations. The computational structure is shown in Figure 4-7 and geometry details are given in Table 4-1.
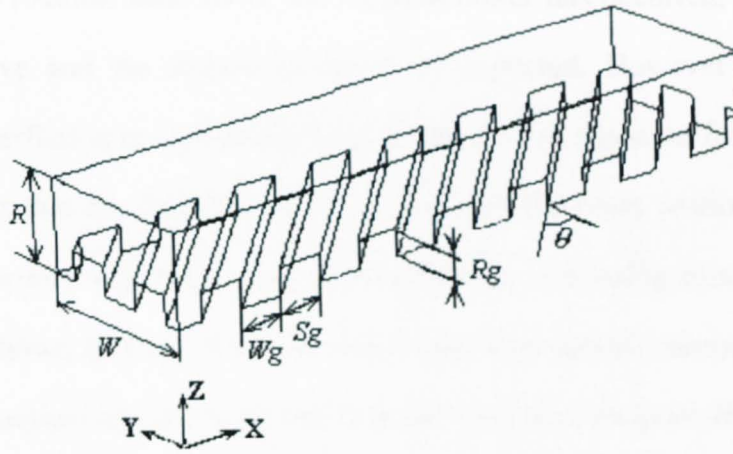
(a) 3D Wireframe of rotation section
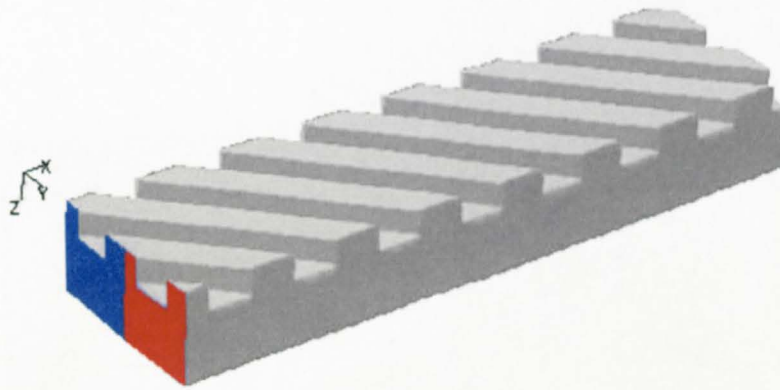
(b) 3D Geometry of rotation section (Seen from bottom)

Fig.4-7 Geometry of Rotation Section of FM for CFD Computation

Figure 4-8 is the vector diagram of transverse velocity in the cross section of the flapjack mixer. Due to the unchanged shape of the slanted ridges at the bottom, the transverse flow created in the cross section of the mixer pushes the fluid moving in the same direction. As a consequence, the interface between species is then turned over under the force of the consistent fluid advection when it passes through the channel. As shown in Figure 4-9, after 2mm along the mixer, the layout of species has changed from the side-by-side position at the inlet into one over the other (red over blue). From

this aspect, the rotation function of the flapjack mixer has occurred, since the turning over is effective and the degree is almost as expected. However this is not true, because the interface is unexpectedly twisted into a bowl shape, as found in Fig4-9 (e), which indicates that the distribution of species over the cross section is not uniform. This non-uniformity will then cause problems in the following mixing section, as in the situation shown in Fig.4-9 (e), in which the blue species surrounds the red one. After being squashed into the wide and shallow pan-shape channel, the red species will still stay in the centre and be sandwiched by the blue side by side, the diffusion distance will consequently increase to 1/3 of the channel width, rather than be reduced into the order of microns as was intended.
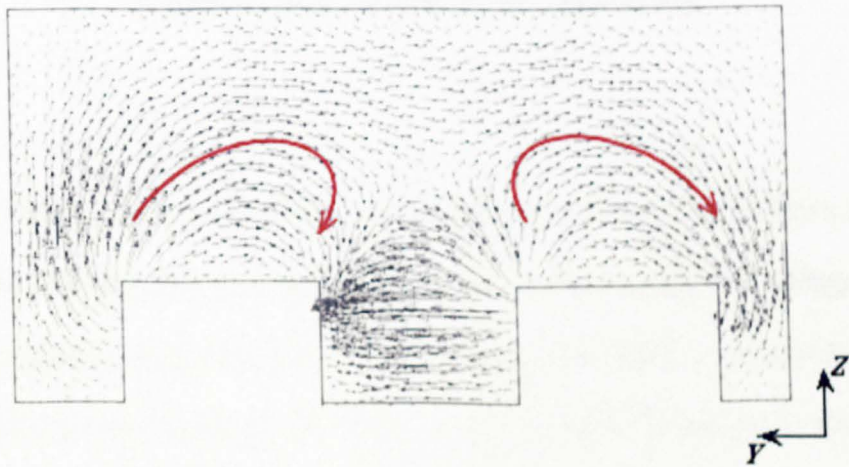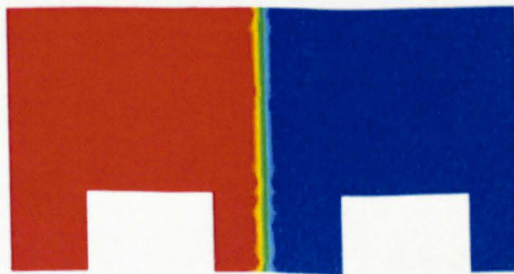

Fig.4-8 Vectors of Transverse Flow of FM

(a) Reagents Fed at the Inlet

| (b) 0.5mm Downstream of Inlet | (c) 1.0mm Downstream of Inlet |

(d) 1.5mm Downstream of Inlet   (e) 2.0mm Downstream of Inlet
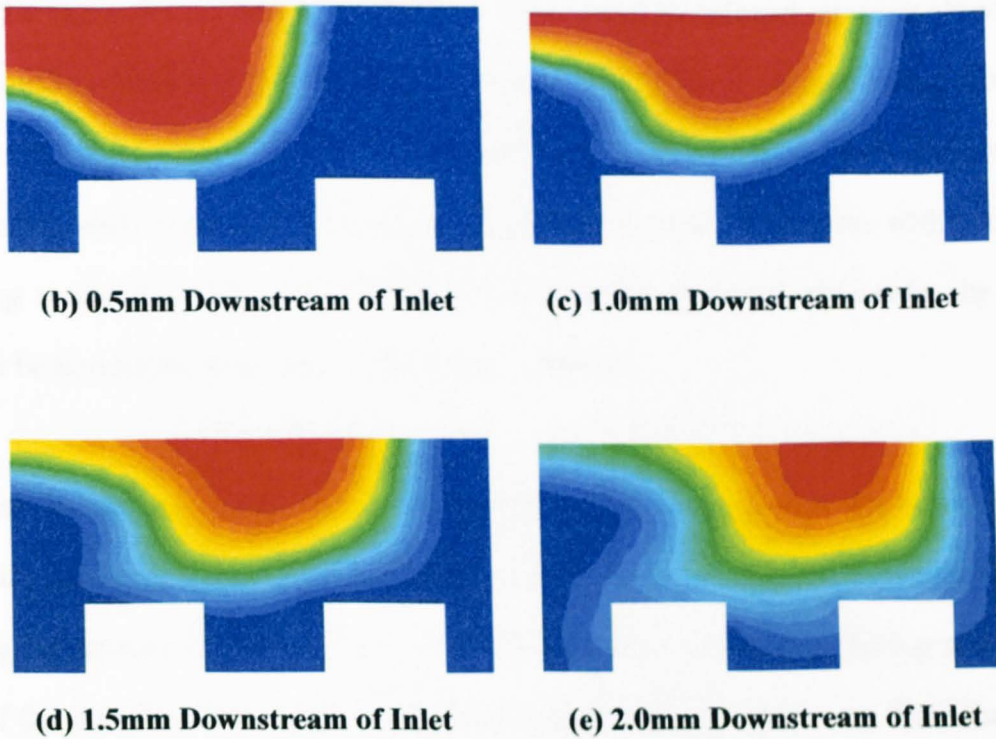
Fig.4-9 Flipping of Species Interface in FM

The twist of the interface is caused by two factors: the strong motion from ridges at the bottom of the channel and the weak flow in the top. Although the oblique ridges are effective in creating transverse flow, the stirring of the fluid is mostly limited to the lower part of the main channel and halted when the fluid rises up to the upper wall because of the low Reynolds number. The velocity vectors shown in Figure 4-8 are a good proof of such a circumstance in which strong fluid flow is found in the lower part of the main channel, with an especially high velocity near the two corners due to the reduction of the flow area. However, in contrast, two dead zones exist in the top corners of the main channel. As the result of the uneven distribution of fluid motion, the fluid volume is pushed strongly in the lower part, whereas it slows down when approaching the upper part of the channel, and finally sticks to the wall and hardly moves because of the weak flow as well as dead zones in the corner. The species interface, at the same time, experiences a process as given in Figure 4-9 (b)-(e), during

which the middle and bottom parts are easily and rapidly rotated and lifted, until they reach the upper part of the channel where their speed is reduced, moving slowly and being pushed further to the top wall by the following fluid volume rising from the ridges. The upper part of the interface, meanwhile, keeps its vertical shape almost unchanged while moving very slowly along the top channel. Therefore, with both ends sticking to the top wall of the channel, the interface between species in the mixer cannot be horizontal; instead, a bowl shape is formed.

As may be deduced from above description, the ideal situation for achieving the desired flipping process is that the species interface can be kept and moved diagonally during the process. To say the least, as an alternative circumstance, the top and bottom tips of the interface must move at a similar speed, being pushed away from the centre simultaneously, then the top being dragged down while the bottom being lifted up, so that the interface can be maintained approximate to a flat surface and a position close to horizontal be obtained.

To achieve such a motion for both the upper and lower part of the species interface, similar transverse flow must be created relatively evenly over the cross-section. Simply changing the geometry such as width and depth of either the channel or the ridges has been considered. However it seems not to be a good choice because fluid motion in these situations will always be strong near the bottom of the main channel and become weaker and weaker when approaching the top. Instead, the most effective method should be using some symmetric geometry. Hence, a new geometry of the flapjack mixer was proposed, referred to as the double grooved flapjack mixer (DGFM), in which the slanted ridges were put on both the top and bottom of the channel (as illustrated in 4-10).
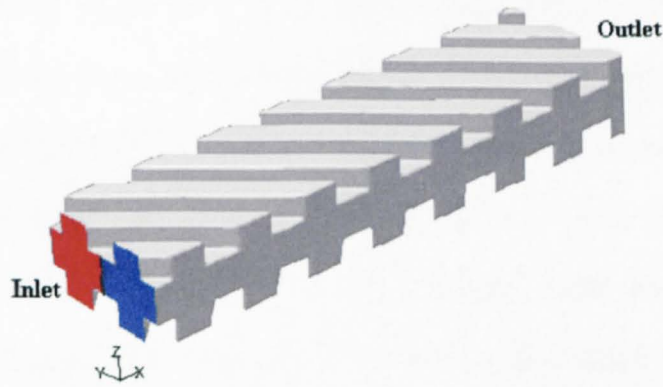
Fig.4-10 Geometry of Double Grooved Flapjack Mixer (DGFM)

Due to the symmetry in the geometry, the transverse flow, created in the cross section, distributes symmetrically, not only in the main channel, but also all over the surface. One strong circulation can be found in the centre of the channel in the velocity vector diagram as given in Figure 4-11, which is the driving force for the flipping of the interface.
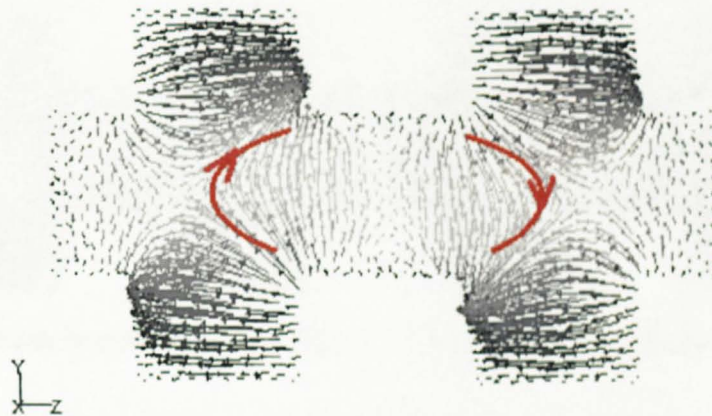

Fig.4-11 Vectors of Transverse Flow of DBFM

As a consequence, any movement of the species interface takes place simultaneously on the cross, as shown in Figure 4-12. In addition, the flipping process occurs more rapidly in the DGFM because the rotation effect is twice as strong as that in the FM. From the results in Figure 4-12, a species interface, which is not really horizontal but close to that, can be achieved within the channel length of 0.3mm. Longer than that, as the fluid volume is further rotated and the interface begins to be twisted, the same non-uniformity in the distribution of species along the channel depth will happen again, resulting in the unnecessary difficulty in diffusion in the following section.

(a) Reagents Fed at the Inlet   (b) 0.1mm Downstream of Inlet

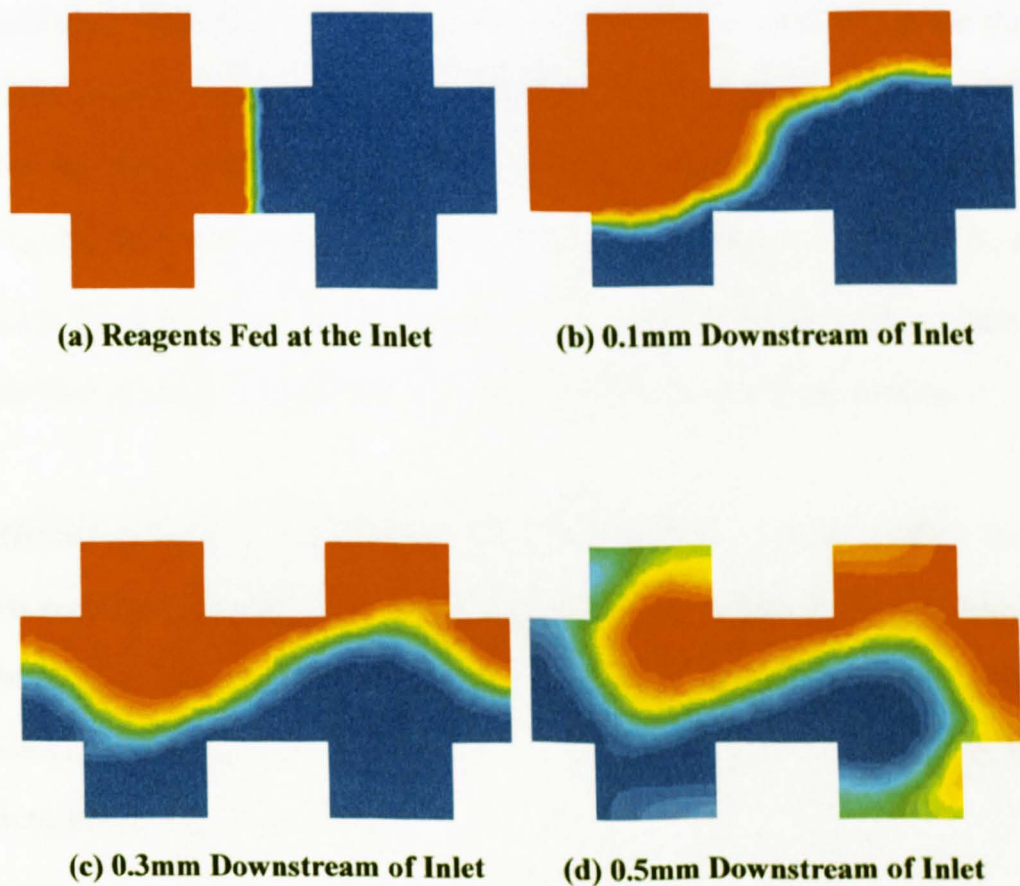(c) 0.3mm Downstream of Inlet   (d) 0.5mm Downstream of Inlet

Fig. 4-12 Flipping of Species Interface in DGFM

The difficulty of flipping the species interface in the DGFM lies in the control of the process. For fluid flow at different Reynolds numbers, the transverse flow created in the main channel is certainly different. So the speed of the fluid rotation varies with

fluid flow and the channel distance to obtain an appropriately flipped interface for the next section also changes. Therefore fluid flow must be controlled with good precision because either inadequate or over flipping of the interface will cause non-uniformity in the distribution of species. However, it is not so easy to meet this requirement and any error will eventually result in bad performance of the mixer.

4.3.2.2 Squashing the interface

Stretching and squashing the interface into a wide and shallow gap may be the most simple but effective method to reduce the diffusion distance. Characterised by the extraordinarily small depth, the mixing section of the FM is a channel in the shape of an ellipse (Figure 4-13(a)). With the gap etched to only 2 microns, the diffusion distance can then be reduced to a micron. Hence good mixing even for species like ionic liquids, of which the diffusivity is in order of magnitude of 10^{-11} m^2/s, can be still achieved in a time of 100 milliseconds. Meanwhile, as the channel is 1.5cm wide, the interface is largely expanded, which will also benefit the mixing process.

A difficulty associated with fabrication of the mixing section resulted from the distortion of the channel geometry during the thermal bonding. Under the force of the weight of glass, the cover glass was observed sunken and its centre area was stuck to the bottom, so that the flow passage in the centre of the pancake was totally blocked (as illustrated in Figure 4-13 (b)).

From the sinking of the top glass that occurred with the pancake, estimation can be made on the distortion rate in such a microchannel over a span in width of W to be:

$$\eta = \frac{0.002}{1.5} W \approx 10^{-3} W \qquad (4-5)$$

So, in a channel that is typically 100 microns wide, the amount of sag that is likely to happen is about $0.1\mu m$. But as the distortion will be less serious when the gap is narrower, the actual amount over the normal channel width could be smaller than the estimation.

(a) Geometry of Mixing section   (b) Schematic of channel distortion
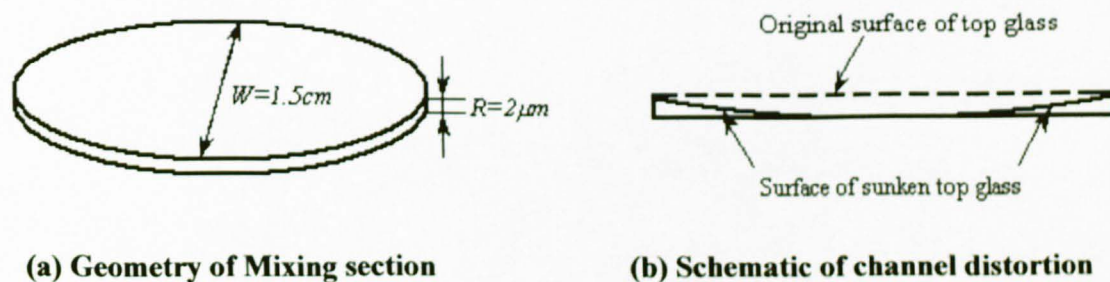
Fig. 4-13 Mixing Section of FM

One solution to the problem is to support the top glass by some pillars, as shown in Figure 4-14. Due to the tolerance of the wet etching method ($\pm 5\mu m$) as well as the precaution to reduce the risk of blockage, the channel depth in this design had to be increased to $10\mu m$. As a result, the diffusion time also increased, to the order of half to one second.
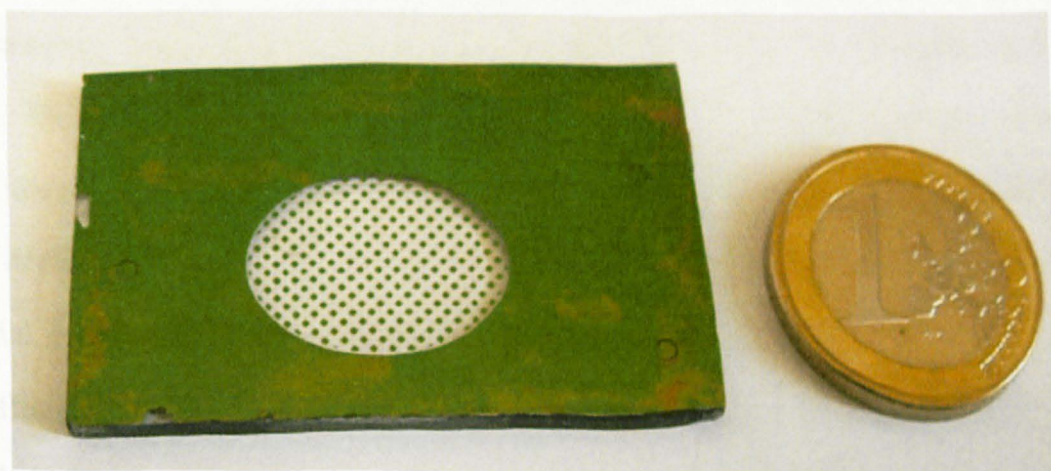

Figure 4-14 Geometry of Improved Mixing Section of FM

4.3.2.3 Fabrication of FM

The first practical flapjack mixer was fabricated by lithographic etching techniques. By etching the straight channel and the slanted ridges separately, the mixer is then made by bonding the two parts together.
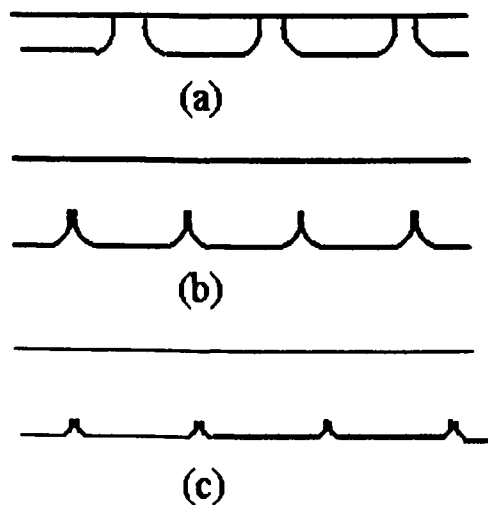

(a)

(b)

(c)

Figure 4-15 Interference Etching of the Slanted Grooves

What is significant in the technology is the etching of the slanted ridges on the bottom of the mixer. The method used is called "interference etching", as illustrated in Figure 4-15. The interference etching is carried out by gradually etching a group of ridges until they intersect with each other, forming small slanted channels of a certain width and depth, as well as ridges between every two adjacent grooves. Time control is crucial in this method because too long or too short etching time will result in either insufficient etching as shown in (a) or over etching like (c). The best example is the result in Figure 4-15 (b), though it is still quite different from the ideal design in the CFD computation.

The first flapjack mixer was made of glass. Table 4-2 gives the dimensions of all parts of the mixer, and Figure 4-16 gives its appearance, of which the mixing section is unfortunately blocked due to the sinking of the covering glass over the large width of the gap.
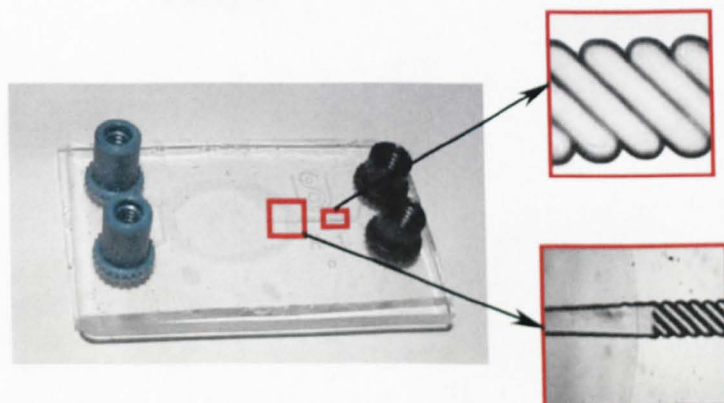

Figure 4-16 Fabricated Flapjack Mixer

Table 4-2 Dimension of Fabricated Flapjack Mixer

Dimension	Rotation section		Mixing section
	Channel	Slanted ridges	
W	600 μm	160 μm	15 mm
R	50 μm	50 μm	2 μm

4.3.3 Folding Network Mixer

A number of structures of a folding network mixer have been reported, such as the rectangular network introduced by Chen and Meiners (2004) and the one proposed by Lee and Lee (2005),which used horizontal and vertical guiding walls in the channel. But no matter what kind of geometry these mixers adopt, the principle is the same, i.e.,

using the channel geometry to repeatedly split and reunite the fluid, thus halving the

diffusion distance and doubling the species interfacial area in each element, as
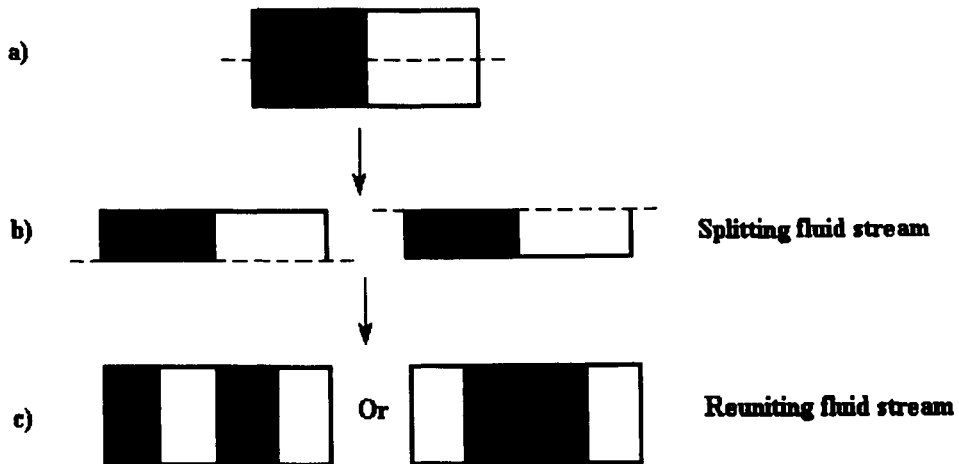
illustrated in Figure 4-17.

Fig. 4-17 Schematic of FNM's Principle

A further variation of the FNM has been investigated in the current research. As shown

in Figure 4-18, the mixer is fabricated on three layers of glass, with channels etched on

the top and bottom layers and interconnected by holes in the middle. A chain of mixing

elements is then formed to split and recombine the fluid streams. Hence, when flowing

through the mixer, the number of the species interfaces increases and the diffusion

distance decreases exponentially.

The mixing performance of the FNM has been reported to be quite efficient. For

example, the relative rms deviation from perfect mixing of about 1% can be achieved

with 6 elements in Chen and Meiners' network at Pe = 500 (2004) and less than 5%

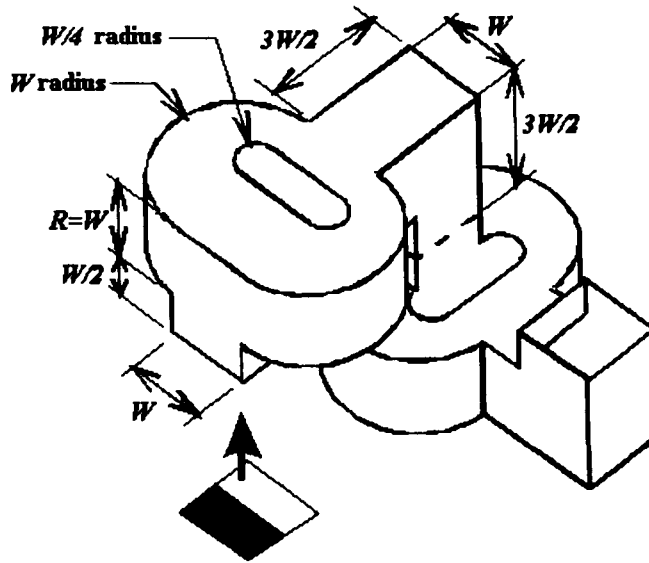be obtained within 6 elements in Lee and Lee's design at Pe = 2000 (2005).

Fig. 4-18 Mixing Element of FNM (MacInnes and Allen 2005)

Simulation has also been carried out on the geometry shown in Figure 4-18. The relative rms deviation of species in the order of 1% is found to be obtainable with 3 elements at Pe = 100 and with 6 elements at Pe = 1000 (MacInnes and Allen 2005). The effectiveness of the mixer thus brings about a shorter channel length and a smaller footprint size of the chip. But more than that, due to the simple flow pattern and short flow passage of each element, the pressure drop across the FNM is also smaller than in other mixers. These features make it the most efficient of the four kinds of micro-mixers.

4.4 COMPARISON OF MIXING SCHEMES

As introduced above, all passive micro-mixers can be divided into four types, the simple channel mixer (SCF), the alternating flow mixer (AFM), the folding fluid mixer (FFM) and the folding network mixer (FNM). Among those having been studied in the current research, the staggered herringbone mixer is a typical FFM, and the flapjack

mixer is combination of the SCF and FFM. Though the AFM has not been tested in experiments, much work has been done and well reported (MacInnes *et al.* 2005). In order to select an appropriate scheme for the design of a microreactor system for the kinetics measurement of chemical reactions, comparisons need to be made between the available mixers and then a choice must be made, so that mixing can be carried out rapidly and effectively.

4.4.1 Parameters for Comparison

Two parameters are used to assess quantitatively the performance of different micro-mixers: one is the relative standard deviation of the concentration profile of the mixture downstream of the mixing elements and the other is the pressure drop to achieve certain mixing uniformity.

Defined as in formula (4-6), the relative standard deviation of the species mass fraction relative to the value for perfect mixing describes the uniformity of the mixture obtained in the cross section after the mixer. When this value is unity, it means the liquid is completely unmixed, and when $\sigma_Y = 0$, the mixture is perfectly uniform.

$$\sigma_Y = \sqrt{\frac{\overline{Y^2}}{(\overline{Y})^2} - 1} \tag{4-6}$$

The over bar in the formula designates the averaging operation. This operation is normally taken over the surface of the cross section or the volume of the domain. However, it sometimes could also be the mass flux weighted over the surface, for example, in some cases when fluid flowing through a surface is of interest.

Using pressure drop for the comparison of the mixers takes the driving force required by the mixers into account. If the mixing is effective but the pressure needed is too

high, the mixer is still unfeasible for the practical application. Using the known relation for pressure drop for flow in microchannels (Eq.(3-29)), expressions can be rewritten into Eq.(4-7) for the alternating flow mixer (AFM), by applying the channel length $\Delta s = 2V\tau_\sigma$ (MacInnes *et al.* 2005):

$$\Delta p = \frac{f\mu}{\tau_w} \mathrm{Pe}^2 \frac{\tau_\sigma}{\tau_w} \qquad (4\text{-}7)$$

in which τ_σ is the mixing time to achieve the required mixing uniformity σ_Y.

The equation for pressure drop of the folding flow mixer (FFM) and the folding network mixer (FNM) is the same, but expressed in terms of required mixer elements k_σ and coefficient for unit element β, as

$$\Delta p = \frac{\beta\mu V k_\sigma}{W} \qquad (4\text{-}8)$$

where $\beta = fWL_e/R^2$ and L_e is the length of one element of the mixer. Hence the time for fluid passing through one element τ_e is:

$$\tau_e = \frac{L_e}{V} \qquad (4\text{-}9)$$

and the mixing time across k_σ elements is:

$$\tau_\sigma = \tau_e k_\sigma \qquad (4\text{-}10)$$

Substituting Eq.(4-9) and (4-10) into (4-8), the pressure drop along the FFM and FNM is:

$$\Delta p = \frac{\beta\mu}{\tau_w} \frac{L_e}{W} \frac{\tau_w}{\tau_\sigma} k_\sigma^2 \qquad (4\text{-}11)$$

Both Eq.(4-7) and (4-11) can be normalised by $\frac{\mu}{\tau_w}$ because for a given channel size and fluid system, the equilibration time τ_w is fixed and the same for mixers. Therefore,

the non-dimensional pressure drops for the AFM, the FFM and the FNM are respectively:

AFM: $\Delta p^* = f Pe^2 \dfrac{\tau_\sigma}{\tau_w}$ (4-12)

FFM and FNM: $\Delta p^* = \beta \dfrac{L_e}{W} \dfrac{\tau_w}{\tau_\sigma} k_\sigma^2$ (4-13)

It is then easy to find out that the normalised pressure drops for all the three mixers are expressed as a function of time ratio τ_σ / τ_w , which indicates how rapid the mixing will be relative to the pure diffusion process.

4.4.2 Comparison of Mixers

Mixing of species for reaction kinetics measurement is crucial for both starting and stopping the chemical reactions. The less time the process takes to achieve a certain level of σ_r, the better the kinetics measurement will be. Thus, for all micro-mixers, the one that can perform mixing acceptably well within a reasonably short time whilst not putting a high demand on the pressure drop will be preferable for the design of a microreactor system.

The comparison of micro-mixers starts with the mixing time needed for different fluids. Figure 4-19 gives a logarithmic plot of the least time required for three mixer types to mix well liquid systems at different Schmidt numbers. Since the analysis has been carried out on the basis of a sufficiently low flow rate for the inertial effect to be negligible, the results in the plot are reliable for Reynolds number lower than 10 (MacInnes and Allen 2005).
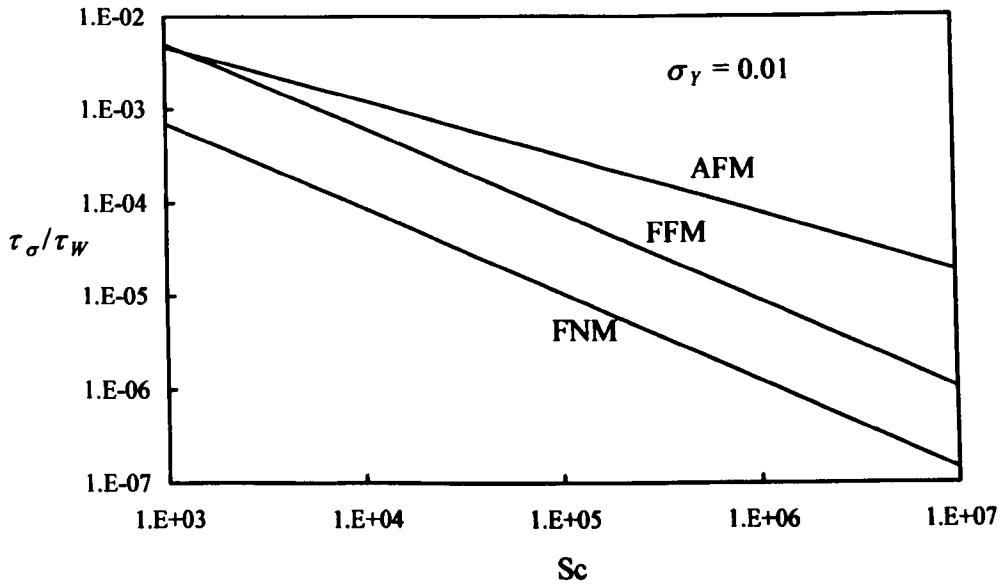
Fig. 4-19 Minimum mixing time as a function of Schmidt number (Re < 10)

(MacInnes and Allen 2005)

In the plot, the performance of the FFM is found to be similar to that of the AFM at low Sc or even worse when $Sc \leq 1000$, but it becomes more and more effective when the Schmidt number increases. When Sc is about 5×10^5, the mixing time in the FFM is about ten times shorter than in the AFM and the gap keeps increasing as the Schmidt number goes up. For the FNM, its plot stays all the way lower than the other two and the mixing in the FNM is always about an order of magnitude faster than the FFM. Therefore, for the three types of mixers, the FNM is the most efficient for a wide range of Schmidt numbers from 10^3 to 10^7.

With respect to the pressure drop, the normalised parameter has also been plotted as a function of the time ratio, for cases where different mixing uniformity is to be achieved. Figure 4-20 gives two results, of which σ_Y is 10% and 1% respectively (MacInnes and Allen 2005).
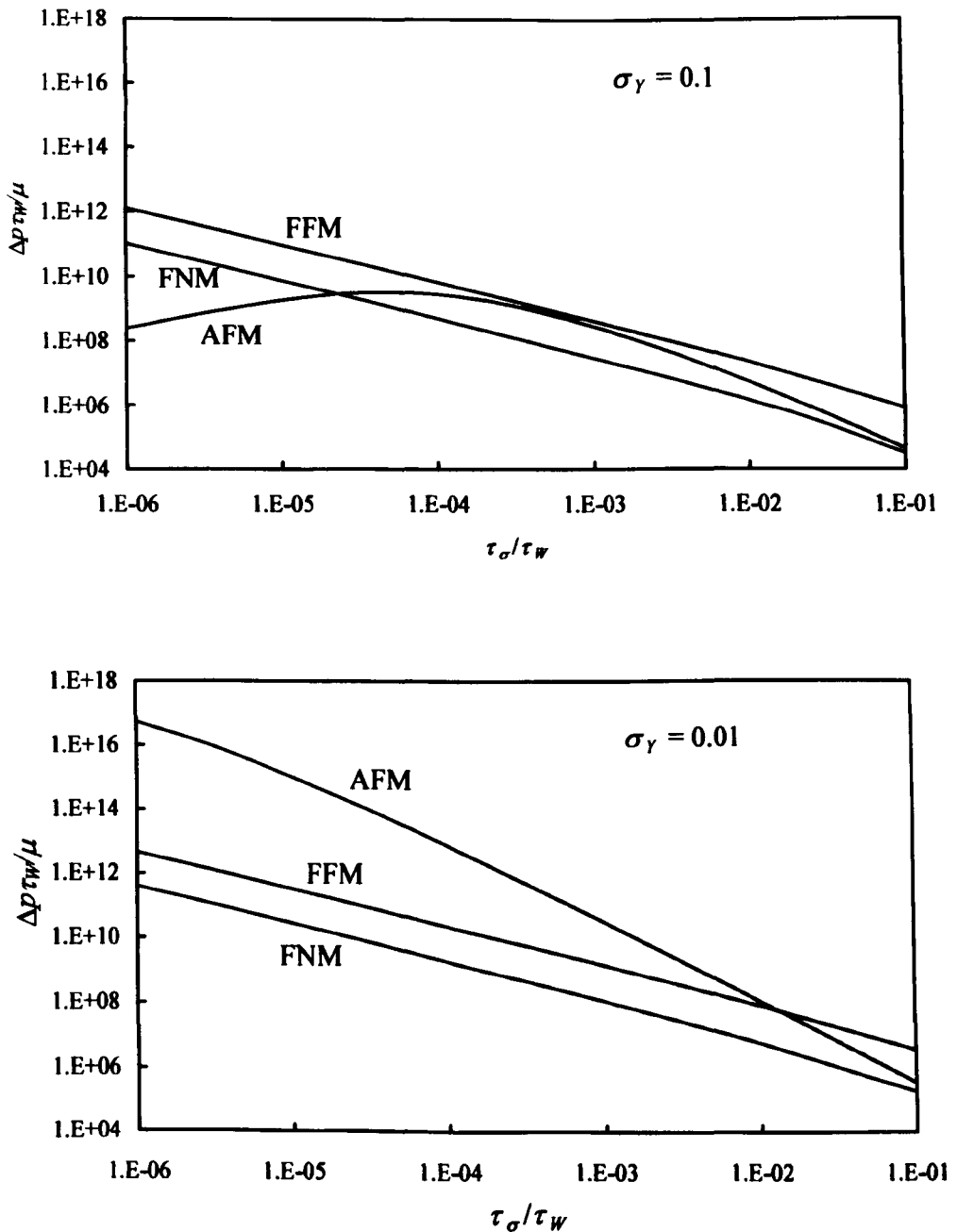
Fig. 4-20 Non-dimensional pressure drop versus mixing time (MacInnes and Allen 2005)

The FNM is found again to be preferable to both the FFM and the AFM at the higher

degree of mixture uniformity, i.e. $\sigma_Y = 0.01$, because it requires the lowest pressure

drop over most of the range. It is about an order of magnitude lower than that of the

FFM for all the range, and several orders of magnitude lower than the AFM at a high

degree of uniformity except for the situation when the reduction in mixing time becomes modest. However, when the requirement of the mixture uniformity is relaxed, say to $\sigma_Y = 0.1$, the situation changes quite a lot and is more complicated. Although the FNM is still better than the FFM, the AFM becomes competitive over the relevant range of time ratios. In the lower requirement of mixing regime, the AFM has the lowest pressure drop when the mixing time is small, increasing to the level close to the FFM at medium time and finally reaching to a little higher than the FNM when the mixing time almost equals the diffusion time.

It may be noticed that the SCM is not included in all these plots. Purely relying on the molecular diffusion, the mixing time in a SCM is just the diffusion time as Eq.(4-2). In order to enhance the mixing process in the mixer, the most effective measure is to reduce the diffusion distance. However, as mentioned above, the mixing section of the flapjack mixer is difficult to manufacture and maintain because it has such a small geometric dimension. Due to this limitation of fabrication technology, the SCM is excluded from the consideration of the mixers for the microreactor system.

4.4.3 Conclusion

Not relying on reducing the dimensions of channel size, approaches such as the AFM, FFM and FNM are effective in producing a uniform mixture. But meanwhile, they usually require a significant pressure drop for the process. Among the three types of passive micro-mixers, the folding network mixer seems especially attractive, because it not only provides the greatest reduction for a wide range of Schmidt number, but also requires the lowest pressure drop to achieve a high degree of mixture uniformity. The FNM then becomes the candidate for the mixer of the microreactor system that will be used for the reaction kinetics measurement.

Furthermore, for the purpose of measuring the reaction kinetics, the mixing time must be as short as possible, or at least, only be a small portion of the total reaction duration. As the reaction to be carried out on chip is in the time scale of seconds, the mixing time within 100ms will result in an error approximately of 10% for the initial measurement, while 10ms for only 1%. In order to guarantee the accuracy of the measurement, the smaller error is of course desired. For the ionic liquids used as the solvents in the chemical reactions, of which $\rho = 1500\,\text{kg/m}^3$, $\mu = 0.03\,\text{Pa} \cdot \text{s}$; $\mathcal{D} = 10^{-11}\,\text{m}^2/\text{s}$, the Schmidt number of the fluid system is in the order of magnitude of 10^6 and the diffusion time in a normal channel in width of 200μm is 10^3s. So if the mixing time is to be limited in the order of 10ms, the time ratio $\frac{\tau_\sigma}{\tau_w}$ is 10^{-5}. Referring back to Figure 4-19, the FFM is just about suitable for such a task, while the FNM is definitely competent. With Figure 4-20, the non-dimensional pressure drops for both mixers at the requirement of $\sigma_Y = 0.01$, $\frac{\tau_\sigma}{\tau_w} = 10^{-5}$ can be worked out thereafter as 10^{12} for the FFM and 10^{10} for the FNM. The pressure drop to drive ionic liquids through two mixers will then be 300bar for FFM and 3bar for FNM respectively.

Therefore, it is quite clear that the folding network mixer will be more promising for the purpose of measuring kinetics of chemical reactions using ionic liquids as solvents.

Chapter 5

DESIGN OF THE MICROCHANNEL KINETICS MEASUREMENT SYSTEM

5.1 INTRODUCTION

A microchannel reactor (MCR) system has been designed for the measurement of reaction kinetics in which ionic liquids are used as solvents. To achieve this purpose, three functions are essential:

- Feeding the reactants in different combinations as required;

- Mixing the reactants, controlling the reaction time by starting and stopping the reaction precisely;

- Sampling and conveying the product to the equipment for analysis.

To carry out all these functions, a reaction network for the mixing and reaction is necessary, as well as other auxiliary equipment such as the computer to control the system and connections to an HPLC for product analysis. The design of the whole system involves selection of proper structures and/or appropriate equipment for each function, assembling them, and making them perform well for the kinetics measurement.

The performance of the MCR system relies on control of the chemical reactions and the repeatability of the results. The control of reactions includes the control of the

reaction time as well as other conditions such as the stoichiometry. Comparatively, the control of the reaction time is more important and more difficult.

The usual concept of "reaction time" in the text comprises three aspects:

- The time to mix reactants right before the reaction so that a uniform mixture can be produced for the reaction;

- The real reaction duration;

- The time to mix the mixture with diluent afterwards in order to quench the reaction in time.

But in fact it is very hard to separate the two mixing times before and afterwards from the reaction duration. Hence, the determination of the start and stop of chemical reactions is critical to the kinetics measurement, and it relies on quick mixing processes to both promote and stop the reaction.

The repeatability of the results depends also on the good control of the process. It includes the precise timing and quick responses of the system. In order to communicate well with and thus to control the apparatus, models are needed to help the understanding of processes. Consequently, the design of the MCR system involves development of useful models.

5.2 DESCRIPTION OF APPARATUS

Taking into account the three essential functions and possible necessary equipment, a concept of the MCR system is proposed as in Figure 5-1.

The system carries out tasks from feeding reactants for reaction to analysing the results automatically under computer control. It consists of three parts: the driving part, the reaction zone and the sampling part.
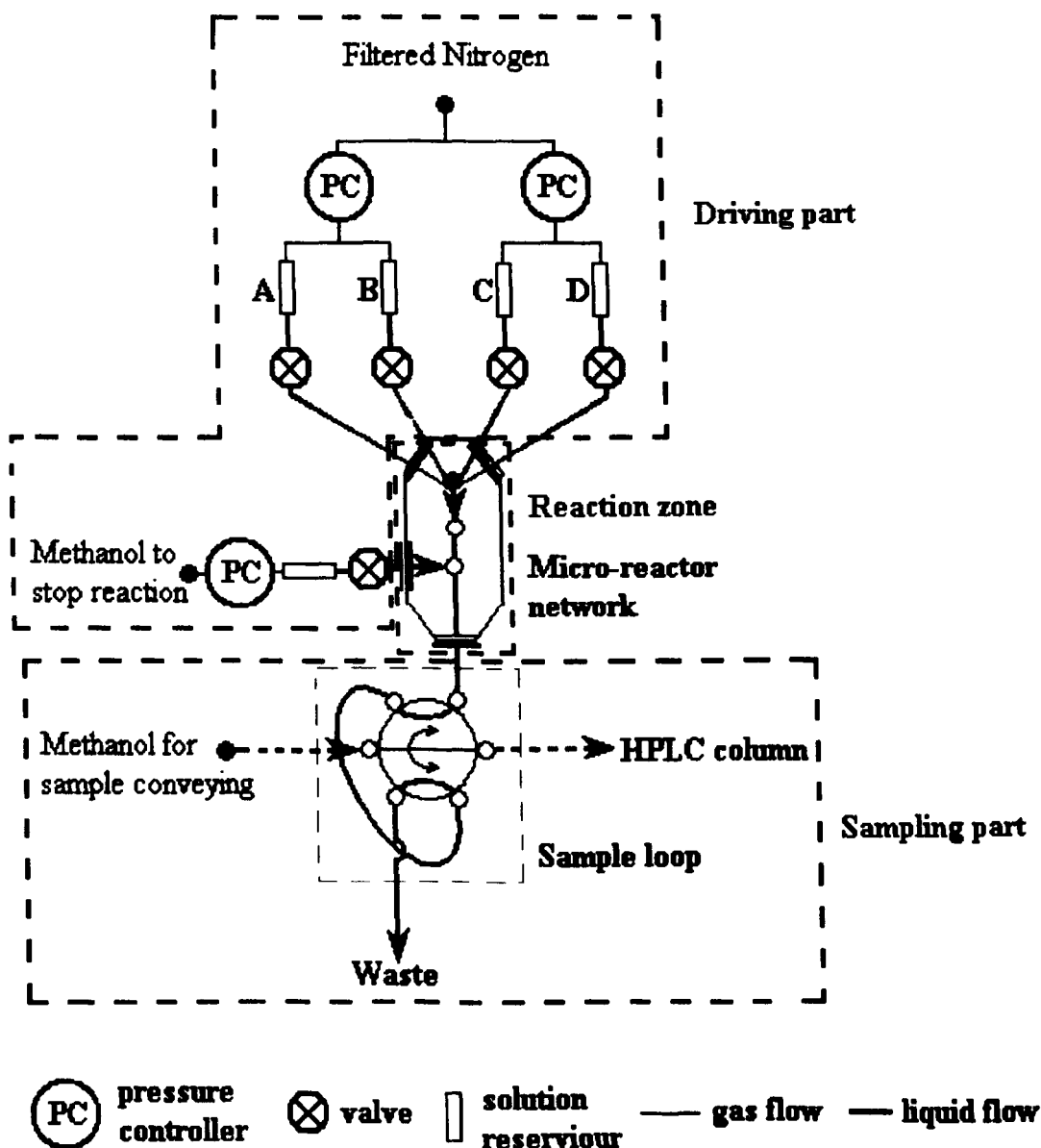
Fig. 5-1 Concept of MCR System

The driving part of the system is responsible for feeding the species and driving the fluid flow. To perform these functions, pressure controllers, valves and connection from reservoirs to the reaction zone are required.

The reaction zone is the core of the system where mixing and reaction take place. By including both the micro-mixer and reaction chamber and channel segments for

connection between parts, the channel network is capable of carrying out duties such as holding of reactants and quenching of reactions on the small chip.

The sampling part actually is a standard auto-sampling unit that performs the connecting or disconnecting of the sample loop to the HPLC equipment automatically. It consists of three parts: a WellChrom® electrical valve drive K-6, a 6-Port/3-Channel injection and switching valve and a sample loop with known volume. Being able to operate under the computer command, the valve switches to different position, thus the fluid contained in the sample loop is sent either to the analysis column or to the waste beaker at the end of the process.

For the sake of making the reaction stoichiometry changeable, the reactants (A and C) and catalysts (B and D) in the system are stored in separate reservoirs and controlled by respective valves and pressure controllers, as illustrated in Figure 5-1. The process of measuring reaction kinetics carried out in the system is then as follows.

On receipt of signals from the computer, the selected valves open and reactants are forced into the chip in desired combinations. In order to get rid of the residuum from last run, the valves are kept open for a few seconds to flush the chip clean. The mixing of reactants begins immediately as streams meet and keeps going all the way when fluid flows through the mixer. At the same time, reaction happens in places where reactants and catalyst are brought together. The residence time in the mixer is kept around 100ms, which is much shorter than the reaction time control that ranges from many seconds to minutes. The product formed during this mixing stage is thus negligible.

After flushing the chip, all reactant valves close, holding the mixtures stagnant in the reaction chamber for a certain period of time, to allow the reaction to progress.

Afterwards, only one reactant valve opens for a short time, ejecting a small amount of fluid into the diluent stream (i.e. methanol) as a sample from the chamber. The reaction is thus quickly stopped, as the sample is rapidly mixed and diluted with excess methanol. The mixture is then pushed by the methanol stream and conveyed to the HPLC column for analysis.

5.3 DESIGN OF MICROREACTOR NETWORK

In order to measure reaction kinetics on-chip, both mixing and reaction are essential. As a result, the design of the microreactor network includes the determination of the mixers and the reaction network. One thing needs to be made clear here is that there were altogether two versions of reaction network adopted for the kinetics measurement, called Mark I and Mark II design respectively in the current research. Following discussions are based on the work of the Mark I design.

5.3.1 Design of Mixer

As described above, two micro-mixers are required in the MCR system. One is before the reaction chamber, referred to as the "reaction mixer", which is responsible for producing a homogeneous mixture for the reaction. The other is after the reaction chamber, called the "dilution mixer", for mixing of the sample with the diluent to stop the reaction. For both mixers, the quicker the mixing process is, the more accurate the set reaction time will be, and more accurate kinetics measurement can be obtained.

In the previous chapter, various micro-mixers were compared. The conclusion was drawn that the folding network mixer is the most promising choice for the required purpose. Based on this conclusion, further computations were carried out for the design of the mixers, with geometries as given in Figure 5-2.
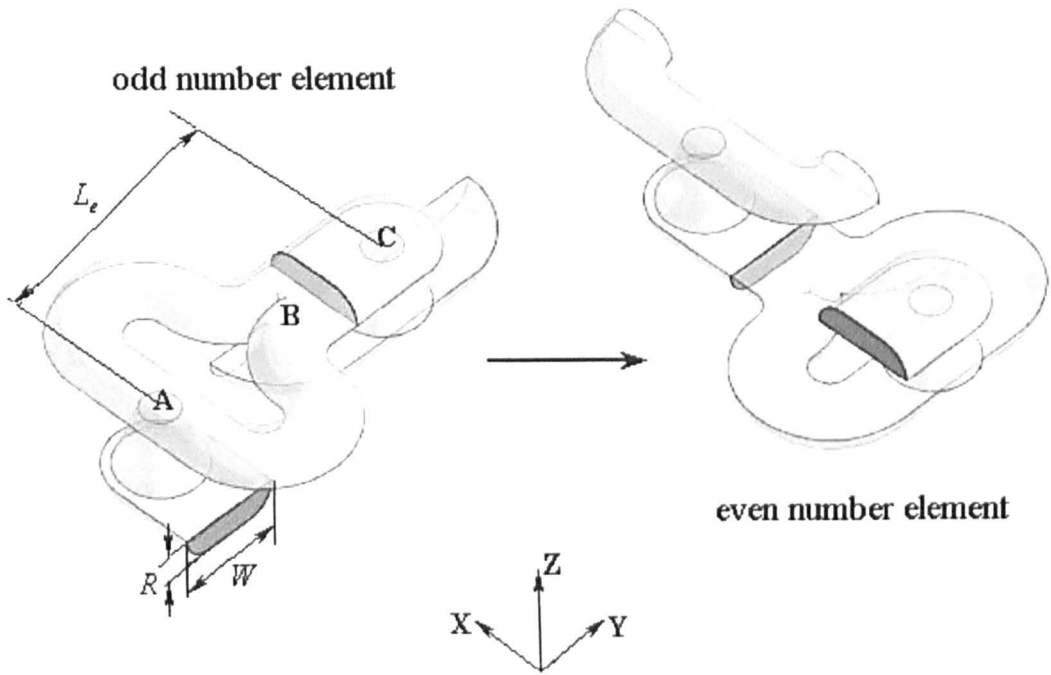
Fig. 5-2 Geometries of FNM's Mixing Elements (Chen *et al.* 2006)

The elements of the computational domains include a splitting part (the curved part) and a recombination part (the straight part), to carry out the split and reuniting of fluid flow. Being both in depth R of 75μm, the width W of the splitting part is 180μm whilst that of the recombination part is 275μm. The total length of the element, L_e, is 720μm. In addition, as the connecting hole tapers from the bottom to the top layer, two computation domains have been created, respectively for element with odd and even numbers, as shown in the Figure above.

The geometry of the splitting channel is designed with particular attention, in order to make the pressure driving two streams along the curved flow path equals to the sum of the flows across the direct distance from the connecting hole to the reuniting position of the fluids ((point A and B respectively in Fig 5-2). With this special design, the

pressure drop across the whole element can then be predicted by Eq.3-29, with the volume flow in the recombination channel and the element length.

Computations have been carried out in collaboration with Dr MacInnes element by element with different geometries as a function of their number. Two-step approaches have been used as in the previous work, which is transferring the result at the outlet surface from one element as the inlet boundary conditions to the next one downstream. After developing geometries as shown in Fig5-2 to generate the velocity profile of developed flow with periodic boundary condition, two dark grey shadow in Figure 5-2 have been determined as the two surfaces of inlet and outlet of each element. In order to prevent the solution at the outlet surface from being affected by the outlet boundary conditions, the surface has to be taken at two channel widths upstream of the connecting holes because, as indicated by Eq.(3-24), the transient effect of flow developing process is limited within one channel width when $Re \leq 10$ ($Re \approx 1$ at this situation). Consequently, the inlet has to be extended as well to the same position of the tail of the upstream element to ensure the data is being transferred correctly (Chen *et al.* 2006).

Computation for the design of the mixer was carried out, for a few cases with coarse grids and at low Peclet numbers due to the limited computer resources. By computing six elements at $Pe = 100$ and ten elements at $Pe = 1000$, an exponential decay was found in σ_Y with the element numbers (as shown in Figure 5-3). An expression was then successfully put forward to fit data points at these two conditions (MacInnes and Allen 2005):

$$\frac{\sigma_Y}{\sigma_{Y_0}} = \exp\left[-\frac{\alpha k}{\ln(Pe) + \zeta}\right]$$
(5-1)

where α, ζ and σ_{Y_0} are all constants, with values as given in Table 5-1 (Chen *et al.* 2006).
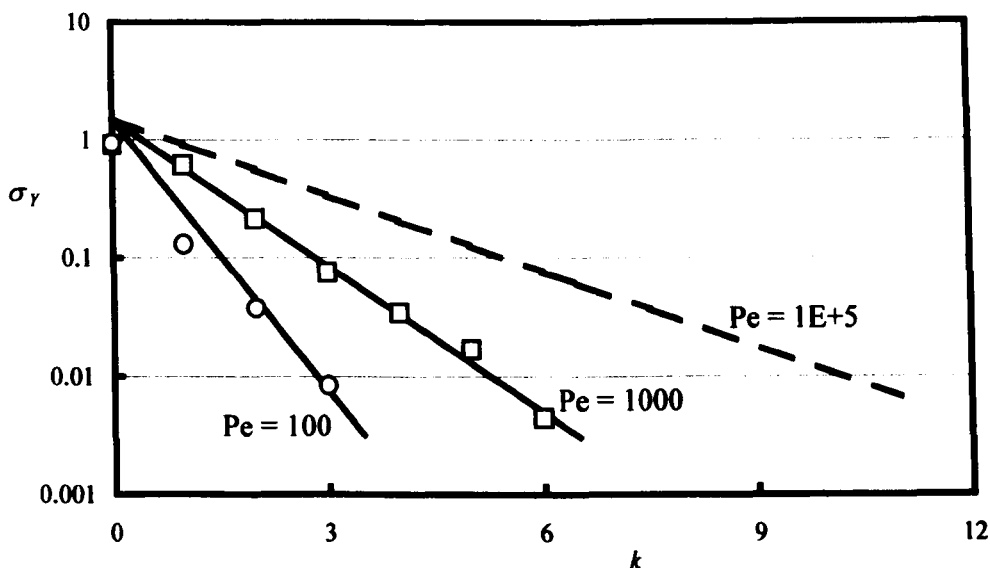
Fig. 5-3 σ_Y **Changing as a Function of Element Numbers** k

Table 5-1 Values of Constants in Exponential Decay Fitting Law

Parameter	Value
α	4.73
σ_{Y_0}	1.49
ζ	1.92

The expression (5-1) was thereafter used for the scale-up prediction of mixing process at high Peclet number. With the values of the constants as given in Table 5-1, only 11 mixing elements were estimated to be needed to achieve $\sigma_Y \leq 1\%$ at $Pe = 10^5$. But, so as to be cautious and also for better arrangement of the mixer in the layout, 13 elements were eventually placed before the reaction chamber. Another 7 elements were put after the chamber to mix the sample with diluent so as to quench the reaction, since the Peclet number in this situation is at the level of 1000 and 6 elements are needed to achieve $\sigma_Y < 1\%$ according to Figure 5-3.

The drawback found in the first design of the mixer is the coarse grid used in the computation. The computational errors were estimated to be within 10% for the computed values of relative standard deviation (MacInnes and Allen 2005). The large errors may lead to over prediction of the mixing process, and the exponential decay deduced from the results may not well represent the real story. As a result, when results are used for the scale-up for high Peclet number, the prediction could be found to produce bigger errors than expected.

5.3.2 Design of Reaction Network

As introduced before, the reaction network is a channel network, in which all the mixing and reaction processes take place. To perform the operations from producing homogeneous mixtures for the reaction, to mixing the sample with diluent to stop the reaction on the chip, the network must include components such as the reactant feeding channels, reaction chamber and dilution channels in addition to the micro-mixer. The design of the reaction network hence is to determine the configurations of each part as well as the layout of the whole network.

The dimensions of the network are determined based on the balance between bigger channel giving lower pressure resistance and limiting the channel width to within the range that has been shown to be able to be fabricated with acceptable tolerance. As a result, the width of 180μm (of which the mask width is 30μm) is used for the reactant feeding channels, because according to previous research experience, the minimum mask width that can be satisfactorily produced is 20μm (Du, 2005). Meanwhile, 275μm is used as the standard channel width for both the micro-mixers and the dilution channel in most parts of the Mark I design, as with this width, the total pressure resistance per unit length of four feeding channels is the same as that of the

wide channel and the mixers, so the pressure drop along the narrow channel can be quickly calculated using the parameters in those channels.

The reaction chamber is the other important part in the network, as it is the platform for chemical reactions and the container of samples. The design considerations for the reaction chamber are based on two aspects, that is, the sample volume for the analysis and the time scale for fluid to pass through it. From the point of view of kinetics measurement, a big chamber is of course preferable, for the sake of providing good samples in reasonable volumes so that an accurate analysis can be achieved. However, a big volume equals a long residence time. Hence, in respect of the time scale, the chamber volume must be limited so that it can filled in a negligibly short time in relation to the reaction durations. Balancing these two points, the decision was made that a volume similar to that of the reaction mixer was used, so that the resistance time in the reaction chamber would be less than 100 milliseconds, which is in a similar scale as that in the reaction mixer. Meanwhile, the design of the reaction chamber was constrained by the layout of the network. Limited by the channel depth of 75μm and the volume around 0.32μl (that is the volume of reaction mixer in the Mark I MCR system), the width of the chamber has to be expanded to increase the volume and the length is fixed by the distance between the end of the reaction mixer and the joint before the dilution mixer. Consequently, the reaction chamber of Mark I design is 1mm wide, 5mm long, in a shape of wide pan and having a volume of 0.36μl.

As shown in Figure 5-4, the final layout design of the reaction network sent for manufacture by the Micronit® (the Netherlands) includes:

1) Four reactant feeding channels (A)

2) One reaction mixer (B) and one dilution mixer (D)

3) One reaction chamber (C)

4) Dilution channels, which include the diluent feeding channel (E) and the mixture outlet channel (F)
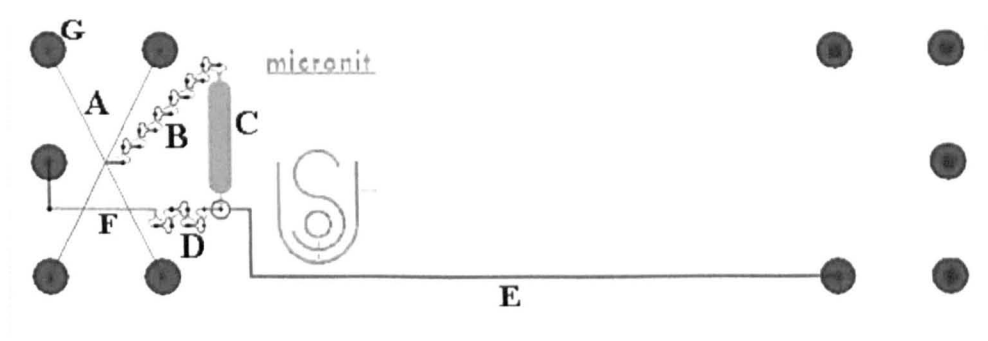
5) Feeding/outlet ports (G)

Fig. 5-4 Layout of Reaction Network

(A. Reactant feeding channels; B. Reaction mixer; C. Reaction chamber; D. Dilution mixer; E. Diluent feeding channel; F. Mixture outlet channel; G. Feeding/outlet ports. Dimensions are given in detail in Appendix-2)

The reaction network is constructed in three layers of glass. On the top and bottom layers, channels are fabricated by wet-etching technology, and on the middle layer, tapered holes are made by powder blasting for fluidic interconnection. By this means, the geometry as given in Fig. 5-2 has been brought into reality, where the odd mixing elements of the FNM mixer are made on the bottom layer of the glass, whilst the even number elements are on the top layer, with fluid passing through via connection holes tapering from the bottom to the top. In the same way, other parts of the network are etched on different layers of glass as well. As illustrated in Figure 5-4, parts in colour of light blue are etched on the top layer of the three-layer glass structure, parts in green are fabricated on the bottom layer, the small dots in black are the interconnection holes made on the middle layer, and the holes in dark blue are the feeding or outlet ports

made through the top layer. For all details of dimensions of each part of the network (corresponding to Figure 5-4), please refer to Table 5-2.

Table 5-2 Designed Dimensions of Reaction Network

Label	Name of part	W (μm)	R (μm)	L (cm)
A	Reactant feeding channel	180		0.559
B	Reaction mixer	275	75	0.72 (per element)
D	Dilution mixers			
C	Reaction chamber	1000		0.5
E&F	Dilution channel	275		3.706 (total length)

		Diameter 1 (μm)	Diameter 2 (μm)	Depth (μm)
G	Feeding/outlet ports	1600	600	1100
-	Interconnection holes	100	200	175

5.4 ASSEMBLY OF THE SYSTEM

In order to measure the reaction kinetics, the microchannel reactor system requires some auxiliary equipment for the control of the fluid flow as well as the sampling and analysis of chemical reactions. Thus, besides the reaction network, the system also includes pressure controllers, valves and the auto-sample unit. A microreactor system corresponding to the concept as described at the beginning of the chapter (Figure 5-1) has been then set up and assembled on the stand, as shown in Figure 5-5.

The criterion for selection of these devices is their quick response to electronic signals. Aiming to reduce the error in the reaction time as much as possible, the response times of the selected equipment are limited to be within one second.
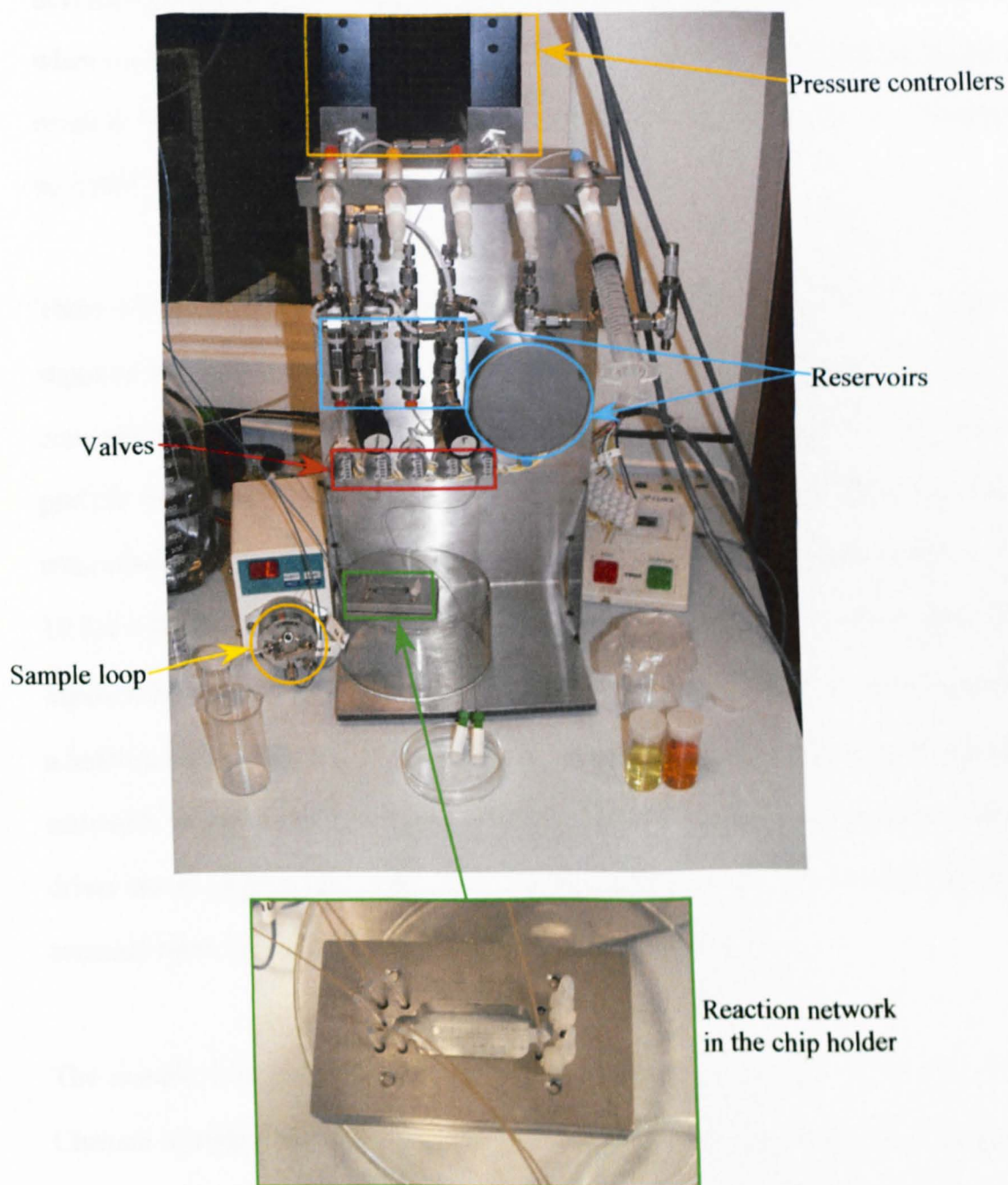
Fig. 5-5 Assembled MCR System

The pressure controller is a product from Brooks Instrument® (the Netherlands). Integrating an electric pressure transducer, a control valve and associated conditioning and control electronics into a compact unit, the controller provides an accuracy of ±0.5% of full scale in the control of either downstream or upstream pressure. More

importantly, the pressure can be built up in a time of 0.5 to 5 seconds, and the deviation between repeated operations is only 0.1% of full range of the controller. So when operated in a reasonable range, for example at half of the full scale, the error resulted in the pressure supplying will be about 1%, which can be satisfactorily accepted as an uncertainty in practice.

There are all-together five valves used in the MCR system. All these valves are supplied by Nresearch Inc[®], together with CoolDrive[™] valve driver from the same company. Functioning under the forces produced by a solenoid and a spring, the valves provide simple on/off operations, which can respond in 5-20/5-30 milliseconds respectively. More importantly, the valve also has small internal volume, that is, 19.7µl between inlet and outlet ports (A and B in Figure 5-6 (Nresearch 2006)). Meanwhile, another advantage of the valves is that the CoolDrive[™] driver circuit uses a holding voltage that can be automatically achieved within 150ms after the solenoid is activated. As the holding voltage applied is only 1/3 of that to activate the valves, the driver circuit prolongs the life of valves because less heat will be produced to hold the solenoid open, thus over-heating problems can be eliminated.

The sample loop unit includes a WellChrom electrical valve drive K-6, 6-Port/3-Channel injection and switching valve and a sample loop in volume of 20µl (the drive and the vale as shown in Figure 5-7, (Knauer 2006). Controlled by external software, the unit can be easily integrated into HPLC system and two operations, i.e., injection and loading, can be performed and indicated on the LCD display of the drive. As shown in the figure, the "L" means the state of loading and the "I" indicates the state of injection. The sample unit will stay at "loading" state for most of the time, during which the sample loop is disconnected from the HPLC analysis and fluid stream is led to the waste. When injection begins, with a capital "I" appearing on the LCD screen, the valve switches to the injection position, connecting the sample loop and leading the

fluid contained to the HPLC analytical column for analysis. The time for valve to switch from port to port is less than 150ms, as introduced by the supplier (Knauer 2006).
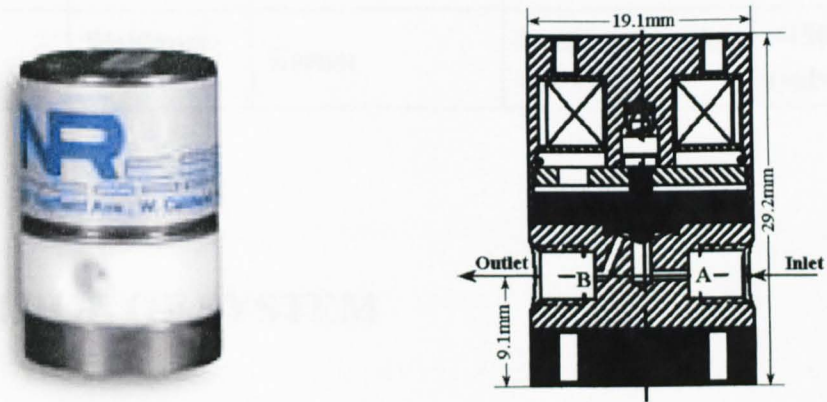
(a) Picture of valve   (b) Section plane of valve (Nresearch 2006)
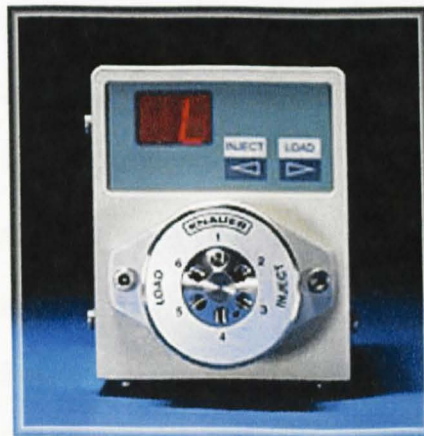
Fig.5-6 Schematic of Valve

Fig.5-7 Auto-sampling Valve and Drive (Knauer 2006)

Details of the selected devices are summarized in Table 5-3.

Table 5-3 Details of Devices in MCR System

Apparatus	Model	Supplier	Range	Response time
Pressure controller	5866 series	Brook Instrument	0 – 10 bar	0.05–5 seconds
Valve	161D5Xxx	Nresearch Ltd	On-off operation	5–20ms for ON; 5–30ms for OFF
Sample unit	Wellkrom K-6	Knauer	Loading-injection operation	<150ms (valve switching)

5.5 CONTROL OF SYSTEM

In order to avoid any confusion in the concept, three terms, i.e. "measurement", "experiment" and "campaign", need to be defined and distinguished before further introduction to be made on the control of the microreactor system. The meanings of these words in text about reaction kinetics measurement are:

- Measurement— the action to measure single parameter, such as pressure, temperature, and mass etc. In particular, in the "kinetics measurement", it means to obtain the species composition of reaction mixture.

- Experiment— several measurements taken to obtain the yield of chemical reaction over certain time.

- Campaign— the action of carrying out a sequence of experiments, so that the changing of yield of chemical reaction versus time can be obtained, with which the kinetics can hence be studied.

5.5.1 Control Programme

To make an accurate measurement of reaction kinetics, control of the MCR system is very important. Feeding the species, holding the fluids for reaction and conveying the

samples for analysis must all take place in the correct order. Moreover, the timing must be accurate, changing with the reaction duration in each experiment.

As described above, there are three processes in each kinetics measurement. According to the time sequence of a specific experiment, these processes and the operations included are:

1) Flushing process: all valves open, species are fed into the network and fluid flows through the chip.

2) Reaction process: valves for reactants close and mixtures are held in the reaction chamber; the valve for diluent opens. For short reaction time ($\tau_R \leq \tau_P$), the pressure is maintained during the process. However, if the reaction time is long ($\tau_R > \tau_P$), the pressure is brought down first, reducing those for reagent reservoirs to zero whilst keeping the one over the diluent reservoir at a very low level. The pressure is then gently brought back again when it approaches the end of the reaction time. The purpose of decreasing the pressure during the long reaction period is mainly to reduce consumption of diluent by keep it flow at very low rate to well clean the residua off the channel. Consideration has also been given on avoiding the compressed nitrogen gas diffusing into liquids thus causing methanol and reagent solution to be saturated with nitrogen. However, due to the low diffusivity of ionic liquids and the big dimension of the diluent reservoir (6cm in diameter, with a volume of 100ml), the saturation process will take much longer than the duration of experiments, hence this factor is of less concern.

3) Sampling process: only one valve of the reactants opens for very short time, ejecting the sample from the reaction chamber; the diluent valve opens and pressure is applied, to mix the diluent with the sample, stopping the reaction and conveying the sample to the analysis unit. A signal is then sent to the

sampling unit. With the valve automatically switching to "injection" position, the sample is pushed into the analysis column of HPLC.

The time sequence of the processes and corresponding operation is illustrated in Figure 5-8. All the time scales appearing in the figure are defined as following:

τ_P — Pressure build-up time, the time allowing pressure to achieve the stable state at the set level.

τ_F — Flushing time, the time for all fluid streams to flow through the system, thus to clean the residua of last measurement.

τ_R — Reaction time, the period between the point when the fluid flow is stopped to hold the mixture in the reaction chamber and when one reactant valve opens to push the reaction mixture out of the chamber.

τ_E — Ejection time, the time for one reactant valve to stay opening soon after the reaction time is due, in order to push part of the reaction mixture out of the reaction chamber as a sample.

τ_S — Sample delay time, the time interval between the points when the sample starts to be ejected from the reaction chamber and when the sample loop is signalled for injection to convey the captured sample into flow path of the HPLC column.

τ_L — Loop opening time, the time for the injection/switching valve stays at the "Injection" state before it switches back to the "Loading" state.
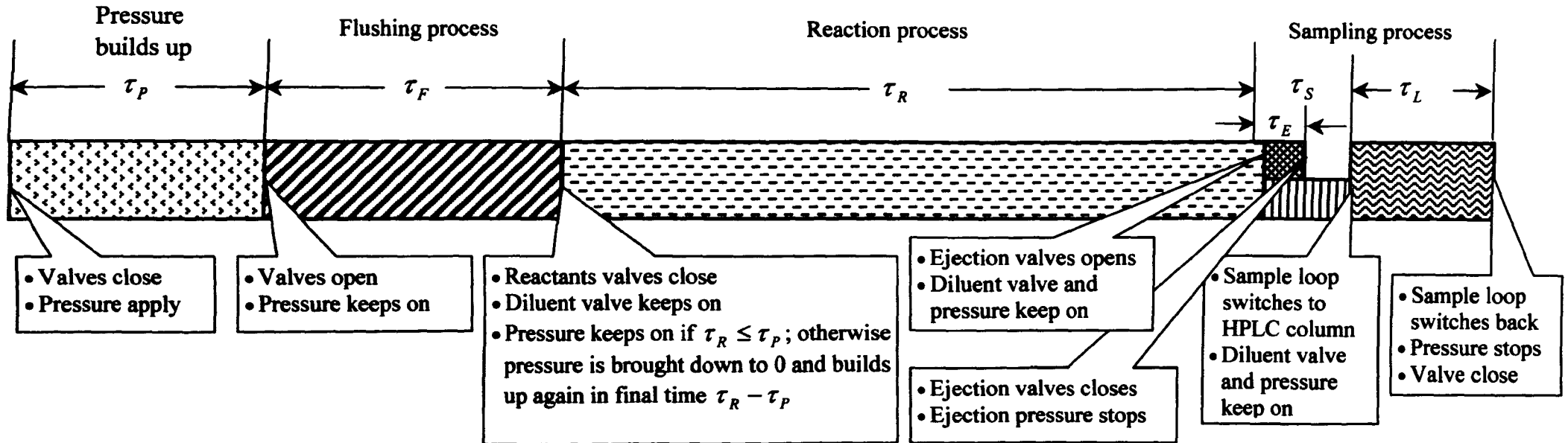
Fig.5-8 Time Sequence and Operation of System Control

To measure the reaction kinetics, a Labview programme has been developed to control the time scale for each process (contribution from Dr. Bown. For programme code, please see appendix). Communication interfaces have also been developed to input information and monitor the progress. Figure 5-9 illustrates the interface for the input of the operating conditions. Variables can be set all in this interface, such as the numbers of experiments to be made, driving pressure for reactants and diluent (P_r and P_m), and time scales including the flushing time τ_F, reaction time τ_R, ejection time τ_E, sampling delay time τ_S and the time for the loop opening to the HPLC column τ_L for each measurement. With all this information, a campaign will then be carried out automatically under the control of the computer, with reactions, sampling and analysis occurring in the MCR system at the design conditions.
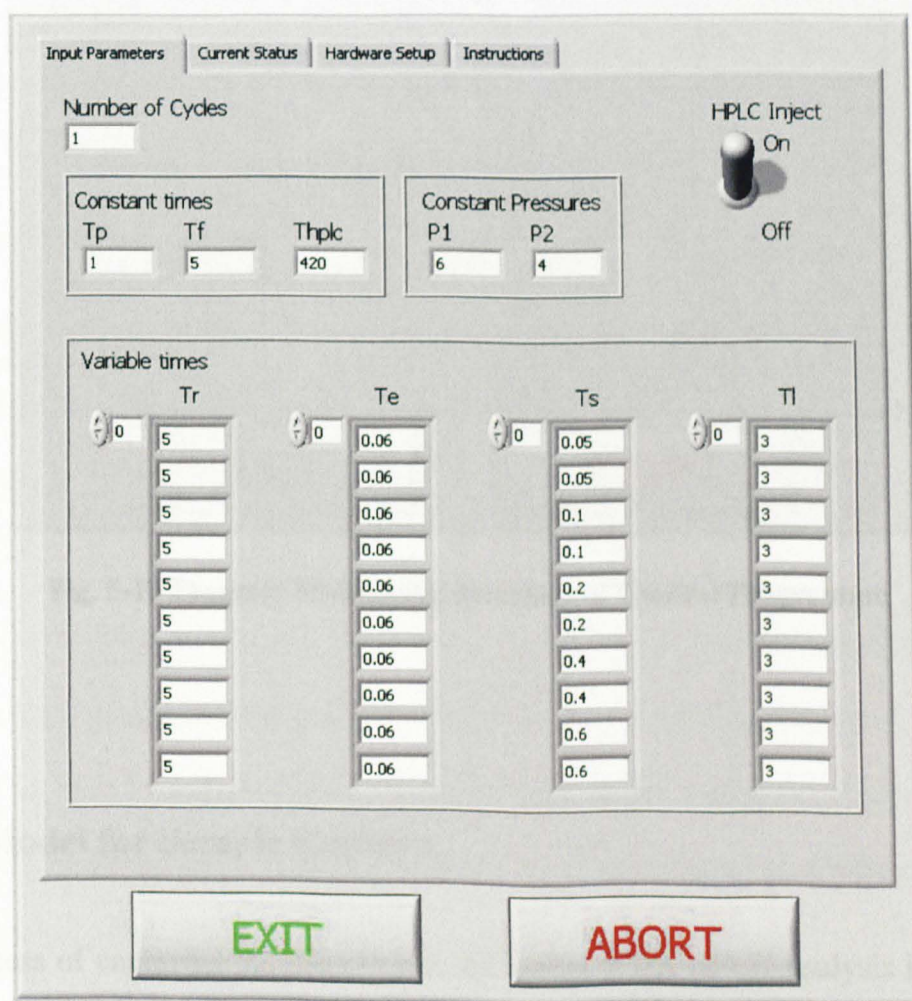
Fig. 5-9 Data Input Interface of Control Programme

Figure 5-10 is the monitoring interface of the control programmes. Besides the settings of the experiment in progress, it also gives the current pressure applied as well as how many experiments left to be made.
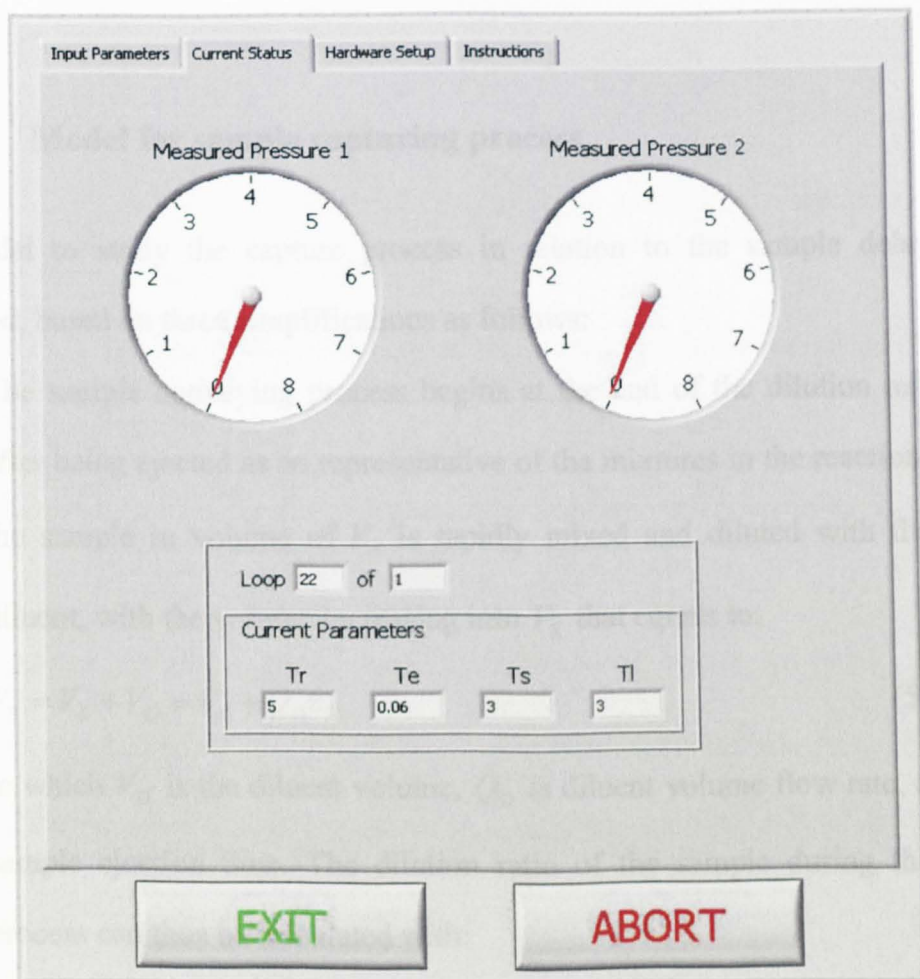

Fig. 5-10 Progress Monitoring Interface of Control Programme

5.5.2 Model for Sample Capture

The process of capturing the sample and delivering it for HPLC analysis involves an important parameter, that is, the sampling delay time τ_S. At different values of τ_S,

different parts of the sample slug are captured in the loop; or in other words, different volume fractions of the diluted sample are obtained. In order to understand how the capture efficiency of the sample loop varies with the sampling delay time, a two-dimensional model has been developed, helping to determine the optimum operation time of the sample loop so that the maximum sample can be captured for the HPLC analysis.

5.5.2.1   Model for sample capturing process

The model to study the capture process in relation to the sample delay time is developed, based on three simplifications as follows:

1) The sample conveying process begins at the end of the dilution mixer. Soon after being ejected as an representative of the mixtures in the reaction chamber, the sample in volume of V_E is rapidly mixed and diluted with the head-on diluent, with the volume increasing into V_S that equals to:

$$V_S = V_E + V_D = V_E + Q_D \tau_E \qquad (5\text{-}2)$$

in which V_D is the diluent volume, Q_D is diluent volume flow rate, and τ_E the sample ejection time. The dilution ratio of the sample during this ejection process can thus be calculated with:

$$DR_E = V_S / V_E = 1 + Q_D \tau_E / V_E \qquad (5\text{-}3)$$

2) During the process that the sample V_S is conveyed to the sample loop, the diffusion effects between the sample and the diluent are ignored. Therefore, when the fluid flow through all the passages, the sample can be regarded as being sandwiched by layers of diluent and in the typical parabolic shape of the fully developed laminar flow.

3) Although the dimensions of the tubing in the system vary from 275μm for the dilution channel to about 650μm for the tubing of the sample loop, all the

sections of the flow passages in the model are considered in the same circular cross section of radius of R_0. In order to preserve the volume so that the residence time in each part will remain the same, the section length then has to be adjusted. Referred as effective length L_i^*, it can be worked out by the actual dimensions of the passage as:

$$L_i^* = L_i \left(\frac{R_i}{R_0} \right)^2 \qquad (5\text{-}4)$$

As shown in Figure 5-11, there are altogether three passages for the sample to pass through on the way being conveyed:

1) The passage leading from the end of the dilution mixer to the sample loop V_P;

2) The sample loop V_L;

3) The passage from the end of the sample loop leading to the outlet V_O.

Concerning the sample capturing, only the sections V_P and V_L are relative and only the volume trapped in V_L can be sent as a value sample for the analysis. The effective lengths of the two sections are respectively L_P and L_L, defined slightly differently as:

$$L_P = \frac{V_P}{\pi R_0^2}, \quad L_L = \frac{V_P + V_L}{\pi R_0^2} \qquad (5\text{-}5)$$

The other effective lengths used in the model are the length of the parabola of the sample in their different stages. As illustrated in Figure 5-11, these variables are:

L_0 — The imagined effective length of the sample parabola in volume of V_S at the end of the dilution mixer;

L_F — The effective distance that the front of the sample parabola has travelled in the flow passage;

L_B — The effective distance that the back of the sample parabola has travelled in the flow passage;
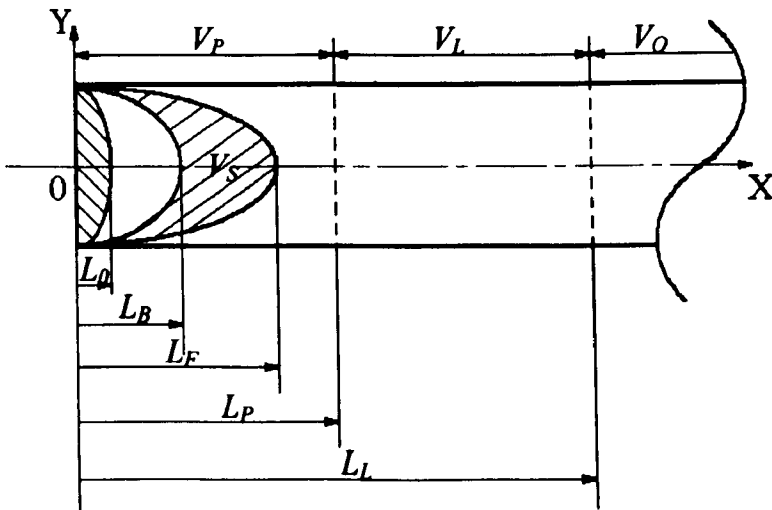

Fig. 5-11 Schematic of Flow Passages for a Sample Ejected to Pass Through

Then depending on the time when the front or the back of the sample parabola reaches and leaves the sample loop respectively, the process of the sample passing through and being captured by the sample loop can be reduced to four cases in the model (as shown in Figure 5-12):

a) $L_B \leq L_P$, $L_P \leq L_F < L_L$: The front part of the sample is in the sample loop while the back tip of the sample parabola is still outside of the sample loop.

b) $L_P < L_B$, $L_F \leq L_L$: Both the front and the back tips of the sample parabola is inside the sample loop.

c) $L_P < L_B \leq L_L$, $L_L < L_F$: The back part of the sample is in the sample loop, however, the front tip of the parabola has gone beyond the sample loop.

d) $L_L < L_B$: Both the front and the back tips of the sample parabola have left, so that only the tail of the sample still resides in the sample loop.
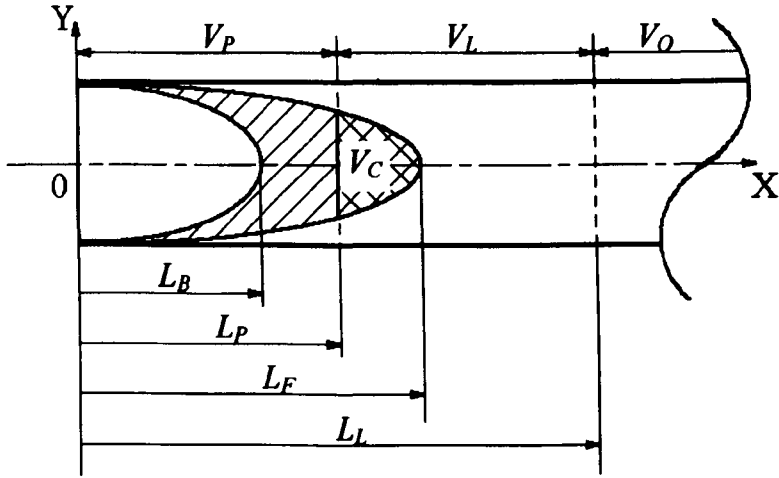
a) $L_B \leq L_P,\ L_P \leq L_F < L_L$
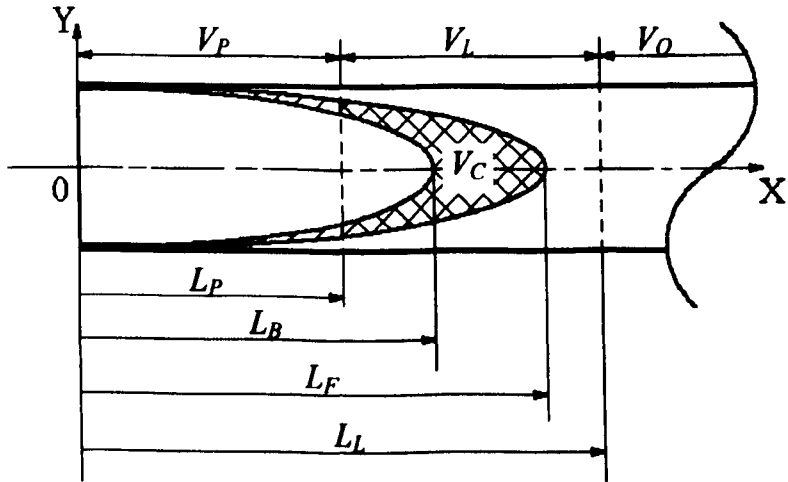
b) $L_P < L_B,\ L_F \leq L_L$
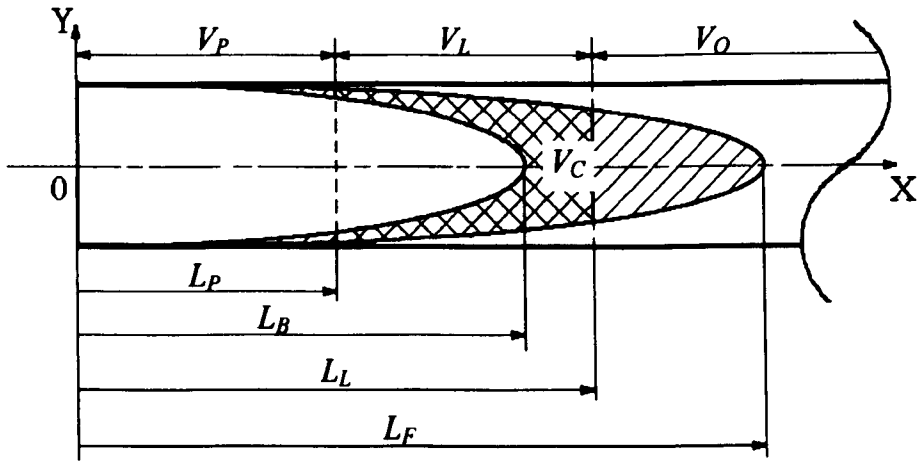
c) $L_P < L_B \leq L_L$, $L_L < L_F$,
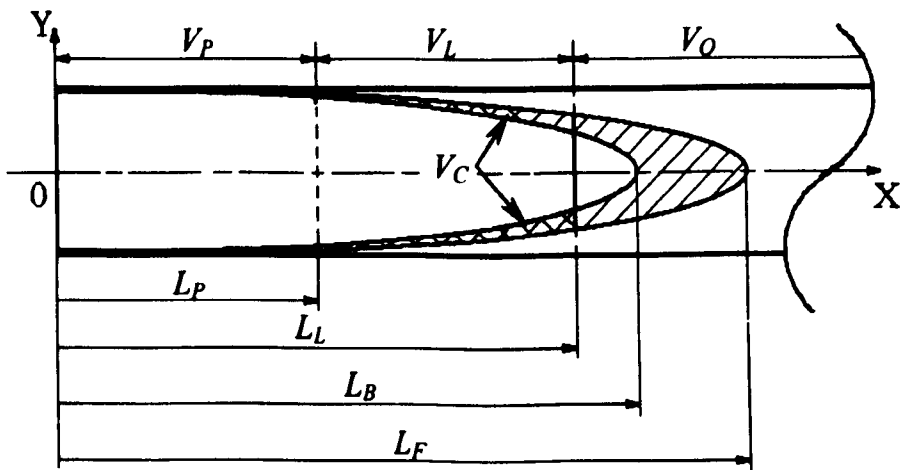
d) $L_L < L_B$

Fig. 5-12 Four Cases for Valid Sample to Be Captured in Sample Loop

A variable called "the capture fraction" f_C is used in the model to assess the capture efficiency of the sample loop. In theory, it is the ratio of the species representative volume captured by the sample loop to that ejected from the reaction chamber, i.e.:

$$f_C = V_{RC} / V_E \tag{5-6}$$

133

But as in the model, the sample conveying process is considered to begin after species are well mixed and diluted through mixer, a practical definition in terms of the diluted sample volume V_S is used instead, given as following:

$$f_C = V_C / V_S \tag{5-7}$$

where:

$$V_C = V_{EC} DR_E \tag{5-8}$$

To solve for the capture fraction, the volume of the sample within the loop must be determined under the condition of each case introduced above. Since only the part in the loop can be conveyed for the analysis, the captured volume is then the segment of the sandwiched sample intersected by the sample loop, namely:

$$V_C = V(front\ parabola\ in\ sample\ loop)$$
$$- V(back\ parabola\ in\ sample\ loop) \tag{5-9}$$
$$= \int_{L_F}^{\min(L_F, L_L)} \pi y^2 dx_F - \int_{L_F}^{\min(L_B, L_L)} \pi y^2 dx_B$$

As for laminar flow in a tube, the velocity profile in a coordinate as shown in Figure 5-12 is:

$$u = u_{max}\left[1 - \left(\frac{y}{R_0}\right)^2\right] \tag{5-10}$$

in which u_{max} is the velocity at the centreline of the flow passage.

In time τ, the distance x that the fluid passes, hence, equals:

$$x = x_{max}\left[1 - \left(\frac{y}{R_0}\right)^2\right] \tag{5-11}$$

where x_{max} is the distance that the centre of the fluid passes.

The equation (5-11) can also be written as:

$$y^2 = R_0^2 \cdot \left(1 - \frac{x}{x_{max}}\right) \qquad (5-12)$$

in which for the front part of the sandwiched sample parabola:

$$x_{max} = L_F \qquad (5-13)$$

and for the back part of the sample parabola:

$$x_{max} = L_B \qquad (5-14)$$

Replacing corresponding variables in Eq.(5-9) with Eq.(5-12) to (5-14), the volume of the diluted sample captured by the sample loop for four cases as illustrated in Figure 5-11 equals to:

$$V_C = \int_{L_p}^{\min(L_F, L_L)} \pi R_0^2 \left(1 - \frac{x}{L_F}\right) \cdot dx$$

$$- \begin{cases} \int_{L_p}^{\min(L_B, L_L)} \pi R_0^2 \left(1 - \frac{x}{L_B}\right) \cdot dx & \text{if } L_B \geq L_P \\ 0 & \text{if } L_B < L_P \end{cases} \qquad (5-15)$$

5.5.2.2   Solutions for capture fraction

The final solution of the capture fraction relies on the equations with which all the effective lengths can be expressed in terms of the known volumes of sections or the parabola that can be easily calculated.

From equation (5-12), the first equation that can be developed is the one to calculate the diluted sample volume:

$$V_S = \int_0^{L_0} \pi y^2 dx = \int_0^{L_0} \pi R_0^2 (1 - \frac{x}{L_0}) dx = \pi R_0^2 L_0 / 2 \qquad (5-16)$$

Therefore the effective length of the diluted sample parabola can be solved in term of its volume by equation:

$$L_0 = 2V_S / \pi R_0^2 \tag{5-17}$$

Meanwhile, since the velocities of the front and the back of the sample parabola travel at the same speed, the imagined effective length also equals:

$$L_0 = L_F - L_B \tag{5-18}$$

In the same way, the distance that the back of the sample parabola travels in the flow passage can be related to the volume flow rate of the diluent Q_D as:

$$Q_D \tau_S = \int_0^{L_B} \pi y^2 dx = \int_0^{L_B} \pi R_0^2 (1 - \frac{x}{L_B}) dx = \pi R_0^2 L_B / 2$$

So:

$$L_B = 2Q_D \tau_S / \pi R_0^2 \tag{5-19}$$

in which τ_S is the sampling delay time.

Rewriting Eq.(5-5), the volume of the two flow passages concerned can be obtained as:

$$V_P = \pi R_0^2 L_P \tag{5-20}$$

$$V_L = \pi R_0^2 (L_L - L_P) \tag{5-21}$$

With equations from (5-17) to (5-21), the sample volume captured in the loop as well as the capture fraction for all four cases described previously can be simplified and solved. For example, for case b where $L_P < L_B$, $L_F \leq L_L$:

$$
\begin{aligned}
V_C &= \int_{L_P}^{L_F} \pi R_0^2 \left(1 - \frac{x}{L_F}\right) dx - \int_{L_P}^{L_B} \pi R_0^2 \left(1 - \frac{x}{L_B}\right) dx \\
&= \pi R_0^2 (L_F - L_B) - \pi R_0^2 \frac{\left(L_F^2 - L_P^2\right)}{2L_F} + \pi R_0^2 \frac{\left(L_B^2 - L_P^2\right)}{2L_B} \\
&= V_S \left(1 - \frac{V_P^2}{4Q_D \tau_S (V_S + Q_D \tau_S)}\right)
\end{aligned}
\tag{5-22}
$$

$$\therefore f_C = V_C/V_S = 1 - \frac{V_P^2}{4Q_D\tau(V_S + Q_D\tau_S)} \tag{5-23}$$

Solutions for all other three cases respectively are:

a) $L_B \le L_P, L_P \le L_F < L_L$:

$$V_C = \frac{(2Q_D\tau_S + 2V_S - V_P)^2}{4(V_S + Q_D\tau_S)} \tag{5-24}$$

$$f_C = \frac{(2Q_D\tau_S + 2V_S - V_P)^2}{4(V_S + Q_D\tau_S)} \Big/ V_S \tag{5-25}$$

c) $L_P < L_B \le L_L, L_F > L_L$:

$$V_C = (V_L + V_P - 2Q_D\tau_S) - \frac{V_L \cdot (2V_P + V_L)}{4(V_S + Q_D\tau_S)} + \frac{4Q_D^2\tau_S^2 - V_P^2}{4Q_D\tau_S} \tag{5-26}$$

$$f_C = (V_L + V_P - 2Q_D\tau_S) - \frac{V_L \cdot (2V_P + V_L)}{4(V_S + Q_D\tau_S)} + \frac{4Q_D^2\tau_S^2 - V_P^2}{4Q_D\tau_S} \Big/ V_S \tag{5-27}$$

d) $L_L < L_B$:

$$V_C = \frac{V_S \cdot V_L \cdot (2V_P + V_L)}{4Q_D\tau_S \cdot (V_S + Q_D\tau_S)} \tag{5-28}$$

$$f_C = \frac{V_L \cdot (2V_P + V_L)}{4Q_D\tau_S \cdot (V_S + Q_D\tau_S)} \tag{5-29}$$

5.5.2.3   Maximum capture fraction

With the model developed above, the capture fraction of the sample loop varying with the sample delay time can then be predicted if the variables including the ejection time, the species volume ejected from the reaction chamber and the diluent volume flow rate are known.

Predictions have been made with the model for five cases. In each case, either the ejected species volume or the diluent flow rate is changed. For example, Case 1 to 3 have the same diluent flow rate but differ in the original sample volume ejected from the reaction chamber; while for Case 4 and 5, they have the same V_E as Case 1 and 3 respectively but different Q_D (as given in Table 5-4).

Table 5-4 Conditions of Cases in Prediction

	V_P (μl)	V_L (μl)	V_E (μl)	V_S (μl)	Q_D (ml/s)	τ_E (s)	DR_E	$f_{C,max}$
Case-1			0.10	0.78	0.013		7.8	0.909
Case-2			0.18	0.96	0.013		5.3	0.908
Case-3	8.302	20	0.24	1.02	0.013	0.06	4.3	0.908
Case-4			0.01	1.0	0.015		10	0.909
Case-5			0.024	0.054	0.005		2.3	0.912

The results of all the cases are plotted in Figure 5-13, in which the curves of Case 1 to 3 are found overlapping with each other, and Case 4 and 5 shifting along the axis of time scale. Considering the differences between the cases, it is apparent that the diluent flow rate determines the conveying speed, and thus the time that it takes for the sample to pass through the loop, while the ejected sample volume has only a trivial effect on the capture efficiency.

Meanwhile, an interesting phenomenon is also found in the plot. Although the conditions of each case varies in V_E or Q_D and so does the shape of the curves, the capture fraction reaches a similar maximum level, which is about 0.91. Moreover, all the maximum f_C occur at the same circumstance, that is the extreme of the second case of the model as illustrated in Figure 5-14.
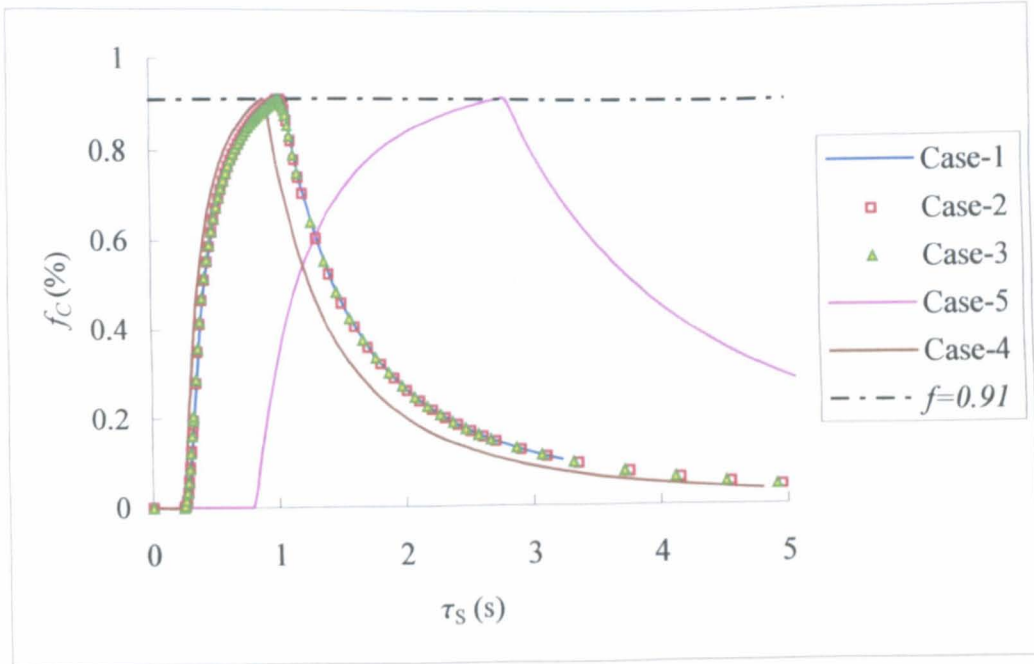
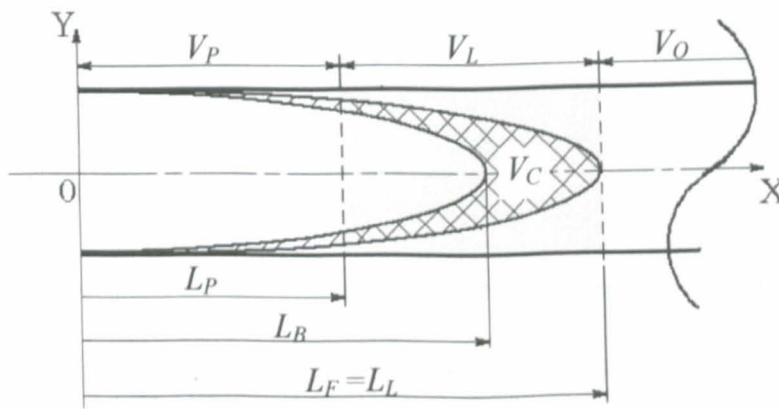**Fig. 5-13 Capture Fraction Changing With Sampling Delay Time**

Fig. 5-14 Circumstance for Maximum f Occurring

As shown in Fig. 5-14, when the front of the sample parabola reaches the end of the loop, a new relation for the effective lengths establishes as:

$$L_F = L_L \tag{5-30}$$

Then the diluent flow rate can be solved by replacing Eq.(5-18) with Eq.(5-19), (5-5) and (5-30) as:

$$Q_D \tau_S = \frac{V_L + V_P - 2V_S}{2}$$

(5-31)

Substituting above formula into Eq.(5-23), the maximum fraction can thus be obtained in the expression in terms of the diluted sample volume, V_S, the volume of the flow passage V_P, and the volume of the sample loop, V_L, as:

$$f_{C,max} = \frac{V_L(V_L - 2V_S) + 2V_P(V_L - V_S)}{(V_P + V_L)(V_P + V_L - 2V_S)}$$

(5-32)

In the developed MCR system Mark I, the volumes of V_P and V_L, are 8.302μl and 20μl respectively, and V_S varies from case to case with the maximum value in the order of 1μl. As V_S is far smaller than the other two parameters, accounting for about 5% or less of V_L, it can be neglected, leaving Eq.(5-32) even simpler as:

$$f_{C,max,s} = \frac{V_L^2 + 2V_P V_L}{(V_P + V_L)^2}$$

(5-33)

From this expression, the simplified $f_{C,max}$ is determined only by the volume of the sample loop and the leading passage from the dilution mixer to the loop, whilst V_S have no effects at all. For the MCR system Mark I, the value of $f_{C,max}$ for all cases is:

$$f_{C,max,s} = 0.914$$

(5-34)

Comparing to the values of cases in Table 8-4, the deviations between $f_{C,max}$ and $f_{C,max,s}$ of the system are all no larger than 0.7%. Therefore ignoring the V_S will not

result in big error in the prediction of $f_{C,max}$ and the simplification can be happily accepted as a quick estimate.

As discussed so far, the model for the sample capturing within the sample loop provides a measure to predict the process, and thus to make decisions on the optimum operation of the process. But more than that, the consistency found in the maximum capture fraction offers the opportunity to capture samples always at the peak time.

5.6 CONCLUSION

In this chapter, the design of the micro-channel reactor system is introduced. Great effort has been made on the design of the mixers, the most difficult and important part of the system. In addition, work has been carried out including deciding the dimensions and layout of the reaction network, selecting and assembling proper auxiliary equipment such as pressure controllers and valves, designing the control interface to communicate with the electronic apparatus, and developing models to understand and predict the sampling process. Since all the design is mainly based on theoretical accounts, the actual performance of the device must be somewhat different because of the accuracy of fabrication and uncertainty of equipment. Therefore tests need to be made on the system to assess its performance before chemical reactions are carried out and kinetics is measured on the chip.

Chapter 6

MEASUREMENT TECHNIQUES

6.1 INTRODUCTION

A range of measurements of parameters required to determine the device performance is necessary for the successful study of chemical kinetics. For example, the composition of a mixture is an important parameter because it provides direct information about changes over the reaction time. Mixture compositions must be obtained both before and after the reaction in order to determine the reaction yield over time. This involves two aspects: the control of fluid flow in the microreactor system and the accuracy of the specific analytical instrument. The chemical composition before the reaction is determined by the flow ratio between feeding streams whilst that of the mixture after reaction is analysed by an HPLC. The resultant errors need to be assessed so that the practical performance of the device can be accurately assessed.

The measurement techniques involved in this research include the determination of the fluid flow in the MCR system, the calibration of the HPLC analytical column, and the characterising of the performance of the micro-mixer. In this chapter, these techniques will be described, together with an assessment of the error they introduced.

6.2 DETERMINATION OF FLUID FLOW

The fluid flow in the microreactor system depends on the pressure applied and the resistance of each segment of the network. With the pressure being regulated by the selected pressure controller, the other factor to affect the flow is the resistance to flow. As indicated by Eq.(3-30), the pressure resistance of a flow passage is proportional to geometric parameters such as width, length and cross-sectional area, as well as the dynamic viscosity. Therefore, for a channel network with a known geometry and controlled pressure conditions, the only unknown variable determining the flow is the viscosity. The method and apparatus developed for viscosity measurement results from the need to obtain information about ionic liquids, the reaction medium quickly and frequently.

The reaction mixture in the MCR system is produced by bringing together up to four different reactant or catalyst solutions and mixing them rapidly on chip. Depending on the flow rate of each feeding stream, the mixture compositions can be calculated with:

$$C_{r,i}Q_{r,i} = \sum_{k=1}^{4} C_{0,i}^{(k)} Q_{0,i}^{(k)} \tag{6-1}$$

in which: $C_{0,i}^{(k)}$ is the original concentration of species i in its corresponding reservoir k; $C_{r,i}$ is the concentration of species i in the mixture in the reaction chamber; $Q_{r,i}$ is the volume flow rate in the reaction chamber; and $Q_{0,i}^{(k)}$ is the flow rate of species i in the feeding passage connected to reservoir k. Since all the leading tubing and the feeding channels of the system are designed to be of the same length and identical cross section, the flow rate of each stream, again as indicated by Eq.(3-30), is a function of the solution viscosities. Thus the species concentrations of the reaction mixtures are functions of the viscosity of each reactant solution as well.

On the other hand, the importance of the fluid viscosity measurement also results from the peculiarities of the ionic liquids. Varying with factors such as temperature, solution concentrations and water content, the viscosities of ionic liquids may change dramatically from 40 times that of water in pure liquids to a level similar to a normal aqueous solution. Therefore, simple measurement of viscosity data for ionic liquids under relevant conditions is of great help in the determination of important experimental parameters.

6.2.1 Theory and Apparatus

The principle of the measurement is based on the theory of fully developed laminar flow. As introduced in Chapter 3, the pressure drop of fluid flow at a low Reynolds number is a function of the volume flow rate as well as the fluid viscosity:

$$\Delta p = f \mu Q \qquad (6\text{-}2)$$

Then by driving the fluid at a known pressure flowing through a passage with regular geometry, viscosity can be deduced from the obtained flow rate using above relation.

To carry out the measurement, a capillary viscometer is employed, of which the coefficient in Eq.(6-2) equals to:

$$f = \frac{128 \Delta s}{\pi D^4} \qquad (6\text{-}3)$$

This method is only suitable for Newtonian fluids. For the ionic liquids used in the research, Bmim[NTf$_2$] is Newtonian. Note that, although pure Emim[NTf2] is reported as a non-Newtonian fluid (Brennan 2006), the behaviour of the actual liquid used in the reaction is Newtonian, because its non-Newtonian behaviour is suppressed by slight water content (<0.02%w/w) and dissolved impurities. Therefore, the method is still applicable.

Figure 6-1 illustrates the apparatus for the viscosity measurement. It consists of a stainless steel reservoir of volume 2ml for the specimen and a glass capillary with a diameter of 150μm (ID) and length of 15mm. In order to maintain the temperature at the set level during the measurement, both the reservoir and the capillary are submerged in a water bath and insulated with a Styrofoam container, which slows down the heat loss and brings the interior temperature towards a uniform level in a short time. A PTFE tube of diameter 800μm (ID) and length 25cm is used as an extension of the glass capillary to the collection vial on the balance. To further reduce the heat loss on the way to the vial, the transfer tubing is sheathed inside another nylon tube.
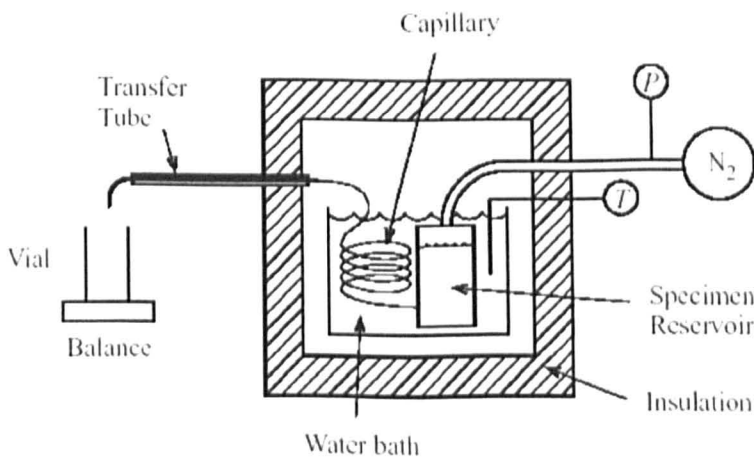
(a) Schematic diagram of apparatus (Shaw et al. 2005)
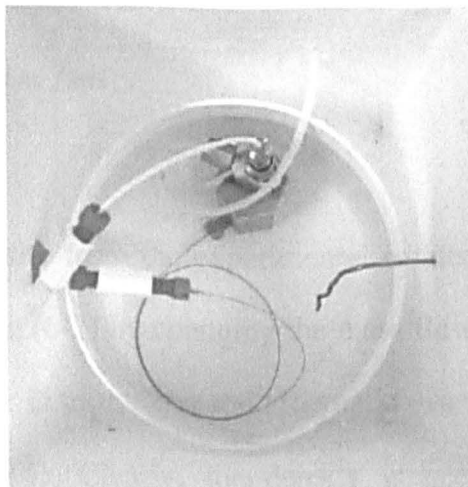
(b) View inside the insulation container
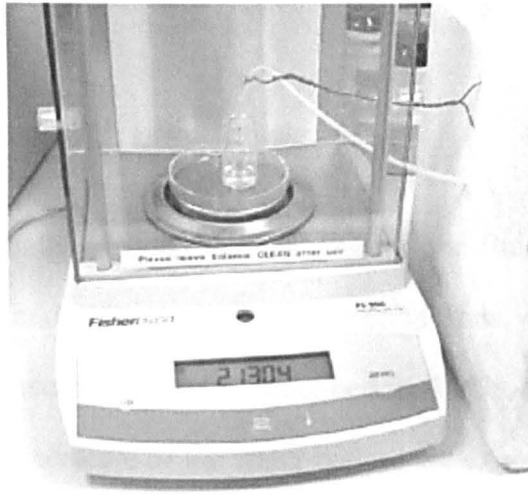
(c) Transfer tubing reaching to the balance

Fig. 6-1. Experimental Apparatus for Viscosity Measurement

The temperature is measured by a 1.5 mm diameter stainless steel-clad thermocouple that is also immersed in the bath. Compressed nitrogen is supplied through an in-line filter and controlled by a regulator to produce the driving pressure for the fluid flow. Drops of liquid are collected in the vial and weighed on an analytical balance. Both the temperature and mass data are accessed and recorded by a computer every second.

Since it is the mass flow rate, $\dot{m}$, to be measured with this apparatus, the method actually determines the kinematic viscosity rather than the dynamic instead. The relation between them can be deduced from Eq.(6-2) as:

$$\Delta p = f\mu Q = f\frac{\mu}{\rho}\dot{m} = f v \dot{m} \tag{6-4}$$

To get the dynamic viscosity from the experimental results, data can be processed in two ways. One is to use Eq.(6-2) by changing the mass flow rate into the volume flow rate beforehand. The other is to transfer the kinematic viscosity into the dynamic one afterwards through Eq.(6-4). Clearly, the density is needed in both cases. More importantly, the change of density with temperature must be taken into account.

6.2.2 Measurement and Error Assessment

The measurement is usually carried out by collecting the fluid mass over a period of time at known pressure and different temperature conditions. As a standard procedure, the operations of the measurement can be described as 4 'A's, that is:

1) Adjusting the temperature of the water bath to the expected level;

2) Allowing a period of about 20 minutes for the equilibration of temperature between the liquids in the reservoir and the water bath;

3) Applying pressure, and allowing another short interval to allow the fluid flow to become steady;

4) Activating the computer program and initializing the balance, to start recording the data of the time, the temperature and the cumulative mass.

The mass flow rate is then the slope of the curve of collected mass versus time.

6.2.2.1   Error in temperature control

The errors of temperature in the experiment derive from two sources, the temperature equilibration between the water bath and the specimen in the reservoir before the measurement; and the temperature variation due to the heat loss during the measurement. Time is crucial in both cases. In the first, a long time is needed in order to achieve the equilibration of temperatures. In the second case, however, a short time is required, to reduce the heat loss during the data-recording period, thus maintaining the temperature with small variations.

In order to find the time needed to achieve a uniform temperature inside the Styrofoam container as well as the rate of heat losses through its lid and walls, the water bath was filled with water and left inside the box for a period of time whilst the temperature was

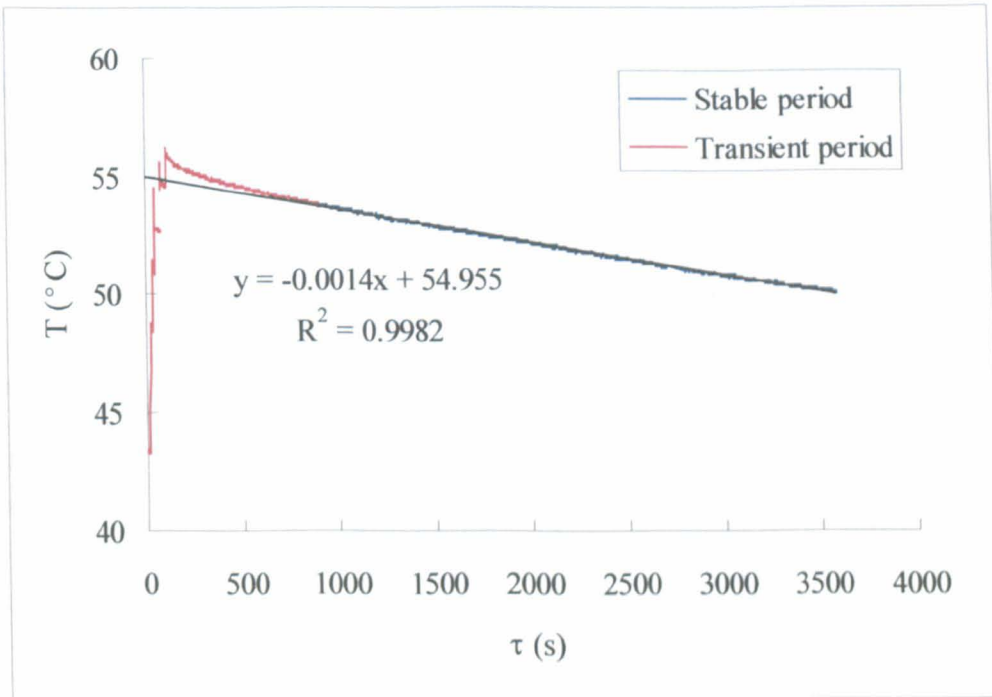recorded. Figure 6-2 gives the measurement results of temperature of water bath changing over time.

Fig. 6-2 Equilibration of Temperature inside the Insulation

According to the behaviour of temperature versus time, the plot shown in Figure 6-2 can be divided into two parts: a transient period and a stable period. In definition, the transient period is the time necessary to equilibrate the temperature. So no measurement should be carried out during this period because the temperature experiences significant changes, especially in the first several minutes. The transient period, estimated from the plot, lasts for about 15 minutes. Thereafter the stable period begins and the temperature drops at the same rate until the end of the experiment. In the viscosity measurement, the practical equilibration time is 20 minutes for the uniformity of temperature, plus another 5 minutes for the developing of steady flow, which therefore proves to be long enough to allow for the transient stage.

As in the experiment, it takes 400 seconds to record 10 data points to determine the flow rate, the temperature keeps changing during this time even when it is in the stable period. In order to assess the error of temperature resulting from the variation in the data-recording process, the variation rate at different temperature level and the changes occurring in the time for data taking were worked out from the experimental results and given in Table 6-1.

Table 6-1 Calculated Variation Rate of Temperature in Stable Period

Difference between ambient and water temperature (°C)	Variation rate (°C/s)	Referred water temperature (°C)	Temperature change in data-recording (°C)	Deviation in temperature (%)
<3	0.0001	25.2	0.04	0.2
3-7	0.0002	28.7	0.08	0.3
7-10	0.0003	32.2	0.12	0.4
10-19	0.0004	38.2	0.16	0.4
19-25	0.0008	45.7	0.32	0.7
25-30	0.0014	51.2	0.56	1.0

Note: average ambient temperature in experiments was 23.7°C.

From the table, it can be easily found that the variation rate increases with the temperature difference between the environment and the water bath, due to the stronger heat transfer and increased heat losses. However, for the temperature range that is of interest in this research, the temperature change during data recording is negligible, since all the deviation can be controlled within ±1%. Moreover, this figure can be further reduced, by taking fewer data points for each flow rate so that experiments can be finished in an even shorter time.

6.2.2.2   Effect of temperature on flow control

The effect of temperature on the flow control also results from the fact that the fluid viscosity, especially for ionic liquids to be measured by the apparatus, can be greatly affected by temperature.

As described above, in the developed apparatus, the leading passage from the specimen reservoir to the vial on the balance consists of two parts: a glass capillary and a Teflon tube. Although only the glass capillary is supposed to be used as the viscometer and most of the pressure drop happens across it, the existence of the Teflon tube will inevitably absorb some driving force, and thus cause some error in the pressure and flow. A parameter called the "pressure fraction" was then defined as in Eq.(6-5) and used in the research, to describe the fraction of the pressure drop over the Teflon tube. Meanwhile, it can be also used to quickly assess the error caused if the pressure drop along the Teflon tube is neglected.

$$\varepsilon = \frac{\Delta p_T}{\Delta p_T + \Delta p_C} \tag{6-5}$$

According to the theory of the viscometer, the definition expression for ε can be further expanded by substituting Eq.(6-2) and (6-3) into Eq. (6-5) to replace the corresponding variables as:

$$\varepsilon = \frac{\Delta p_T}{\Delta p_T + \Delta p_C} = \frac{1}{1 + \dfrac{f_C \mu_C Q}{f_T \mu_T Q}} = \frac{1}{1 + \dfrac{\mu_C}{\mu_T} \dfrac{\Delta s_C}{\Delta s_T} \left(\dfrac{D_T}{D_C} \right)^4} \tag{6-6}$$

where the subscripts of C and T stand for the parameters of the glass capillary and the transferring tube respectively.

As indicated by the above formula, the effect on the pressure fraction along the sections of flow passage can result from two aspects: the viscosity ratio of the fluids

and the geometric ratios including the length ratio and diameter ratio. But as the geometric parameters are usually fixed in a developed apparatus, the fluid viscosity is the more important factor.

Typically, for the designed device as shown in Figure 6-1, by replacing the geometric ratios in Eq.(6-6) with their real numbers, the pressure fraction is then only a function of the ratios of the fluid viscosities.

$$\varepsilon = \frac{1}{1 + \dfrac{\mu_C}{\mu_T} \dfrac{15}{25}\left(\dfrac{800}{150}\right)^4} = \frac{1}{1 + 485.45 \times \dfrac{\mu_C}{\mu_T}} \qquad (6\text{-}7)$$

From Eq.(6-7), the effects of temperature on the pressure and flow are evident. In the apparatus, the glass capillary is kept inside the Styrofoam container whilst the Teflon tube is put outside. Heat loss along the Teflon tube must be more serious than that over the glass capillary, especially when the temperature difference between the specimen and the environment is large. Consequently, the fluid temperature along these two sections must be different. Since the viscosity of ionic liquids can be significantly affected by temperature, different temperature variations could result in different pressure fractions, and thus errors in the control of the fluid flow.

Also from Eq.(6-7), bigger pressure fractions over the Teflon tube results in bigger errors in the pressure when the temperature in the insulation container is much higher than the environment, because greater heat loss occurs during delivery of the specimen to the collection vial and the viscosity of ionic liquids increases along the transferring tube. As the ionic liquids' viscosities may vary from $0.007\,\text{Pa}\cdot\text{s}$ at 90°C to $0.042\,\text{Pa}\cdot\text{s}$ at 20°C (value of Emim(NTf2), measured by Brookfield viscometer at Queen's University Belfast), the largest pressure drop over the Teflon tube estimated by Eq.(6-7) is 1.2% of the total value. Therefore, if this part of effect is ignored, it will result in a

maximum error of 1.2% in the pressure, and thus the same value in the calculation of fluid flow.

However, the situation for measurements of viscosities will be much better than that, because the temperature difference between the environment and the specimen will be normally within 30°C, and the errors caused in the fluid flow will be less than 0.5%, which is considered negligible.

6.2.2.3   Error in data processing of flow rate

During the measurement, as the liquid accumulates at the outlet of the transferring tube until a drop is finally formed and suddenly falls into the vial, the cumulative mass always exhibits a discrete change rather than a continuous curve with the time. Accordingly, two methods were found to obtain the mass flow rate from the experimental data. One is to fit all the data points using the least-square-error criterion; and the other is to fit with the same rule but only one data point (the average or the one in the same position of the data sequence) at each mass level.

Figure 6-3 illustrates the same data being processed in both ways. In Fig.(6-3-(a), all the data points are displayed, and fitted with a linear function by the least-square-error criterion. The slope of the fitted line is then the mass flow rate. In Fig.(6-3-(b)), the same data are processed, but with the second method. In this method, only the last data point at each mass level was selected and fitted. The slope of the line again is the flow rate wanted.
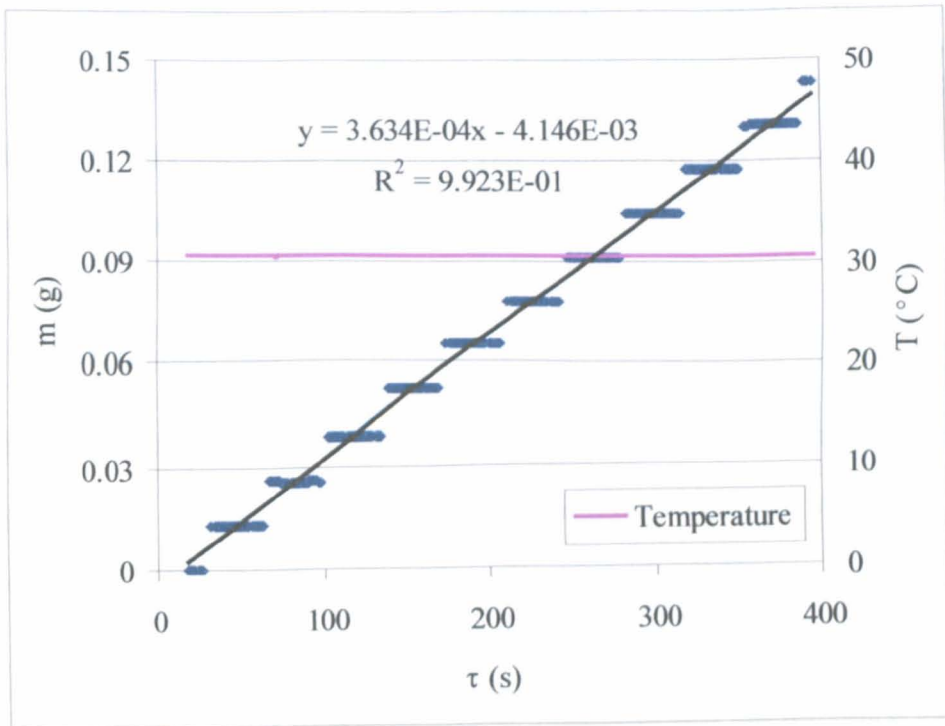
(a) Mass flow rate obtained by fitting all the data points
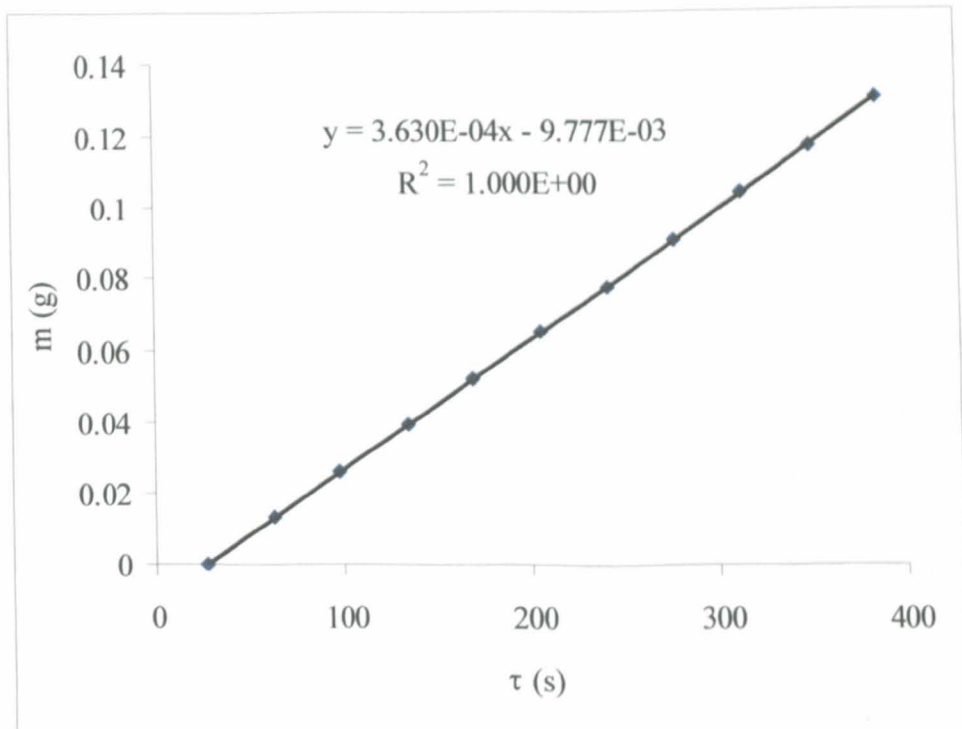
(b) Mass flow rate obtained by fitting the last data points

Fig. 6-3 Determination of Mass Flow Rate in Viscosity Measurement

The deviation between these two methods is found to be negligible. For example, for the case given in the figure, it is only 0.1%. However the second method gave a slightly better fit. Therefore, the mass flow rate required for the viscosity measurement is obtained afterwards by fitting the last point of the collected data at each mass level versus the time.

The method to get the dynamic viscosity is to obtain the kinematic viscosity by replacing the mass flow rate in Eq.(6-4), and changing it into the dynamic viscosity using the corresponding density data. Due to the lack of an instrument conveniently to measure the density variation with temperature, the density of ionic liquids used in the transferring of v into μ has to be assumed as a constant and the reference value is the liquid property at the temperature of 25°C.

The density of ionic liquids is known to change with temperature as well. So the assumption made above will also result in some error in the data processing. However, since the density fortunately changes at a modest rate, the error can be controlled by limiting the temperature of the experiment to be within a small range.

As an example, consider the Emim(NTf2), the ionic liquid that was used as the solvent for the reactions in the kinetics measurement. By plotting densities against temperature over the range of 25-60°C (see Figure 6-4), it can be found that the density changes at a rate of 0.001 g/cm$^3 \cdot$C (The density values were measured using the commercial Anton Paar DMA 4500 density meter at Queen's University, Belfast). The maximum error consequently resulting from the changing rate is then 1.6% for the viscosity measurements (of the reference value, which is 1520 kg/m^3 at 25°C), in which the temperature ranges from 0 to 40°C. But in the experiments carrying out reactions on

chip, the error is limited to be no more than 0.65%, as the ambient temperature in the

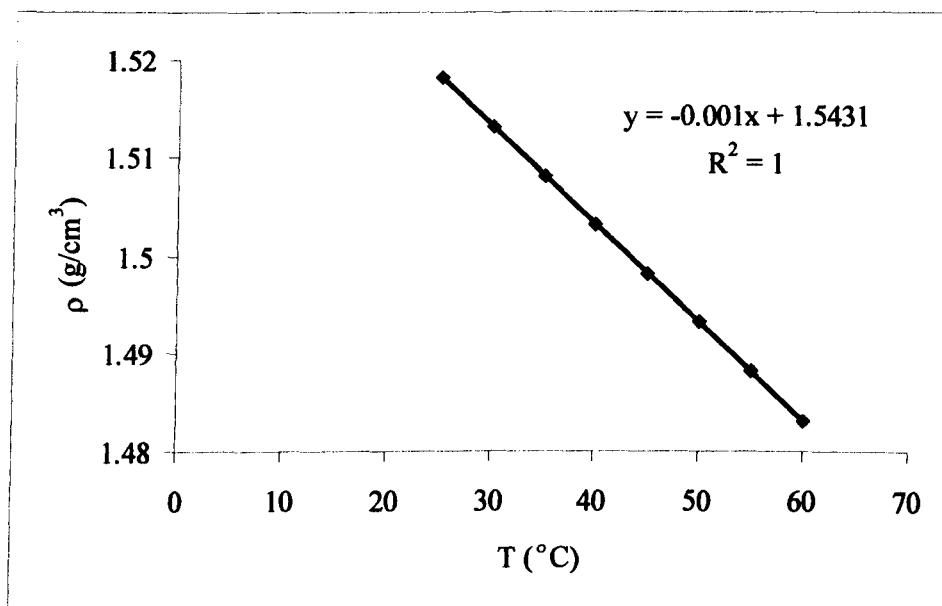lab varies between 18-30°C at most in a day.

Fig. 6-4 Density of Emim(NTf2) Varying with Temperature

6.2.3 Total Error of Measurement

Errors of the viscosity measurement are also limited by the accuracy of other

instruments. For instance, the precision of reading the analytical balance is 0.1mg, the

thermo couple is believed to have an uncertainty of less than 1% in the temperature

range of interest, and the pressure meter has an uncertainty of 1% of its 2 bar full-scale.

Moreover, the diameter of the glass capillary from different delivery was found, by

direct measurement using a microscope of several cut sections, to have a deviation of

1% (varying from 149 to 152μm, comparing to the specified 150μmID), which thus

results in about 2% in the measurement. With the uncertainty from the capillary

dimension, plus an uncertainty of 1% from the factors of temperature and pressure, and

another 1% from the assumption of uniform density, the total error of the viscosity measurement of ionic liquids is then expected to be in the order of 3%.

As an example, water viscosity has been measured with this method and apparatus as introduced above, and the result has been compared with the data reported in the literature (ThermExcel 2006), in order to further assess the accuracy of the measurement. A constant density of 1000 kg/m^3 was used for the data process to change the kinematic viscosities into dynamic values, and the average recorded ambient temperature was 21.9°C.

Figure 6-5 gives both the measurement results and the value of viscosity reported in literature at similar temperature levels. The biggest error between the two is 3.5%, occurring at the biggest temperature difference (water temperature is 0°C). The figure may seem a little bit high. But as an effective measure for obtaining the viscosities of ionic liquids quickly and conveniently, it is considered acceptable.
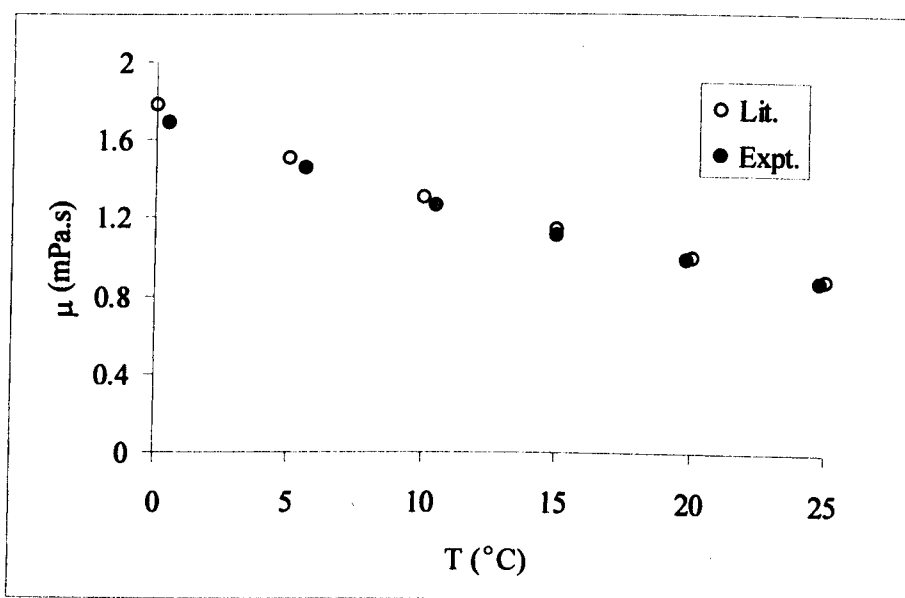
Fig. 6-5 Comparison between Water Viscosity Data from Experiment and Literature

6.2.4 Results

With the apparatus and technique developed, the viscosity of Emim[NTf$_2$], the ionic liquid that is used as a solvent for the chemical reactions on the chip, has been measured and compared in different situations.

The first attempt was made to study the effect of the water composition on the viscosity of ionic liquids. In order to compare how the viscosity changes when the ionic liquid is stored, a batch of newly manufactured Emim[NTf2] (Batch-1)was divided into two halves. For one half of the batch, the liquid was further divided, with one part kept dry and the other saturated with distilled water. The viscosities of both samples were then measured with the Brookfield viscometer instrument (carried out by a collaborator at Queen's University, Belfast). At the same time, the other half batch was posted to Sheffield, and the viscosity was measured with the apparatus described above.

The results of the three measurements made on the Emim[NTf$_2$] are plotted in Figure 6-6. For comparison, the viscosity of Emim[NTf$_2$] from a batch (Batch-2 in the figure) received several months earlier was also measured, with data added as the diamonds in the plot. With all the data put together, a fall in liquid viscosity with the water content can be clearly found in the figure.

There are altogether four plots displayed in Figure 6-6, of which the solid and empty circles are the dry and water saturated Emim[NTf$_2$] measured with Brookfield viscometer instrument respectively, the cross is the batch of ionic liquids measured by the developed apparatus upon receiving the delivery (Batch-1 in the figure), and the hyphen is the result of a batch (Batch-2) received several months previously. As illustrated by the plots, the dry ionic liquid exhibits the highest viscosity among the

four results, while the water saturated one gives the lowest value. Between these two

limits are the results of Batch-1 and Batch-2. Moreover, the liquid viscosity of Batch-1

is found to be higher than that of Batch-2 at corresponding temperature points. This is

considered to be due to the equilibration between the ambient vapour and the ionic

liquids over the storage period despite the tight seal of the bottle. It also indicates how

important a quick and accurate viscosity measurement technique is to the kinetics

measurement.
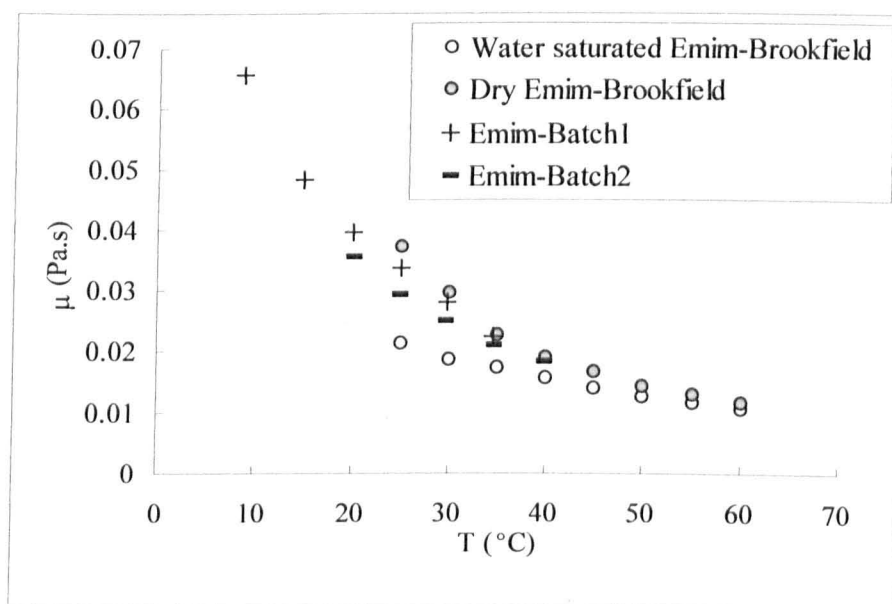
Fig.6-6 Comparison of viscosity measured by Brookfield viscometer and the experimental apparatus

Meanwhile, it is also found that the effect of water content on the ionic liquid's

viscosity decreases with the temperature. For example, the viscosity of the dry

Emim[NTf2] is nearly twice the value of the wet liquid at 25°C, however, their

difference reduces to about 10% when the temperature approaches 60°C. Hence, the

viscosity of ionic liquids seems to be less sensitive to the water level at higher temperatures.

Since the Emim[NTf2] is used as the solvent for the chemical reactions, a question is then raised of how the liquid viscosity is influenced by the concentration of reagent solution. To answer this question, reagents and catalyst were dissolved in the Emim[NTf2] at the concentration as given in Table 6-2, and solution viscosities were measured with the capillary viscometer.

Table 6-2 Concentrations of Solutions in Fig.6-7

	Name of Solute	Concentration (M)
Catalyst solution	Sc	0.00235
Reagents solution	NBA	0.189143
	DHF	0.416124
	Pyrene	0.02068

The measured viscosities of the solutions, together with the pure Emim[NTf2], are plotted in Figure 6-7. From the results, the viscosity of the catalyst solution is found to be quite close to that of the Emim[NTf2], due to the low concentration of the solution. The reagent solution, however, is less viscous than both the pure ionic liquid and the catalyst solution. This is not only because there are three solutes dissolved in the ionic liquid, with two of them at a concentration hundreds times that of the catalyst solution, but also because the added DHF is believed also to play an important role in decreasing the viscosity of the solution. The viscosity of the reagent solution at low temperature (10°C) is about 15% lower than that of the pure Emim[NTf2]. But again, when the temperature increases, the difference becomes less and less conspicuous.

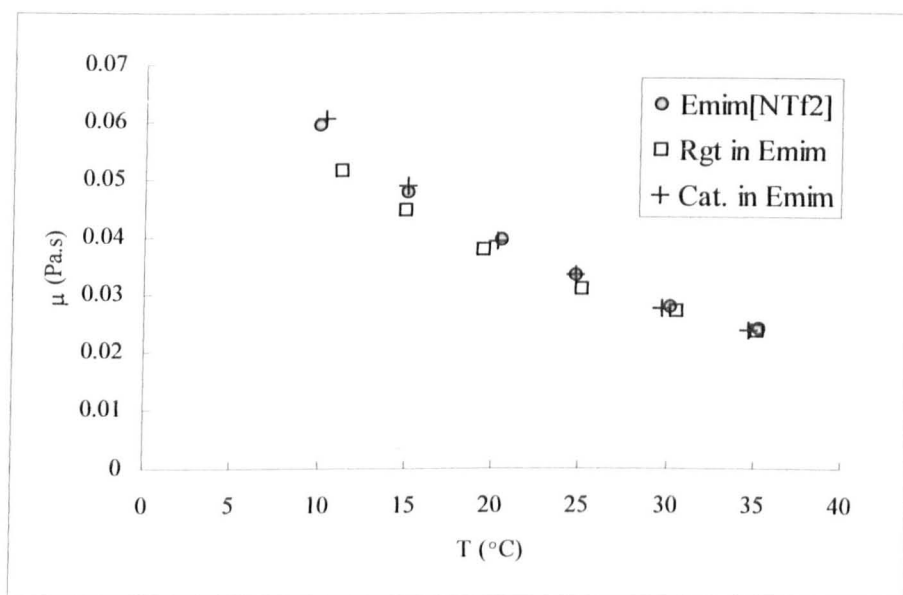When the temperature goes up to over 30°C, the solution viscosities differ less than 2%.

Fig. 6-7 Measured Viscosity of Pure solvent, Catalyst and Reagent solution

6.3 MEASUREMENT OF SPECIES COMPOSITION

The measurement of species composition in the kinetics measurement is achieved with a Varian® HPLC (high performance liquid chromatography) instrument, of which a C18 reserved-phase analytical column is employed for the separation of compounds. A Knauer® injection/switching valve together with a 20μl sample loop is used for the introduction of the sample. The mobile phase used for the analysis is an acetonitrile-water solvent mixed at a volume ratio of 70:30. In addition, a guard column is added to protect the analytical column from the precipitated materials and fine particles in the solvent.

Measuring the species composition means both identifying and quantifying the compounds in the mixture. To achieve these two tasks with the HPLC, a calibration is necessary before any analysis of samples. Two results must be obtained through the calibration work. First, the peak retention time is needed to identify each analyte; and second, the calibration factor (CF) (Meyer 1994) is required to change the peak area of the chromatography into the concentration of species in the actual analysis.

To achieve a good result, two kinds of standard solutions were prepared at different stages of the calibration. To identify the molecule in the chromatography, solutions were prepared by dissolving only one analyte of good purity every time in methanol at a proper concentration. This kind of solution is referred to as the "sole analyte solution" infra in the thesis. Since there is no other chemical presenting in the solution, the peak detected by the instrument no doubt indicates the single analyte in the solution, therefore the retention time (the time that the peak appears) can be used for the identification of the analyte.

Theoretically, the sole analyte solution can be used for quantification purpose as well. But, as all species are mixed and delivered together to the column in the actual analysis process, there might be some interference between the chromatographic results of the analytes. Although it is considered unlikely to happen, utilization of so-called "analyte mixture solutions" has been suggested in order to avoid the potential effect. In the analyte mixture solutions, all analytes are dissolved in the same bulk of methanol, and the concentrations are prepared to cover the range of that to be measured in the experiment. With the solutions being introduced through exactly the same path as experienced by the samples in the analysis process, the analyte is then identified with its known retention time in the chromatography, and its response intensity (peak areas) is recorded corresponding to the concentration. Afterwards, by relating all the response intensities to the series of concentrations of the analyte mixture solutions, a calibration

factor (CF) can be obtained, with the peak area expressed in terms of the analyte's concentration.

As an example, Figure 6-8 is the calibration curve obtained for NBA (N-Benzylideneaniline, 99%, Ardrich) at 224nm wavelength. By repeating the calibration three times with the same series of solutions, good reproducibility can be found in the operation. The maximum deviation among the data points in the plot is estimated to be 1.8%. As a component of the kinetics measurement, the deviation will result in an uncertainty of about 2% in the final results for the reaction data.
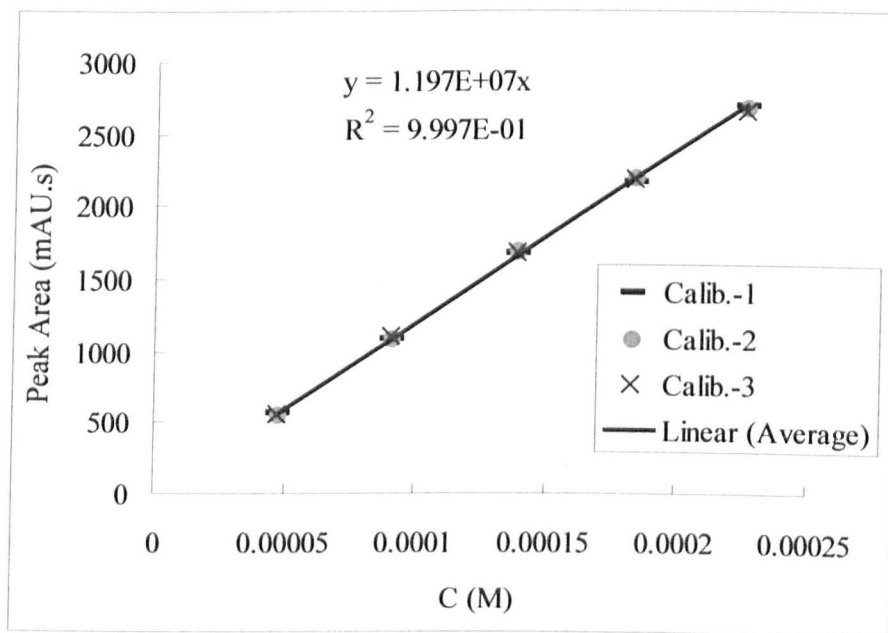
Fig. 6-8 Calibration of HPLC Column for NBA

One thing needs to be added here is that there are several options for the absorption wavelengths provided in the HPLC, which enables the analytes to be analysed under the most suitable choice. Although the retention time will not be affected by the option chosen, the response intensity differs greatly from wavelength to wavelength.

Therefore, in the situation when different wavelengths are chosen in the analysis of the sample, the calibration factor for each analyte must be obtained at and used only for the same wavelength as the one at which its response intensity is to be read. Otherwise, higher uncertainty will be caused in the result. For example, by using the calibration factor of NBA at 224nm to quantify the peak area at a wavelength of 254 nm, a further error in the order of 2% will be brought into the species composition, in addition to the uncertainty of 2% found in calibration.

6.4 MEASUREMENT OF MIXING UNIFORMITY

In order to assess the performance of the micro-mixers, a method has been developed to measure the mixture uniformity in the microchannel with a fluorescent dye. Carried out using the Axiovert 100 inverted microscope, the measurement aims to obtain information on the fluorescence concentration distribution across the channel section. Thus the parameter σ_γ (defined in Eq.(4-6)) is to be used to evaluate the homogeneity of the species in the cross section of the mixer. In this way, the experimental results can be compared with the CFD computation.

6.4.1 Description of Method

The measurement of the mixing uniformity developed in the experimental work is based on the theory that the fluorescence emission intensity is proportional to its concentration in the specimen.

Rhodamine B (RhB) is used in the measurement, dying one stream of the ionic liquid by including a small amount of the chemical. Simultaneously, another stream of the ionic liquid, without fluorescent dye in it, is fed from its respective inlet. The

Rhodamine B molecules in the dyed solution then redistribute over the channel's cross-section whilst the two streams of fluid flow through the micro-mixer and mix with each other. The uniformity of the fluorescent molecules distributed in the cross-section depends on the performance of the micro-mixer. Accordingly, by knowing how uniform a distribution of the Rhodamine B concentration is from its emitted light intensity in the surface, the effectiveness of the mixing process can be assessed.

To obtain the Rhodamine B concentration over the cross section of the channel, three fluorescence illumination images need to be taken for each location, that is, an illuminated image of the mixing flow, a reference image and a dark image.

The illuminated image is taken at the moment when the mixing of species is in progress whilst the dyed and un-dyed ionic liquids are flowing through the micro-mixer. Using the emission light intensity I given off by the fluorescent dye, the story of the mixing process can be deduced by making the measurement of I element by element through the micro-mixer.

The reference image is the one of the micro-mixer filled with a uniform mixture at a known concentration C_0. In the measurement, this uniform solution is prepared by mixing thoroughly the dyed and un-dyed ionic liquids at 1:1 volume ratio. Giving a light intensity of I_0, the reference image then represents the state when the streams of the dyed and un-dyed ionic liquids are perfectly mixed in the micro-mixer.

The dark image is used to correct the light noise from the environment in the measurement. To take the dark image, the incident light should not be switched off but blocked so that the same effect of the light in the environment can be caught and the background noise intensity I_D can be removed from the other two images.

With the above three images taken, the concentration of Rhodamine B in any cross-section of the mixer can be determined from the recorded light intensity at each pixel position as:

$$C = \frac{I - I_D}{I_0 - I_D} C_0 \qquad (6\text{-}8)$$

and the relative standard deviation of the Rhodamine B concentration of interest is:

$$\sigma_Y = \sqrt{\frac{\overline{C^2}}{\overline{C}^2} - 1} \qquad (6\text{-}9)$$

One thing to be noticed is that, in the wet-etched channel, the channel depth approaches to zero near the edge of the curved bottom. Therefore, the above equation will become less accurate and a significant error will unavoidably occur at the edge of the channel. To guarantee the accuracy of the measurement, the region near the channel edges must be located, so that data from this area can be discarded. To achieve this point, another geometry image is then needed, which should be taken at the same position of the mixer, however without fluorescence filters. In this way, a clear image of the channel geometry can be obtained and used as a reference for the correct positioning of the channel edges in the fluorescence images.

6.4.2 Settings of Microscope

As illustrated in Figure 6-9, the Axiovert 100 inverted microscope comprises: 1) a transmitted-light illumination system; 2) an incident-light fluorescence illumination system; 3) a charge-coupled-device (CCD) camera and image recording system.

- - - ➤   Light path of incident-light fluorescence illumination system

- - - ➤   Light path of transmitted-light illumination system
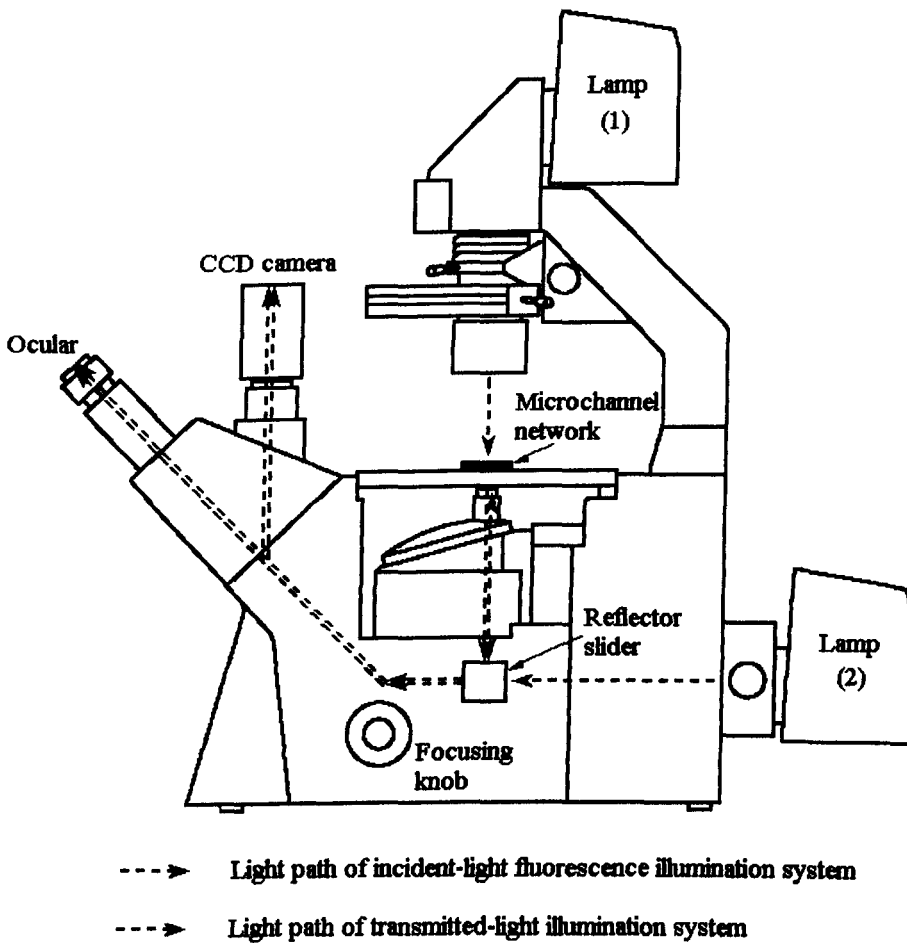
Fig.6-9 Schematic of microscope setting

Located on the top of the microscope, the transmitted-light illumination system is used

in the measurement to take the geometry image. It includes a 12V 100W halogen lamp

as the light source, a potentiometer to adjust the light intensity and other optical

components such as the aperture diaphragm and condenser. The transmitted-light

illumination system enables the image to be taken at conditions independent from the

fluorescence illumination. Thus filters can be removed by moving the reflector slider,

and the light intensity can be reset for the best result for the geometry details.

Moreover, since the condenser helps the objective to collect the diffracted light from

the specimen better, a sharper image of the geometry can be obtained with the

transmitted-light, which will help the precise positioning of the channel edges from the recorded pixel values.

The incident-light system at the bottom of the microscope is employed for the fluorescence illumination. As shown in Figure 6-9, it consists of: 1) a HBO 50W mercury short-arc lamp; 2) a filter slide with three positions, i.e. the dark slider blocking the light path (used to take the dark image), the red-attenuating filter that eliminates the disturbing IR-light and a free aperture; and 3) a reflector slider with four click-stop positions (Zeiss 1998).

As the Rhodamine B used in the measurement absorbs and emits light at different wavelengths (554nm and 627nm respectively (Sigma-Aldrich 2006)), an excitation filter (546nm band pass with 10nm width at half maximum, Zeiss) and an emission filter (600nm band pass with 25nm width at half maximum, Zeiss) are used, together with a reflector mirror placed at the same position as the reflector slider. As demonstrated in Figure 6-10, travelling from the HBO lamp, the incident light first impinges on the excitation filter, with the unwanted band blocked and the desired band passing and then reaches the reflector mirror. Tilting at an angle of 45° with respect to the incoming light, the mirror acts as the dichromatic beam splitter, reflecting the excitation light vertically via the objective to the specimen without any loss. The emission light produced by the Rhodamine B molecules is then gathered by the objective. At a higher wavelength than the excitation illumination, the emission light is able to pass through the reflector mirror, whilst most of the concomitant scattered excitation light hitting the dichromatic mirror is reflected back. Before reaching the eyepiece or the CCD camera, the emitted light must travel through another filter (the emission filter), with which the residual excitation light is blocked and only the desired long emission wavelength is permitted to pass by.

A C4742-95 CCD camera (Hamamatsu Photonics Ltd.) connected to a computer finally acquires the image formed in either light illumination system. The software Wasabi is used to record the image and a small programme was developed (contribution from Dr. Bown) to export the light intensity of each pixel of the image into a text file.
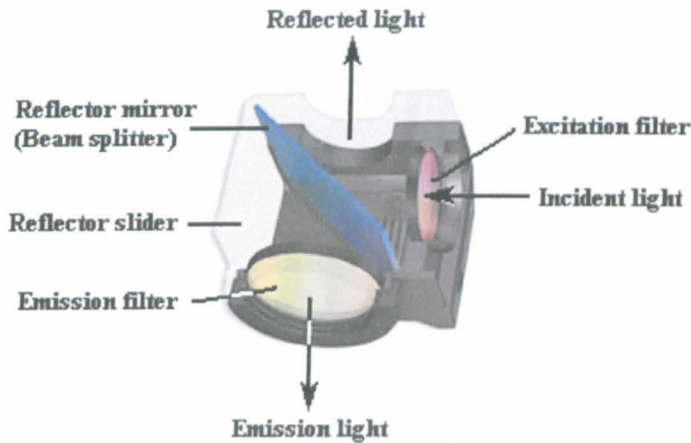

Fig.6-10 Illustration of light through the reflector slider

6.4.3 Features of Measurement

The advantage of measuring the mixing uniformity with a fluorescent dye is that the light intensity of each pixel in the image can be obtained, thus the concentration corresponding to each pixel can be achieved and compared with the perfectly mixed state. By this means, the mixing process in the microchannel can be assessed through the relative standard deviation of the uniformity of the distribution of fluorescent molecules over the channel's cross-section.

Moreover, the usage of both the transmitted-light illumination system and the fluorescence illumination system enables the best results to be achieved for both the geometry image and the fluorescence images respectively. Moreover, as the two systems can be conveniently switched from one to the other, causing no interference in the position of the specimen on the stage, the geometry image can be used to help the processing of the fluorescence data, thus good accuracy can be ensured.

It is worth mentioning that, what the method determines is the average concentration of fluorescent dye along the channel depth. Although no details can be obtained along the depth of the cross-section, the measurement carried out along the micro-mixer gives a good opportunity to observe and understand the mixing process in the microchannels.
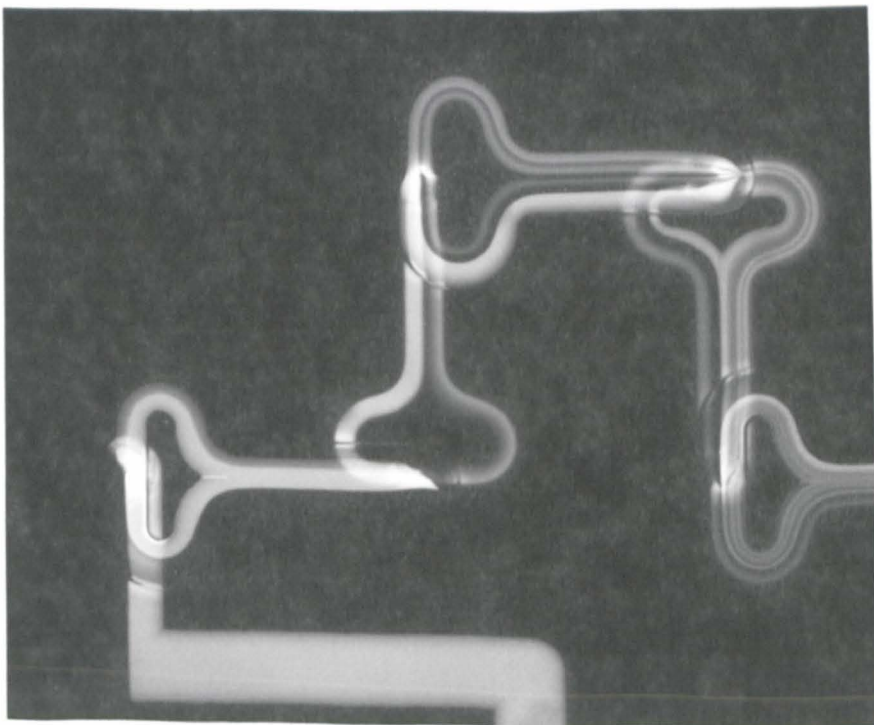
Fig. 6-11 Fluorescence study of mixing process in FNM

As an example, Figure 6-11 displays the fluorescence images taken for the first four elements (including the inlet and part of element No.5) of the folding network micro-mixer. The dyed and un-dyed ionic liquids are fed side by side from the inlets. Then the fluid streams experience repeated splitting and reuniting element by element, with the numbers of bright and dark striations increasing along the mixer. Meanwhile, the thickness of the striation in the same element has also been found to be asymmetric. For instance, in the second element, the left bright striation is bigger than the right one, and the same for the bottom and top one in the third element. This is considered to be a result of the uneven splitting of the fluid streams. Hence, the fluorescence illumination study of the species mixing not only highlights the characteristics of the process, but also demonstrates some unexpected features.

Chapter 7

KINETICS MEASUREMENT DEVICE

MARK I

7.1 INTRODUCTION

As described in Chapter 5, the microreactor (MCR) system developed in the research functions in the following steps:

- Producing a homogeneous mixture of known composition by rapid and effective on-chip mixing for the chemical reaction;

- Maintaining the mixture in the reaction chamber for a given reaction time;

- Rapid quenching of the reaction by effective mixing with the diluents in the dilution mixer;

- Conveying the quenched mixture to an HPLC sample loop for measurement of species quantities.

As the performance of the device depends on the satisfactory control of each process, a series of tests are needed to assess the processes before any kinetics measurement are made on the chip. For example, the mixing process in the micro-channel should be first studied and the performance of the mixers should be evaluated, in order to understand the extent of homogeneity that can be achieved through the mixers. Meanwhile, work to determine the strategy of controlling the system should also be involved, which includes how to obtain a valid sample of the reaction mixture, what sample delay time

is to be used to achieve good measurement as well as good repeatability, and what operating conditions are to be adopted to achieve good performance of the system.

These tests are of great importance. In this chapter, the tests carried out with a non-reacting solution system to assess the performances of the MCR system Mark I are introduced, and determinations are made on the operating conditions of the device for kinetics measurement.

7.2 MIXING PERFORMANCE

The mixing of species is a key process in carrying out chemical reactions in the micro-channel. In the device Mark I, two folding network mixers (FNMs) of the same pattern are adopted, aiming to produce uniform mixtures to either start or quench the chemical reactions instantly on-chip. Hence, the performance of the mixers needs to be assessed, in order to obtain detailed information on species mixing as well as mixture homogeneity in the microchannel.

7.2.1 Performance of the FNM in the MCR System

As introduced in Chapter 6, the performance of the mixer was assessed through measuring the mixing uniformity with fluorescence dye. The same method was used for the study of mixing process in the folding network mixer of the MCR system. However, due to the highly compact geometry, a difficulty then rises for the measurement of mixture uniformity element by element in the diagonal reaction mixer. As the elements are arranged so close to each other, the fluorescence emitting from one will greatly affect and also be affected by its neighbours. Hence, only at the final outlet of the mixing chain and in the reaction chamber itself are the convenient places to obtain valuable information on mixing uniformity.

The measurement was therefore carried out downstream in the reaction chamber. This results in additional advantages. First, the extraordinary big channel width of the chamber provides a good window for the optical study and makes the measurement more convenient. Second, as the flow spreads out into a much wider space, the lateral diffusion is halted by the increased spatial separation, so that the measurement becomes more accurate. Moreover, the big aspect ratio of the reaction chamber decreases the complexity of the question by reducing the effect of a two-dimensional measurement of mixing into a one-dimensional system. And finally, the uniformity of mixture in the reaction chamber is very important because it provides the information on the homogeneity of the mixture for chemical reactions.

The measurement was carried out on a Mark I microreactor network, in which a FNM with 13 elements were used as the reaction mixer before the reaction chamber. Special arrangements for the feeding of fluid streams were made in order to create the same conditions as that used when chemical reactions are carried out on-chip. Instead of feeding the reagents and catalyst solutions, two other solutions are used for the measurement. These are the pure $Bmim(NTf_2)$ ionic liquid (referred to as un-dyed solution *infra*), and the fluorescent dye solution (referred to as dyed solution *infra*) that dissolves Rhodamine B into $Bmim(NTf_2)$ at a concentration of 0.0006M.

As shown in Figure7-1, the dyed and un-dyed ionic liquids were fed diagonally into the four ports of the MCR system in the measurement. As a result, a flow with three interfaces between streams was produced in the junction and led into the mixer, as displayed in Figure 7-2. The uniformity of the mixture produced after the mixer is then assessed by measuring the concentration of the fluorescent dye of the mixture in the reaction chamber using the method introduced in Section 6.4.

Un-dyed
solution

Dyed
solution

Y

←1 mm

X

Dyed
solution

Un-dyed
solution
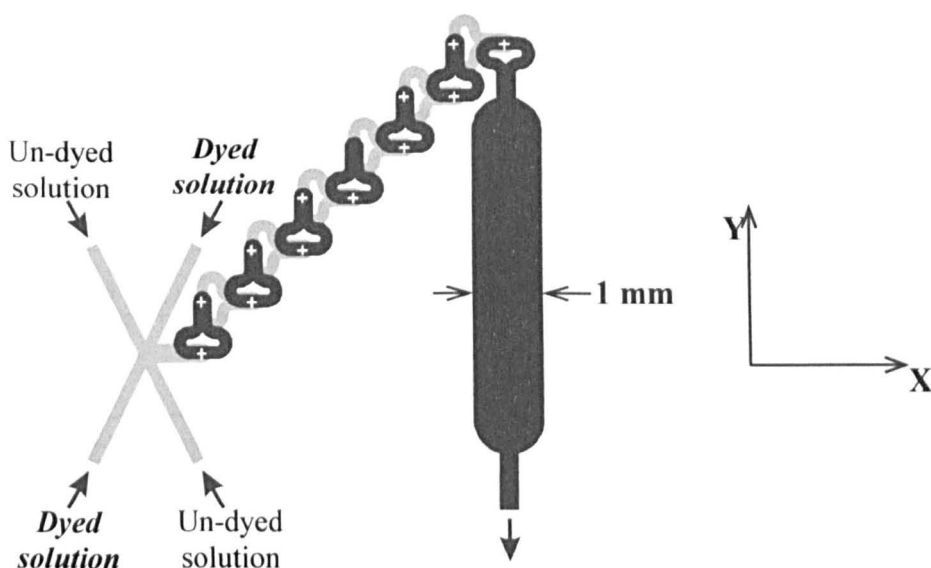
Fig.7-1 Experimental Settings for Measurement of Mixture Uniformity
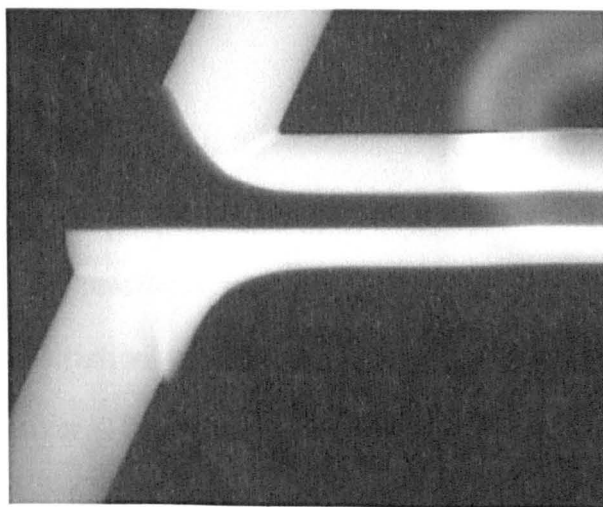
Fig.7-2 Flow Leading to Reaction FNM

Conditions for the measurement and the value of the relative parameters are given in Table 7-1. From them, the Reynolds number and Peclet number based on the channel depth, R, are calculated as:

$$\mathrm{Re} = \frac{\rho V R}{\mu} = 0.19 \tag{7-1}$$

$$Pe = \frac{VR}{\mathcal{D}} = 4.14 \times 10^5 \qquad\qquad (7\text{-}2)$$

Table 7-1 Conditions and parameters of mixture uniformity measurement

Dimension of mixer		Relative Parameters	
W (m)	275×10^{-6}	Density of Bmim (NTf$_2$) (at 25 °C) (kg/m^3)	1500
R (m)	75×10^{-6}		
Experimental conditions		Viscosity of Bmim (NTf$_2$) (at 25 °C) $(N \cdot s/m^2)$	0.0497
Driven pressure (bar gauge)	6		
Ambient temperature (°C)	23.9	Diffusivity of Bmim (NTf2) (m^2/s)	1.54×10^{-11}
Average velocity (m/s)	0.085		

The fluorescent image of mixture in the reaction chamber is then observed under the microscope. In the image as displayed in Figure 7-3, fluid striations of uneven thickness are found in the reaction chamber, especially the big bright one that exists in the centre. The uneven striations are considered to be due to by the uneven splitting of fluid streams in the mixer. They greatly affect the mixing process, as large diffusion distance may form, as found in the centre of the chamber. The rms of mixing uniformity in this case was calculated as $\sigma_Y = 25.0\%$, which is obviously higher than the design value. It then seems that the error resulting from scale-up based on coarse-grid computations is significant. Hence, more computations are needed in order to find a new expression to better fit the decay of σ_Y with numbers of mixing elements.
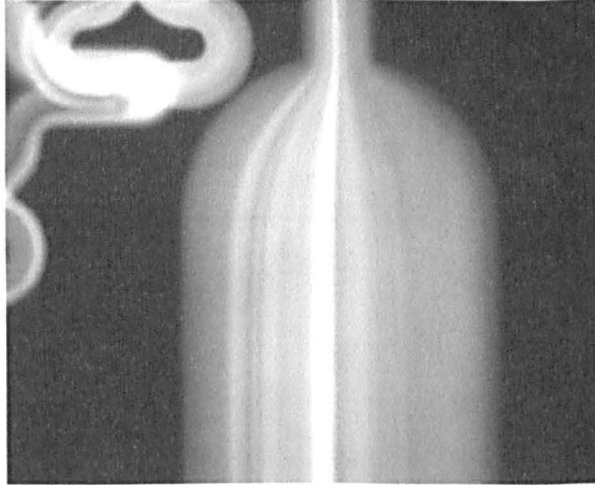
Fig.7-3 Fluorescence image of mixture concentration in the reaction chamber

Although still being limited at low Peclet numbers by the computer resources, computations were carried out by including one more case at $Pe = 320$ in addition to the two at $Pe = 100$ and $Pe = 1000$ in the previous work. More importantly, finer grids were used and more elements were computed for each case, in order to refit the changing trend of σ_Y.

The computational results for the more intensive computation is show in Figure 7-4. An exponential decay of σ_Y is found again with the number of mixing element k. However, its changing rate is much slower comparing to that in Figure5-3. For example, 6 elements are needed to achieve $\sigma_Y = 1\%$ at $Pe = 100$ and 16 elements at $Pe = 1000$ in this design, compared to 3 and 11 elements required respectively in previous prediction.

A expression is also proposed, in the same form as Eq.(5-1), which is:

$$\frac{\sigma_Y}{\sigma_{Y_0}} = \exp\left[-\frac{\alpha k}{\ln(Pe) + \zeta}\right] \tag{7-3}$$

However different values are decided for the constants to fit the data points (please see

Table 7-2) (Chen *et al.* 2006).
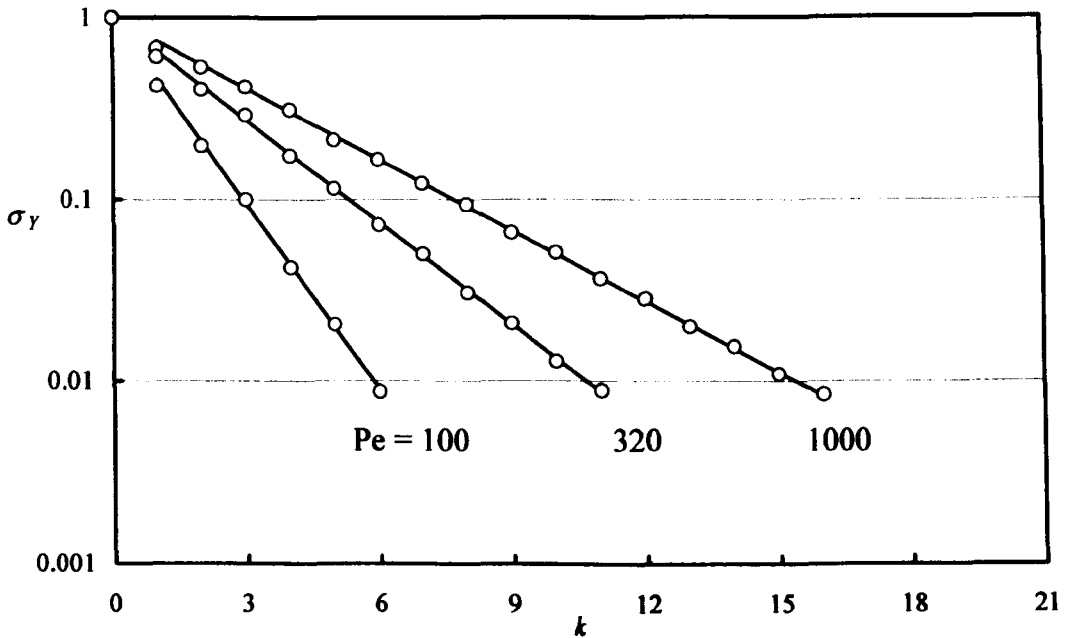
Fig.7-4 Exponential Decay of σ_Y with k in FNM (Chen *et al.* 2006)

Table 7-2 Values of Constants in Exponential Decay Fitting Law

Parameter	α	σ_{Y_0}	ζ
Value	1.12	1.01	-3.18

With these new values, the rms deviation were re-estimated for the Mark I design to be

$\sigma_Y = 17.6\%$ for the reaction mixer with 13 elements at $Pe \approx 10^5$ and $\sigma_Y = 12.3\%$ for

the dilution mixer with 7 elements at $Pe = 1000$. It was also predicted that, to achieve

a homogeneous mixture with $\sigma_Y = 1\%$ for the reaction of ionic liquids where $Pe \approx 10^5$,

34 elements are needed for the reaction mixer. Moreover, as the Peclet number of the

dilution mixer was found in the experiments to be in the same order of magnitude as that of the reaction mixer, rather than $Pe = 1000$ as thought previously, another 34 mixing elements are needed for the dilution mixer in order to quench the reaction well. Hence, it is clear that the performance of the FNM in the Mark I design has been over-estimated, especially for the dilution mixer, so that it is not surprising to find a worse mixing performance in the measurement.

7.2.2 Mixing Process in the FNM

Further study was also carried out to understand the mixing process in detail in the FNM mixer. In order to investigate the species mixing element by element, a horizontal mixer of 16 elements was designed, as shown in Figure 7-5 (a). Being fabricated in the same three-layer glasses, the investigation mixer has the same channel width and depth as the reaction mixer. The only difference between them is that a longer combination part is used for the element of the investigation mixer (as illustrated in Figure 7-5 (b)), in order to conveniently measure the mixing performance after each element. Meanwhile, another group of 16 elements in the same type but bigger sizes are placed below the investigation mixer. The big mixer is designed for the study of mixing process in microchannels, especially at relatively high Reynolds number, due to its lower resistance resulting from bigger dimensions.
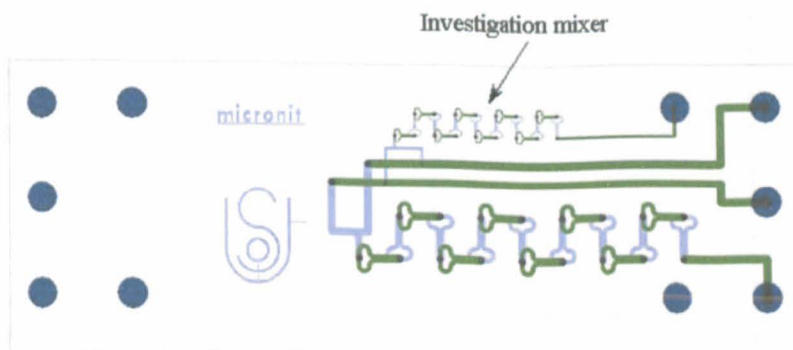
(a) Design diagram for manufacture of investigation mixer
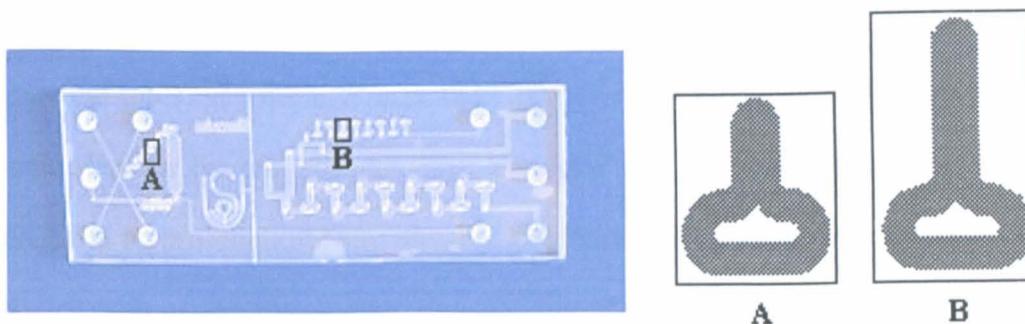
(b) Comparison between elements of reaction mixer and investigation mixer

Fig. 7-5 Investigation Mixer for Study of Mixing Process in FNM

(Dimension details are given in Appendix-2)

The same method described above was used to measure the mixing uniformity element by element in the investigation mixer. The un-dyed and dyed solution used in the measurement were the pure Bmim(NTf$_2$) ionic liquid and the solution prepared by dissolving Rhodamine B in Bmim(NTf$_2$) at a concentration of 0.0078M. For details of other experimental conditions, please refer to Table 7-3.

Table 7-3 Conditions of Measurement in Investigation Mixer

Experimental conditions		*Dimension of mixer*	
Ambient temperature (°C)	~23	Width (m)	275×10^{-6}
Velocity of flow (m/s)	0.068	Depth (m)	75×10^{-6}
Density of Bmim(NTf$_2$) (at 25 °C) (kg/m^3)	1500	*Non-dimensional numbers*	
Viscosity of Bmim (NTf$_2$) (at 25 °C) ($N \cdot s/m^2$)	0.0497	**Reynolds Number**	0.15
Diffusivity of Bmim (NTf2) (m^2/s)	1.54×10^{-11}	**Peclet Number**	3.2×10^5

The dye and un-dyed solutions were fed side by side into the mixer through its leading channels. Driven by the nitrogen gas, the fluid streams repeatedly experienced the splitting and recombination from element to element. By taking the fluorescent images of all elements of the investigation mixer, the characteristic pattern of mixing in the FNM is evident as illustrated as in Figure 7-6.

Figure 7-6 is a composite of three fluorescent images taken under low magnifications in order to show the entire cascade of sixteen elements of the investigation mixer. More and more striations can be seen formed and the thickness of the striation reduces along the mixer. Moreover, the uneven thickness of striation can be found in the picture as well. For example, a thick black stripe can be continuously found in the lower part of the element 3 and 6, as well as in the left side of element of 4 and 8. Since the unevenness of splitting and recombination can be observed in both the reaction mixer and the investigation mixer, it is thought to be related to the chip structure, for example, the offsets between the layers of glass where the channels are etched.

Meanwhile, the mixing performance was assessed through measuring the average fluorescence concentration along the channel depth. The rms deviation of the mixture uniformity was found to decay exponentially with the number of the mixing elements, as it might be generally expected. Curiously, an oscillating behaviour is found in a cycle of every four elements, when the experimental results are plotted as shown in Figure 7-7.
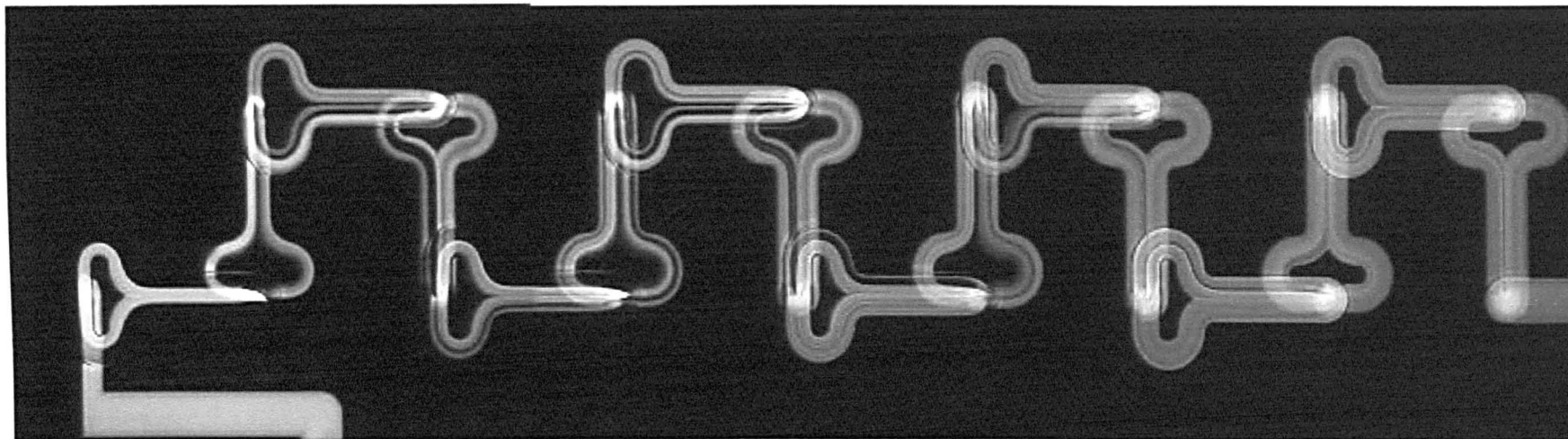
Fig.7-6 Mixing Process in FNM

Eq.(7-1) together with the constant value in Table 7-2 was also used for prediction at

the experimental condition of $Pe = 3.2 \times 10^5$. As shown in Figure 7-7, the predicted

value of σ_Y in each element is generally higher than that measured in the experiment,

however, its exponential decay is somewhat slower. This is because, for the

measurement, only the average concentration of fluorescence over the channel depth

can be obtained, thus the contribution of the varying concentration along the depth to

the rms deviation has to be ignored in the assessment of the mixing uniformity.
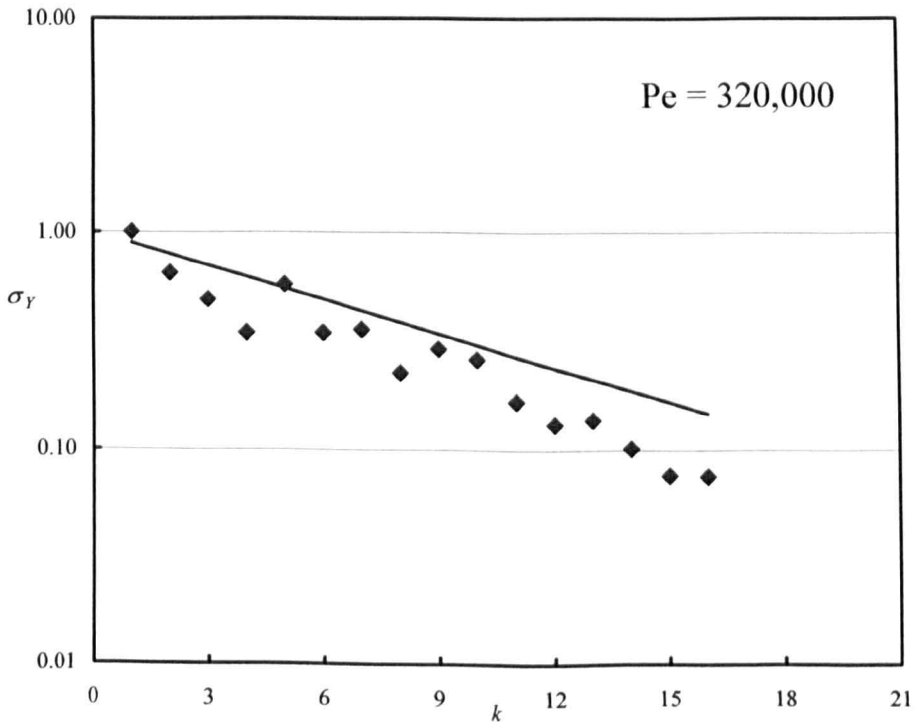
Fig.7-7 Experimental Results of σ_Y Decaying with Element Number k in the FNM
(The line is the theoretical fit with Eq. (7-3) and parameter values in Table 7-2)

7.2.3 Effect of Offset

As described previously, the folding network mixers are constructed in three layers of

glass, of which the top and bottom layers have the channels etched and the middle one

has connection holes made by powder blasting. Hence the alignment between layers is a challenge in the fabrication technology. Although this chip is made by a commercial manufacturer, some misalignments between the layers of the fabricated mixer can still be found when the reaction network is examined under microscope. For instance, as illustrated in Figure 7-8, the top layer in the diagonal reaction mixer is offset 12μm relatively to the bottom layer in the direction of negative X and positive Y.
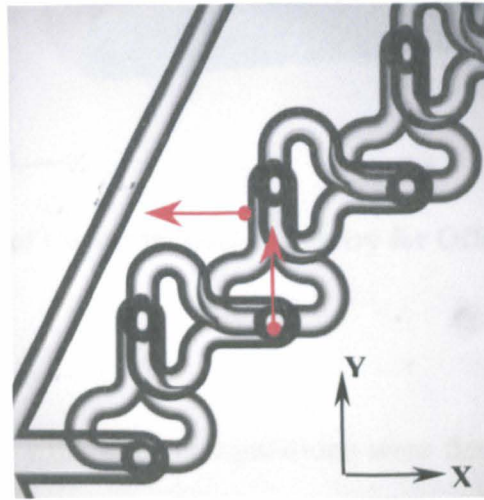
Figure 7-8 Offsets between Layers of Reaction Mixer

To understand how the misalignments in the structure affects the performance of the mixer, CFD computations were carried out. The position of the connection hole was used as reference in the computation. Then, both the offsets of top and bottom layers to the hole and the tapering of the hole (positive or negative to the flow direction) were taken into account in the computations.

As an example, Figure 7-9 gives one of the geometries used in the computation, in which the connecting hole tapers in the same direction of the fluid flow. The upstream combination part and the downstream splitting part of mixer in the geometry have been simplified into two straight channels in their respective dimensions. In order to prevent

the output results from being affected by the computational outlet boundaries, the lengths of the splitting channels were extended by one channel width in both directions over the interfaces for output of data.
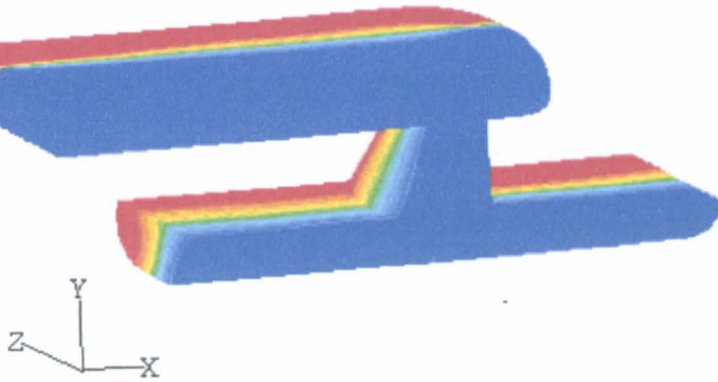
Fig.7-9 Example of Computational Geometry for Offset Effect in FNM

To cover all the possible situations, computations were designed based on two main changes in the structure, which is:

1) The tapering directions of the connecting hole, i.e. the direction of the fluid flow and against the flow;

2) The possible offset position of the top and bottom layer relatively to the connecting hole, which can be further divided into four circumstances as:

   • Only the top layer is offset to the connecting hole

   • Only the bottom layer is offset to the connecting hole

   • Both the top and bottom layers are offset, while in the same direction to the connecting hole

   • Both the top and bottom layers are offset, however in the opposite directions to the connecting hole.

In these cases, the offsets were all set to be 15μm, no matter on which layer and in which direction it happens.

Hence, there were altogether eight cases generated by combining the above conditions and each is referred to by its offset conditions. For example, for cases where the hole tapers in the direction of fluid flow, it is referred to as "top-offset-up-hole" when the top layer is offset, and referred to as "bottom-offset-up-hole" when the bottom layer is offset. For cases when both layers are offset, they are referred to as "both-same offset-up-hole" and "both-opposite offset-up-hole" respectively according to the situation whether the top and bottom switch to the same direction or not. Besides, there were two other cases included in the computations as well, which were the perfect alignment achieved for both situation of the hole pointing upward or downward. Results of all these cases are displayed in Figure 7-10.

The effects of the offset of the fluid flow on the mixing performance can be seen from the contours of concentration on central plane of the connecting hole and the outlets of the splitting channel. An interesting trend has been found from these results. That is, for both up-hole and down-hole cases, the offset of the feeding channel (the recombination part of the mixer) usually results in a twist of fluid flow in the horizontal cross-section of the connecting hole, whilst the offset of the outlet channel (the splitting channel) causes a tilt of fluid in the vertical central section of the hole.

Taking the cases where the connecting hole tapers in the same direction of fluid flow as an example, as shown in Figure 7-10 (I), when the top and bottom layers are perfectly aligned to the central hole, the fluid streams pass straight down through the connecting hole, and no twist occurs within the connecting hole. As a result, the interface between species coincides well with the symmetry of channel geometry. However, for the case where only the top layer offsets relatively to the hole (top-offset-up-hole), the species interface is soon twisted when it flows into the hole. As the twist of interface remains through the hole, the composition consequently fed into the two

splitting channel is not the same. For the case when only the bottom layer is offset, although the fluid looks to pass the hole symmetrically, the species interface is distorted by the flow out of the hole, and a tilted end can be found in the central section of the hole. Hence the species interface is no longer vertical either, when it enters and flows through the splitting channel.

The most powerful case to demonstrate the effect of misalignment on the flow may be the one where both channels offset to the connecting but in opposite directions (both-opposite offset-up-hole). In this case, since both twist and tilt of fluid flow occur due to the offset of both layers, the distortion of the interface looks the worst of all cases. The composition of the split streams is of course impossible to be the same at all.

The effects of offset on the uneven composition of two split fluid streams, however, are hard to be related to the mixing performance. When flowing through the mixer, fluid may be twisted and interface distorted to different extent in each element. More importantly, this distortion could be possibly be reinforced, or on the contrary, be compensated, as the process repeats over a number of elements. Therefore, in this sense, the details of the mixing process in the FNM are very complicated.

No matter how the mixing process is influenced in each element, the perfect alignment of the channel structure is still what is desired. Some new microreactor networks were then fabricated, with great effort to minimize the misalignment. The offsets between the top and bottom layers of the new chip were measured under microscope. The results are given in Table 7-4, which have been reduced greatly from 12μm as the one shown in Fig. 7-8. Consequently, the rms deviations σ_Y are also found decreased to less than 10% for the examples given in Figure 7-11.

(I). Perfect alignment
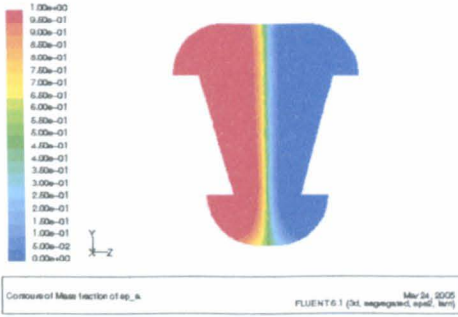
a) Symmetric-up-hole

b) Symmetric-down-hole
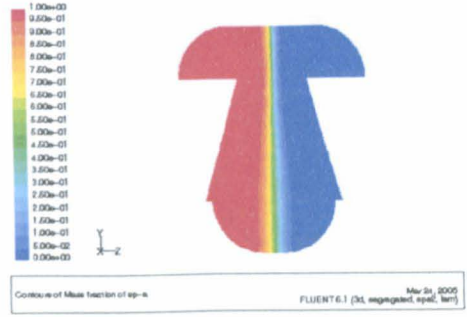
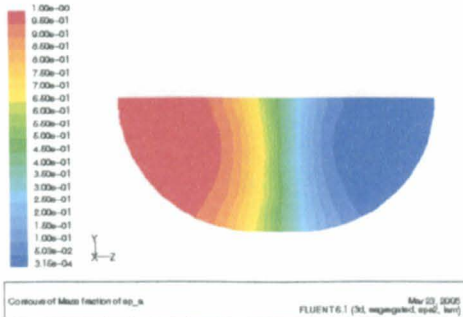Central surface of connecting hole
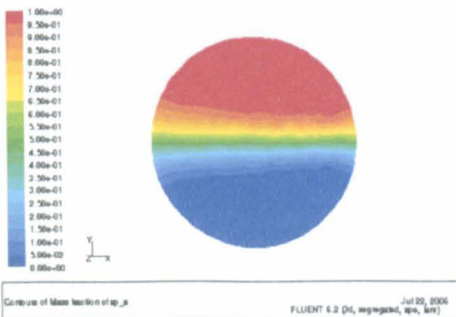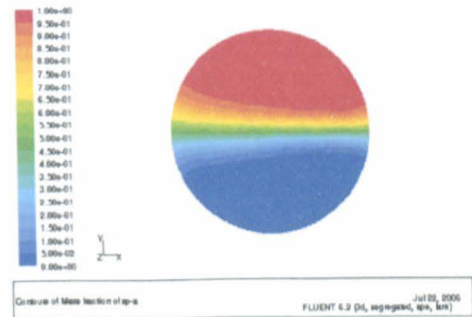
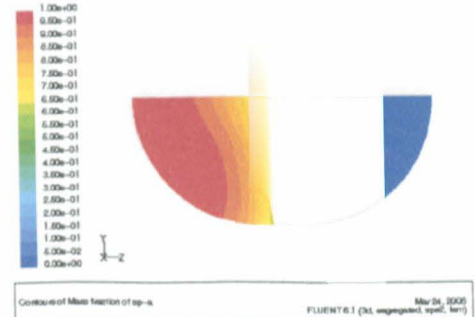Central surface of connecting hole
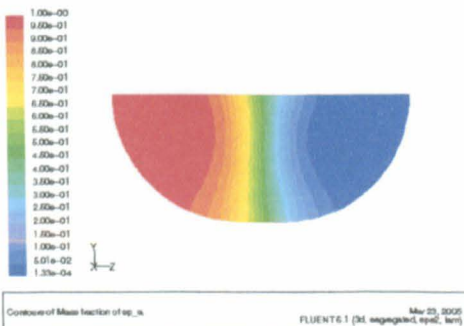

Cross section of connecting hole

Cross section of connecting hole
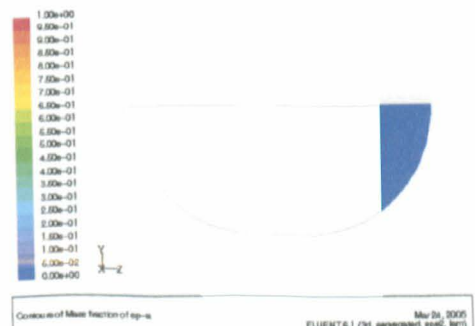

Channel outlet-1

Channel outlet-1

Channel outlet-2

Channel outlet-2

(II). Only the top layer offsets
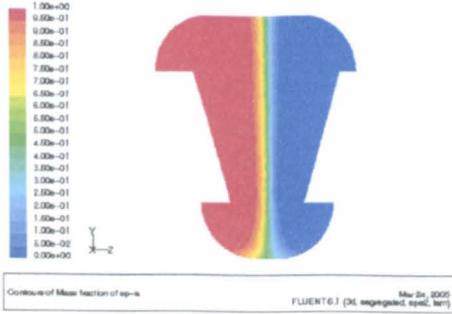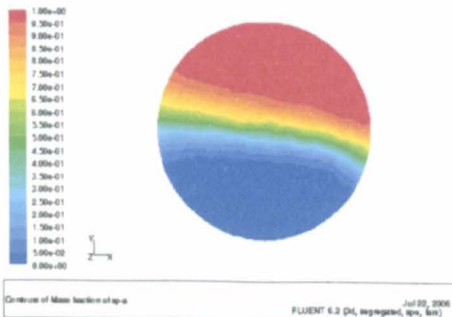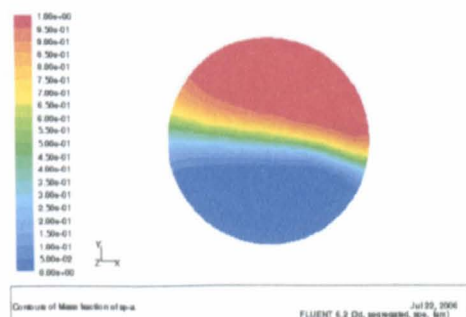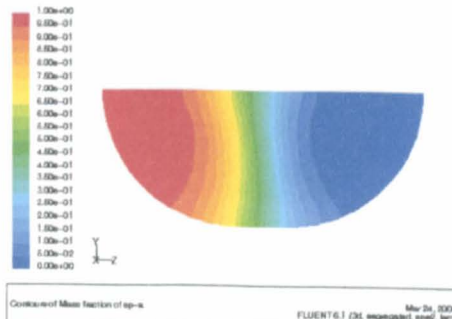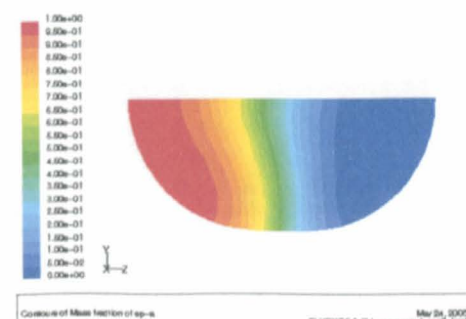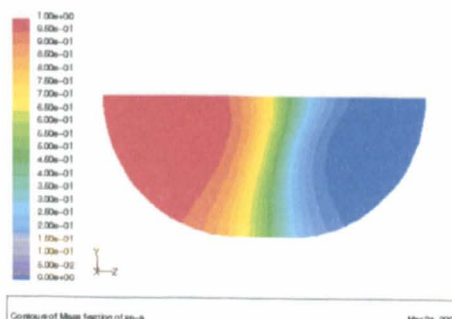
a) Top-offset-up-hole   b) Top-offset-down-hole

Central surface of connecting hole   Central surface of connecting hole

Cross section of connecting hole   Cross section of connecting hole

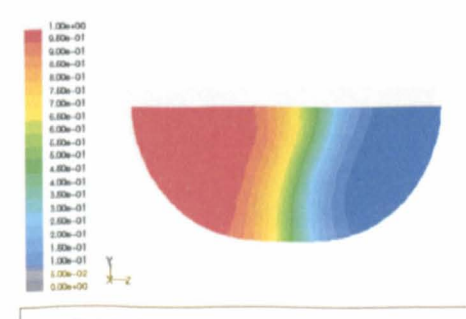Channel outlet-1   Channel outlet-1
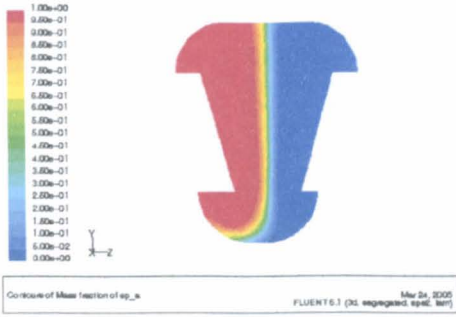

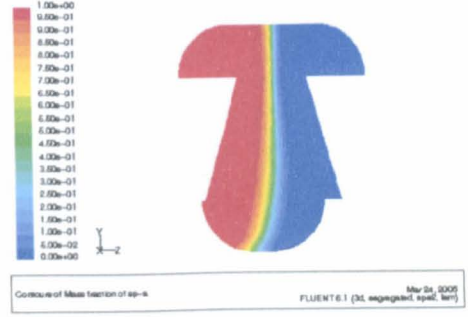Channel outlet-2   Channel outlet-2

188

(III). Only the bottom layer offsets
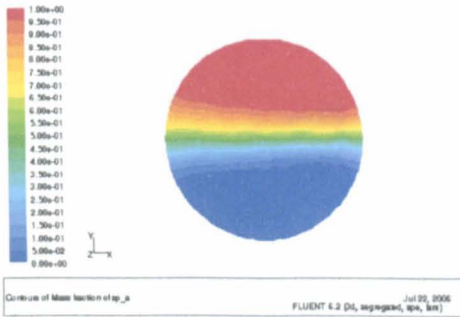
a) Bottom-offset-up-hole

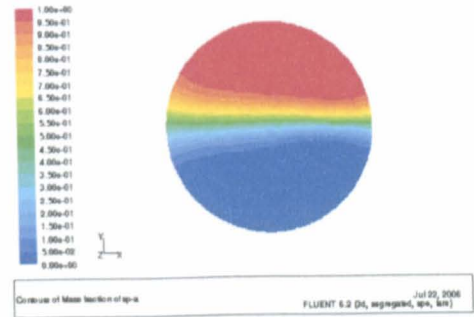Central surface of connecting hole

b) Bottom-offset-down-hole

Central surface of connecting hole

Cross section of connecting hole

Cross section of connecting hole

Channel outlet-1

Channel outlet-1

Channel outlet-2

Channel outlet-2

(IV). Both layers offset in the same directions

a) Both-same offset-up-hole   b) Both-same offset-down-hole
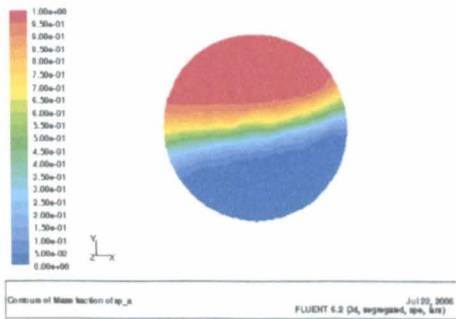
Central surface of connecting hole   Central surface of connecting hole

Cross section of connecting hole   Cross section of connecting hole

Channel outlet-1   Channel outlet-1

Channel outlet-2   Channel outlet-2

190
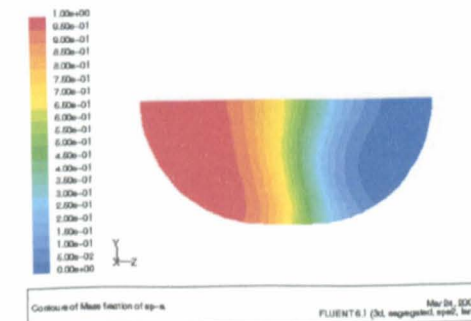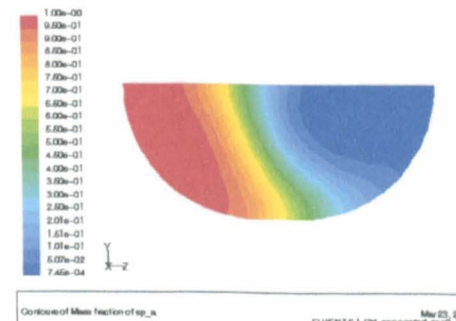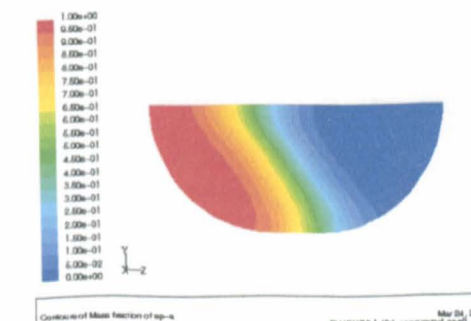
(V). Both layers offset in opposite directions
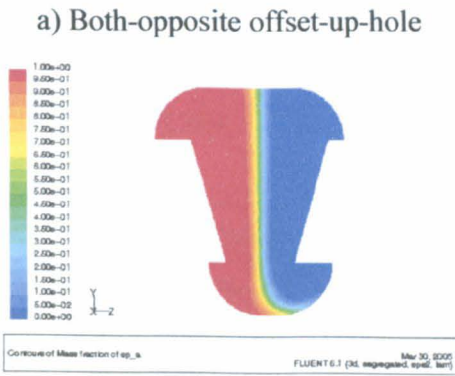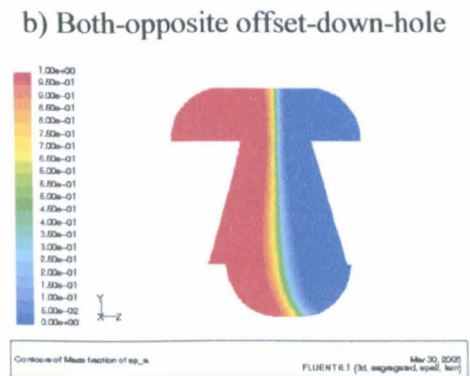
a) Both-opposite offset-up-hole   b) Both-opposite offset-down-hole

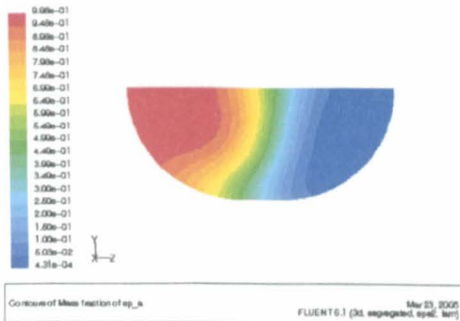Central surface of connecting hole   Central surface of connecting hole
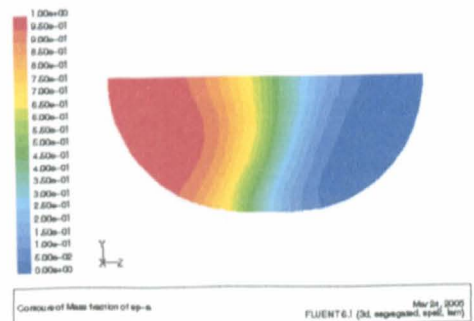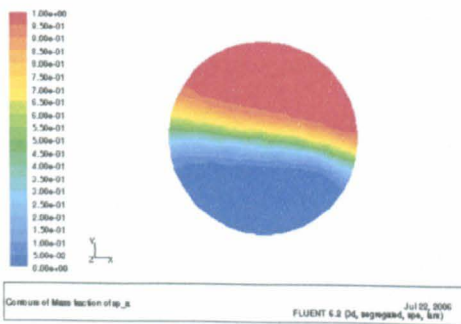

Cross section of connecting hole   Cross section of connecting hole
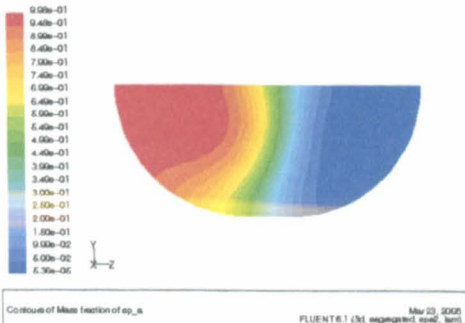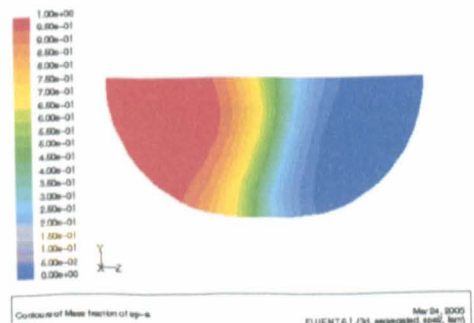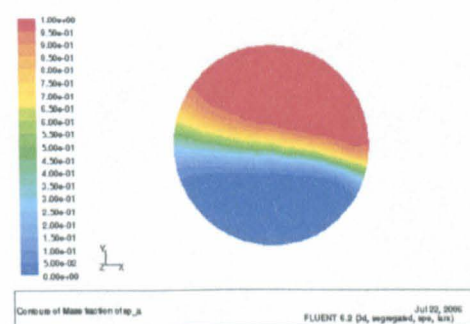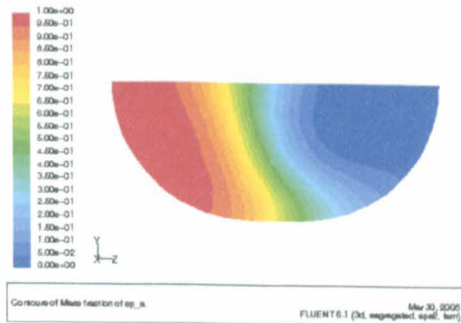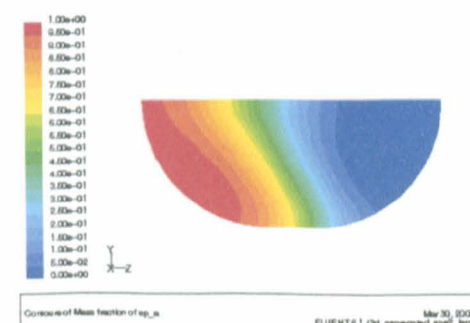

Channel outlet-1   Channel outlet-2
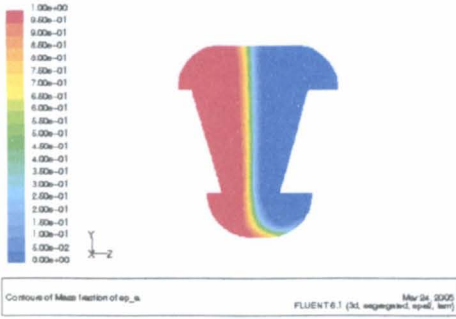

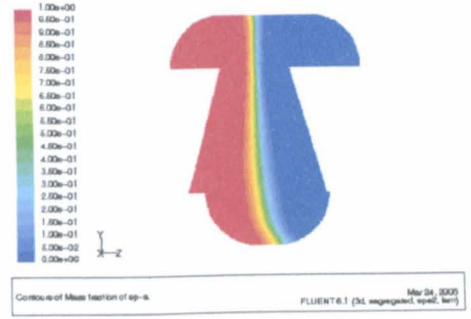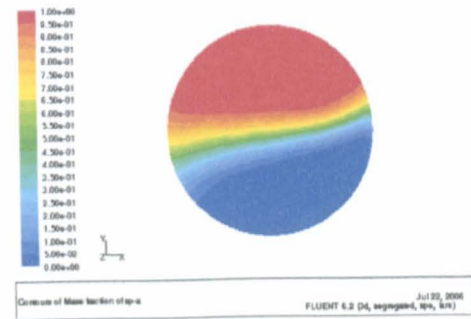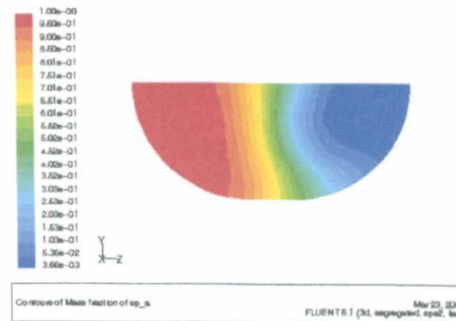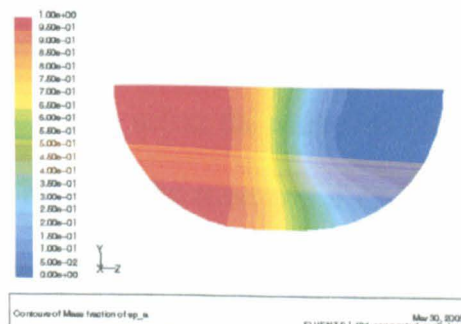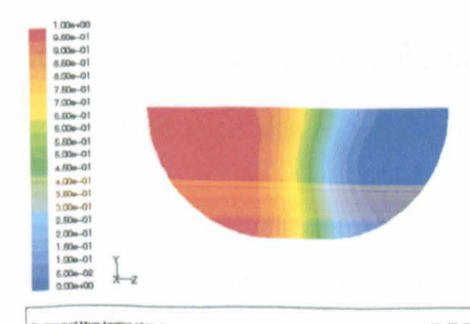Channel outlet-2   Channel outlet-2

Fig.7-10 Computational Results of Offset between Layers of FNM

Table 7-4 Offset of Wafer B

Chip	Top layer (relative to the middle)		Bottom layer (relative to the middle)	
	δx (μm)	δy (μm)	δx (μm)	δy (μm)
Wafer B-No.8	-5.7	-3.7	-6.4	0.1
Wafer B-No.10	-2.9	-3.7	-2.5	0.1
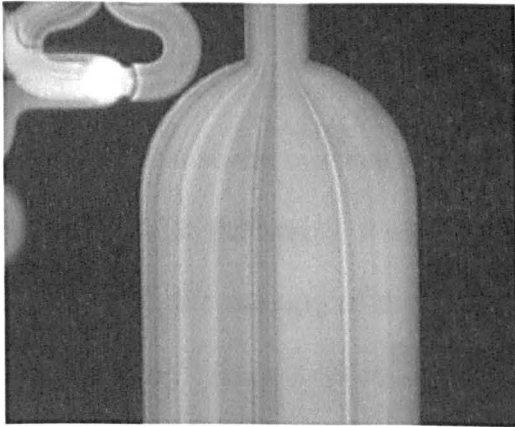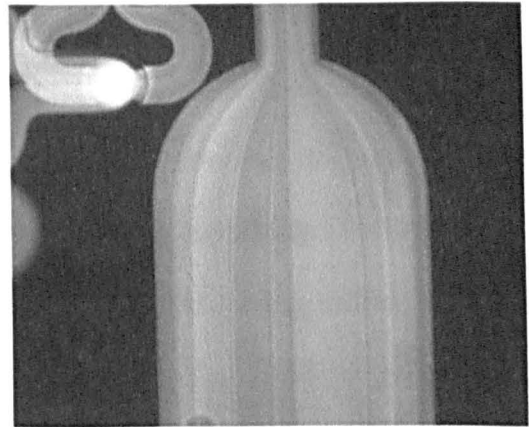
Wafer B-No.8, $\sigma_Y = 8.0\%$ **Wafer B-No.10, $\sigma_Y = 6.9\%$**

Fig.7-11 Rms Deviation of Chip from Wafer B

7.3 PERFORMANCE OF VALVE

The valves in the MCR system play an important role in the control of fluid flow. Aiming to reduce the error that might be caused in the kinetics measurement, the initial criterion to select the valves is focused on a quick response time that is negligible to the reaction duration. As a result, five solenoid valves functioning at the balance of magnetic force and a spring were used. As given by the manufacturer, these valves can respond in 20ms for the simple operation of opening and 30ms for closing for fluid such as nitrogen gas. This seems more than enough for the requirement of the system

control. However, when tests were carried out to assess the performance of the system, the valves were found to behave differently, due to the special properties of the fluid.

The first point that was noticed regarding the valve performance is that it did not respond as quickly as expected. It was first found in testing how the sample volume changes with the valve open time (i.e., the total length of the time for which the valve was held open during an experiment). As shown in Figure 7-12, the changing rate of ejected volume with time is not linear. It increases more rapidly at the shorter ejection times. This is considered to be due to the opening process of the valve, in which the solenoid produces a magnetic force to pull the pintle up, while the spring produces a resistance because the movement causes its compression. Since the magnetic force is a constant, whilst the spring force increases (because it is proportionally to its elastic deformation), the moving of the pintle becomes slower as it moves further during the valve opening. As a consequence, the volume opened for fluid to pass through increases slower during the process, until it reaches the steady state of valve fully opening. Bearing this process in mind, the time scale of 0.04s found in Figure 7-12 is thought to be that needed for the valve to fully open for ionic liquids flow. The valves then have a real response time twice of that indicated by the manufacturer for the opening operation. This may be partly due to the different performance existing between products. But it is considered more likely to be because of the high viscosity of ionic liquid. After being wetted, the surfaces are covered by layer of the sticky liquid, and surface tension and friction increase. Hence, it is more difficult for the pintle to be pulled up and it takes longer for the valve to fully open.
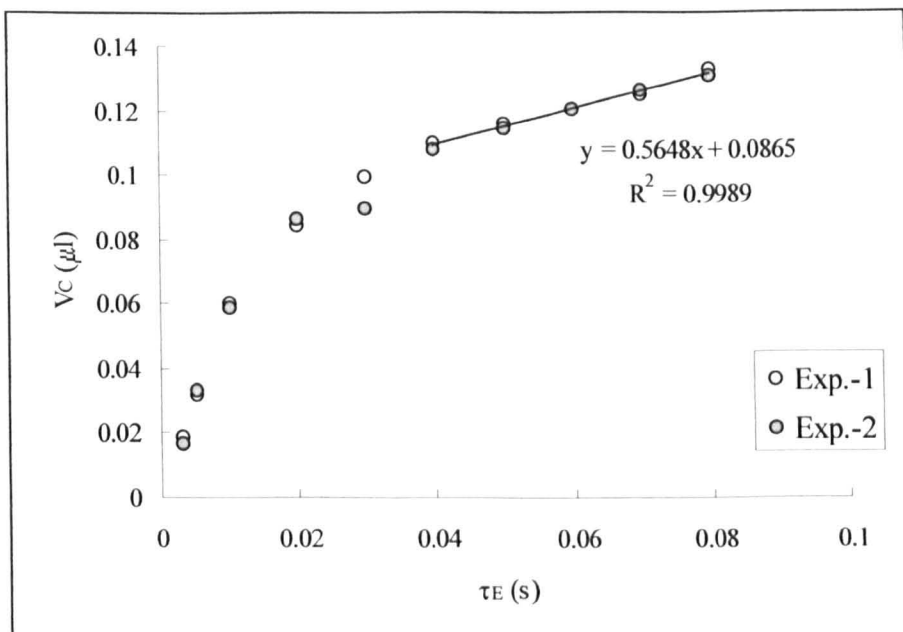
Fig. 7-12 Captured Sample Volume Changing with Ejection Time (Pr=4 bar)

The second point is, a poor repeatability can be found in the plot as shown in Figure 7-12. When carried out at same conditions, including experimental setting and the order of arrangement of ejection time, the relative error between two experiments is found to range from 3% up to 20%. And more importantly, the larger error does not happen under specific circumstances. It is then very difficult to estimate the volume of ejected sample via models or measurement beforehand because it varies during a campaign.

In order to overcome this rather significant problem, something inert to the reaction is used as an indicator of the sample volume ejected and captured. This enables the compositions of reaction mixtures to be calculated from the results of HPLC analysis. The technique is discussed in detail in the next section.

However, using the internal standard technique, the flow rate estimated by fitting the captured volume versus time is found larger than that calculated in the network analysis at the same pressure conditions. This is supposed to be caused by two factors,

the closing operation of the valve, and the relaxation of the material forming the flow passages after the valve closes. During the closing process, since the current is cut off in the solenoid, the pintle drops under only the force of the compressed spring. When the pintle quickly moves down, an extra pressure is produced and applied to the fluid. This seems to result in an increase of the flow rate during the short ejection interval. Meanwhile, during the ejection time, the Teflon flow passage in the valve expands under the effect of high pressure. When the valve closes after the ejection, the pressure drops due to the stopping of the fluid flow, hence the Teflon material relaxes gradually because of the reduction in the pressure. The relaxation of the Teflon hole (see Figure 5-6 (b)) then causes a force pushing the liquid out more rapidly than at its steady state. As a result, a higher sample volume is found and captured in the sample loop. But to prove the effect of these two factors is very difficult, and no direct evidence has been found in the experiment.

The relaxation phenomena after the valves close may cause the valve response to vary with the reaction duration. After being closed for different time to hold the fluid for reaction, the relaxation of the Teflon material of the valve may be different. For a short reaction duration, since the Teflon relaxes just a little bit before it opens again for ejection, the hole is still in the expanded state. It seems that the pintle can then move more easily than after a long reaction time, during which the Teflon hole relaxes more, thus holding the pintle more firmly. Therefore, the response time of the valve after the reaction is likely to increase with the reaction durations. This was observed in the experiments discussed below.

7.4 INTERNAL STANDARD

Due to the poor repeatability of the solenoid valves, a substance called an "Internal Standard" was used both in the tests of the MCR system and in the real kinetics

measurement on-chip. Functioning as an indicator, it provides information on the sample volume captured for HPLC analysis and changes in species compositions along the MCR system. Hence, judgement can be made on whether the sample is valid and the kinetics measured correct.

7.4.1 Internal Standard

Mentioned briefly in the last section, the internal standard used in the experiments enables measurement of how much fluid flows through the device. It is then possible to calculate the conversion and the productivity of the chemical reactions. This approach is simple but very important, particularly in the reaction experiments.

As mixing and reaction take place on-chip, the compositions of both the reagents and the product are changing with time. In the simple case, the change in the composition with time shows how the reaction progresses, on the premise that the sample volume captured and analysed each time is identical. However at the condition under which the sample is ejected in reality, the relation becomes complicated because the amount of every captured sample is different so that the composition measured is not based on the same mass. Hence, an internal standard is necessary, to track the concentration changes of species through the system. As it flows through the system, it is ejected together with the reagents. Measurement of mass and concentration of the internal standard can then provide information as follows.

- Amount of reactant being captured by the sample loop;
- Validity of sample captured for the analysis;
- Concentration of reacting species of interest;

To function as an indicator of the changes occurring in the reactants, the substance used as the internal standard must meet several requirements, such as:

1) It can be well dissolved in the ionic liquid that is used as the solvent of the chemical reaction.

2) It must be inert to the chemical reaction that is performed in the MCR system, so its composition will not change during the course of reaction; and meanwhile, its presence will not have any influence on the reaction kinetics.

3) It must have a high extinction coefficient to the UV light, so that it can be easily detected in the HPLC column at low concentration.

4) It must have a unique retention time (the time takes for a compound to come through the analytical column to reach the detector) in the HPLC analysis, so that it can be easily distinguished from other reacting species, and it should not cause any effect on the analytical peaks of other chemicals.

7.4.2 Pyrene — Internal Standard in Experiments

The internal standard used in the experiments was pyrene ($C_{16}H_{10}$, 99%, Sigma-Aldrich), a polycyclic aromatic hydrocarbon consisting of four fused benzene rings (the structure is given in Figure 7-13) (Sigma-Aldrich 2006).
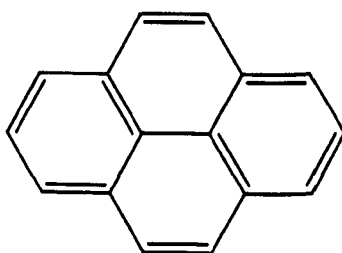
Fig.7-13 Structure of Pyrene

The reason for choosing pyrene is because the colourless or pale yellow solid has all properties required as the internal standard in the experiment. Firstly, for instance, it is soluble in Emim(NTF_2) ionic liquid, the solvent used for the reaction. Secondly, it will

not react with any reactants and it will not interfere with the chemical reaction either. Moreover, with four aromatic rings conjugated and the pi-electrons delocalised over the whole molecule, it can strongly absorb the UV light, so it can be easily detected in the HPLC column even at low concentration. This is very important because as the internal standard, the concentration of pyrene must be limited for the sake of not affecting the fluid properties of the solution system. In the practical experiment, the concentration of pyrene was controlled at around 0.01M, which is 1/10 of the detectable reactant NBA. At such a low concentration, the existence of pyrene was estimated to have an effect less than 3% on the viscosity of the reactant solution at the experimental temperature condition of around 20°C and it decreases to around 1% when temperature approaches 30°C. However, it gives a clear reading of the peak area in the chromatogram of HPLC analysis. Lastly, the long retention time is another advantage of using pyrene as the internal standard. As will be discussed in Section 7.7, there are altogether six kinds of species existing in the reaction system, which are the reactant NBA and DHF, the catalyst, the product THQ, the solvent Emim(NTf$_2$) and the internal standard pyrene. However, in the HPLC analysis, only the NBA, THQ and pyrene can be accurately measured, since others appear too close and have their peak areas overlapping with each other, it is too difficult to distinguish them. As shown in Figure 7-14, the retention time of pyrene found in the chromatogram appears nearly 5 minutes later than that of the NBA and THQ, and its peak area is well apart from the reacting system. Hence the presence of pyrene will not cause any effect on the accuracy of HPLC measurement of the reaction mixtures.
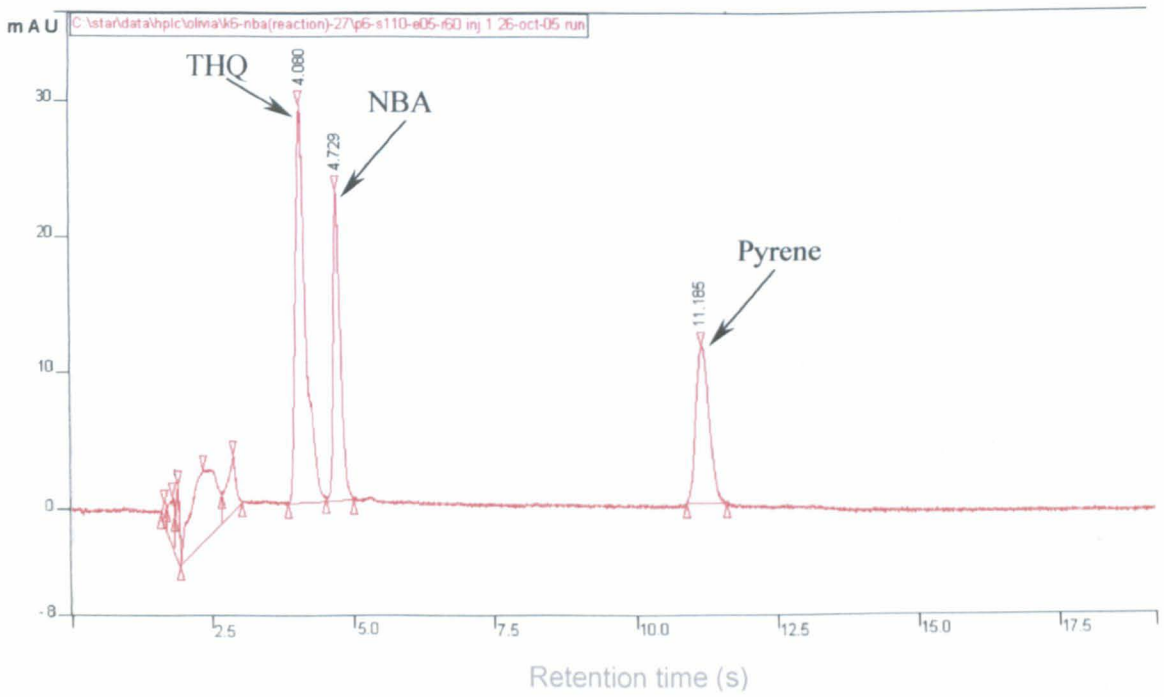
Figure 7-14 HPLC Analytical Result of Reaction Mixture

7.4.3 Dilution Ratio

As described previously, the purpose of introducing the internal standard is to track the composition changes in the reacting system. In order well to describe the changing of species composition before the reaction and after it, a variable referred to as the "dilution ratio" (DR) is defined, using the concentrations of the internal standard in the reaction chamber and measured in the HPLC, as:

$$DR = \frac{C_{r,P}}{C_{m,P}} \tag{7-4}$$

in which, $C_{r,P}$ and $C_{m,P}$ are the concentrations of the pyrene respectively in the reaction chamber and measured by the HPLC.

According to Eq.(7-4), the concentration of the internal standard in the reaction chamber must be known for the calculation of the dilution ratio. For any species i, its

composition in the chamber can be worked out on the basis of the conservation of mass, as given in Eq.(7-5), which can be de deduced from the original solutions in the reservoirs and the corresponding flow rate feeding into the chip.

$$C_{r,i}Q_{r,i} = \sum_{k=1}^{4} C_{0,i}^{(k)}Q_{0,i}^{(k)} \tag{7-5}$$

where: $C_{0,i}^{(k)}$ is the original concentration of species i in the reservoir k; $C_{r,i}$ is the concentration of species i in the reaction chamber; $Q_{r,i}$ is the flow rate in the reaction chamber; and $Q_{0,i}^{(k)}$ is the flow rate in the feeding passage connected to reservoir k.

In the kinetics measurement device, with all the leading capillaries and the feeding channels being designed to be of the same length and identical cross-section, the flow rate of each stream then depends on the solution viscosities only (see Eq3-30). When the experiments are carried out under ambient conditions, the solution viscosities were assumed uniform along the feeding passage from a given reservoir to the channel junction, as the change in temperature was negligible. Therefore by substituting Eq.3-30 into Eq.(7-5), the formula of the species compositions can be simplified as:

$$C_{r,i} = \frac{\displaystyle\sum_{k=1}^{4} \frac{C_{0,i}^{(k)}}{\mu^{(k)}}}{\displaystyle\sum_{k=1}^{4} \frac{1}{\mu^{(k)}}} \tag{7-6}$$

where: $\mu^{(k)}$ is the viscosity of the solution from reservoir k.

7.5 DETERMINATION OF SAMPLE DELAY TIME

As introduced in Chapter 5, changes in the sample delay time will result in different parts, or different volume fractions, of the diluted mixture being captured by the sample loop. Varying the sample delay time allows determination of how the capture fraction of the sample loop changes with time. In turn, this permits a decision on the

optimum operation time of the sample loop, so that the maximum fraction of the sample can by captured for HPLC analysis.

The experiments on sample delay time were to find the sample delay time τ_S corresponding to the maximum captured fraction. They were usually carried out with a non-reacting solution system, in which the reagents solution was normal, while the catalyst solution was in fact the pure solvent without catalyst. In such a way, the solution will behave the same as in the reactions while avoiding the composition changing as it does during reactions. Meanwhile, with the reactions deactivated, both the traceable reagent and the internal standard can be used to calculate the dilution ratio. This experiment then provides a good chance to assess the deviation between the two results.

In the experiment, by varying the sample delay time, different amounts of sample were captured by the sample loop and the corresponding concentrations were obtained from the HPLC. Based on the mass balance, the concentration of sample (species i) in the loop $C_{m,i}$ can be related to the concentration of the same species residing in the reaction chamber $C_{r,i}$ as:

$$C_{m,i} \cdot V_L = C_{r,i} \cdot V_C \qquad (7\text{-}7)$$

Hence the volume of the sample captured in the loop is:

$$V_C = \frac{C_{m,i} \cdot V_L}{C_{r,i}} \qquad (7\text{-}8)$$

Then the concentration data obtained from the HPLC are transferred into the volume of the captured sample, so that the maximum sample volume can be found more easily.

By varying the sample delay time, the captured sample volume V_C is found changing with τ_S. But more importantly, since the volume ejected from the reaction chamber is

determined only by the ejection time, a maximum sample capture can be found at a certain sample delay time. The time, corresponding to the maximum capture fraction can then be used for later experiments with the same solvents. This is why the experiment to determine τ_S is usually carried out first when a new solvent is used.

Figure 7-15 gives result from an experiment on the sample delay time. It shows the effect of delay time on the amount of sample captured in the loop. The peak of the sample delay time corresponding to the maximum captured volume found in the experiment was 0.8s, and it was used for other experiments with the same batch of solvent.
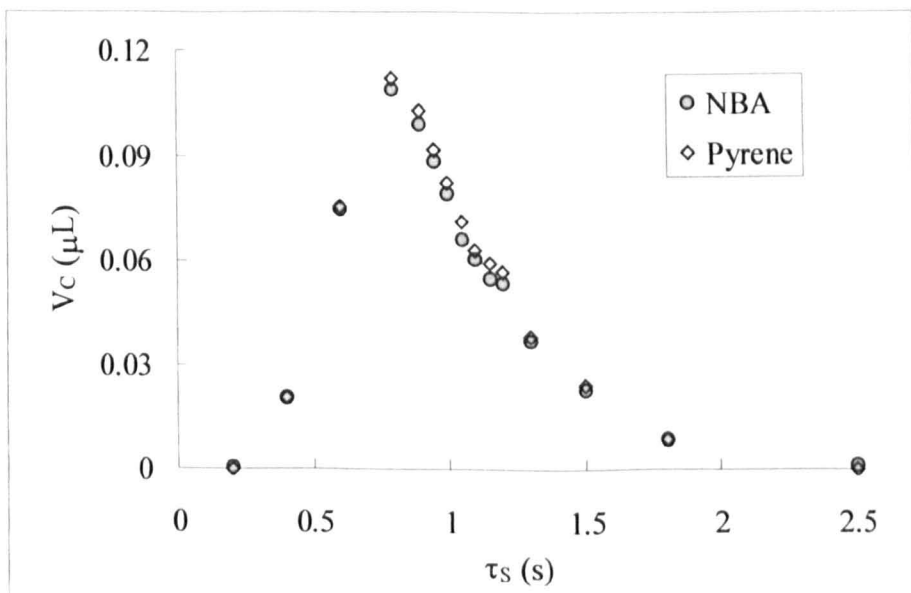
Figure 7-15 Experimental Result of Sample Delay Time

$$(P_r = 6 \, \text{bar} \, , \ P_d = 4 \, \text{bar} \, , \ \tau_R = 5 \, \text{s} \, , \ \tau_e = 0.05 \, \text{s})$$

Meanwhile, the captured volume was worked out independently from the concentration of the NBA and pyrene in the loop. The deviation found between the results is 2.3% at the peak delay time. However, bigger figures are found appearing at

the sharp back slope, for instance, 7.8% was detected as the maximum value at $\tau_S = 1.15$ s. This is due to the method chosen for HPLC analysis. As the analysis duration was not long enough to clean the column thoroughly, the residua left caused the baseline to be lifted at the early times of the measurement. As a result, the peak area read for the NBA was always on the low side, and so was the calculated captured volume. Noticing the problem, some extra time has been added to the period used for HPLC analysis, in order to clean the column well.

7.6 DETERMINATION OF VALID SAMPLE

A valid sample is any representative part of the material that resided in the reaction chamber of the device during the reaction period. The importance of determination of a valid sample results from the different homogeneity existing between the mixture along the mixer and that in the reaction chamber.

As is known, the mixing process occurs when the fluid flows through the mixer, so mixtures of different uniformity are produced along the mixing elements. Compared to that in the mixer, mixture in the reaction chamber, anyway, is the best that can be achieved over a number of elements. Due to the difference in homogeneity of mixtures, reactions progressing in the chamber must be at a different rate from that along the mixer. As a result, samples from the mixer will represent kinetics different from the reactions occurring in the reaction chamber. Whether a sample is valid or not is crucial, because anything coming upstream from the mixer will cause an incorrect measurement of the reaction kinetics. In order to achieve a good result, a representative sample must be guaranteed to come only from the reaction chamber.

7.6.1 Maximum Valid Sample

To judge whether a sample is valid or not, its volume must be known. A sample with a volume larger than that of the reaction chamber is obviously invalid, because it must contain species coming from the mixer, thus the measured material includes a range of compositions. On the other hand, a sample with too little volume is not much better than over-sized ones, because too small a sample captured in the loop results in very low concentration for the analysis. Since HPLC measurement has its limit for detecting of analyte, the analysis for low concentration samples will be easily influenced by the background noise, such as solvent, and thus producing inaccurate results. Hence, an effective way to make the judgement is to find the maximum limit of the volume for a sample to be valid. Then within the limit, the larger the sample volume is, the better it is for the measurement.

The maximum valid sample to be ejected comes from consideration of flow in the reaction chamber. As shown in Figure 7-16, the extreme for a sample to be ejected as valid is when the front of fluid coming from the mixer (the dotted line) reaches the outlet of the reaction chamber. In this case, all volume that has been ejected is no doubt a good representative for the past reaction period. However, the material remaining is considered invalid because any further ejection will bring substance from mixer into the sample to be measured.
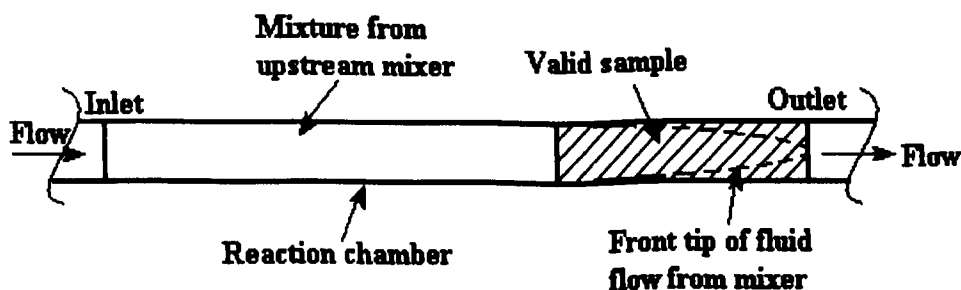
Fig. 7-16 Schematic of Maximum Valid Sample
(View from the side of the reaction chamber)

As the aspect ratio of the reaction chamber is 0.075 (1mm in width and 75μm in depth), the fluid flow inside can be regarded as Poiseuille flow between two parallel plates. The average velocity of the fluid flow in the chamber V is then (White 2006):

$$V = \frac{2}{3}u_{max} \qquad (7\text{-}9)$$

in which: u_{max} is the velocity of the central fluid stream.

Assuming it takes time τ for the tip of fluid from the upstream mixer to reach the outlet of the reaction chamber, that is to flow through the chamber length L, i.e.,

$$L_{tip} = L = u_{max}\tau \qquad (7\text{-}10)$$

the length that total fluid volume pass through during the same time is then:

$$\overline{L} = V\tau = \frac{2}{3}L_{tip} \qquad (7\text{-}11)$$

Therefore, the volume occupied by the material from the mixer in the case as shown in Figure 7-16, which is also the maximum volume of a valid sample, is approximately:

$$V_{valid,max} = \overline{L}A = \frac{2}{3}L_{tip}A = \frac{2}{3}V_{reactor} \qquad (7\text{-}12)$$

where A is the cross sectional area of the reaction chamber.

With the volume of the reaction chamber in Mark I design having been designed to be 0.36 μl, the volume V_E for an ejected sample to be valid must satisfy the limit as:

$$V_E \le V_{valid,max} = \frac{2}{3} \times 0.36 = 0.24 \, \mu l \qquad (7\text{-}13)$$

Meanwhile, taking the capture fraction into account, the volume of a valid sample to be captured in the HPLC sample loop is:

$$V_C \le V_{C,max} = V_{valid,max} \times f_{C,max,s} \approx 0.24 \times 0.91 = 0.22 \, \mu l \qquad (7\text{-}14)$$

7.6.2 Experiments to Determine Sample Validity

The experiments to determine the validity of a captured sample were a series of tests aimed to find the conditions under which valid samples are guaranteed so that these conditions could be used for later chemical reactions on-chip. In theory, the judgement on the validity of a sample should be based on its volume ejected from the reaction chamber. This means, the sample loop must be well cleaned before the ejection; afterwards, it should also be flushed with lots of methanol, in order to push all the ejected volume into the collection vial. However, as the ejected sample is so small, it usually becomes too diluted for the HPLC analysis after mixing with methanol during the cleaning and flushing processes. Thus, it is hard to obtain the ejected sample volume directly in the experiments. As an alternative, the validity of the sample can be determined from its volume captured in the loop. In this sense, the sample must be captured at the peak delay time, so that the maximum captured volume is proportional to the ejected sample volume, because $f_{C,max}$ is a constant and independent of the peak delay time, as discussed previously. Knowing the maximum volume for valid sample to be captured, any sample captured at the peak delay time in a smaller volume is hence valid.

Then, in the same way as for the sample delay time, experiments were also carried out with the non-reacting solution system, of which the reaction was deactivated in the absence of the catalyst in the solution. The original compositions of reagents C_0 (in reservoir) were all the same as in the reaction system; therefore the properties of the fluid remained the same as well. Knowing the compositions in the reaction chamber from the solution viscosities with Eq.(7-6), the captured volume was deduced from HPLC measurement with Eq. (7-8).

Since the ejection details may vary with conditions, the experiments must be carried out under different conditions. The pressure of the reagents and the ejection time are usually two of the most important parameters in the test. Combining them over a wide range of conditions, tests were then performed and information about valid sample validity was obtained for the reaction experiments.

Figure 7-17 shows the experimental results obtained by varying the ejection time τ_E at different reactant pressure P_r. The red line is the maximum of the valid sample, which is 0.22μl as given by Eq. (7-14).
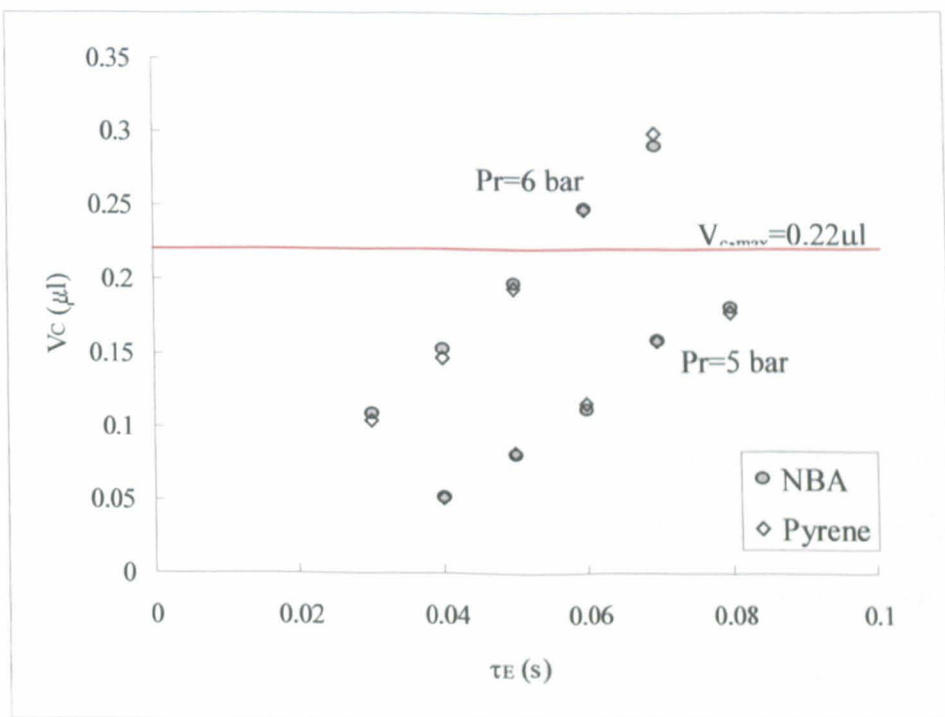
Figure 7-17 Experimental Result of Valid Sample Volume

$$(P_d = 4\,\text{bar}, \tau_R = 5\,\text{s}, \tau_S = 0.8\,\text{s})$$

These tests tell us that, at a lower pressure as $P_r = 5\,\text{bar}$, valid samples can be guaranteed when the ejection time ranges from 0.04s to 0.08s. However at a higher

pressure as $P_r = 6\,\text{bar}$, operation must be more careful since the ejection time has to

be limited within 0.05s in order to ensure the sample ejected is valid.

Again in the same way as the experiments on the sample delay time, the experiments

on the valid sample volume can be also used to assess the error caused in the kinetics

measurement by the introduction of the internal standard. Adding another 10 minutes

to the time required by the HPLC analysis method, the deviation found between the

captured sample volumes respectively based on the NBA and Pyrene concentration is

within 3% at condition of $P_r = 5\,\text{bar}$, $\tau_E = 0.06\,\text{s}$; and less than 4% at

$P_r = 6\,\text{bar}$,$\tau_E = 0.04\,\text{s}$. It then proves that extending the analysis time is helpful to

clean the HPLC column, thus reduce the error of measurement.

7.7 CHEMICAL REACTION ON-CHIP

7.7.1 The Chemical Reaction

The chemical reaction performed on the microreactor system is a simple $A + B \rightarrow C$

type reaction. Specifically, it is between two reactants that are N-Benzylideneaniline

(NBA, 99%, Aldrich) and 2,3-Dihydrofuran (DHF, 99%+, Aldrich), and forms only

one product, Tetrahydroquinoline (THQ). Scandium trifluoromethane sulphonate (Sc,

99%, Aldrich) is used as the catalyst in the process. Figure 7-18 illustrates the reaction

structure.

The reason for choosing this reaction to be performed on-chip is because known from

previous studies, it is simple, it works on a reasonable time scale that is suitable for the

microreactor system, and it has no side reactions and forms a stable product etc. As a

simple reaction, it is a good system to begin with to measure kinetics with a

microreactor device.
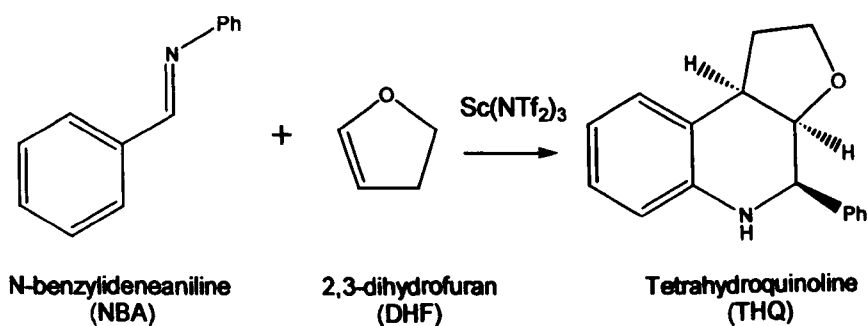
Fig. 7-18 Structure of Reaction Performed On-chip

Both the reactants and catalyst of the reaction are dissolved in the ionic liquid Emim(NTf$_2$),. By putting two reactants in the same solution whilst the catalyst is in a separate one, two solutions are available. They are referred to as "reactant solution" and "catalyst solution" respectively. The two solutions are then kept separately, by putting them in different reservoirs and feeing them into the chip through their respective tubing, so that no reaction takes place until the reactants and catalyst finally meet in the junction of the reaction mixer. From then, the reaction progresses while reactants and catalyst streams mix along the mixer and the reaction chamber. But the reaction is regarded to start at the point when the mixed reactants and catalyst streams are held in the reaction chamber because the residence time of fluid in the mixer is negligible.

For the reaction of interest, the reaction rate can be expressed by either the consumption rate of NBA or the formation rate of THQ, as only these two substances besides the internal standard can be accurately measured by HPLC.

$$\text{NBA} + \text{DHF} \xrightarrow{\text{Sc}} \text{THQ} \qquad\qquad (7\text{-}15)$$

Choosing to be expressed by the production of THQ in the process, the rate law of the second-order chemical reaction as in Eq.(7-15) is then:

$$\frac{dc}{dt} = k'([NBA]_0 - c)([DHF]_0 - c) \tag{7-16}$$

in which, k' is the reaction rate coefficient, $[NBA]_0$ and $[DHF]_0$ are the initial concentration of reactants NHA and DHF respectively, and c is the changed amount of species concentration (Atkins and De Paula 2002).

The concentration of NBA changing with reaction time is solved as:

$$[NBA] = [NBA]_0 \frac{\gamma \exp(-\gamma t/t^*)}{\gamma + 1 - \exp(-\gamma t/t^*)} \tag{7-17}$$

in which the two dimensionless parameter γ and t^* are:

$$\gamma = \frac{[DHF]_0 - [NBA]_0}{[NBA]_0}, \quad t^* = 1/k'[NBA]_0 \tag{7-18}$$

The concentration of THQ forming with reaction time is:

$$[THQ] = [NBA]_0 - [NBA] \tag{7-19}$$

A simple and rapid method to determine the rate coefficient k' of a chemical reaction is through its half-life $t_{1/2}$. For second-order chemical reactions, the value of $t_{1/2}$ depends on the initial concentration of reactant $[A]_0$, i.e.:

$$t_{1/2} = \frac{1}{k_2[A]_0} \tag{7-20}$$

Knowing $[A]_0$ and working out the value of $t_{1/2}$ from the experimental data, a plot can then be made of $t_{1/2}$ against $1/[A]_0$, and the slope is the value of $1/k_2$. This in return gives a check on the assumption of the reaction order if a linear fitting is found to fit the data points. (Atkins and De Paula 2002)

210

The standard half-life time method to determine the reaction order and reaction rate coefficient from raw experimental data is as follows. (Atkins and De Paula 2002)

a) Plot reagent concentration $[A]$ changing with reaction time t.

b) Choose a sequence of concentration $[A]_{0i}$ as "initial" concentrations and record corresponding time $t([A]_{0i})$.

c) In the plot, find the time $t([A]_{0i}/2)$ for the "initial" concentrations to reduce to its half vale by interpolation. The half-lift time corresponding to concentration $[A]_{0i}$ then is:

$$t_{1/2}([A]_{0i}) = t([A]_{0i}) - t([A]_{0i}/2) \qquad (7\text{-}21)$$

d) If $t_{1/2}([A]_{0i})$ is independent of $[A]_{0i}$, then the reaction is first-order. Otherwise, plot $t_{1/2}([A]_{0i})$ against $1/[A]_{0i}^{n-1}$. The general expression of $t_{1/2}$ in terms of $[A]_0$ in nth-order reaction is:

$$t_{1/2} = \frac{2^{n-1}-1}{(n-1)k_n[A]_0^{n-1}} \quad (n \geq 2) \qquad (7\text{-}22)$$

Hence, if a straight line can be obtained, the reaction order is n, and the slope is the vale of $\dfrac{2^{n-1}-1}{(n-1)k_n}$.

The catalyst in the chemical reaction has no effect on the reaction order. However, it influences the reaction rate. Therefore, for different catalyst concentrations, the reaction rate constants would be different. This is of particular importance for making reasonable comparison between reactions.

7.7.2 System Operation over Regimes of Reaction Time

Initial reaction tests were also made on the captured sample volume versus the reaction time in exactly the same way as for the experiments on sample delay time.

Surprisingly, the data points were found to fall into two regimes above and below the reaction time $\tau_R = 30\,s$. As shown in Figure 7-19, for the reaction times greater than 30s, the captured sample volume was about 0.15µl and gently decreased with time scale. However, once the reaction times became over 30s, the captured volume reduced dramatically to be around 0.01µl. The different results of the captured sample volume in two reaction time regimes are caused by different reasons.
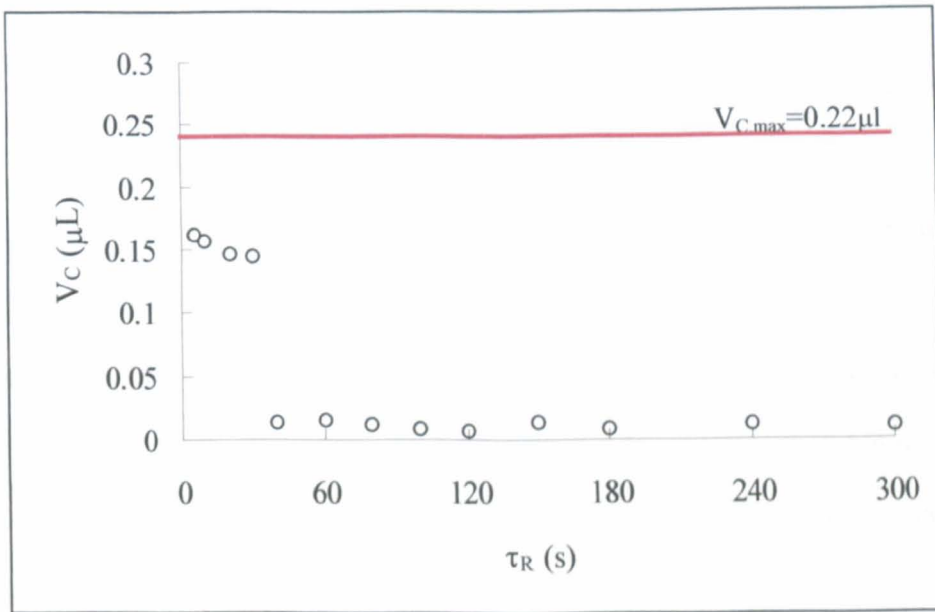
Figure 7-19 Different Regimes of Reaction Time

$(P_r = 5\,\text{bar}, P_d = 4\,\text{bar}, \tau_E = 0.06\,\text{s}, \tau_S = 1.0\,\text{s})$

For the short reaction times, the gentle decreasing in the captured sample volume is mainly caused by the relaxation of the Teflon hole in the solenoid valves. As discussed previously, the expanded Teflon material over long flushing time relaxes with the time when the pressure is withdrawn from the fluid. Hence, the longer the reaction time is, the closer the Teflon hole is to the normal and comparatively the more tightly it holds the pintle. As a result, the volume passing through the hole in the same ejection time reduces because it takes longer for the pintle to reach the same opening position.

However, since the effect of the relaxation of the Teflon hole is small, the decreasing of the sample volume occurs gradually over the reaction time.

The reason for the dramatic change in the captured sample volume at reaction time over 30s is considered to be partly due to the same reason as for the regime of short τ_R. However, in later fluorescence studies (see Chapter 8), it was found to be more because of the conditions applied to operate the MCR system. As illustrated in Figure 5-8, when $\tau_R > 30s$ ($\tau_P = 30s$), the pressure was brought down to zero and built up again in the last 30s of the reaction time. During the pressure's building up, before the ejection of the reaction sample, the diluent valve opened whilst all the other four reactants valves were kept closed. It was then possible for the methanol stream to flow back through the dilution mixer and even back to the end of the reaction chamber (as the fluorescence images shown in Figure 7-20), due to the re-expanding of the relaxed upstream flow passages. Therefore, the ejected volume in this case contained some methanol, thus the volume of real reaction sample was greatly decreased, depending on how much methanol was added to the sample before the ejection started.
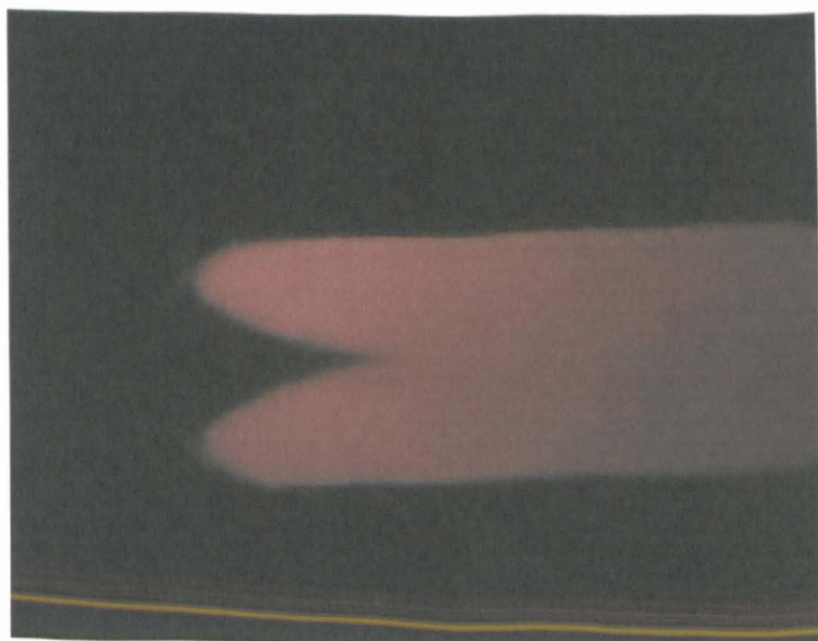
Figure 7-20 Diluent Flowing Back into Reaction Chamber

To solve this problem, a decision was made to extend the ejection time, so that a sample with proper volume could be ejected and captured for HPLC analysis for the reaction times longer than 30s. As shown in Figure 7-21, different ejection times were used for the two regimes of the reaction times, of which 0.06s was used for the short reaction time and 0.3s for the long one. Accordingly, the captured sample volume in the long reaction time regime approached a level similar to that in the short reaction time, thus samples in both regimes fell in the range of the HPLC measurement.
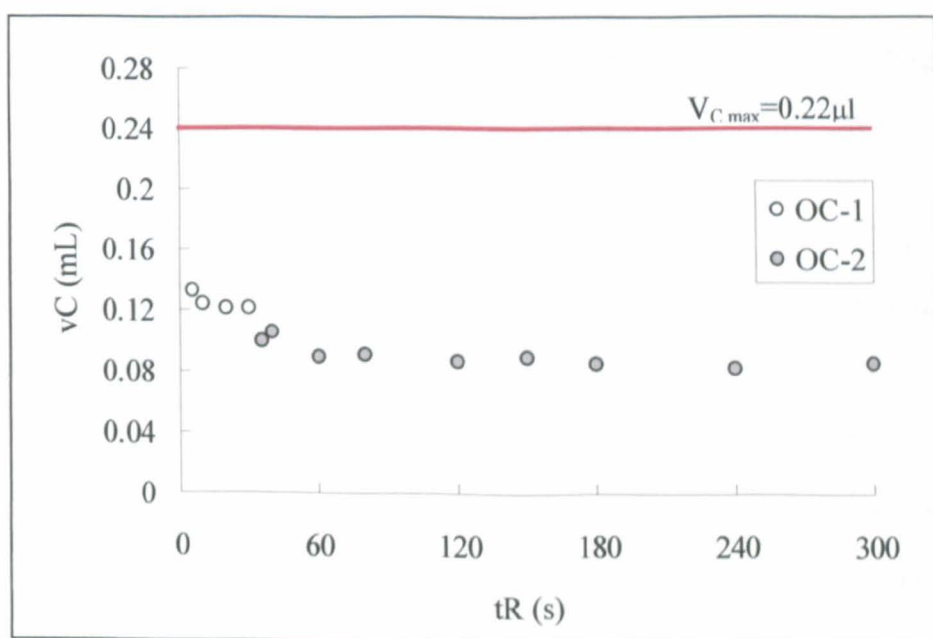
$(P_r = 5 \, \mathrm{bar} , P_d = 4 \, \mathrm{bar} ; \tau_S = 1.2 \, \mathrm{s} ; \mathrm{OC\text{-}1}: \tau_E = 0.06 \, \mathrm{s} ; \mathrm{OC\text{-}2}: \tau_E = 0.3 \, \mathrm{s})$

Figure 7-21 Controls for Different Regimes of Reaction Times

7.7.3 Chemical Reaction On-chip

With sample delay time and ejection time determined, the chemical reaction was then carried out in the microreactor system Mark I with the reactants and catalyst solution introduced.

Tests were first made to study the effect of the catalyst concentrations on the reaction rate. In each test, different reaction times were set through the interface as shown in Figure 5-9 for a sequence of measurements, so that a campaign of kinetics study could be carried out automatically under the computer control, and the yield of the chemical reaction changing with time was obtained. The reactant solutions in the tests were prepared at similar concentrations, but the catalyst loadings were quite different (details are given in Table 7-5). Results of both tests are plotted in Figure 7-22.

Table 7-5 Conditions of Reaction Tests on Effect of Catalyst Loadings

		Test-1	Test-2
Species concentrations (M)	NBA	0.0855	0.0825
	DHF	0.178	0.176
	Sc	0.0014	0.000696
	$[NBA]_0/[Sc]_0$	61.1	118.5
Operating conditions	Pressure	$P_r = 6\,bar$, $P_m = 4\,bar$	
	Time scale	$\tau_E = 0.3\,s$	$\tau_E = 0.5\,s$
		$\tau_P = 30\,s$, $\tau_F = 20\,s$, $\tau_S = 0.9\,s$	
	Temperature	$T = 25.6\,°C$	$T = 28.1\,°C$

Due to the lack of enough data points, especially in early reaction stage, it is difficult to determine the reaction orders and reaction rate constants of these two tests. Instead, the theoretical fit had to be made with the second-order reaction law by simply changing t^* in Eq.(7-17), and the one that best fits the experimental data was determined by the least rms of the relative deviations between the theoretical fie and experiments. The simple method however decided a relatively accurate value of t^*. As

illustrated in Figure 7-22(a), further changes of t^* by $\pm10\%$ would result in the rms deviations to increase about 5%.
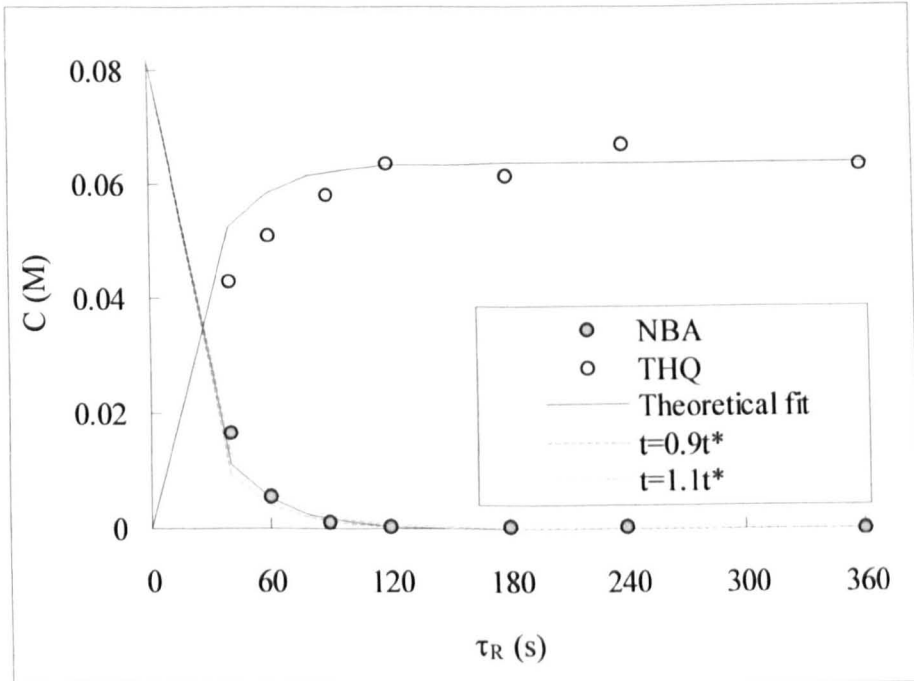
(a) Test-1
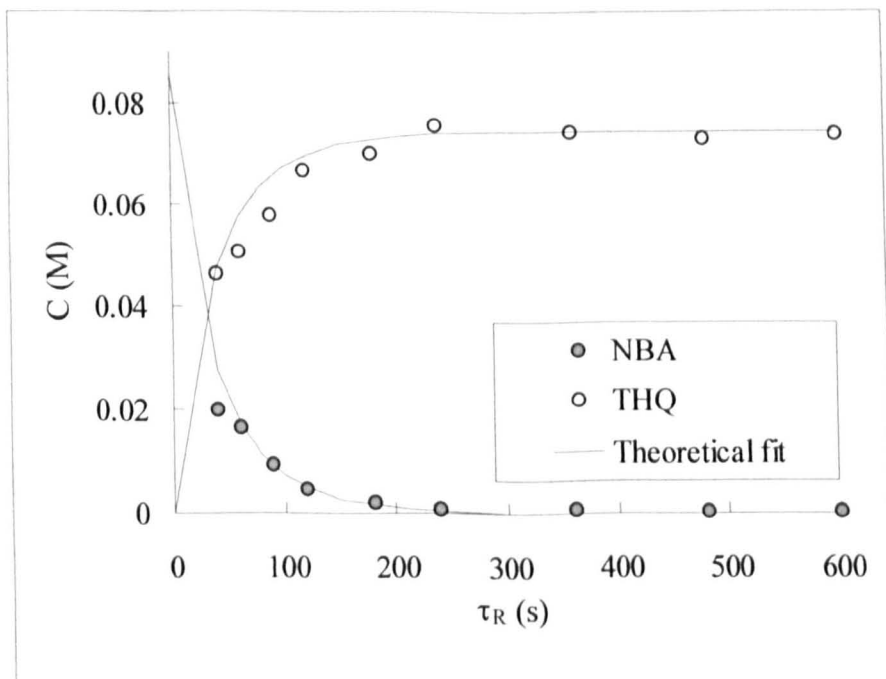
(b) Test-2

Fig.7-22 Effect of Catalyst Loading on the Reaction Rate

Nevertheless, the theoretical prediction is found not to meet the experimental results very well, especially for the product THQ. This is due to the impurity of the solvent. The density of Emim[NTf$_2$] used for the tests was found to be only 1421 kg/m^3, in relation to the normal value 1500-1540 kg/m^3 of the pure liquid. Meanwhile, the total concentration of NBA and THQ in the reaction was found to be lower than the initial concentration [NBA]$_0$. Hence, NBA was suspected to decompose due to the impurity of the solvent, so that the reaction kinetics was different from the theoretical prediction.

However, despite these shortcomings, the effect of catalyst loading on the reaction rate can still be seen to be significant. Comparing these two plots, the reaction of Test-1 seems to reach an asymptote at about 120s whilst Test-2 took at 240s. As the concentration of the catalyst solution in Test-1 is nearly twice that in Test-2, this indicates that the reaction rate increases with the concentration of catalyst solution. This is an important point because to make a reasonable comparison of reaction kinetics, catalyst loading must be taken into account.

More tests were then made to study the reaction kinetics in Emim[NTf$_2$]. Of an example, the species concentrations and conditions used for the chemical reaction are listed in Table 7-6. Purity of the ionic liquid was also confirmed by its density, which was 1547 kg/m^3.

Reaction kinetics was first checked with the raw experimental data. By plotting the half-life against the initial concentration of NBA, a straight line fitted well the data points (as given in Figure 7-23). As indicated by Eq.(7-20), the linear relation between $t_{1/2}$ and $1/[NBA]_0$ then confirms that the NBA reaction is a second-order reaction. The

reaction rate constant k_2 for the reaction at the specific catalyst concentration and experimental conditions is 0.923 $M^{-1} \cdot s^{-1}$.

Table 7-6 Conditions of Chemical Reaction in Emim[NTf2]

Species Concentration (M)		Operating conditions	
NBA	0.103	Pressure	$P_r = 5\,bar$, $P_m = 4\,bar$
DHF	0.231	Time scale	$\tau_P = 30\,s$, $\tau_F = 20\,s$
Sc	0.00101		$\tau_E = 0.05/0.5\,s$, $\tau_S = 1.1\,s$
[NBA]o/[Sc]o	101.6	Temperature	$T = 18.4\,°C$
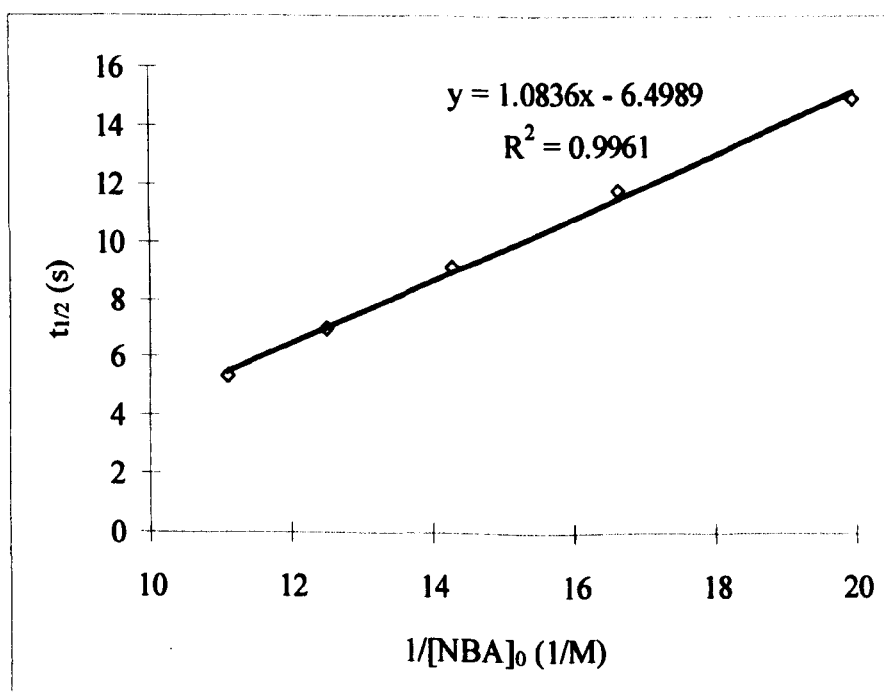
Fig.7-23 Determination of Reaction Order and Rate Coefficient

All the reaction results are shown in Figure 7-24. Using the criterion of least rms of

relative deviation, the second-order reaction law is used to fit the data since the

reaction order has been confirmed.
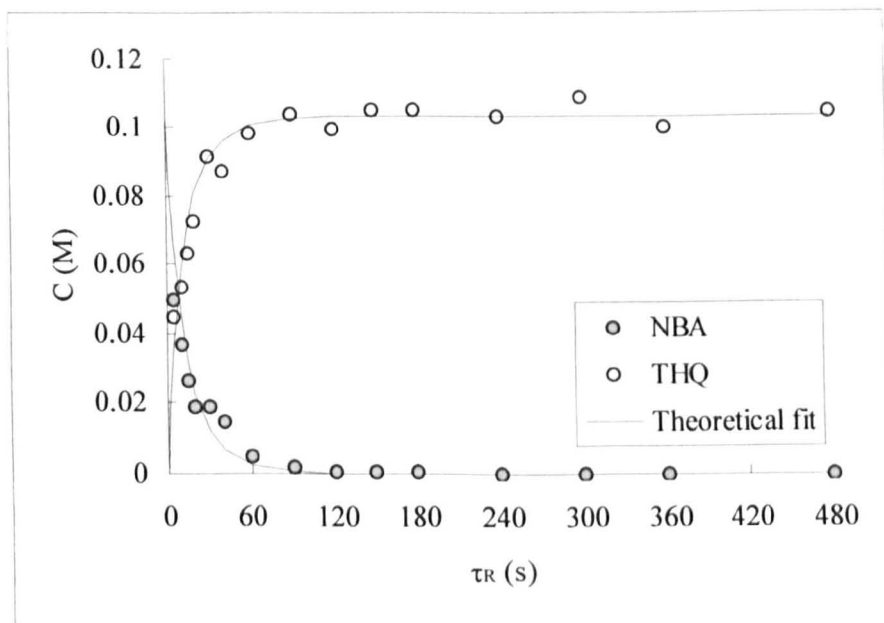
Figure 7-24 NBA Reaction in Emim[NTf2] On-chip

In relation to the theoretically fitted curves, the scatter of experimental data can easily

be seen in both the NBA and THQ profiles. The scatter may result from several causes.

The decreasing trend of the NBA concentration changing at $\tau_R = 30s$ is mainly caused

by the diluent flowing back into the reaction chamber when the pressure was built up

at the end of the reaction time. As the reaction mixture was then partly diluted, and the

reaction stopped, the captured sample contained a mixture of different reaction times.

Meanwhile, the THQ results seem to scatter more than the NBA, and the concentration

of some points are even higher than the original value of the reactant. This is because

an isomer of THQ was formed in the reaction due to the impurity of the ionic liquid.

As their peak areas were too close to be distinguished, readings had to be made

through simply taking them as a total and then converting into absolute concentrations with the calibration factor of the THQ. The resultant error is estimated to be about 15%, deduced from a calculation on the mass balance of the process.

Because of a lack of corresponding data, a comparison could not be made between the kinetics measured manually and automatically by the MCR system of the reaction under the same conditions. But from the experiments carried out on-chip, it was found that the purity of ionic liquids has a big impact on the chemical reactions. For instance, impure ionic liquids were found to be able to catalyse the reaction even without the presence of the catalyst, or even worse, unexplained crystals could form during the reaction on-chip.

Compared to conventional manual kinetics operations, the measurable time scale of the chemical reaction is much improved in the MCR system. Typically, for a manual system, the shortest measurable reaction time is about 30 seconds for an experienced experimenter. However, it is now 5 seconds or even less for on-chip kinetics study. Therefore, automatic measurement, small hold-up of solvents and a wide measurable range of time scale are the advantages of the MCR system over the manual method in the measurement of reaction kinetics in ionic liquids.

7.8 CONCLUSION

Through a series of experiments, the performance of the MCR system, such as the mixing performance, the behaviour of solenoid valves, and the operating conditions, have been tested before a chemical reaction was carried out on-chip. As a result, appropriate methods and conditions have been determined for the operation of the system. Meanwhile, drawbacks including high deviation in the mixing performance, unexpected valve behaviour and inappropriate operating conditions for long reaction

time have also been identified. Based on the study discussed in the chapter, improvements will then be made, in order to make the measurement of reaction kinetics with the MCR system more reliable and accurate.

221

Chapter 8

KINETICS MEASUREMENT DEVICE MARK II

8.1 INTRODUCTION

Drawbacks have been identified in the performance of the Mark I MCR system through a series of tests with both reacting and non-reacting solution systems. These included:

- Large standard deviations in the mixture uniformity produced through 16 elements of the FNM type reaction mixer;

- Pseudo random behaviour of solenoid valves during the opening/closing process of ejection

- Lack of precise control of pressure conditions during long reaction times, which caused the backflow of diluent in the reaction chamber, thus resulting in smaller amount of reaction sample being captured for the HPLC analysis.

Realising these problems, efforts have then been made to improve the design and produce a Mark II version of the system. Specifically, new designs of the reaction mixer as well as the dilution mixer have been proposed for a mixing performance of $\sigma_Y = 1\%$. The sampling method has also been changed to mitigate the impact of the non-ideal valve performance. In addition, appropriate operating conditions were also determined, to achieve a good control of the MCR system. These developments enable

more reliable and accurate measurements to be made for the study of reaction kinetics in ionic liquids.

8.2 IMPROVEMENTS OF THE DESIGN OF MIXERS

As discussed in detail in Chapter 7, the mixing performance of the developed folding network mixer in the MCR system was not as good as expected, due to the coarse grids used in the design computations and the fewer cases computed at low Peclet number for the design of the mixer. The resulting error in the computation thus led to an overestimation of the decay rate of σ_Y with the numbers of mixing elements k, and the situation became even worse when the law was applied for the scale-up to high Peclet number cases.

To make improvements to the mixers, more computations have been carried out, with finer grids as well as under cases of a wider range of Peclet numbers. As a result, a new decay law has been found for the decreasing of σ_Y over k, which is in the same expression as Eq.(7-3), but with different values of the constants (see Table 8-1). By rewriting Eq.(7-3) into the form of Eq.(8-1), the new exponential decay law was used to determine the mixing elements required to well mix the reactants streams through both the reaction and dilution mixers.

$$k = -\frac{\ln\dfrac{\sigma_Y}{\sigma_{Y_0}} \times \left(\ln(Pe) + \zeta\right)}{\alpha} \qquad (8\text{-}1)$$

Table 8-1 Values of Constants in Exponential Decay Fitting Law

Parameter	α	σ_{Y_0}	ζ
Reaction mixer	1.81	0.657	-3.94
Dilution mixer	14.3	1.56	-1.01

With such an equation, 23 elements are found to be needed in a FNM in order to achieve $\sigma_Y = 1\%$ at $Pe = 10^6$. Hence 29 elements were specified for the reaction mixer, for reasons of caution and good arrangement in the layout of the network as well. The standard deviation of the mixing uniformity is then estimated to be about 0.5% in the situation where a perfect alignment is achieved. But it is found that, even if an offset occurs between the layers of glass, the mixing performance of the new reaction mixer will still be acceptable. For instance, for the mixers of Mark I, σ_Y increases 1.4 times due to the offsets between glass layers, from 17.6% predicted with the decay law to 25% found in the performance assessment. Deduced with the value, if the same alignment occurs in the chip of Mark II, the standard deviation of the new reaction mixer will then be in the order of 1% after 29 elements.

Improvements have been made on the design of the dilution mixer as well. But in addition to considering the insufficient number of mixing elements, Reynolds number has also been taken into account. The diluent flow was found to be at a Reynolds number around 100 at the operating condition of the MCR system. Since at such a high value of Re, the fluid flow is already in the inertial-affected range, an alternative design of the dilution mixer was proposed. Referred to as the "swirl mixer", its mechanism is to mix the fluid streams by distorting the interfaces when the flow at high Reynolds number swirls through the two chambers and a connecting hole (as shown in Fig.8-1 (b)).

CFD computations have been carried out with the help of Dr. MacInnes on both the folding network mixer and the swirl mixer, in order to make a comparison between the two. Both computational geometries are shown in Figure 8-1, of which the cross section is in the shape of a trapezium since the channel was manufactured by powder-blasting method.

(a) Folding network mixer   **(b) Swirl mixer**
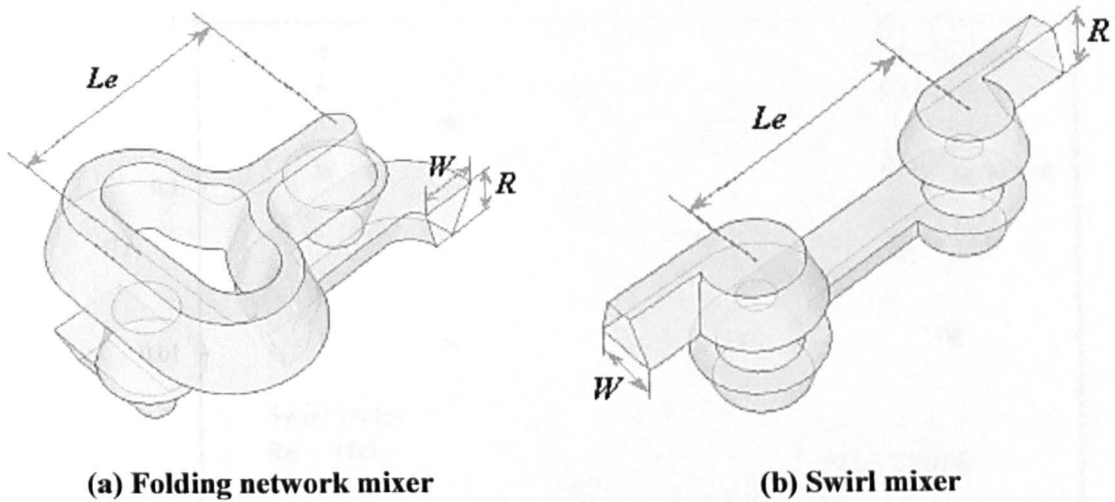
Fig. 8-1 Computational Geometry of Swirl Mixer

Computations have then been made on both mixers at $Pe = 1000$ and two Reynolds numbers conditions of $Re = 0.1$ and $Re = 100$ respectively. As given in Figure 8-2, the two mixers show different behaviour in respect of Reynolds number. Comparatively, the FNM looks less sensitive to a change of Reynolds number, since its results at two values of Re are quite close. The performance of the swirl mixer, however, differs greatly with Re. As shown in the figure, it behaves very poorly at low Reynolds number, but it exhibits an even better performance than that of the FNM at $Re = 100$. For instance, to achieve a deviation of $\sigma_Y = 1\%$, 6 elements of the FNM type mixer are needed, however, for the swirl mixer, the number decreases to only 2. Therefore, concerning the elements required to achieve the same mixing performance at Reynolds number in the order of magnitude of 100, the swirl mixer is more effective than the folding network mixer that had been previously used as the dilution mixer.
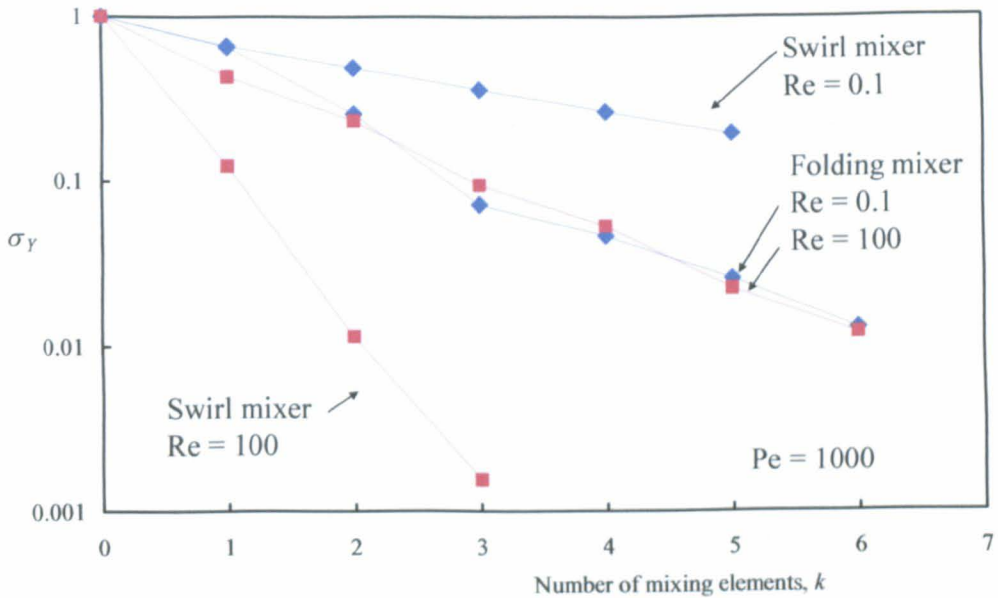
Fig. 8-2 Computational Results of FNM and Swirl Mixer at Different Re

Comparison has also been made between the pressure drop needed along the two mixers. Figure 8-3 gives the computational results of non-dimensional pressure drop in one element of two mixers as a function of Reynolds number. It can be found that at $Re = 100$, the normalised pressure drop per element of the swirl mixer is nearly twice that of the FNM. However, as the number of mixing elements required by the swirl mixer is only 1/3 of that in the FNM, the overall pressure drop will be still lower for the swirl mixer to achieve the same mixing performance.

Based on the comparison discussed above, the swirl mixer shows advantages over the FNM in both the required mixing elements and pressure drop to achieve a good mixing performance at high Reynolds number of 100. Hence, it was selected to be type of the dilution mixer in the Mark II design of the reaction network. A swirl mixer with 5 elements was specified, since as indicated by Eq.(7-3) and the values of corresponding parameters in Table 8-1, it will produce a mixture with $\sigma_Y = 0.5\%$ at $Pe = 10^6$.
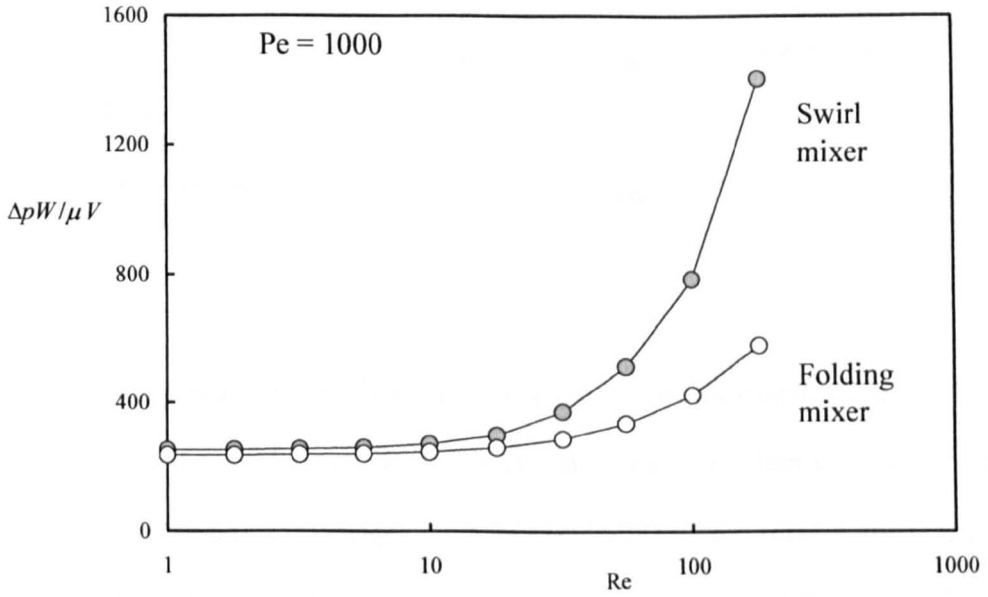
Fig. 8-3 Non-dimensional Pressure Drop in One Mixing Element as

A Function of Reynolds Number For Two Mixers.

The layout of the reaction network with new reaction mixer and dilution mixer is illustrated in Figure 8-4. For dimensions of both mixers, please refer to Table 8-2.
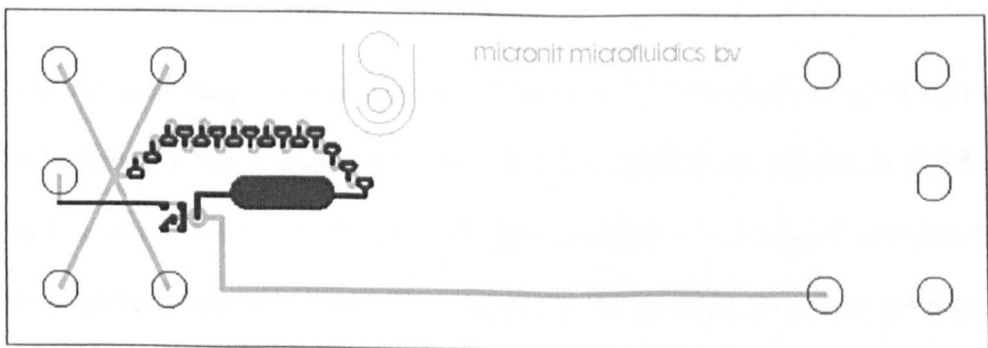
Fig. 8-4 Layout of New Design of Reaction Network

(Dimension details are given in Appendix-3)

Table 8-2 Dimensions of Improved Design of Reaction Network

	W (μm)	R (μm)	L_e (μm)	Number of elements
Reaction mixer	200	150	75	29
Dilution mixers			90	5

Unfortunately, the performance of the mixers could not be assessed in the way that was undertaken for the Mark I reaction network. Because the channels were made by powder-blasting method, the rough channel bottom would reflect the light in all directions. Thus the light intensity measured would contain contributions of scattered light from somewhere else, rather than be in proportion to the number of fluorescent molecules in the channel depth. Therefore, the measurement would be meaningless, since a large error is unavoidable and unpredictable. But, according to above discussions, a mixing performance of $\sigma_Y = 1\%$ can be estimated for the reaction mixer and maybe even less for the dilution mixer.

8.3 IMPROVEMENTS IN THE SAMPLING PROCESS

Concerning the sampling process, the drawbacks of the old method lie in two aspects: the small volume of the reaction chamber and the method to capture a valid sample. The small reaction chamber of the old network resulted in both small volume for valid sample and limited time for the ejection process. As a result, to obtain a valid sample, the valve had to be opened and closed in very short time before the ejected volume reached the sample loop. Then the impacts of both the opening and closing action of the valve on the fluid flow were included in the sample to be captured. For example, due to the operating conditions applied and the relaxation of the flow passages, the sample ejected at the very beginning might contain the methanol which had flowed

back into the reaction chamber, and thus strictly speaking, was an invalid sample. Moreover, the closing of the valve would add an extra volume to the sample, hence the ejection of the sample became unpredictable and information could only be obtained through experiments. In addition, because the sample is so small, accurate measurement of the ejected sample volume was impossible. Consequently, a valid sample had to be determined via its captured volume by the loop, and, whilst a method to capture it at the peak delay time was successfully used in order to judge the validity of sample with the constant maximum capture faction, the system was not ideal.

Accordingly, improvements are made on the two aspects of the sampling process as discussed above. First, the reaction chamber in the new design of the network has been enlarged. Extending the width to 1.5mm and the length to 4.77mm and a depth of 0.15mm, the volume of the new powder blasted reaction chamber has been increased to 1μl, which is about three times that of the old one. Second, the operating pressure conditions have been changed. Instead of being brought down to zero for a reaction duration longer than that set for pressure building-up, the pressure is maintained at the same level all the time until the end of one measurement. And finally, the sampling method has been improved to avoid the impacts of the uncertain valve opening/closing actions. Specifically, two changes have been made for the capture of a valid sample. First, to avoid the possible contamination of the sample tip that may happen when the valve is opening for ejection, the sample is to be captured after its front has left the loop whilst the invalid part has not arrived yet. Second, to avoid the effect of the valve's closing, the ejection valve is to be kept open. As a result, a continuous stream of mixed diluent and materials from the reaction chamber will fill the loop and the upstream flow passages when the part contained in the loop is caught and conveyed to the HPLC column. In this way, the validity of the sample is better guaranteed, but the time control becomes crucial to obtain a good sample for the kinetics measurement. In order to distinguish the method from the old one that used before, the new sample method is

referred to as "sampling with valve open", while the old one referred to as "sampling with valve closed".

A new model has also been developed to help to understand the new sampling method. Using the same approach as in the model for the sampling with valve closed, the entire process of the sample passing through and being captured in the loop can then be reduced to two simple cases. As illustrated in Figure 8-5, depending on the time that the parabolic front of the volume ejected from the reaction chamber reaches and leaves the loop, these cases are:

a) $L_P \leq L_F < L_L$: The tip of the ejected volume is inside the loop.

b) $L_F > L_L$: The tip of the ejected volume has gone beyond the loop.

The equation to calculate the captured sample volume can be borrowed from the old model as:

$$V_C = \int_{L_P}^{\min(L_F, L_L)} \pi R_0^2 \left(1 - \frac{x}{L_F} \right) \cdot dx \qquad (8\text{-}2)$$
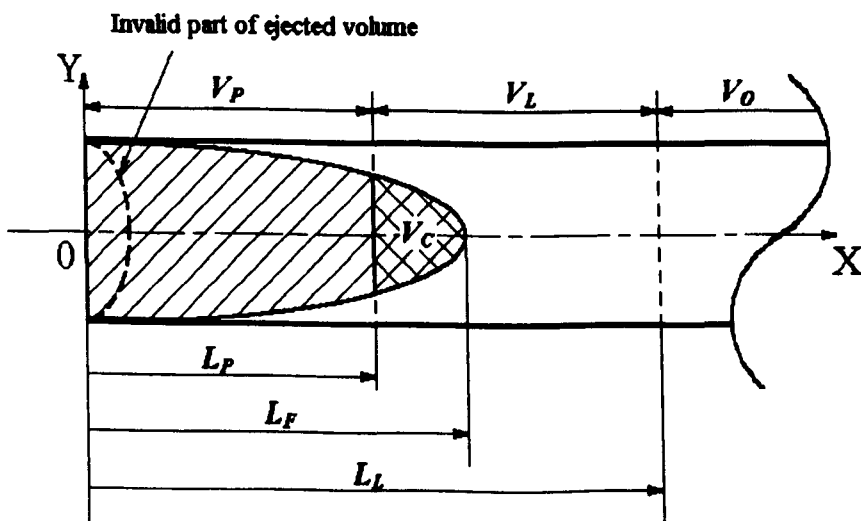
(a) $L_P < L_F \leq L_L$
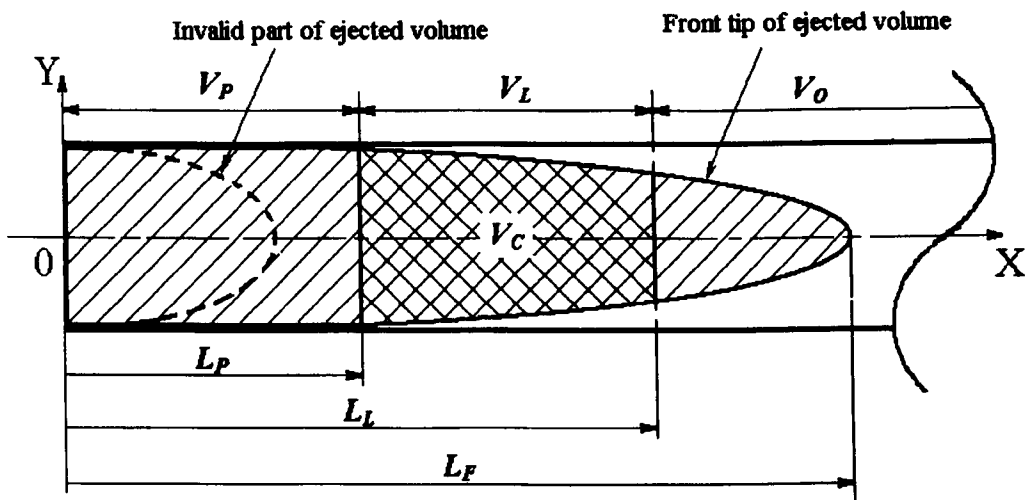
(b) $L_F > L_L$

Fig. 8-5 Schematic of Sampling with Valve Open

As the ejection process in the new sampling method is a continuous process, the diluted sample volume in the passage leading to the loop is a function of the time τ_S and the sum of the flow rate of stream ejected from the reaction chamber Q_I and that of the diluent flow Q_D as:

$$V_S = Q_t \tau_S \qquad (8\text{-}3)$$

in which,

$$Q_t = Q_I + Q_D.$$

And in a steady state of the fluid flow, there is:

$$DR_E = \frac{Q_D}{Q_I} \qquad (8\text{-}4)$$

Then replacing L_0 with L_L in Eq.(5-16) and substituting corresponding variables with Eq.(5-20) and (5-21), solutions are obtained for case a) and b) as:

a) $L_P \leq L_F < L_L$:

$$
\begin{aligned}
V_C &= \int_{L_P}^{L_F} \pi R_0^2 \left(1 - \frac{x}{L_F}\right) dx \\
&= \pi R_0^2 (L_F - L_P) - \pi R_0^2 \frac{\left(L_F^2 - L_P^2\right)}{2L_F} \\
&= Q_t \tau_S - V_P + \frac{V_P^2}{4Q_t \tau_S}
\end{aligned}
\tag{8-5}
$$

b) $L_F > L_L$:

$$
\begin{aligned}
V_C &= \int_{L_P}^{L_L} \pi R_0^2 \left(1 - \frac{x}{L_F}\right) dx \\
&= V_L - \frac{V_L^2 + 2V_P V_L}{4Q_t \tau_S}
\end{aligned}
\tag{8-6}
$$

Comparisons are then made between the experimental data and the prediction with the model for the sampling process with the valve open. As shown in Figure 8-6, the same trends are found in both the prediction and the experiment. That is, after a sharp increase in slope, the captured sample volume becomes stable as a result of the steady state established between the diluent flow and the stream ejected from the reaction chamber after the valve is fully opened.

Moreover, results of two cases where $\tau_R = 30s$ and $\tau_R = 60s$ are given simultaneously in the figure as well. One may remember that, for these two reaction times, it was found in the old sampling regime that the captured sample volume reduced dramatically from the short time scale to the long one, due to the pressure dropping and the relaxation of flow passages during the long reaction time. However, this phenomenon is obviously improved under the new operation of pressure condition, where the pressure is maintained at the same level regardless of the reaction time. The captured volumes corresponding to the same τ_S at the two reaction times are very close to each other, if taking into account the difference existing between experiments (details are given in Table 8-3).
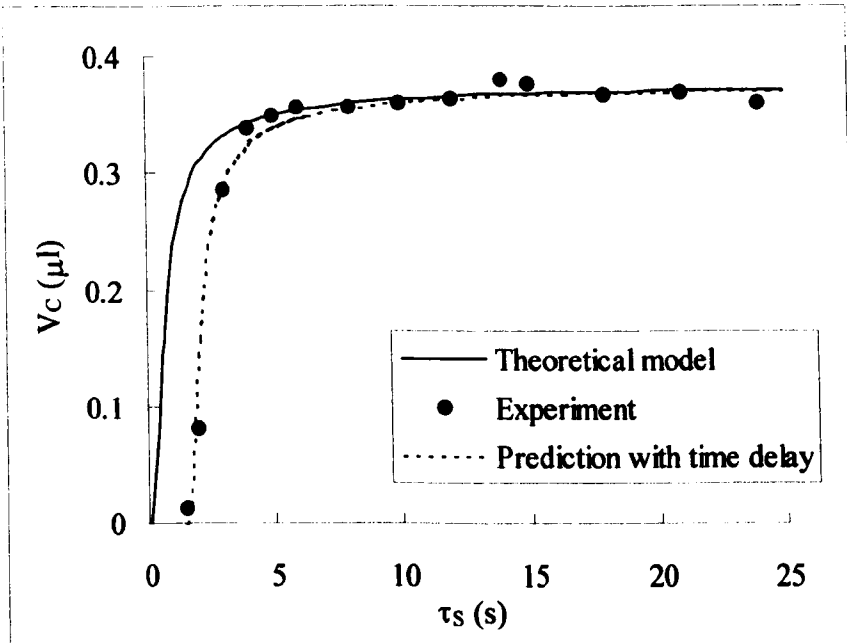
(a) $\tau_R = 30$s
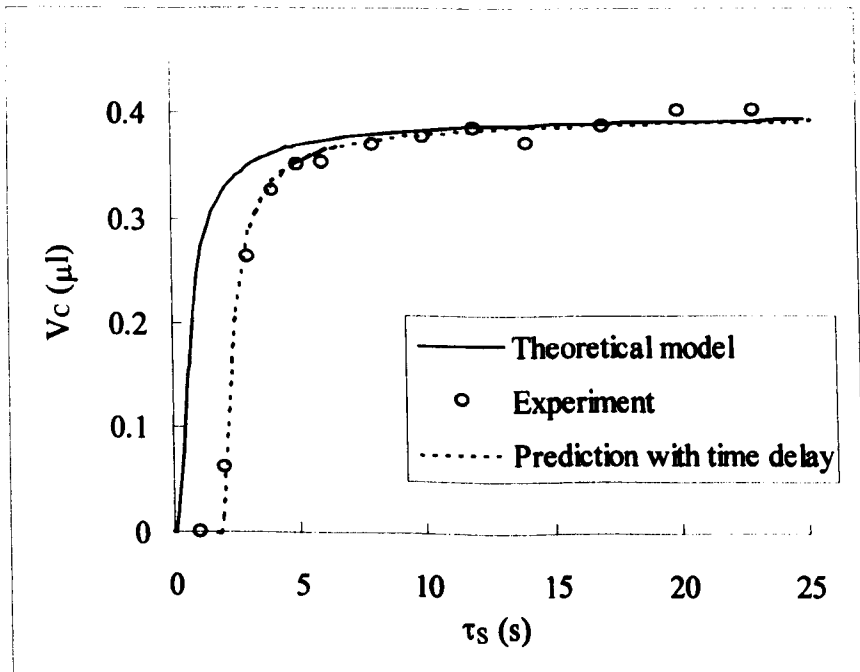
(b) $\tau_R = 60$s

Fig. 8-6 Comparison Between Experiment and Model of Sampling with Valve Open

Table 8-3 Conditions of Data in Figure 8-6

	P (bar)	V_P (μl)	V_L (μl)	Q_t ($\mu l/s$)	DR_E
$\tau_R = 30s$	$P_r = 6$	3.99	20	18.86	52
$\tau_R = 60s$	$P_m = 4$			18.52	49

Regarding the prediction of the model and the experimental data, one may notice there is a time delay between the model and the reality for both cases, which are about 1.4s for $\tau_R = 30s$ and 1.7s for $\tau_R = 60s$. This could not be really explained until further study with fluorescent dye could be carried out under microscope.

As shown in Figure 8-7, by feeding the reactant reservoirs with fluorescent dye Rhodamine B in ionic liquid Emim[NTf$_2$] at a concentration of 0.008M, whilst the diluent reservoir with methanol as usual, a series of images for the sample ejection have been taken at the diluent mixer under the microscope.

(a) $\tau_E = 0$ s

234
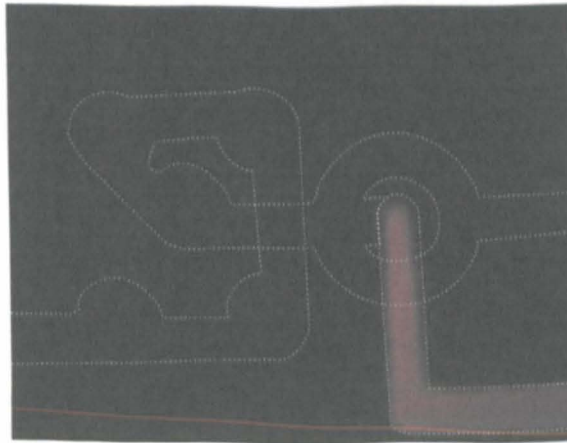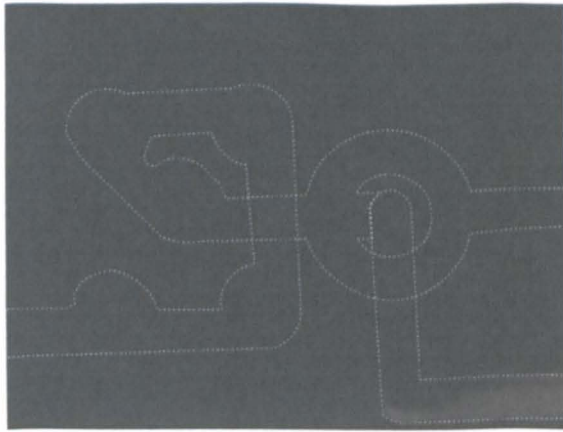
(b) $\tau_E = 0.6\,\mathrm{s}$
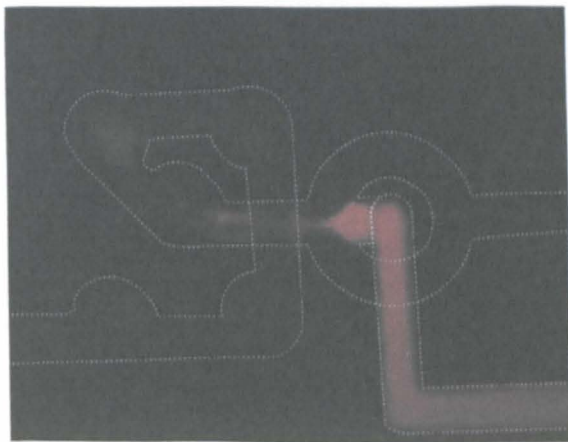
(c) $\tau_E = 1.0\,\mathrm{s}$
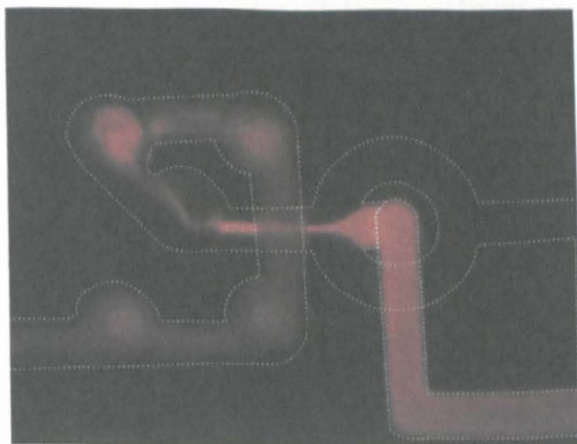
(d) $\tau_E = 1.5\,\mathrm{s}$
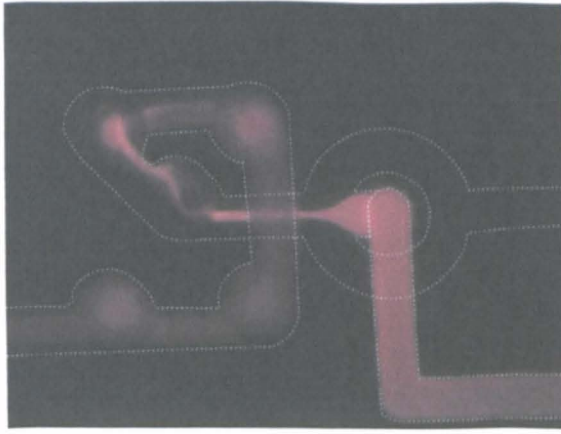
(e) $\tau_E = 2.2\,\text{s}$
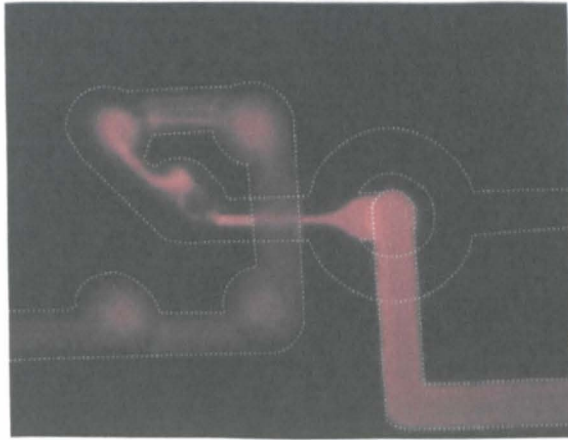
(f) $\tau_E = 2.6\,\text{s}$
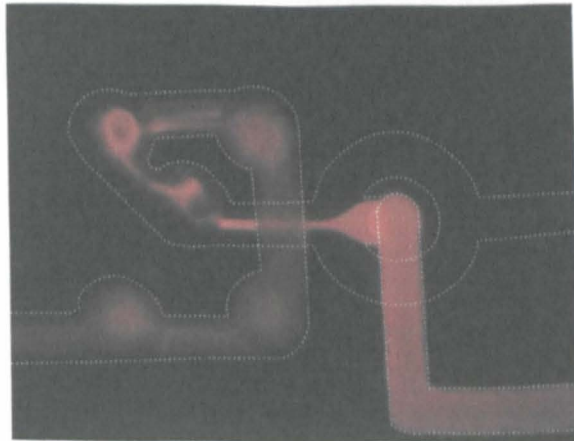
(g) $\tau_E = 3.1\,\text{s}$

Fig. 8-7 Study of Ejection Process with Fluorescent Dye ($P_r = 6\text{bar}$, $P_m = 5\text{bar}$)

(The white dotted line is the outline of the channel)

According to the time sequence, the ejection started at $\tau_E = 0s$. At this moment, the end part and both edges of the channel leading from the outlet of reaction chamber to the dilution mixer was found filled with methanol. This is caused again by the relaxation of the Teflon liner of the solenoid valves. Although the pressure in the new operating conditions is kept high during the reaction time, the pressure at the outlet of the valve still decreases, to the value at the junction before the dilution mixer, due to the stopping of the flow. As the pressure gradually decreases, the Teflon liner relaxes, squeezing some material out until the pressure reaches the same level as that at the junction. Since the relaxed Teflon hole provides capability for more fluid, a small amount of methanol then flows back into the leading channel from the reaction chamber and causes the Teflon liner of the valve to expand again. With Figure 8-7 (a), by roughly measuring the channel length and width that were occupied by methanol before the ejection, the relaxation of the Teflon liner is estimated to be about $0.015\mu l$.

As soon as the ejection starts, the methanol flow was found to continue to move back into the leading channel, but at a far faster speed, until the fluorescent stream started to flow and push the methanol out of the channel (as shown in Figure 8-1 (b)). This process, however, could not be demonstrated in previous experiments. The further back flowing of methanol at the very early stage of the ejection is thought to be associated with the valve's opening action. When the ejection valve opens, some fluid is drawn back because a temporary low pressure may be caused due to the fast movement of the pintle and the high viscosity of the fluid. With channel length estimated from Figure 8-1 (b), the volume of the fluid drawn back during the process is approximate $0.031\mu l$ for a single valve.

Since half the downstream channel is occupied by the methanol before the ejected stream begins to move forwards, it takes longer for it to reach the junction before the

dilution mixer. As given in Figure 8-7 (c), the time scale found in the study is about

1.0s. It is longer than that calculated with channel volume and the flow rate of the

ejected stream, because at the beginning of ejection, the fluid flow is somewhat

different from that of the steady state.

Figure 8-7 (d)-(g) illustrate the developing process of the mixing of the ejected material

and the diluent stream. During the process, the ejected fluorescent stream was found to

flow through the dilution mixer in different patterns during the developing process until

it reaches the steady state. Regarding the time needed for the ejected stream to develop,

it was found to be 2.1s in the experiment ($\Delta t = 3.1s - 1s = 2.1s$). However, with the

volume of the dilution mixer and the total flow rate Q_t , the time for two streams to fill

the mixer is only 0.01s. The large difference between the experimental and the

predicted figures is considered to be caused by the flow of the ejected stream. When the

ejected stream meets the diluent flow at the junction, the denser material is pushed

close to the bottom wall of the channel, instead of being sandwiched by methanol in the

centre. Thus flow of the ejected stream is retarded, and it takes much longer for the

fluid to make its way through the mixer. As a proof, a big width of the fluorescent

stream was found in the feeding channel to the mixer, as shown in Figure 8-8 (the

magnified Figure 8-7(g)). Taking the flow rates of two streams at the condition of

$Q_I = 0.23\,\text{ml/s}$ and $Q_M = 27.3\,\text{ml/s}$, the width of the fluorescent stream should be less

than 1% of the channel width. However, the value estimated from Figure 8-8 is about

25% of the channel width. Therefore, the ejected stream must flow along the wall at a

far lower speed, until it is well mixed with diluent flow after 4 elements along the

dilution mixer, as shown in the image below. As a result, a time delay was found

between the ideal model and the experiment of the new sampling method, as shown in

the plot of Figure 8-6, and it may vary with the flow conditions, such as the flow rate

and the dilution ratio between two streams.
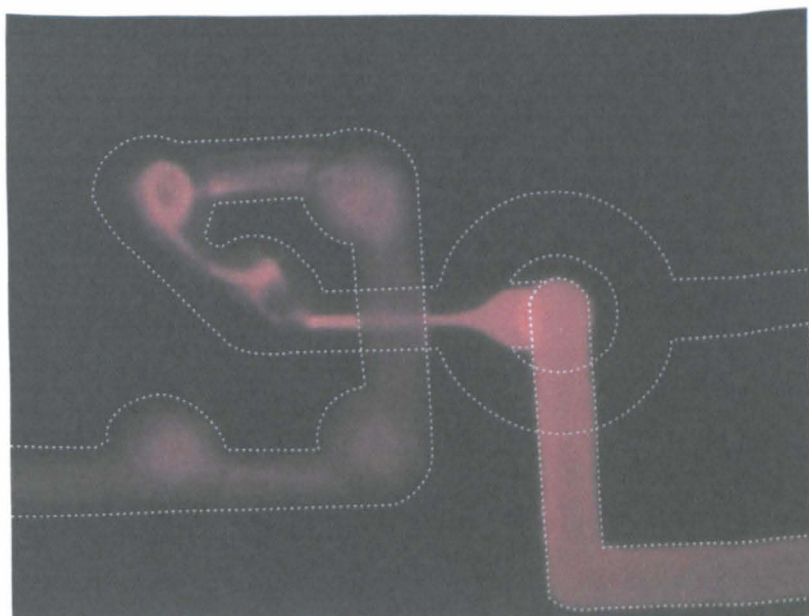
Fig. 8-8 Steady State of Mixing Process in the Dilution Mixer

8.4 DETERMINATION OF OPERATING CONDITIONS FOR THE MCR SYSTEM

The determination of operating conditions enable decision on the parameters for all the processes involved in the kinetics measurement with the MCR system. In detail, these processes include the preparation of the system, the flushing of the reaction network, and the control of the reaction and sampling process. Based on a good understanding of all the process, appropriate parameters can be determined for each operation of the kinetics measurements.

8.4.1 Preparation of the MCR System

To make the MCR system ready for kinetics measurement, some work must be done, such as drying the system thoroughly by blowing nitrogen gas through it, and feeding

the solutions into their respective reservoirs. However, the most important thing is to fill the chip properly with fluids, in order to prevent the fluid flow from being affected by the gas trapped in the system. It is a simple process, but needs to be carried out very carefully. Since the diluent flow responds much faster than the ionic liquid, it is easy for the diluent to flow back along the feeding capillary of reagents/catalyst into their reservoirs and thus to cause contamination.

To look for a method for a good preparation of the system, a lot of tests have been performed on the chip. As a result, a protocol is given as follows as the standard operation procedure to make the MCR system ready for the kinetics measurement.

1) Blow nitrogen gas through the system for at least 15 minutes to make the reservoir, the feeding capillary and the chip fully dry.

2) Feed solutions into their respective reservoirs through a filter. It is important to note that:

   - Use a new filter for each feeding.

   - Air must be removed from the syringe before injecting the solution into the reservoir.

   - The relief valve must be opened to avoid pressure being accumulated during the feeding process.

   - Solutions must be fed gently, in order to avoid causing chaos in fluid in the reservoir.

3) In turn, apply the conditions as given in Table 8-4, to prepare the reaction network for kinetics measurement.

Table 8-4 Conditions for Preparation of the MCR System

	P_r (bar)	P_m (bar)	τ_P (s)	τ_F (s)	τ_R (s)	τ_E (s)	τ_S (s)	τ_L (s)	Run times
1	6	0.5		5	0	0	0		3
2	6	1		5	0	0	0		1
3	6	2		5	0	0	0		1
4	6	3	30	5	0	0	0	3	1
5	6	4		10	0	0	0		1
6	6	4		20	5	0.05	1		1
7	6	4		30	5	0.05	1		3

8.4.2 Operating Conditions for Kinetics Measurement

The operating conditions required for kinetics measurement are parameters such as pressures, flushing time, reaction time, sample delay time and loop opening time. The determination of the values of these parameters relies on the system configuration as well as corresponding method used for the experiment.

I. Pressure conditions

The two pressure conditions to be applied in the experiment are determined mainly by a balance between two factors. First, to achieve a good accuracy, the residence time of fluid through the mixer must be small enough compared to the reaction duration. Thus the faster the fluid flows through the reaction mixer, the better the result will be. Second, considering the effect of the valve relaxation and opening, it is better to keep the diluent pressure low, since it may reduce the amount of methanol that could flow back into the upstream channel. However, the pressure cannot be too low, because to make the swirl mixer function well, a diluent flow at $Re \approx 100$ must be maintained. Balancing these two points, the pressure conditions decided for the kinetics

measurement are: $P_r = 6\,\text{bar}$ and $P_m = 4\,\text{bar}$, and the time for pressure to build up is: $\tau_p = 30\,\text{s}$.

II. Flushing time

The flushing time is the time required to remove the residua of last run and to clean the reaction network for next measurement. More often, it means the time needed for the ionic liquid stream (stream of mixed reactant solution and catalyst solution) to well clean the reaction chamber, since the flow rate of the diluent is much higher. The time scale of the flushing process depends on the channel volumes to be cleaned and the flow rate of fluid stream. Specifically, for the Mark II reaction network, since the total volume of the reaction mixer and the reaction chamber is around 2μl, a flushing time of 30 seconds is specified so that an ionic liquid stream of 20 times the volume of the hold up on the chip will flow through the mixer and the reaction chamber.

III. Minimum reaction time

To determine the shortest time scale that is measurable for the MCR system, it is necessary to take the time delay of order 1.5s in the valve opening action into account. Assuming a similar delay will occur during the valve closing, a reaction time less than 3 seconds will then be impractical for the MCR system. For reaction times larger than that, there should be no problem, but the accuracy will be affected if the time scale is too close to the limit. To be practical, the shortest reaction time is considered to be 5 seconds, and measurement at this time scale has been achieved on-chip. Meanwhile, there is an upper limit for the reaction time as well. This value, however, depends on the volume of the diluent reservoir, because the diluent will keep flowing during the whole reaction duration. For the present system, the longest time is over 25 minutes, but it can be further improved, through replacing the existing reservoir with an even bigger vessel or reducing the methanol flow rate in the reaction time. Therefore, only the low reaction time is limited for the kinetics measurement, and that is 5 seconds.

IV. Sample delay time and loop opening time

The new sampling method requires the valve to be kept open until a sample is captured in the loop. The sample delay time in the new method is of greater importance to the measurement, while the ejection time only needs to be longer than it.

The determination of an appropriate sample delay time still relies on considerations of the validity of an ejected sample. As the reaction chamber in the improved network has been enlarged to a volume of $1\,\mu l$, the limit of a valid sample has also been increased to 2/3 of the value, that is, $0.67\mu l$. At the pressure conditions of $P_r = 6\,bar$ and $P_m = 4\,bar$ to be applied, the time it takes for all the volume to be ejected as valid sample from the reaction chamber is about 1.6s. Taking the time delay found previously between the model and the experiment into account, the latest time to switch the sample loop will be round $\tau_S = 1.6 + (1.4\,to\,1.7) = 3.0\,to\,3.3\,s$. However, according to the plot in Figure 8-6, sample delay time from 2 to 3.3 seconds will all provide a valid sample in the volume that can be accurately analysed by HPLC. Hence, a range of sample delay times is determined, instead of a fixed value, for the kinetics measurement. Ranging from 2 to 3.3 seconds, the sample delay time should be selected with the experimental conditions. For instance, the high value is suggested for low temperature and high viscosity of ionic liquid, whilst the low one is for less viscous liquid and warm conditions.

After selecting the sample delay time, the ejection time and the loop opening time can then be decided. To avoid the impact of the valve closing, the ejection time for the kinetics measurement needs to be longer than the sample delay time. Usually, the valve is set to be closed 1 second after the switching of the loop. The loop open time, however, does not relate too much to the sample delay time. To give enough time to

convey the sample into the HPLC column, its time scale in the measurement is decided to be 3 to 5 seconds, but the latter is more often used for the new sampling method.

All the operating conditions for measurement of reaction kinetics with the MCR system are summarised in Table 8-5.

Table 8-5 Summary of Operating Condition for the MCR System

Pressure (bar)		Time scale (s)				
P_r	P_m	τ_P	τ_F	τ_R	τ_S	τ_L
6	4	30	30	≥ 5	2-3.3	5

8.5 MEASUREMENT OF REACTION KINETICS

The chemical reactions were then carried out on the Mark II chip, and reaction kinetics was measured with conditions as recommended in Table 8-5. Using the same approach as described in Section 7.7, two NBA+DHF reaction tests were performed independently in the same batch of Emim[NTf$_2$]. The purity of the ionic liquid was checked again with its density, which was 1541 kg/m^3 . Details of the reaction conditions such as species concentrations are listed in Table 8-6.

Table 8-6 Conditions of Tests on Chemical Reactions in Emim[NTf2]

		Test-1	Test-2
Species compositions (M)	NBA	0.082	0.086
	DHF	0.168	0.181
	Sc	0.0027	0.0026
	$[NBA]_0/[Sc]_0$	30.4	33.1
Temperature (°C)		23.9	23.1
Sample delay time (s)		2	2.2

By plotting their half-life against the initial concentrations, the kinetics of these two tests are confirmed again to be second-order, since a linear relation can be found in both plots, as shown in Figure 8-9.
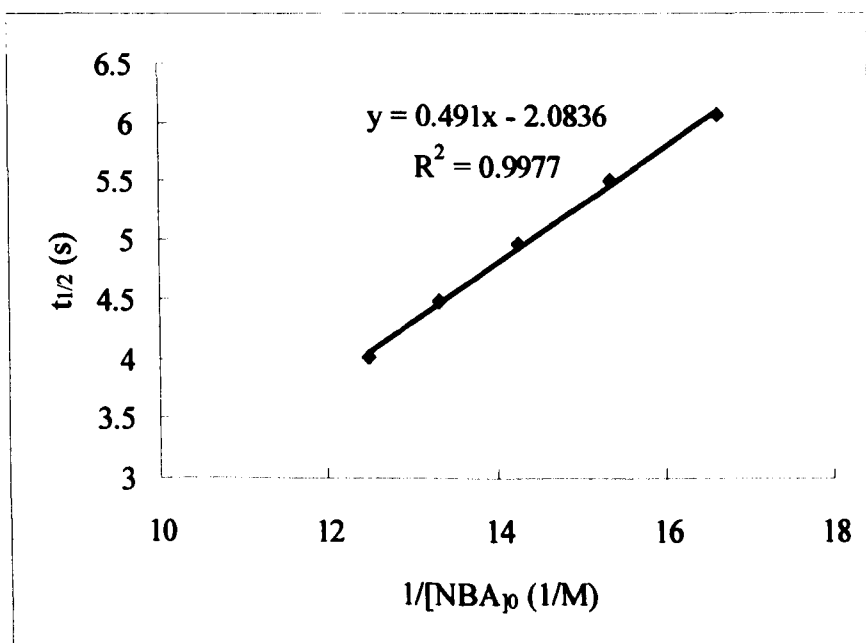
(a) Test-1
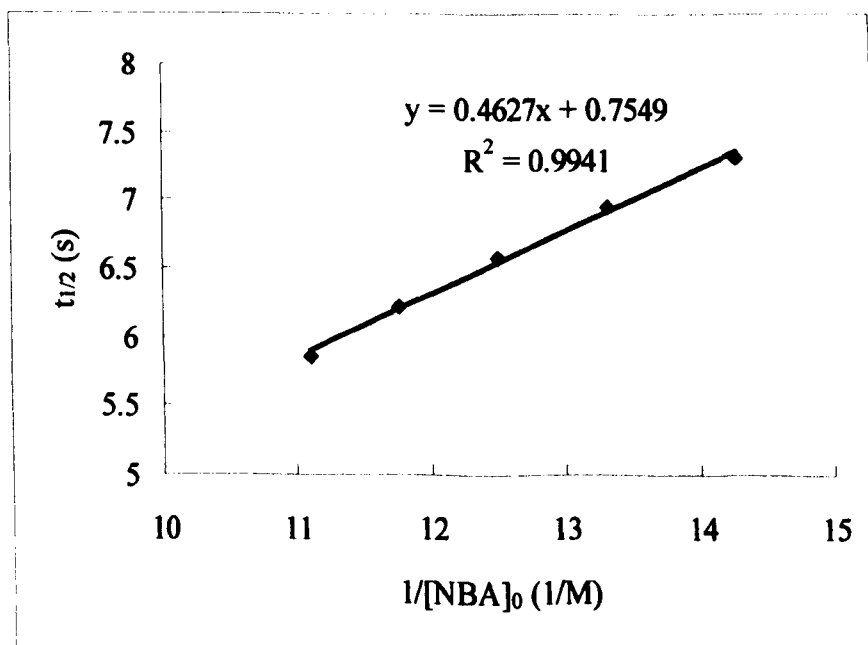
(b) Test-2

Fig. 8-9 Reaction Order and Rate Coefficient of Two Reaction Tests

The second-order law are then used to fit the experimental data of these two tests in the same way as described in Chapter 7, and the results are given in Figure 8-10.
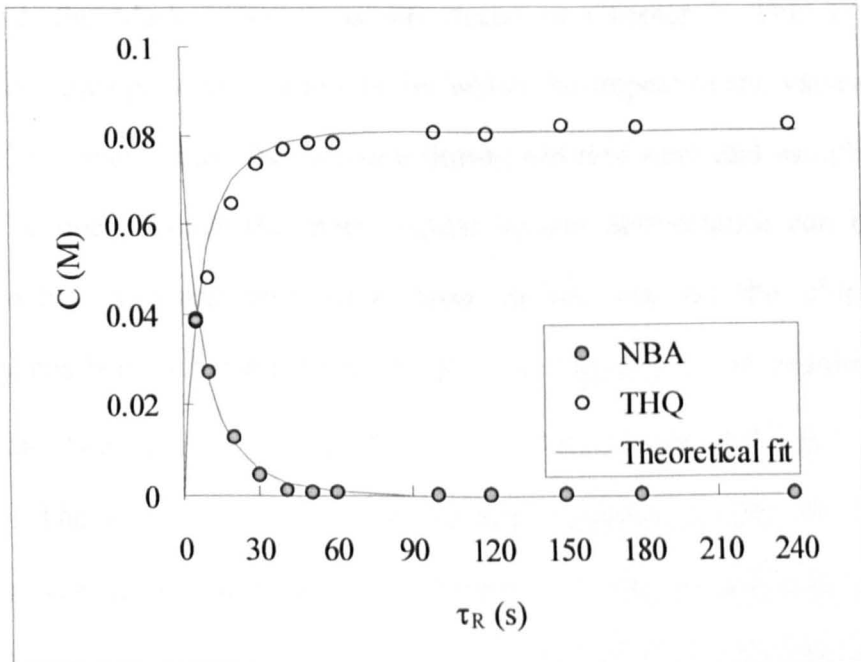
(a) Test-1
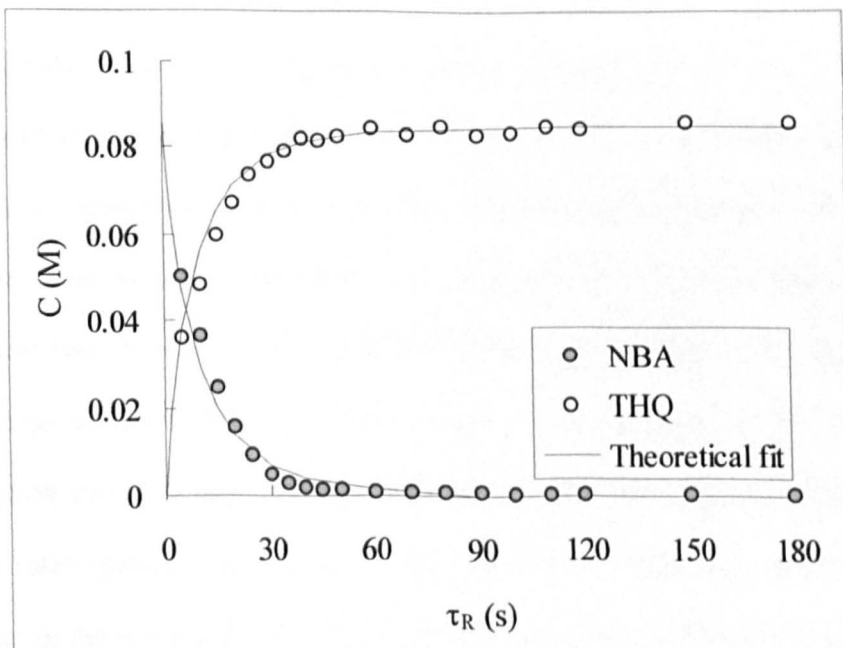
(b) Test-2

Fig. 8-10 Experimental data of NBA Reactions on Chip Fitted with Second-order law

Compared to the result of Mark I chip (see Figure 7-23), two improvements can be found in the results of the Mark II device. First, although the scatter still exists in the data of kinetics measurement, it is much smaller. Specifically, the scatter of the THQ concentration result is about 3% in Test-1 and 2% in Test-2, in relation to 15% obtained with the Mark I device as introduced in Chapter 7. This is due to the application of new operating conditions, by which the impact of the valves' behaviour was reduced by maintaining the pressure during reaction time and sampling with the ejection valve open. Hence the more regular system performance can be achieved. Second, kinetics measurements have been carried out on the chip and good repeatability has been achieved. From the plots in Figure 8-9, the reaction rates were found, in the two tests, to be $2.04\ M^{-1} \cdot s^{-1}$ (Test-1) and $2.16\ M^{-1} \cdot s^{-1}$ (Test-2) respectively. The difference in the reaction rate constants is only 6% between two experiments. Taking into account the deviation in reaction conditions, of which the reactant solution of Test-2 was 5% more concentrated than of Test-1 whilst the temperature was 3% lower, the error resulting from the measurement device and approach can be fairly predicted to be less than 5%. This is due to the improved mixing performance, with which a homogeneous mixture was produced both for the reaction itself and to quench the reaction. Moreover a valid sample was obtained for the analysis under the new operating conditions. Thus the measurements of reaction kinetics became more accurate and repeatable. In respect of the reaction rate constants, the results of these two tests are not comparable to the results obtained on the Mark I chip. This is because of the difference in the catalyst concentration in the two tests. The catalyst solution was at a concentration more than twice that of the previous test, so that the reaction rates obtained on the new chip are higher. However, the higher reaction rate constants in the tests with the Mark II MCR system are also believed to result from the improved performance of the two mixers.

8.6 CONCLUSION

In the Mark II design of kinetics measurement, the mixing performance has been improved by adding more mixing elements to the reaction mixer and by re-designing the dilution mixer to make it suitable for high Reynolds number fluid flow. Meanwhile, operating conditions have been greatly altered, to allow sampling with valve open and maintaining pressure during the reaction duration. As a result, more accurate and repeatable kinetics measurements have been achieved. By carrying out two reaction tests independently on-chip, the scatter of experimental data is found to decrease, and the deviation of the reaction rates obtained in two experiments is of order 6%. The error of the kinetics measurement with the device is thus believed to be within 5%.

Chapter 9

CONCLUSION

The aim of the research was the development of a microreactor system for the kinetics measurement of chemical reactions that use ionic liquids as solvents. As an achievement, the design and construction of the system has been completed, the device has been tested by carrying out measurements of reaction kinetics in Emim[NTf$_2$] experimentally, and the operating conditions required to achieve reliable and accurate measurement of reaction kinetics in ionic liquids have been determined. All the work carried out in the research can be summarised as follows.

- A microreactor system has been designed, constructed and tested for the kinetics measurement of chemical reactions in ionic liquids.

- The development of the system took a substantial amount of research time and effort to achieve the aim because there were challenges that needed to be overcome, such as the control of flow in a network of microchannels. Based on the fluidics theory, equations were established for CFD computation, and a network analysis model was developed to predict the fluid flow in each segment of the channel network. Moreover, as the assumption was made in the network analysis model that the flow was fully developed since the beginning of the channel, studies were also carried out on the entrance effect and bends effect, to assess the error resulting from this assumption.

- The greatest challenge to the research resulted from the special properties of ionic liquids. Being highly viscous and giving low diffusivities, ionic liquids presented the problem of achieving species mixing at high Peclet numbers with fluid flow at Reynolds number approaching zero. More than that, the kinetics measurement required the mixing time to be negligibly short, which further increased the difficulty of the project. Intensive work was then carried out to design a proper mixer to meet the requirements. Consequently, several mixing schemes were discussed, including the simple channel mixer, the folding fluid mixer and the folding network mixer. Careful comparison was made via CFD computations and experimental tests. As a result, the folding network mixer was selected because of its advantages over other candidates in both the mixing performance and the required pressure drop.

- Other difficulties of the research involved the selection of appropriate apparatus for each process needed in the kinetics measurement and the determination of operating conditions. In the Mark I design, the reaction network was fabricated by a commercial manufacturer, in which the FNM was used as both the reaction mixer and the dilution mixer. Meanwhile, taking the response time as the main criterion of selection, apparatus such as pressure controllers, solenoid valves, switching/injection valve and HPLC equipment were assembled and put under the same computer control. Conditions for operating the whole system were also decided, including the sequence and time scales for each operation in the kinetics measurement.

- Measurement techniques were developed in the research, in order to conveniently obtain information needed for the kinetics study. The work included the development of a viscometer to quickly access ionic liquids' properties, the calibration of a HPLC column for composition analysis and the

measurement of mixing performance with fluorescent dye. Procedures for each measurement were described in detail, and errors were assessed as well.

- Before kinetics measurement was ever tried with the developed Mark I MCR system, performances of the device were assessed. The species mixing was then found to be not as good as expected for two reasons, the overestimation of the performance resulting in insufficient mixing elements used in the mixer, and the misalignment in the structure causing uneven diffusion distances for mixing. Moreover, the solenoid valves were found to behave differently from their indicated performance. To gain control over the system with the identified drawbacks, measures such as introducing an internal standard into the reagent streams were proposed. Meanwhile, a model was developed to understand the sampling process. As a result of the model, the method of sampling with the ejection valve closed was used in the kinetics measurement, by which a valid sample of chemical reaction was captured at the peak delay time for HPLC analysis.

- Measurement of reaction kinetics in Emim[NTf$_2$] was carried out as an attempt using the Mark I MCR system. Reaction order found in the experiment agreed well with theory. Moreover, a reaction rate was obtained from the experimental data. Due to a lack of corresponding data for batch reaction in the same solvents, the results of this automatic measurement could not be compared with manual operation. However, in the experiment, the Mark I MCR system exhibited its advantages over the conventional manual method, such as automatic measurement, low consumption of ionic liquids, and a wider measurable range of reaction times.

- Further improvement was made to the Mark I MCR system at the end of the research. The work involved an improvement of the reaction mixer by increasing the number of mixing elements, and the redesign of the dilution mixer by adopting a new type of mixer that functions better for the high Reynolds number flow. As a result, the Mark II design has been put forward and manufactured. Meanwhile, a protocol of operating conditions has been developed, in which the pressure was maintained rather than dropped during the reaction time, and a new sampling method was used to keep ejection valve open until the sample was conveyed to the HPLC column. Accordingly, conditions of pressure and time scale have also been decided for the Mark II MCR system, to achieve better performance of the system.

- Chemical reactions in Emim[NTf$_2$] were carried out with the Mark II MCR system as well. As a result of the improved mixing performance and system control, good repeatability was found in the experimental results. More important, a deviation of less than 5% was achieved for the kinetics measurement with the device.

Due to the limits in time and funding, there remains future work on this project. First, as the new reaction network was fabricated by the powder-blasting technique, the mixing performance of mixers, especially the dilution mixer could not be assessed exactly. Although the CFD computation indicated that the swirl mixer would produce a uniform mixture of $\sigma_\gamma < 1\%$ at Re = 100 after five elements, this remains to be proven. A wet-etched channel with good alignment between layers of glass is suggested for the assessment. Secondly, the solenoid valves can be much improved. An alternative to provide better repeatability and performance for viscous fluids like ionic liquids is desirable. Thirdly, batch reactions are suggested, to be carried out at the same condition as for the automatic measurement. Since the reaction kinetics can be

influenced by factors such as the catalyst concentration and purity of ionic liquids, it would be better to use the same solutions for both measurements, in order to make the results comparable.

253

REFERENCES

Ali, M. F.; Kirby, R.; Goodey, A. P.; et al. (2003). "DNA Hybridization and Discrimination of Single-Nucleotide Mismatches Using Chip-Based Microbead Arrays." *Analytical Chemistry*, 75(18): 4732-4739.

Atkins, P. and De Paula, J. (2002). *Atkins' Physical Chemistry (7th edition)*. Oxford, Oxford University Press.

Aubin, J.; Fletcher, D. F. and Xuereb, C. (2005). "Design of Micromixers Using CFD Modelling." *Chemical Engineering Science*, 60(8-9): 2503-2516.

Baier, T.; Drese, K. S.; Schonfeld, F.; et al. (2005). "A M-Fluidic Mixing Network." *Chemical Engineering Technology*, 28(3): 362-366.

Banks, D. (2005). "Introduction On Microengineering." Available from: http://www.dbanks.demon.co.uk/ueng/. Accessed on 20/11, 2005.

Bau. H. H.; Zhong, J. and Yi, M. (2001). "A Minute Magneto Hydro Dynamic (MHD) Mixer." *Sensors and Actuators B: Chemical*, 79(2-3): 207-215

Bates, E. D.; Mayton, R. D.; Ntai, I.; et al. (2002). "CO_2 Capture by a Task-Specific Ionic Liquid." *Journal of the American Chemical Society*, 124(6): 926-927.

Benson, R. S. and Ponton, J. W. (1993). "Process Miniaturization - a Route to Total Environmental Acceptability." *Chemical Engineering Research and Design*, 71(A2): 160-168.

Bertsch, A.; Heimgartner, S.; Cousseau, P.; et al. (2001). "Static Micromixers Based on Large-Scale Industrial Mixer Geometry." *Lab on a Chip*, 1(1): 56-60.

Bessoth, F. G.; De Mello, A. J. and Manz, A. (1999). "Microstructure for Efficient Continuous Flow Mixing." *Analytical Communications*, 36: 213-215.

Brennan, V. A. (2006). *Reaction Engineering in Ionic Liquids*. School of Chemistry and Chemical Engineering. Belfast, U.K., The Queen's University of Belfast. Dorctor of Philosophy: 238.

Boberge, D. M.; Ducry, L.; Bieler, N.; et al. (2005). "Microreactor Technology: A Revolution for the Fine Chemical and Pharmaceutical Industries?" *Chemical Engineering Technology*, 28(3): 318-323.

Boon, J. A.; Landers, J. S.; Levisky, J. A.; et al. (1987). "Catalysis and Reactivity of Electrophilic Reactions in Room-Temperature Chloroaluminate Molten-Salts." *Journal of the Electrochemical Society*, 134(8B): C510.

Boon, J. A.; Levisky, J. A.; Pflug, J. L.; et al. (1986). "Friedel-Crafts Reactions in Ambien-Temperature Molten Salts." *Journal of Organic Chemistry*, 51(4): 480-483.

Bradley, D. (1999). "Super Solvents." in *Technology Ireland*.

Chabinyc, M. L.; Chiu, D. T.; McDonald, J. C.; et al. (2001). "An Integrated Fluorescence Detection System in Poly(Dimethylsiloxane) for Microfluidic Applications." *Analytical Chemistry*, 73(8): 4491-4498.

Chambers, R. D. and Spink, R. C. H. (1999). "Microreactors for Elemental Fluorine." *Chemical Communications*, (10): 883-334.

Charpentier, J.-C. (2005). "Process Intensification by Miniaturization." *Chemical Engineering Technology*, 28(3): 255-258.

Chauvin, Y.; Gilbert, B. and Guibard, I. (1990). "Catalytic Dimerization of Alkenes by Nickel-Complexes in Organochloroaluminate Molten-Salts." *Journal of the Chemical Society: Chemical Communications*, (23): 1715-1716.

Chauvin, Y.; Mussamann, L. and Olivier, H. (1995). "A Novel Class of Versatile Solvent for Two-Phase Catalysis: Hydrogenation, Isomerization and Hydroformylation of Alkenes Catalyzed by Rhodium Complexes in Liquid 1,3-Dialkylimidazolium Salts." *Angewandte Chemie International Edition in English*, 34(23-24): 2698-2700.

Chauvin, Y.; Olivier, H. and Mussamann, L. (1999). "Process of Hydroformylation of Olefinic Compounds". Office, U. S. P. France, Institue Francais du Petrole. 5 874 638.

Chen, H. and Meiners, J. C. (2004). "Topologic Mixing on a Microfluidic Chip." *Applied Physics Letters*, 84(12): 2193-2195.

Chen, Z.; Bown, M.; O'Sullivan, B.; et al. (2006). "Analysis of a High Peclet Number Mixer Design." *To be submitted to Lab On a Chip*.

Coddens, M. E.; Furton, K. G. and Poole, C. F. (1986). "Synthesis and Gas Chromatographic Stationary Phase Properties of Alkylammonium Thiocyanates." *Journal of Chromatography*, 356: 59-77.

Cong, P.; Doolen, R. D.; Fan, Q.; et al. (1999). "High-Throughput Synthesis and Screening of Combinatorial Heterogeneous Catalyst Libraries." *Angewandte Chemie International Edition*, 38(4): 483-488.

Cull, S. G.; Holbery, J. D.; Vargas-Mora, V.; et al. (2000). "Room-Temperature Ionic Liquids as Replacements for Organic Solvents in Multiphase Bioprocess Operations." *Biotechnology and bioengineering*, 69(2): 227-233.

Davis, J. H. and Fox, P. A. (2003). "From Curiosities to Commodities: Ionic Liquids Begin the Transition." *Chemical communications*, (11): 1209-1212.

De Bellefon, C.; Tanchoux, N.; Caravieilhes, S.; et al. (2000). "Microreactors for Dynamic, High Throughput Screening of Fluid/Liquid Molecular Catalysis." *Angewandte Chemie International Edition*, 39(19): 3442-3445.

Delsman, E. R.; Croon, M. H. J. M. d.; elzinga, G. D.; et al. (2005). "The Influence of Differences between Microchannels on Microreactor Performance." *Chemical Engineering Technology*, 28(3): 367-375.

Du, X. (2005). *Switched Electrokinetic Flow of Non-uniform Liquids in Microchannel Systems*. Department of Chemical and Process Engineering. Sheffield, U.K., The University of Sheffield. Dorctor of Philosophy: 288.

Earle, M. J.; McCormac, P. B. and Seddon, K. R. (1999). "Diels-Alder Reaction in Ionic Liquids." *Green chemistry*, 1(1): 23-25.

Earle, M. J. and Seddon, K. R. (2000). "Ionic Liquids: Green Solvents for the Future." *Pure and Applied Chemistry*, 72(7): 1391-1398.

Earle, M. J.; Seddon, K. R.; Adams, C. J.; et al. (1998). "Friedel-Crafts Reactions in Room Temperature Ionic Liquids." *Chemical Communications,* (19): 2097-2098.

Ehrfeld, W. (1996). "Potential and Realization of Microreactors." *Workshop on Microsystem Technology for Chemical and Biological Microreactors*, Mainz, Germany, VCH VERLAGSGESELLSCHAFT, Weinheim.

Ehrfeld, W. (1998). "Microreactors for Chemical Systhesis and Biotechnology - Current Developments and Future Applications." *Topics in Current Chemistry*. Manz, A. and Becher, H. Berlin Heidelberg, Springer Verlag. 194: 234-252.

Ehrfeld, W.; Hessel, V.; Lowe, H.; et al. (1999). "Materials for Liga Technology." *Microsystem Technology*, 5(3): 105-112.

Ehrfeld, W. and Lehr, H. (1995). "Deep X-Ray Lithography for the Production of Three Dimensional Microsturctures from Metal, Polymers and Ceramics." *Radiation Physics and Chemistry*, 45(3): 349-365.

Einloft, S.; Dietrich, F. K.; De Souza, R. F.; et al. (1996). "Selective Two-Phase Catalytic Ethylene Dimerization by Ni(Ii) Complexes/Aletcl2 Dissolved in Organoaluminate Ionic Liquids." *Polyhedron*, 15(19): 3257-3259.

Erickson, D. and Li, D. (2004). "Integrated Microfluidic Devices." *Analytica Chimica Acta*, 507(1): 11-26.

Fannin, A. A.; Floreani, D. A.; King, L. A.; et al. (1984). "Properties of 1,3-Dialkylimidazolium Chloride-Aluminium Chloride Ionic Liquids: 2. Phase Transition, Densities, Electrical Conductivities and Viscosities." *Journal of Physical Chemistry*, 88(12): 2614-2621.

Fischer, T.; Sethi, A.; Welton, T.; et al. (1999). "Diels-Alder Reactions in Room-Temperature Ionic Liquids." *Tetrahedron Letters*, 40(4): 793-796.

Fletcher, P. D. I.; Haswell, S. J.; Pombo-Villar, E.; et al. (2002). "Micro Reactors: Principles and Applications in Organic Synthesis." *Tetrahedron*, 58(24): 4735-4757.

Freemantle, M. (1998). "Designer Solvent - Ionic Liquids May Boost Clean Technology Development." *Chemical and Engineering News*, 76(13): 32-37.

Fuller, J.; Breda, A. C. and Carlin, R. T. (1997). "Ionic Liquid-Polymer Gel Electrolytes." *Journal of the Electrochemical Society*, 144: L67-L70.

Fuller, J. and Carlin, R. T. (1994). "Structure and Electrochemical Characterization of 1,3-Bis(4-Methylphenyl)Imidazolium Chloride." *Journal of Chemical Crystallography*, 24(8): 489-493.

Fuller, J.; Carlin, R. T.; De Long, H. C.; et al. (1994). "Structure of 1-Ethyl-3-Methylimidazolium Hexafluorophosphate: Model for Room Temperature Molten Salts." *Journal of the Chemical Society: Chemical Communications*, (3): 299-300.

Furton, K. G. and Morales, R. (1991). "Effect of Anion Chain Length on the Solvent Properties of Liquid Tetrabutylammonium Akylsulfonate Salts Studied by Gas-Liquid Chromatography." *Analytica Chimica Acta*, 246(1): 171-179.

Gale, R. J.; Gilbert, B. and Osteryoung, R. A. (1978). "Raman-Spectra of Molten Aliuminium-Chloride-1-Butylpyridinium Chloride Systems at Ambient-Temperatures." *Inorganic Chemistry*, 17(10): 2728-2729.

Gavriilidis, A.; Angeli, P.; Cao, E.; et al. (2002). "Technology and Applications of Microengineered Reactors." *Transaction ICHemE*, 80, Part A: 3-29.

Glasgow, I. and Aubry, N. (2003). "Enhancement of Microfluidic Mixing Using the Pulsing." *Lab on a Chip*, 3(2): 114-120.

Hardt, S.; Drese, K. S.; Hessel, V.; et al. (2005). "Passive Micromixers for Applications in the Micro-Reactor and Mtas Fields." *Microfluidics and Nanofluidics*, 1(2): 108-118.

Haswell, S. J.; Middleton, R. J.; O'Sullivan, B.; et al. (2001). "The Application of Micro Reactors to Synthesis Chemistry." *Chemical Communications*, (5): 391-398.

Haswell, S. J. and Watts, P. (2003). "Green Chemistry: Systhesis in Micro Reactors." *Green chemistry*, 5(2): 240-249.

Hendershot, D. C. (2000). "Process Minimization: Making Plants Safer." *Chemical Engineering Process*, 96(1): 35-40.

Holbery, J. D. and Seddon, K. R. (1999). "Ionic Liquids." *Clean Products and Processes*, (1): 223-236.

Howell, P. B. J.; Mott, D. R.; Fertig, S.; et al. (2005). "A Microfluidic Mixer with Grooves Placed on the Top and Bottom of the Channel." *Lab on a Chip*, 5(5): 524-530.

Hu, J.; Wang, Y.; VanderWiel, D.; et al. (2003). "Fuel Processing for Portable Power Applications." *Chemical Engineering Journal*, 93(1): 55-60.

Hussey, C. L.; Scheffler, T. B. and Wilkes, J. S. (1986). "Chloroaluminate Equlibria in the Aluminum Chloride-1-Methyl-3-Ethylimidazolium Chloride Ionic Liquid." *Journal of the Electrochemical Society*, 133(7): 1389-1391.

Jacobson, S. C.; McKnight, T. E. and Ramsey, J. M. (1999). "Microfluidic Devices for Electrokinetically Driven Parallel and Serial Mixing." *Analytical Chemistry*, 71(20): 4455-4459.

Jaeger, D. A. and Tucker, C. E. (1989). "Diels-Alder Reactions in Ethylammonium Nitrate: A Low-Melting Fused Salt." *Tetrahedron*, 30(14): 1785-1788.

Janicke, M. T.; Kestenbaum, H.; Hagendorf, U.; et al. (2000). "The Controlled Oxidation of Hydrogen from an Explosive Mixture of Gases Using a Microstructured Reactor/Heat Exchanger and Pt/Al2o3 Catalyst." *Journal of Catalysis*, 191(2): 282-293.

Jen, C. P.; Wu, C. Y.; Lin, Y. C.; et al. (2003). "Design and Simulation of the Micromixer with Chaotic Advection in Twisted Microchannels." *Lab on a Chip*, 3(2): 77-81.

Jensen, K. F. (1999). "Microchemical Systems: Status, Challeges and Oppotunities." *AIChE Journal*, 45(10): 2051-2054.

Jensen, K. F. (2001). "Microreaction Engineering - Is Small Better?" *Chemical Engineering Science*, 56(2): 293-303.

Johnson, T. J.; Ross, D. and Locasio, L. E. (2002). "Rapid Microfluidic Mixing." *Analytical Chemistry*, 74(1): 45-51.

Kaufmann, D. E.; Nouroozian, M. and Henze, H. (1996). "Molten Salts as an Efficient Medium for Palladium Catalyzed C-C Coupling Reactions." *Synlett*, (11): 1091-1092.

Keoschkerjan, R.; Richter, M.; Boskovic, D.; et al. (2004). "Novel Multifunctional Micoreaction Unit for Chemical Engineering." *Chemical Engineering Journal*, 101(1-3): 469-475.

Knauer. (2006). "Knauer Online Catalogue: Injection/Swithing Valves." Available from: http://www.knauer.net/e/e_index.html. Accessed on 09/07, 2006.

Knight, J. B.; Vishwanath, A.; Brody, J. P.; et al. (1998). "Hydrodynamics Focussing on a Silicon Chip: Mixing Nanolitres in Microseconds." *Physical Review Letters*, 80(17): 3863-3866.

Koch, M.; Chatelain, D.; Evans, A. G. R.; et al. (1998). "Two Simple Micromixers Based on Silicon." *Journal of Micromechanics and Microengineering*, 8(2): 123-126.

Koel, M. (2000). "Physical and Chemical Properties of Ionic Liquids Based on the Dialkylimidazolium Cation." *Proceedings of the Estonian Academy of Science: Chemistry*, 49(3): 145-155.

Lamping, S. R.; Zhang, H.; Allen, B.; et al. (2003). "Design of a Prototype Manuature Bioreactor for High Throughput Automated Bioprocessing." *Chemical Engineering Science*, 58(3-6): 747-758.

Lang, W. (1996). "Silicon Microstructuring Technology." *Materials Science and Engineering. R: Reports*, 17(1): 1-55.

Lee, S. W. and Lee, S. S. (2005). "Microfabrication of the Split and Recombination Micromixer and the Effect of Its Cross-Sectional Rotation." *3rd International Conference on Microchannels and Minichannels*. Toronto, Canada.

Lerou, J. J.; Harold, M. P.; Ryley, J.; et al. (1996). "Microfabricated Minichemical Systems: Technical Feasibility." *Workshop on Microsystem Technology for Chemical and Biological Microreactors*, Mainz, Germany, VCH VERLAGSGESELLSCHAFT, Weinheim.

260

Liu, R. H.; Stremler, M. A.; Sharp, K. V.; et al. (2000a). "Passive Mixing in a Three-Dimensional Serpentine Microchannel." *Journal of Microelectromechanical Systems*, 9(2): 190-197.

Liu, Y.; Cong, P.; Doolen, R. D.; et al. (2000b). "High-Throughput Synthesis and Screening of V-Al-Nb and Cr-Al-Nb Oxide Libraries for Ethane Oxidation Dehydrogenation to Ethylene." *Catalysis Today*, 61(1-4): 87-92.

Loechel, B. (2000). "Thick-Layer Resists for Surface Micromachining." *Journal of Micromechanics and Microengineering*, 10(2): 108-115.

Lu, L. H.; Ryu, K. S. and Liu, C. (2002). "A Magnetic Micromixer and Array for Microfluidic Mixing." *Journal of Microelectromechanical Systems*, 11(5): 462-469.

MacInnes, J. M. and Allen, R. W. K. (2005). "Mixing Strategies for Flow in Microchannel Devices." *7th World Congress of Chemical Engineering*. Glasgow, Scotland, UK.

MacInnes, J. M.; Chen, Z. and Allen, R. W. K. (2005). "Investigation of Alternating-Flow Mixing in Microchannels." *Chemical Engineering Science*, 60(13): 3453-3467.

MacInnes, J. M.; Du, X. and Allen, R. W. K. (2003). "Prediction of Electrokinetic and Pressure Flow in a Microchannel T-Junction." *Physics of Fluids*, 15(7): 1992-2005.

Madou, M. J. (2002). *Fundamentals of Microfabrication: The Science of Miniaturization. (2nd Edition)*. CRC Press.

Manz, A.; Miyahara, Y.; Miura, J.; et al. (1990). "Design of an Open-Tubular Column Liquid Chromatograph Using Silicon Chip Technology." *Sensors and Actuators B*, 1(1-6): 249-255.

McCreedy, T. (2000). "Fabrication Techniques and Materials Commonly Used for the Production of Microreactors and Micro Total Analytical Systems." *Trends in Analytical Chemistry*, 19(6): 396-401.

McCreedy, T. (2001). "Rapid Prototyping of Glass and Pdms Microstructures for Micro Total Analytical Systems and Micro Chemical Reactors by Microfabrication in the General Laboratory." *Analytica Chimica Acta*, 427(1): 39-43.

261

Meyer, V. R. (1994). *Practical High-Performance Liquid Chromatography*. New York, John Wiley & Sons Ltd.

Mills, P. L. and Nicole, J. F. (2004). "A Novel Reactor for High-Throughput Screening of Gas-Solid Catalyzed Reactions." *Chemical Engineering Science*, 59(19): 5345-5354.

Nardi, J. C.; Hussey, C. L. and King, L. A. (1978). "Alcl3 1-Alkyl Pyridinium Chloride Room Temperature Electrolytes." Office, U. S. P. U.S.A., The United States of America as represented by the Secretary of the Air. 4 122 245.

Nresearch. (2006). "Solenoid Valves." Available from: http://www.nresearch.com. Accessed on 09/07, 2006.

Oddy, M. H. S., J.G. and Mikkelsen J.C. (2001). "Electrokinetic Instability Micromixing." *Analytical Chemistry*, 73(24): 5822-5832.

Olivier-Bourbigou, H. and Magna, L. (2002). "Ionic Liquids: Perspectives for Organic and Catalytic Reactions." *Journal of Molecular Catalysis A: Chemical*, 182-183: 419-437.

Parshall, G. W. (1972). "Catalysis in Molten-Salt Media." *Journal of the American Chemical Society*, 94(25): 8716-8719.

Pattekar, A. V. and Kothare, M. V. (2004). "A Microreactor for Hydrogen Production in Micro Fuel Cell Applications." *Journal of Microelectromechanical Systems*, 13(1): 7-18

Pennemann, H.; Watts, P.; Haswell, S. J.; et al. (2004). "Benchmarking of Microreactor Applications." *Organic Process Research & Development*, 8(3): 422-439.

Peterson, K. E. (1979). "Fabrication of an Integrated Planar Silicon Ink-Jet Structure." *IEEE Transactions on Electron Devices*, 26(12): 1918-1920.

Pomaville, R. M. and Poole, C. F. (1988). "Solute Solvent Interactions in Liquid Tetrabutylammonium Sulfonate Salts Studied by Gas-Chromatography." *Analytical Chemistry*, 60(11): 1103-1108.

Pomaville, R. M. and Poole, C. F. (1990). "Gas Chromatographic Study of the Solution Thermodynamics of Organic Solutes in Tetraalkylammonium

Alkanesulfonate and Perfluoroalkanesulfonate Solvents." *Journal of Chromatography*, 499: 749-759.

Poole, S. K.; Shetty, P. H. and Poole, C. F. (1989). "Chromatographic and Spectroscopic Studies of the Solvent Properties of a New Series of Room-Temperature Liquid Tetraalkylammonium Sulfonate." *Analytica Chimica Acta*, 218: 241-264.

Potyrailo, R. A.; Lemmon, J. P. and Leib, T. K. (2003). "High-Throughput Screening of Selectivity of Melt Polymerization Catalysts Using Fluorescence Spectroscopy and Two-Wavelength Fluorescence Imaging." *Analytical Chemistry*, 75(17): 4676-4681.

Pretti, C.; Chiappe, C.; Pieraccini, D.; et al. (2006). "Acute Toxicity of Ionic Liquids to the Zebrafish (Danio Rerio). " *Green Chemistry*, 8(3): 240-249.

Renner, R. (2001). "Ionic Liquids: An Industrial Cleanup Solution." *Environmental Science & Technology*, 35(19): 410A-413A.

Rife, J. C.; Bell, M. J.; Horowitz, J. S.; *et al.* (2000). "Minuature Valveless Ultrasonic Pumps and Mixers." *Sensors and Actuators A: Physical*, 86(1-2): 135-140

Schwarz, M. A. and Hauser, P. C. (2001). "Recent Developments in Detection Methods for Microfabricated Analytical Devices." *Lab on a Chip*, 1(1): 1-6.

Seddon, K. R. (1997). "Ionic Liquids for Clean Technology." *Journal of Chemical Technology and Biotechnology*, 68(4): 351-356.

Seddon, K. R. (1999). "Quill Rewrites the Future of Industrial Solvents." *Green Chemistry*, 1(3): G58-G59.

Seddon, K. R. (2002). "Ionic Liquids: Designer Solvents for Green Synthesis." *The Chemical Engineer*, 2002(730): 33-35.

Senkan, S.; Krantz, K.; Ozturk, S.; et al. (1999). "High-Throughput Testing of Heterogeneous Catalyst Libraries Using Array Microreactors and Mass Spectrometry." *Angewandte Chemie International Edition*, 38(18): 2794-2799.

Shah, K.; Ouyang, X. and Besser, R. S. (2005). "Microreaction for Microfuel Processing: Challenges and Propects." *Chemical Engineering Technology*, 28(3): 303-313.

Shah, R. K. and London, A. L. (1978). *Laminar Flow Forced Convection in Ducts*. New York, Academic.

Shaw, A.; Brennan, A.; O'Sullivan, B.; et al. (2005). "Ionic Liquids Viscosity Measurement Using a Simple Microchannel Chip." *7th World Congress of Chemical Engineering*. Glasgow, Scotland, UK.

Shetty, P. H.; Youngberg, P. J.; Kersten, B. R.; et al. (1987). "Solvent Properties of Liquid Organic Salts Used as Mobile Phases in Micro-Column Reversed-Phase Liquid Chromatography." *Journal of Chromatography*, 411: 61-79.

Sigma-Aldrich. (2005). "Pyrene." Available from: http://www.sigmaaldrich.com/catalog/search/ProductDetail/FLUKA/82648. Accessed on 21/12, 2005

Sigma-Aldrich. (2006). "Fluorescent Probes: Wavelength Index." Available from: http://www.sigmaaldrich.com/Brands/Fluka___Riedel_Home/Analytical/Fluorescent_Probes/Wavelength_Index.html. Accessed on 20/03, 2006

Song, H.; Tice, J. D. and Ismagilov, R. F. (2003). "A Microfluidic System for Controlling Reaction Networks in Time." *Angewandte Chemie International Edition*, 767-772.

Stone, H. A. and Kim, S. (2001). "Microfluidics: Basic Issues, Applications, and Challenges." *AIChE Journal*, 47(6): 1250-1254.

Stroock, A. D.; Dertinger, S. K.; Whitesides, G. M.; et al. (2002a). "Patterning Flows Using Grooved Surface." *Analytical Chemistry*, 74(20): 5306-5312.

Stroock, A. D.; Dertinger, S. K. W.; Ajdari, A.; et al. (2002b). "Chaotic Mixer for Microchannels." *Science*, 295(5555): 647-651.

Stroock, A. D. and Whitesides, G. M. (2003). "Controlling Flows in Microchannels with Patterned Surface Charge and Topography." *Accounts of chemical research*, 36(8): 597-604.

Suarez, P. A. Z.; Dullius, J. E. L.; Einloft, S.; et al. (1996). "The Use of New Ionic Liquids in Two-Phase Catalytic Hydrogenation Reaction by Rhodium Complexes." *Polyhedron*, 15(7): 1217-1219.

Suarez, P. A. Z.; Dullius, J. E. L.; Einloft, S.; et al. (1997). "Two-Phase Catalytic Hydragenation of Olefins by Ru(Ii) and Co(Ii) Complexes Dissolved in 1-N-Butyl-3-Methylimidazolium Tetrafluoroborate Ionic Liquid." *Inorganica Chimica Acta*, 255(1): 207-209.

Sugden, S. and Wilkins, H. (1929). "The Parachor and Chemical Constitution. Part Xii: Fused Metals and Salts." *Journal of the chemical Society*, Part 1: 1291-1298.

Swatloski, R. P.; Visser, E.; Reichert, W. M.; et al. (2002). "On the Solubilization of Water with Ethanal in Hydrophobic Hexafluorophophate Ionic Liquids." *Green chemistry*, 4(2): 81-87.

Tanaka, S.; Chang, K.-S.; Min, K.-B.; et al. (2004). "MEMs-Based Components of a Miniature Fuel Cell/Fuel Reformer System." *Chemical Engineering Journal*, 101(1-3): 143-149.

Terry, S. C.; Jerman, J. H. and Angell, J. B. (1979). "A Gas Chromatographic Air Analyzer Fabricated on a Silicon Wafer." *IEEE Transactions on Electron Devices*, 26 (12): 1880-1886.

Tesar, V.; Tippetts, J. R.; Low, Y. Y.; et al. (2004). "Development of a Microfluidic Unit for Sequencing Fluid Samples for Composition Analysis." *Chemical Engineering Research and Design*, 82(A6): 708-718.

ThermExcel. (2006). "Physical Characteristic of Water." Available from http://www.thermexcel.com/english/tables/eau_atm.htm. Accessed on 05/02, 2005.

Thornell, G. and Johansson, S. (1998). "Microprocessing at the Fingertips." *Journal of Micromechanics and Microengineering*, 8(4): 251-262.

Torres, M. J. (2001). *Characterization of Ionic Liquids*. School of Chemistry. Belfast, U.K., The Queen's University of Belfast. Dorctor of Philosophy: 383.
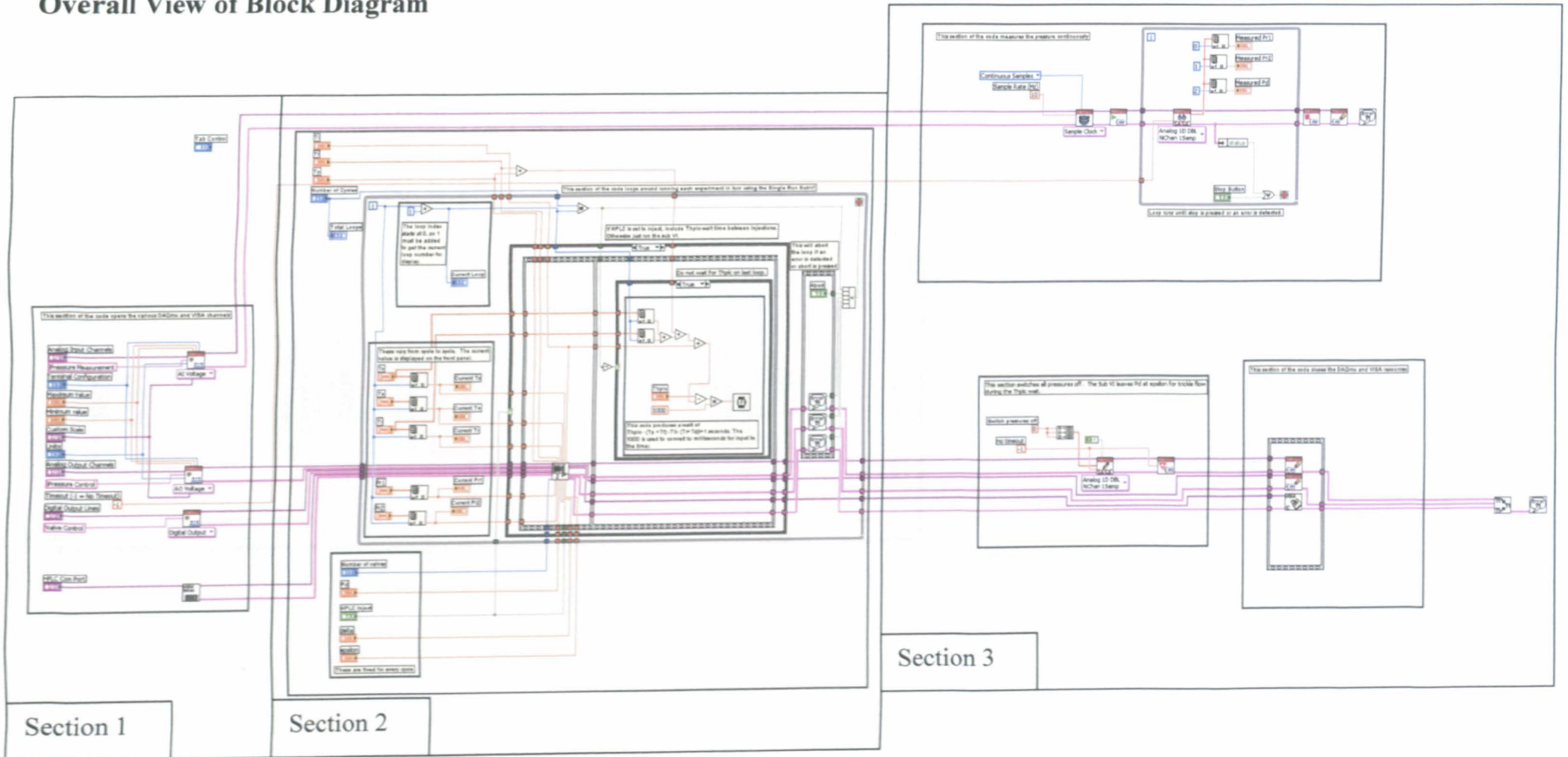
Visser, A. E.; Holbery, J. D. and Rogers, R. D. (2001). "Hydrophobic Ionic Liquids Incorporating N-Alkylisoquinolinium Cations and Their Utilization in Liquid-Liquid Seperations." *Chemical Communications*, (23): 2484-2485

Wang, H.; Iovenitti, P.; Harvey, E.; et al. (2002). "Optimizing Layout of Obstacles for Enhanced Mixing for Microchannels." *Smart Materials and Structures*, 11(5): 662-667.

Wasserscheid, P.; Sesing, M. and Korth, W. (2002). "Hydrogensulfate and Tetrakis (Hydrogensulfato) Borate Ionic Liquids: Synthesis and Catalytic Application in Highly Bronsted-Acidic Systems for Friedel-Crafts Alkylation." *Green chemistry*, 4(3): 134-138.

Watts, P. and Haswell, S. J. (2003). "Continuous Flow Reactors for Drug Discovery." *Drug Discovery Today*, 8(13): 586-593.

Watts, P. and Haswell, S. J. (2005). "The Application of Microreactors for Small Scale Organic Synthesis." *Chemical Engineering Technology*, 28(3): 290-301.

Wegeng, R. W.; Call, C. J. and Drost, M. K. (1996). "Chemical System Miniaturization." *AIChE Spring National Meeting*, New Orleans, U.S.A.

Welton, T. (1999). "Room-Temperature Ionic Liquids: Solvents for Synthesis and Catalysis." *Chemical Review*, 99(8): 2071-2083.

White, F. M. (2006). *Viscous Fluid Flow (3rd Edition)*, McGraw-Hill.

Whitesides, G. M. and Stroock, A. D. (2001). "Flexible Methods for Microfluidics." *Physics Today*, 54(6): 42-48.

Wier, T. P. and Hurley, F. H. (1948). "lectrodeposition of Aluminum" Office, U. S. P. U.S.A., The silliam Marsh Rice Institute of the Advancement of Literature, Science and Art, a corpotation of Texas. 2,446,349.

Wiggens, S. and Ottino, J. M. (2004). "Foundation of Chaotic Mixing." *Philosophical Transactions of the Royal Society of London*: Series A, 362(1818): 937-970.

Wilkes, J. S. (2002). "A Short History of Ionic Liquids--from Molten Salts to Neoteric Solvents." *Green chemistry*, 4(2): 73-80.

Wilkes, J. S.; Levisky, J. A.; Wilson, R. A.; et al. (1982). "Dialkylimidazolium Chloroaluminate Melts-a New Class of Room-Temperature Ionic Liquids for Electrochemistry, Spectroscopy and Synthesis." *Inorganic Chemistry*, 21(3): 1263-1264.

Wilkes, J. S. and Zaworotko, M. J. (1992). "Air and Water Stable 1-Ethyl-3-Methylimidazolium Based Ionic Liquids." *Journal of the Chemical Society: Chemical Communications*, (13): 965-967.

Wise, K. D. (1998). "Special Issue on Integrated Sensors, Microactuators and Microsystems (Mems)." *Proceeding of the I.E.E.E.*, 86: 1531-1533.

Worz, O.; Jackel, K. P.; Richter, T.; et al. (2002). "Microreactors, a New Efficient Tool for Optimum Reactor Design." *Chemical Engineering Science*, 56(3): 1029-1033.

Xia, Y. and Whitesides, G. M. (1998a). "Soft Lithography." *Angewandte Chemie International Edition*, 37(5): 550-575.

Xia, Y. and Whitesides, G. M. (1998b). "Soft Lithography." *Annual Review of Material Science*, 28: 153-184.

Yang, Z.; Goto, H.; Matsumuto, M.; *et al.* (2000). "Active Micromixer for Mirofluidic System Using Lead-Zirconate-Titanate (Pzt) Generated Ultrasonic Vibration." *Electrophoresis*, 21(1): 116-119

Zech, T.; Bohner, G. and Klein, J. (2005). "High-Throughput Screening of Supported Catalysts in Massively Parallel Single-Bead Microreactors: Workflow Aspects Related to Reactor Bonding and Catalyst Preparation." *Catalysis Today*, 110(1-2): 58-67.

Zeiss, C. (1998). *Axiovert 100, Axiovert 135 and 135m: Transmitted Light and Incident-Light Fluorescence (Operating Instructions)*. Germany, Carl Zeiss.

Ziaie, B.; Baldi, A.; Lei, M.; et al. (2004). "Hard and Soft Micromachining for Biomems: Review of Techniques and Examples of Applications in Microfluidics and Drug Delivery." *Advanced Drug Delivery Reviews*, 56(2): 145-172.
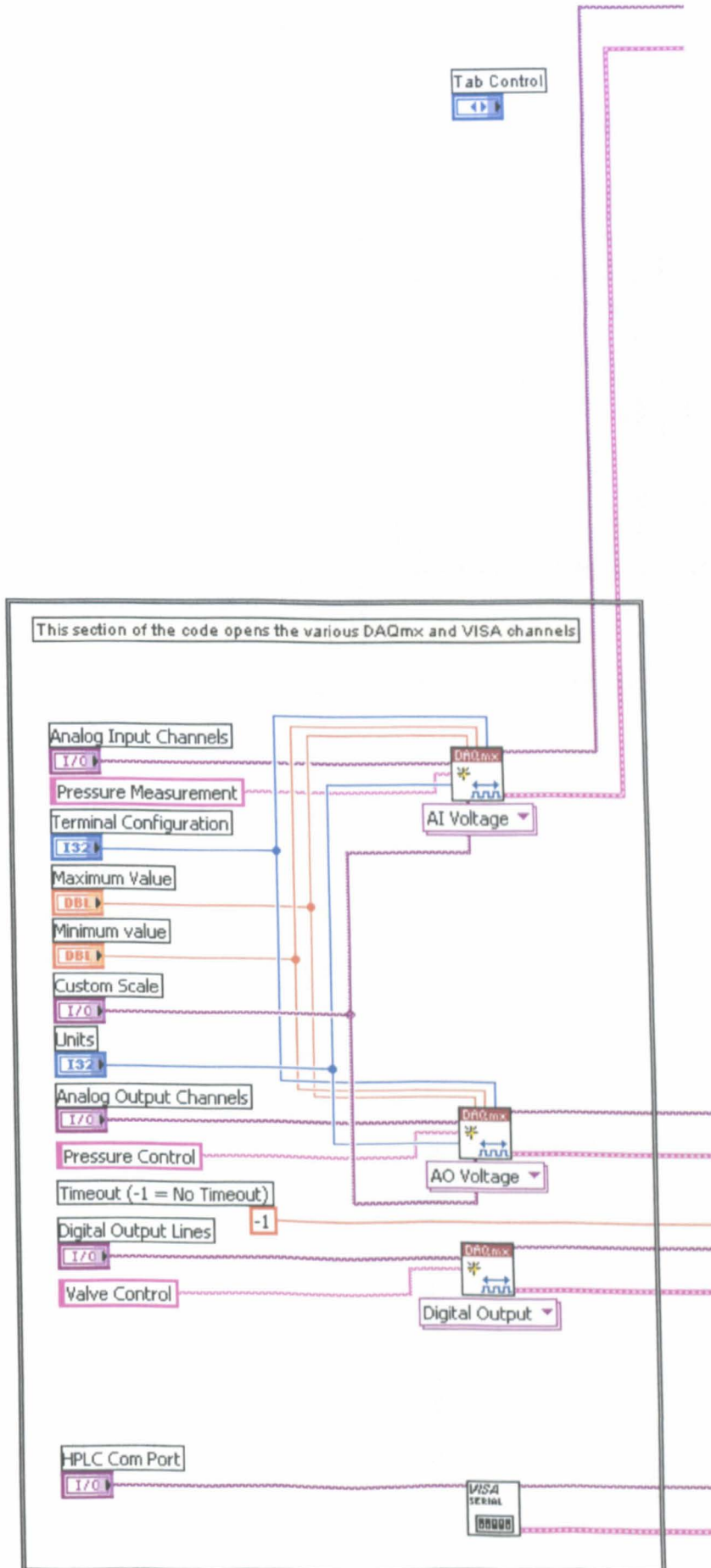
APPENDIX-1: LabVIEW® Code for Reaction Kinetics Device Controller

Reaction Controller

Overall View of Block Diagram

Section 1

Section 2

Section 3

Section 1: Inputs and Channel Opening

Tab Control

This section of the code opens the various DAQmx and VISA channels

Analog Input Channels
I/O

Pressure Measurement

Terminal Configuration
I32

Maximum Value
DBL

Minimum value
DBL

Custom Scale
I/O

Units
I32

Analog Output Channels
I/O

Pressure Control

Timeout (-1 = No Timeout)
-1

Digital Output Lines
I/O

Valve Control

AI Voltage

AO Voltage

Digital Output

HPLC Com Port
I/O

VISA
SERIAL

Section 2: Principle Loop (Note Sub VI to control each reaction)
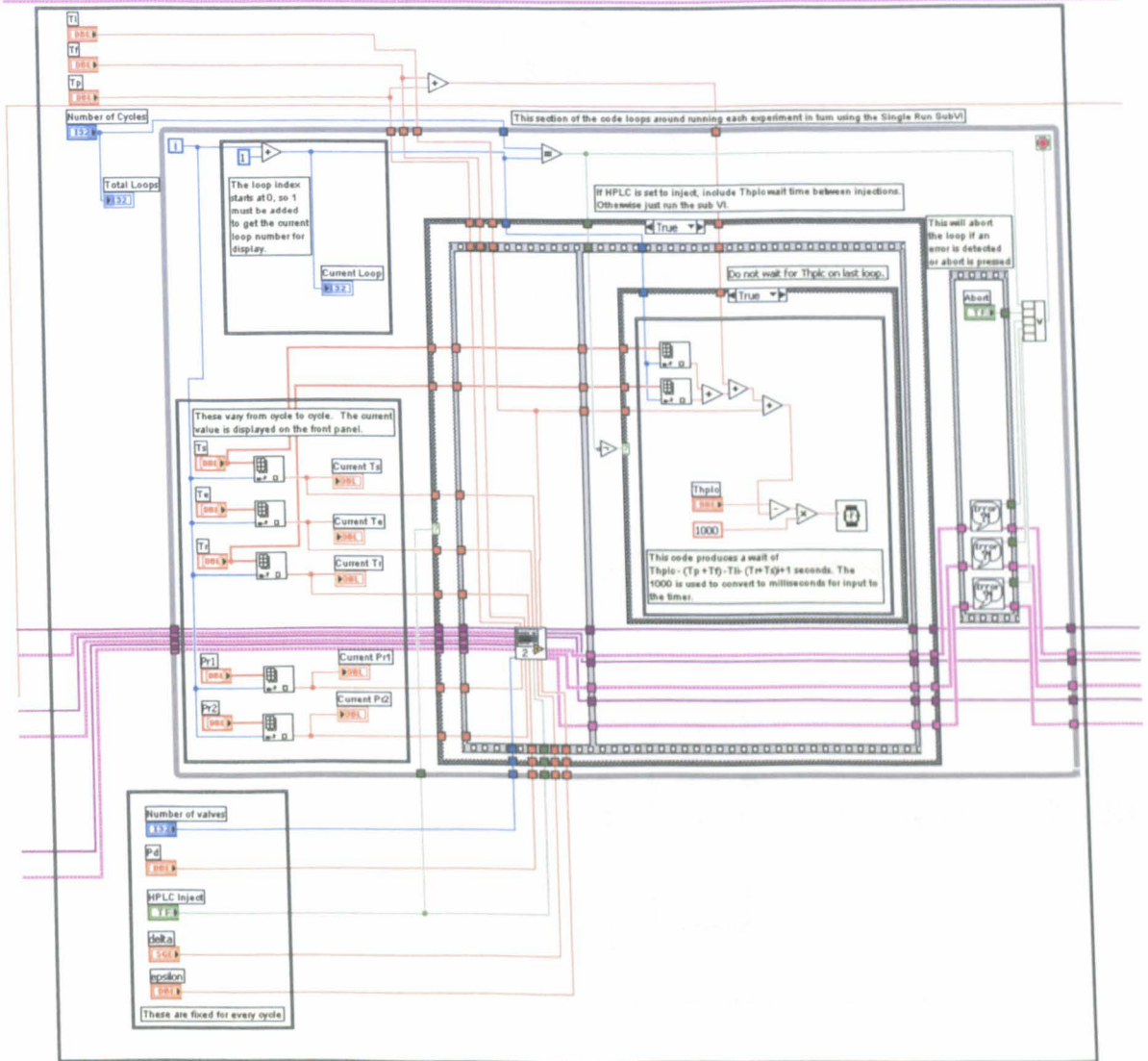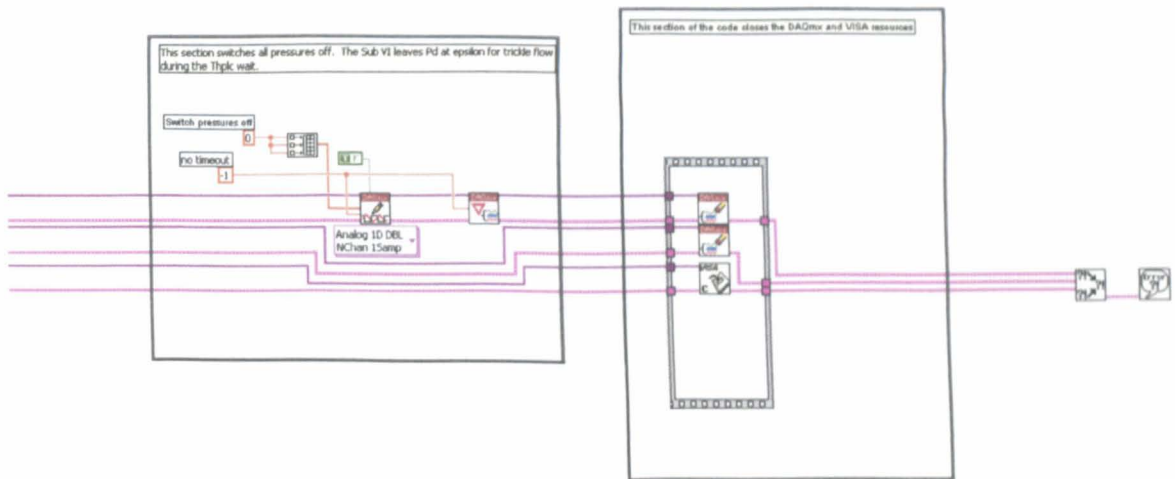

False cases
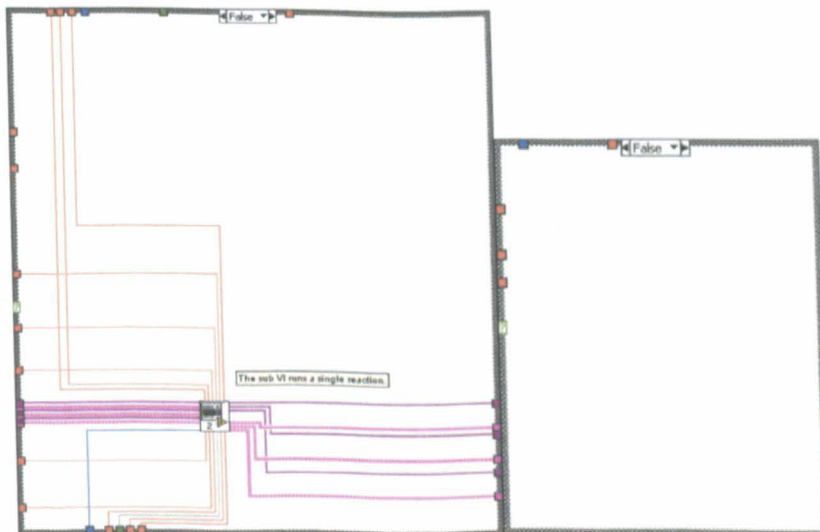
Section 3: Pressure Measurement and Channel Closing

Sub VI

Connections

TI
Ts
Te
Tr
Tf
Tp
Analog Output Task
Analog Output Error
Digital Output Task
Digital Output Error
VISA resource
VISA error
Number of valves
Pr1
Pr2
Pd
HPLC Inject on/off
delta
epsilon

Analog Output task out
Digital Output task out
VISA resourceout
Analog Output error out
Digital Output error out
VISA error out
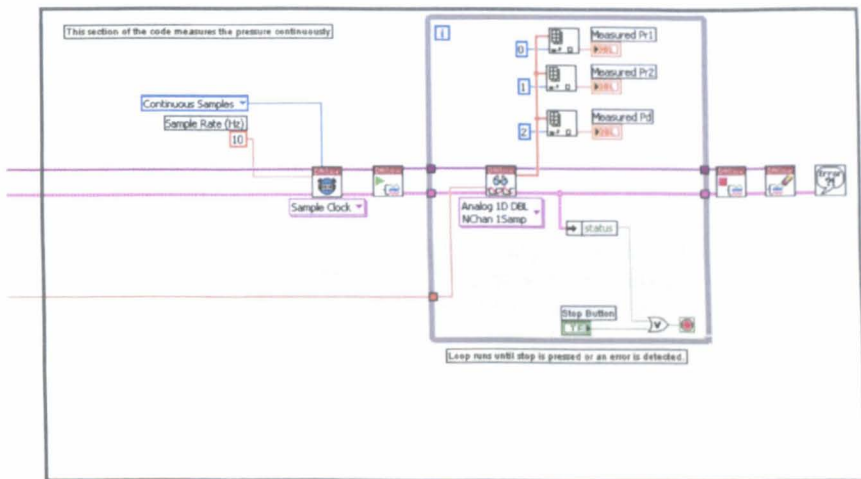
Overall View of Block Diagram
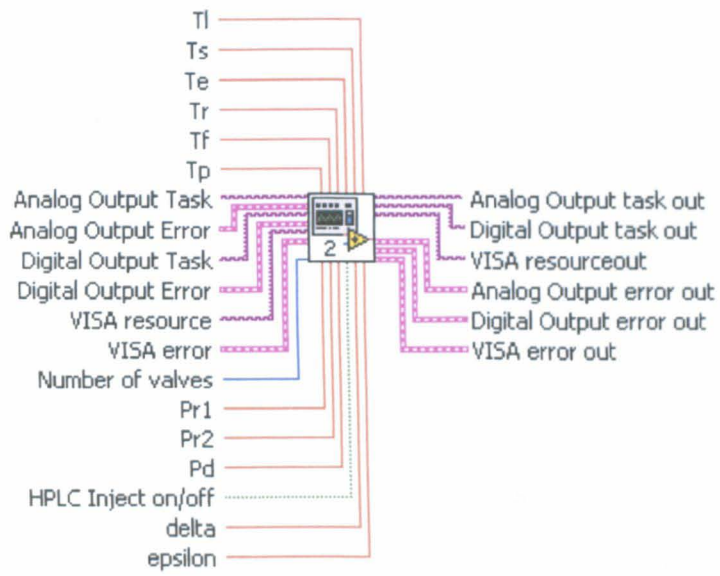
Section 1

Section 2
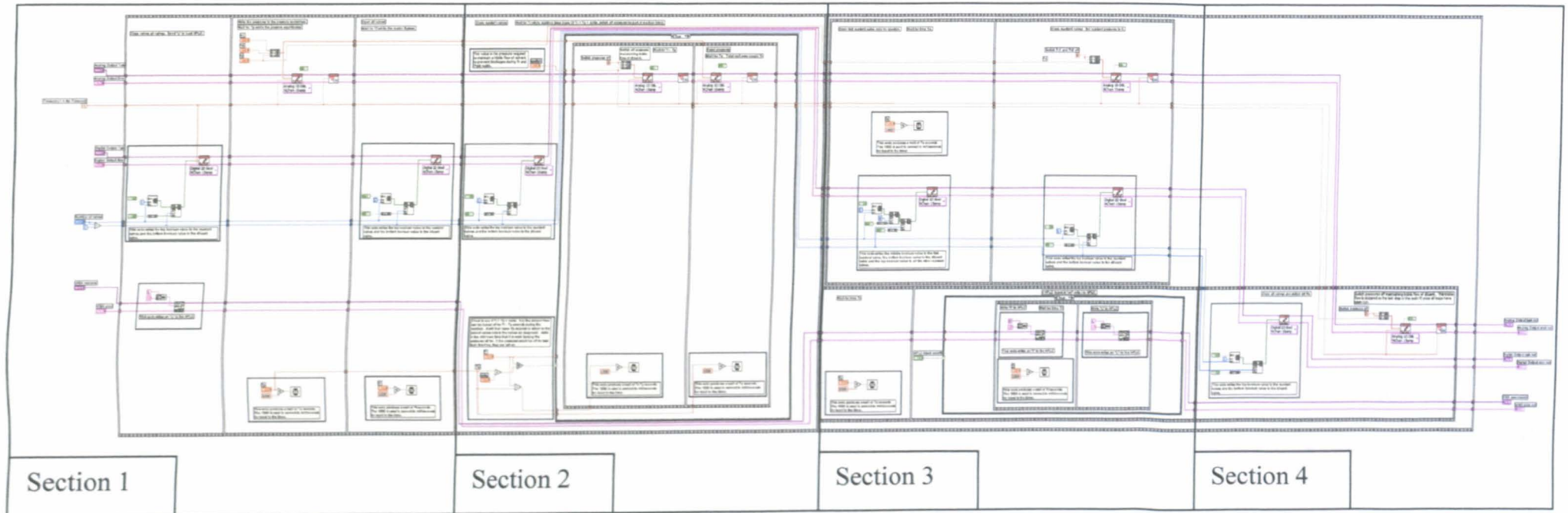
Section 3

Section 4

Section 1: Equilibrate Pressure and Flush Reactor
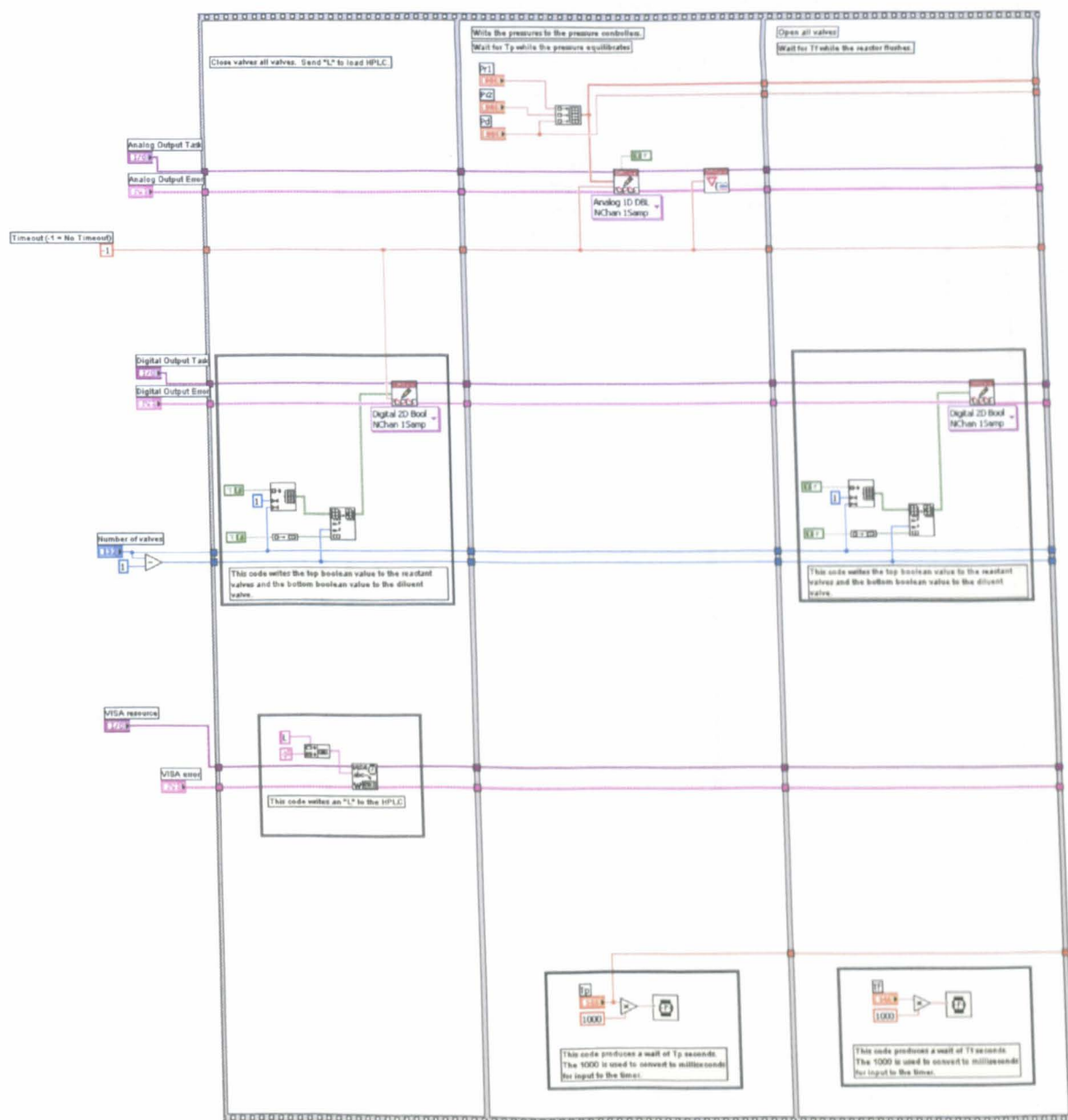
Section 2: Reaction

False Case

| False ▾ |

Wait for Tr seconds.

1000

This code produces a wait of Tr seconds.
The 1000 is used to convert to milliseconds
for input to the timer.

Section 3: Eject Sample from Reactor to HPLC
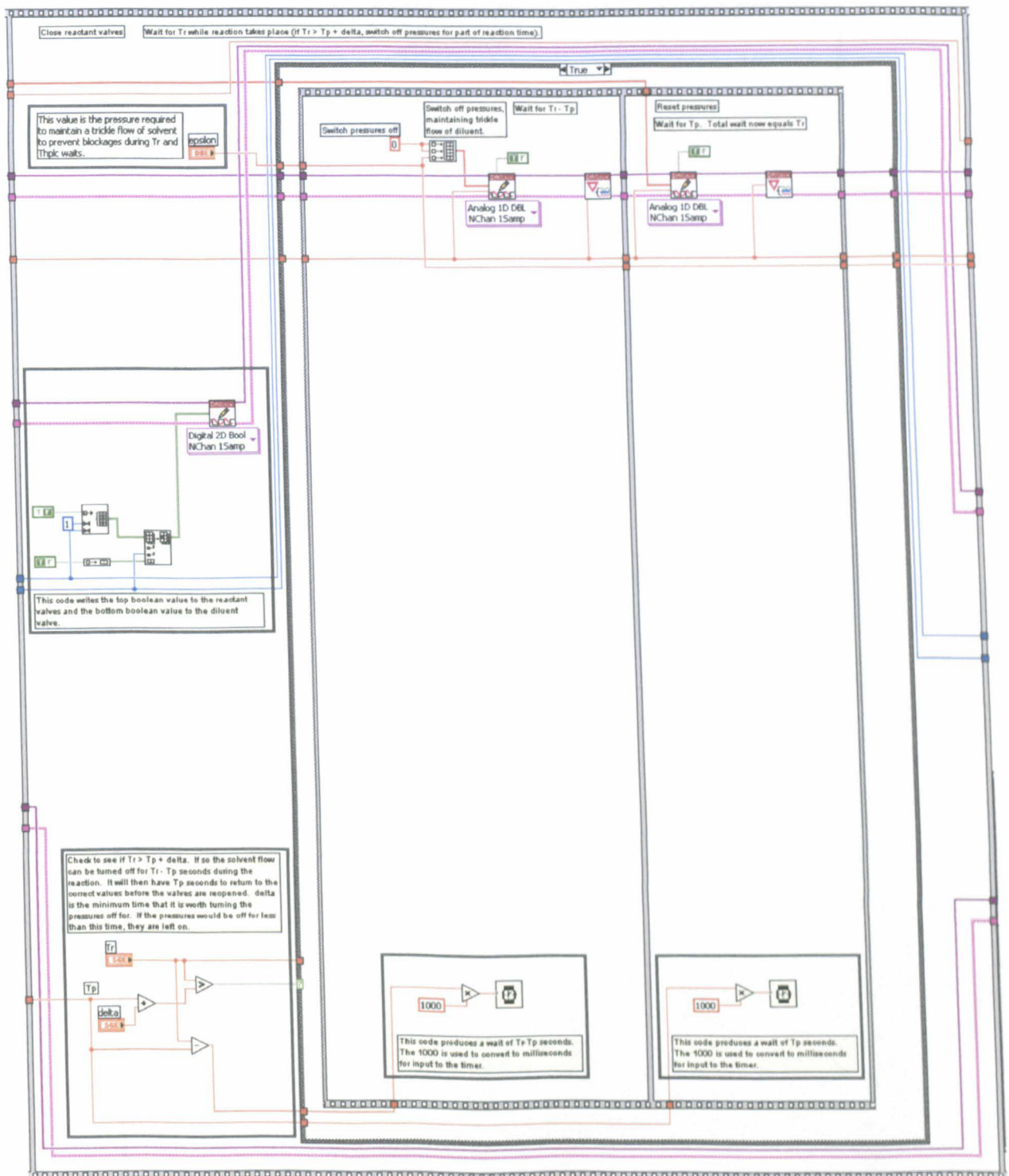
False Case
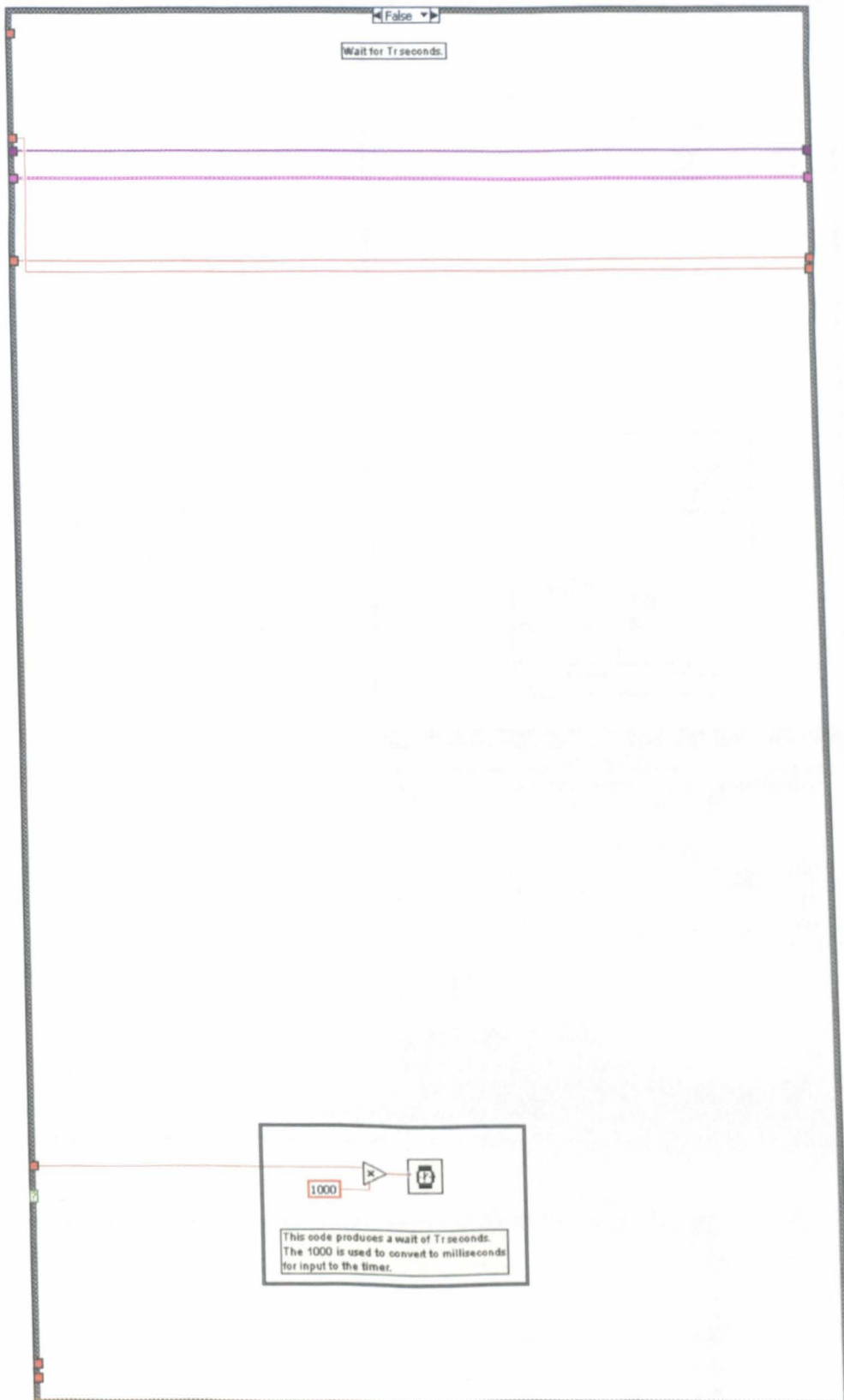
Section 4: Close Valves and Reduce Pressures

Close all valves and switch off Ps.

Switch pressures off maintaining trickle flow of diluent. This trickle flow is stopped as the last step in the main VI once all loops have been run.

Switch pressures off

Digital 2D Bool
NChan 1Samp

Analog 1D DBL
NChan 1Samp

This code writes the top boolean value to the reactant valves and the bottom boolean value to the diluent valve.

Analog Output task out
Analog Output error out

Digital Output task out
Digital Output error out

VISA resource out
VISA error out

Front Panel

Panel 1: Input Parameters

Input Parameters	Current Status	Hardware Setup	Instructions

Number of Cycles
1

HPLC Inject
On

Off

Constant Parameters

Tp	Tf	Tl	Thplc	Pd
30	30	3	1230	4

delta	epsilon
1	0.05
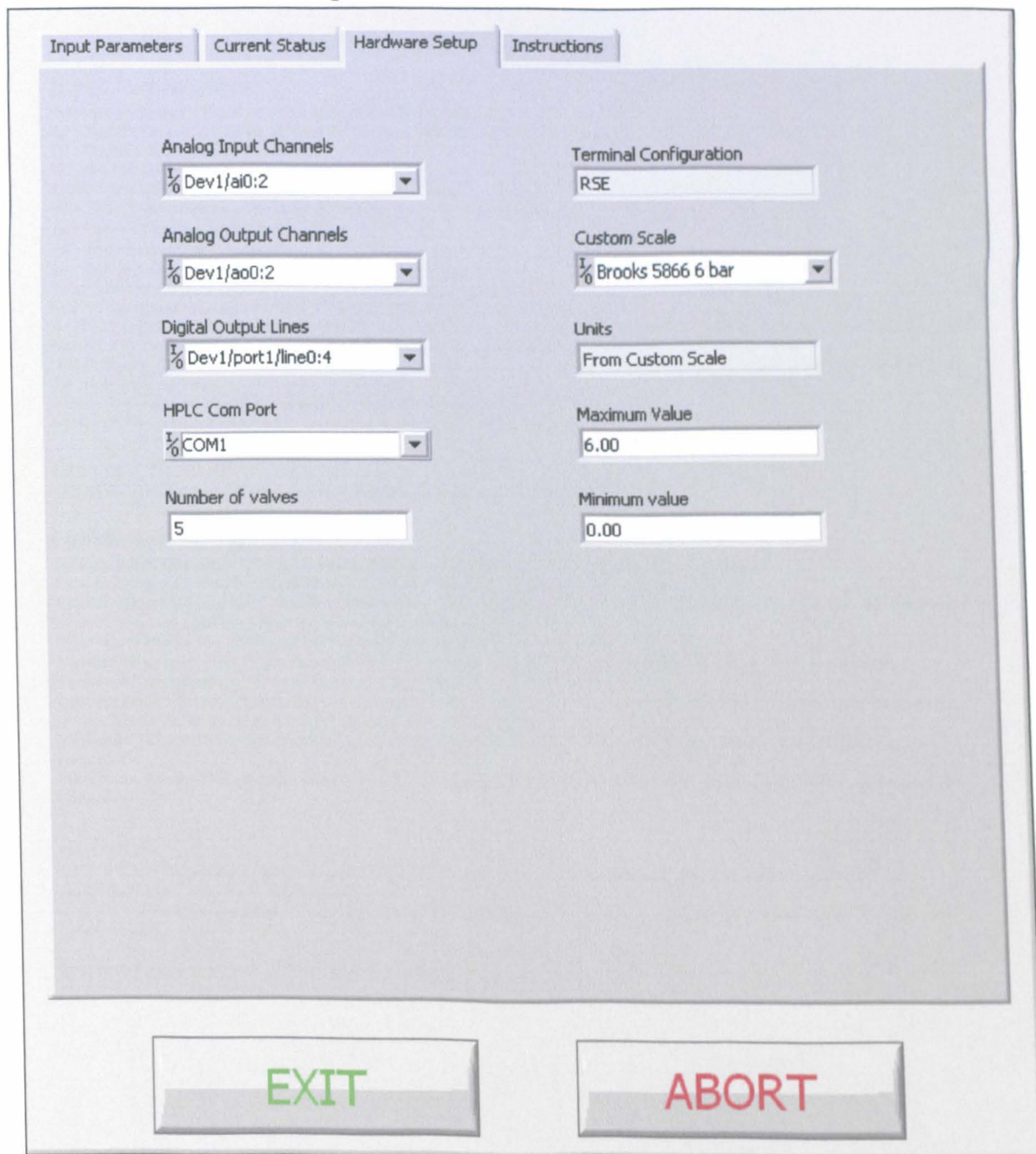
Variable Parameters

	Tr		Te		Ts		Pr1		Pr2
0	5	0	0.3	0	1.2	0	6	0	6
	0		0		0		0		0
	0		0		0		0		0
	0		0		0		0		0
	0		0		0		0		0
	0		0		0		0		0
	0		0		0		0		0
	0		0		0		0		0
	0		0		0		0		0
	0		0		0		0		0

EXIT   ABORT

Panel 2: Current Status
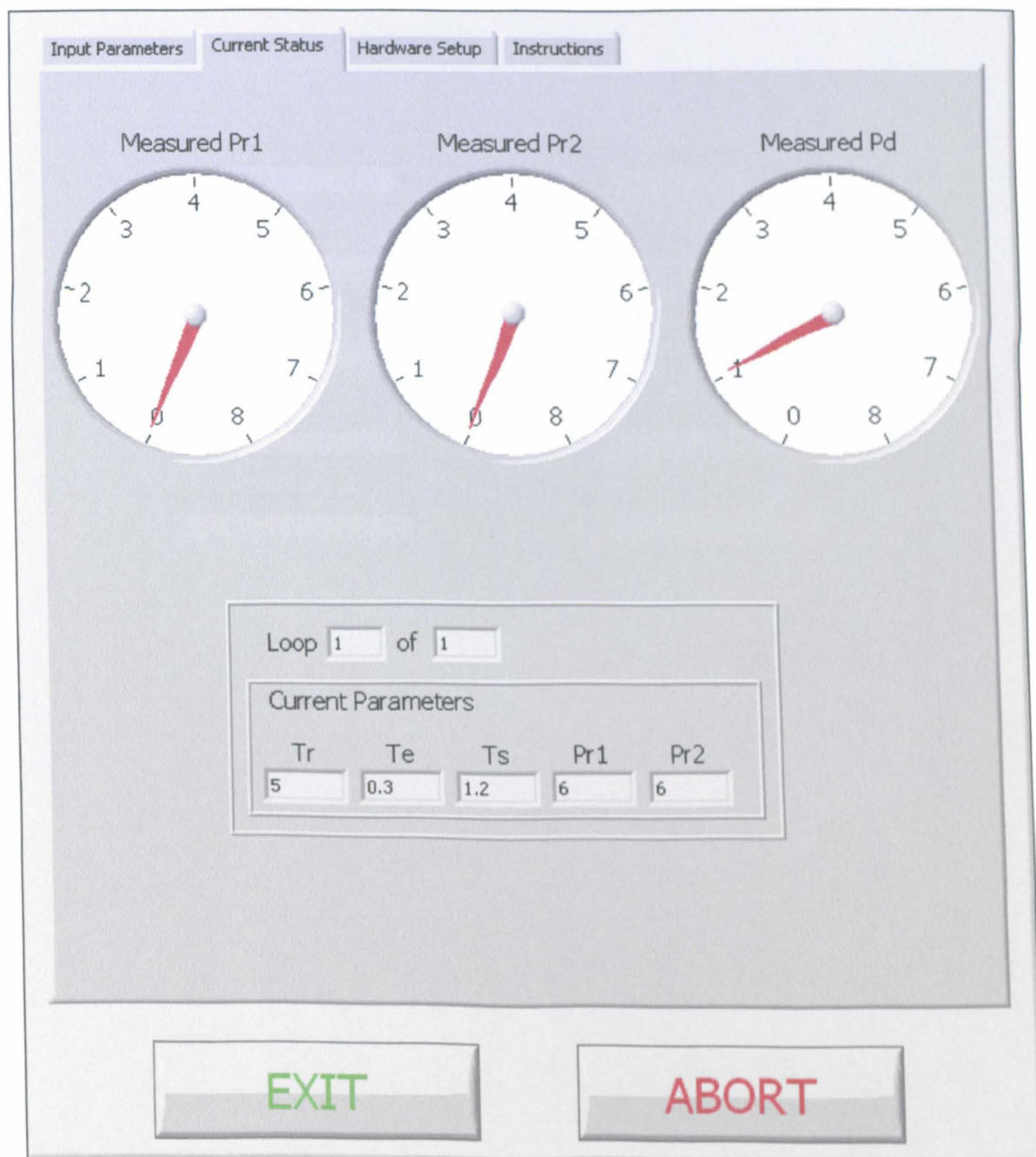
Panel 3: Hardware Setup

| Input Parameters | Current Status | Hardware Setup | Instructions |

Analog Input Channels
I/O Dev1/ai0:2

Analog Output Channels
I/O Dev1/ao0:2

Digital Output Lines
I/O Dev1/port1/line0:4

HPLC Com Port
I/O COM1

Number of valves
5

Terminal Configuration
RSE

Custom Scale
I/O Brooks 5866 6 bar

Units
From Custom Scale

Maximum Value
6.00

Minimum value
0.00

EXIT   ABORT

Panel 4: Instructions

| Input Parameters | Current Status | Hardware Setup | Instructions |

Input Parameters:

Number of Cycles - The number of experiments to be run.
Tp - The time in seconds to be allowed for pressure equillibration.
Tf - The time in seconds to be allowed for flushing.
Tl - The HPLC load time in seconds.
Thplc - The time in seconds for the HPLC column to flush.
Pd - The diluent pressure. The units depend on the custom scale selected.
Tr - The reaction time in seconds.
Te - The ejection time in seconds.
Ts - The sampling time in seconds.
Pr1 - The first reactant pressure. The units depend on the custom scale selected.
Pr2 - The second reactant pressure. The units depend on the custom scale selected.
Tr, Te, Ts, Pr1 and **Pr2** must be filled in for each iteration up to the **Number of Cycles**. When the index at the top left of the column is 0, the first iteration is on the top line. Lines below the **Number of Cycles** are ignored.
HPLC Inject - If on, the sample will be injected to the HPLC. The setting is the same for all cycles and cannot be changed once the program is running.
delta - The minimum time that it is worth reducing pressures for during the reaction.
epsilon - The pressure required to maintain a trickle flow of diluent during the reaction and HPLC analysis waits.

Current Status:

Shows the current cycle number, current variable parameters and current pressures.

Hardware Setup:

Analog Input Channels - Three channels, the first measures **Pr1**, the second **P2** and the third **Pd**.
Analog Output Channels - Three channels, the first sets **Pr1**, the second **Pr2** and the third **Pd**.
Digital Output Channels - One channel per valve. The first channel is the reactant valve used for ejection, the last channel is the diluent valve. All others are reactant valves not used for ejection.
HPLC Com Port - The COM port connected to the HPLC.
Number of valves - The total number of valves to be used. If only one valve is used it will act as a the diluent valve.
Terminal Configuration - Should be set to RSE (referenced single ended).
Custom Scale - If blank, pressures should be set in volts. Custom scales can be defined to allow the pressures to be set in bar.
Units - The units for the analog output channels **Pr1, Pr2** and **Pd**.
Minimum Value - The minimum pressure. (This should not correspond to less than the minimum voltage of the pressure controller).
Maximum Value - The maximum pressure. (This should not correspond to greater than the maximum voltage of the pressure controller).

Buttons:

EXIT - Stops the pressure measurements. This button must be pressed once all the cycles arecomplete. All cycles will be completed unless **ABORT** is also pressed.
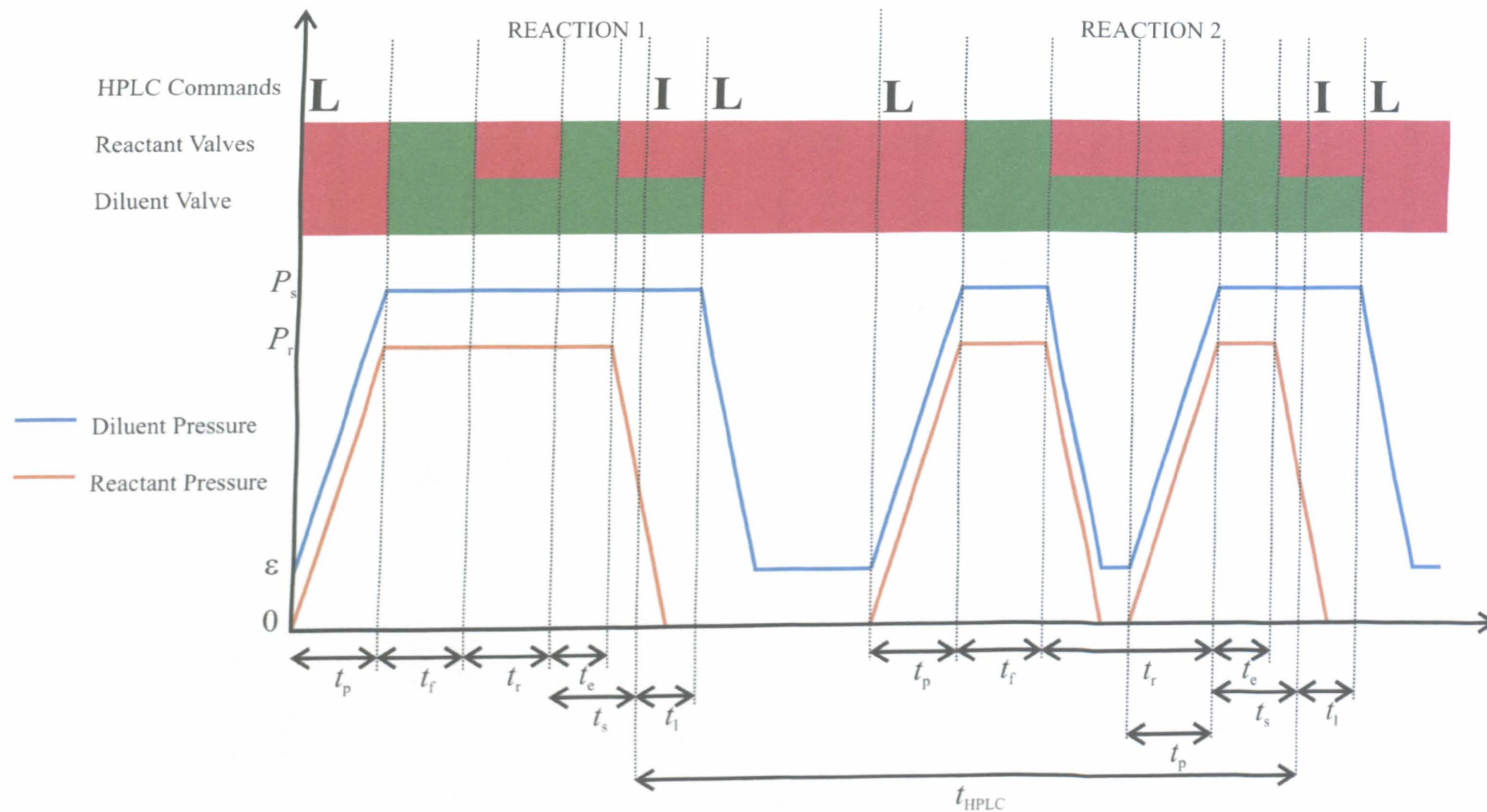**ABORT** - Aborts the experiment at the end of the next cycle. The **EXIT** button should also be pressed to stop the pressure measurements.

Password for altering the VI and sub VI is IonicLiquids.

| EXIT | ABORT |

Schematic of Programme Flow (see notes overleaf)

Notes on Programme Flow Schematic

P_s – Diluent pressure set by user.

P_r – Reactant pressure set by user. In practice there are two different reactant pressures, but they are always applied at the same time.

ε – Pressure to retain a trickle flow of diluent to prevent blockages.

δ – The minimum time that it is worth reducing the pressure during the reaction time.

t_p – Time to reach full pressure. In practice the diluent and reactant pressures may require different times to stabilise. In this case t_p should be longer than the longest stabilisation time.

t_f – Flushing time.

t_r – Reaction time. If the reaction time is sufficiently long it is worth reducing the pressures whilst the reaction occurs. This minimum time is the parameter in the programme. The schematic shows the case where the pressures are not reduced (reaction 1) and where they are reduced (reaction 2).

t_e – Ejection time. The time to open the valve to eject a small sample of the reaction mixture. Only 1 reactant valve need be opened during this time, the others remain shut.

t_s – Sample time. The time for the ejected sample to reach the correct point in the injection loop of the High Pressure Liquid Chromatograph (HPLC).

t_l – Load time. The time taken for the sample to be injected into the HPLC.

t_{HPLC} – HPLC processing time. The time taken for the HPLC to analyse the sample. There must be a sufficient wait between reactions for the HPLC to finish the analysis of one sample before the next is injected. Note that the programme has the option to turn off the HPLC sampling, in which case t_s, t_l and t_{HPLC} become unnecessary.

Valves – Green shows open valves, red shows closed valves.

HPLC Commands – "L" instructs the valve controlling the HPLC to run in "loop" mode. In this case nothing is sent to the HPLC. "I" switches the valve to "inject" mode and the sample is directed into the HPLC.

APPENDIX-2: Design Drawing of Reaction Network – Mark I

CHANNEL SIZES: Top layer   Bottom layer
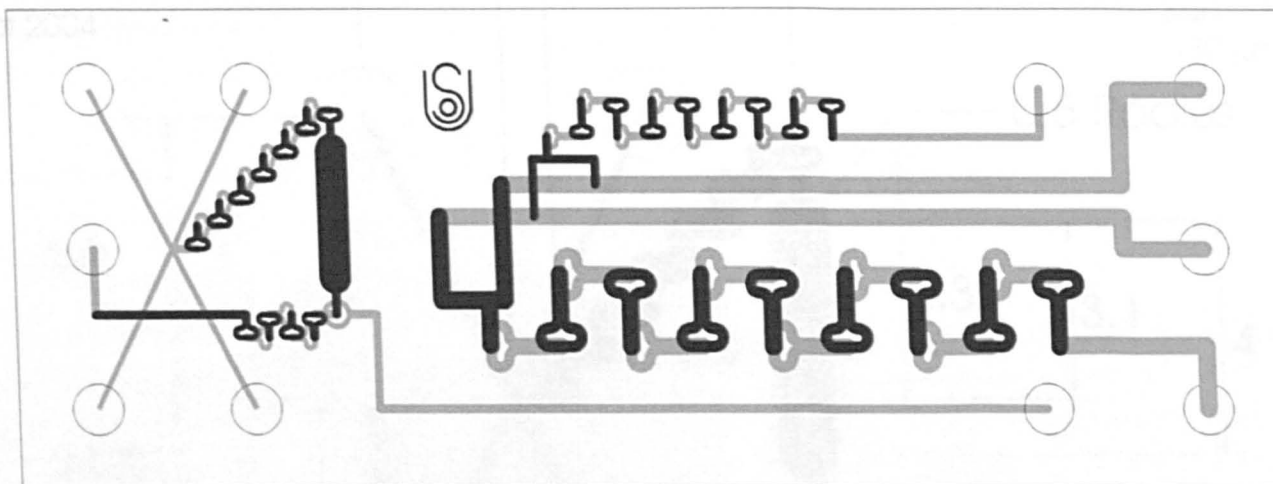
Etched depth is
75 μm

(see also the
detail drawings)

550 μm (400 μm mask)

360 μm (210 μm mask)

275 μm (125 μm mask)

180 μm (30 μm mask)

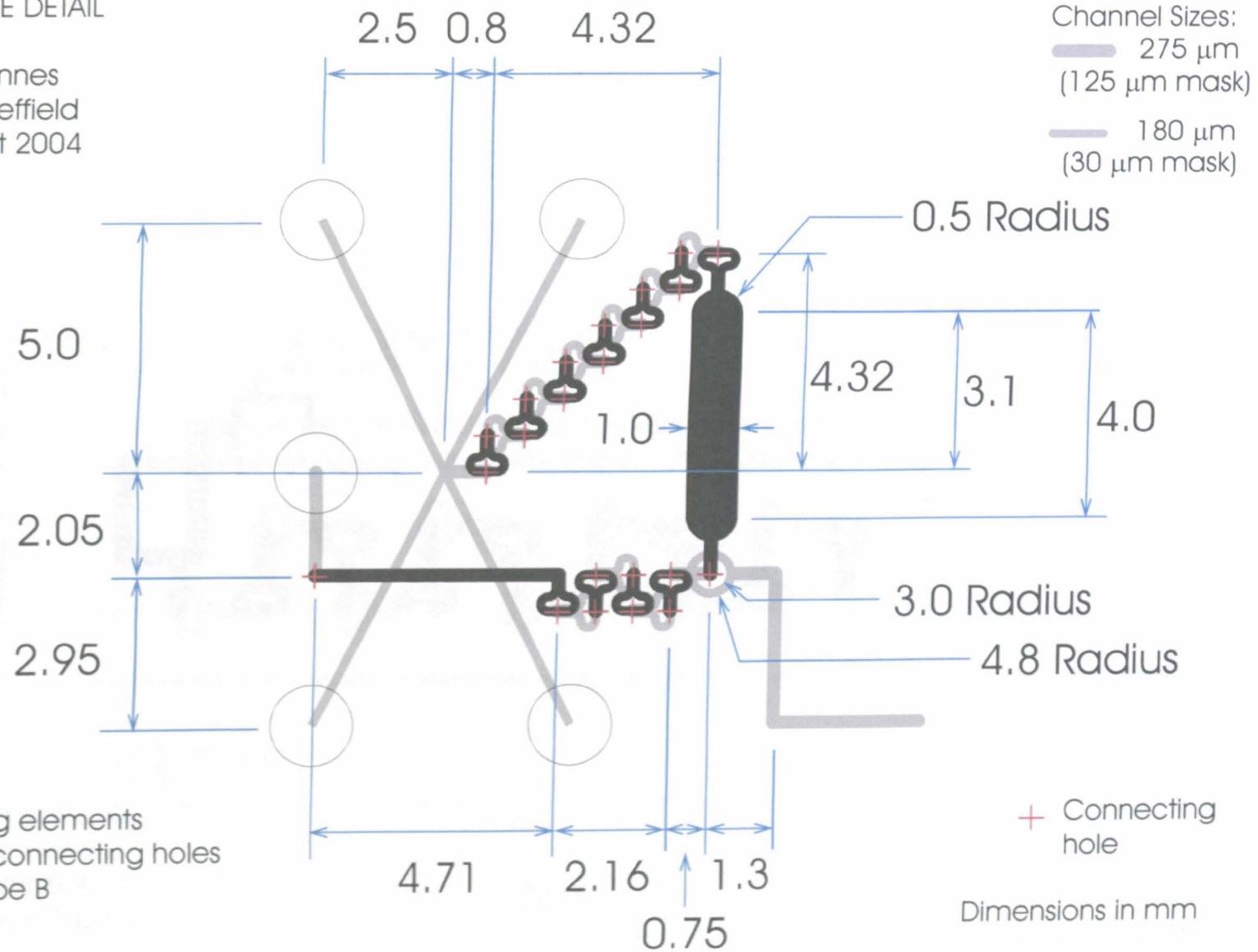LEFT SIDE DETAIL

J MacInnes
U of Sheffield
28 Sept 2004

Channel Sizes:
━━━ 275 μm
(125 μm mask)

━━━ 180 μm
(30 μm mask)

2.5 0.8 4.32

0.5 Radius

5.0

4.32 3.1 4.0

1.0

2.05

2.95

3.0 Radius

4.8 Radius

Mixing elements
and connecting holes
all Type B

4.71 2.16 1.3

0.75

+ Connecting
hole

Dimensions in mm

286

RIGHT SIDE DETAIL

J MacInnes
U of Sheffield
28 Sept 2004

Channel Sizes:

550 μm
(400 μm mask)

275 μm
(125 μm mask)

+ Connecting hole

19.5

2.5

1.0

8.96

6.54

2.5

1.5

0.5

1.5

1.5

0.7

0.8

1.0

3.0

5.0

10.0

2.6

1.0

1.4

5.0

2.0

2.0

0.5

1.5

Mixing elements,
connecting holes:
Top mixer, Type A
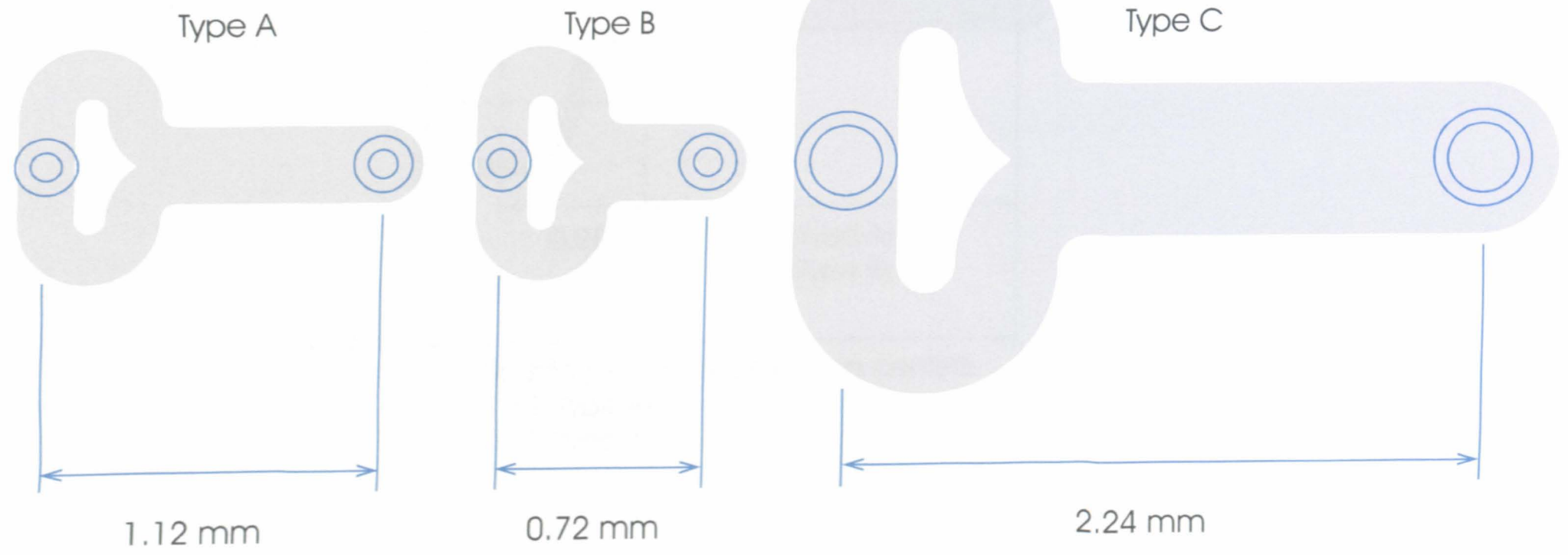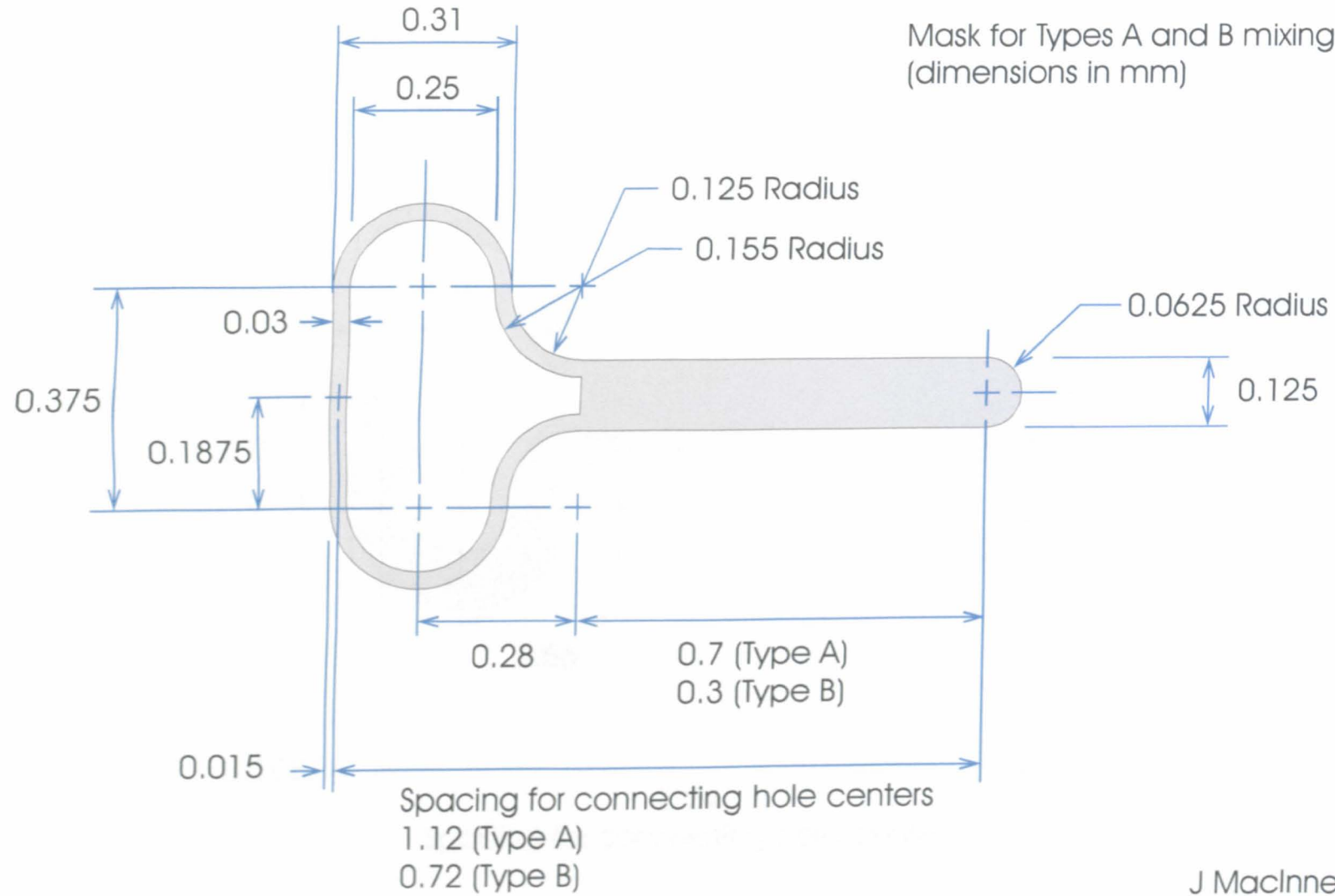Bottom mixer, Type C

17.92

4.58

24.0

Dimensions in mm
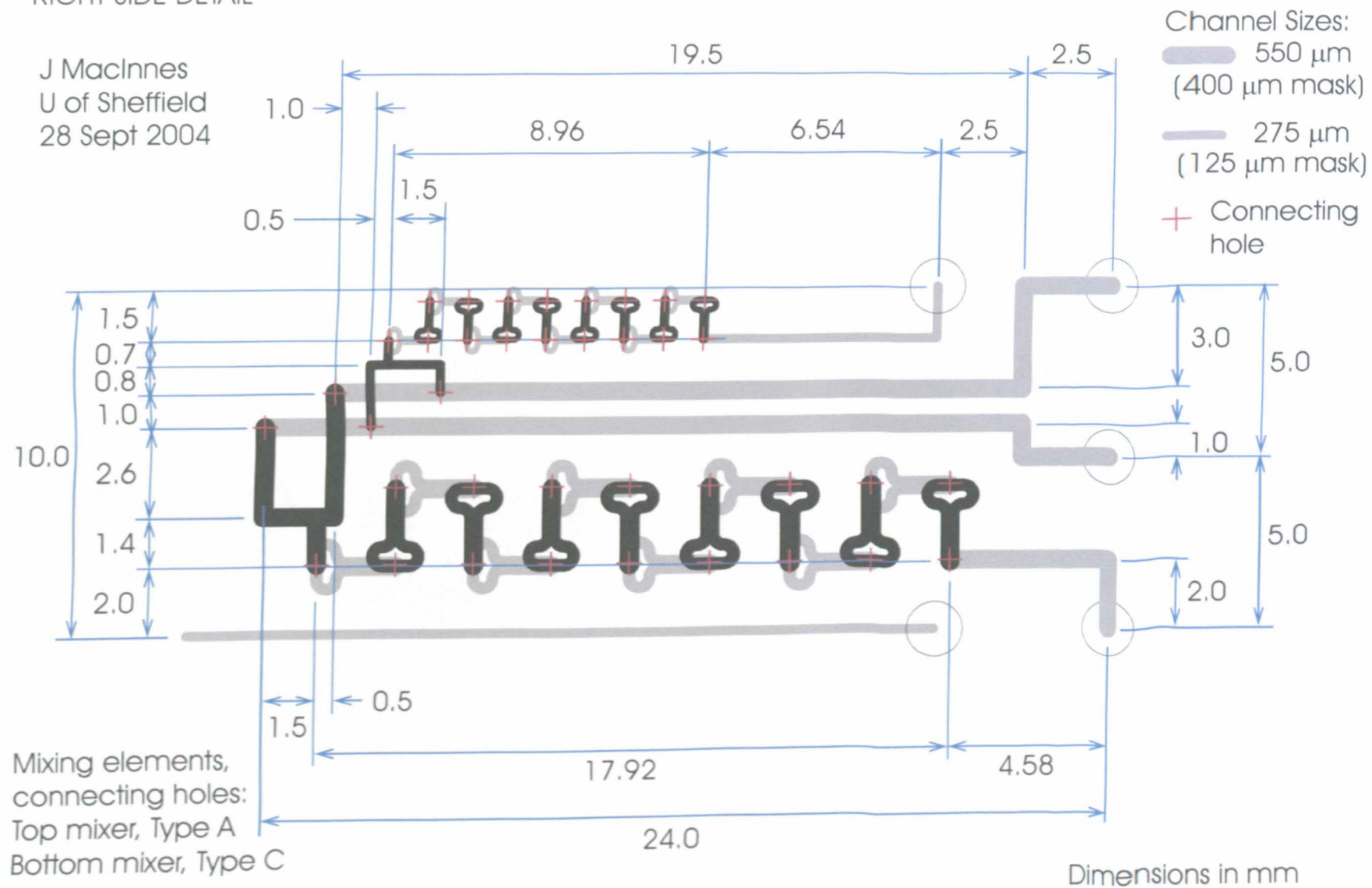
Mixing Elements
(shapes after etching)
connecting hole diameters and spacings

J MacInnes
U of Sheffield
28 Sept 2004

200 to 100 mμ dia. holes

350 to 250 mμ dia. holes

Type A

Type B

Type C

1.12 mm

0.72 mm

2.24 mm

288

0.31

0.25

0.125 Radius

0.155 Radius

0.0625 Radius

Mask for Types A and B mixing elements
(dimensions in mm)

0.03

0.375

0.1875

0.125

0.28

0.7 (Type A)
0.3 (Type B)

0.015

Spacing for connecting hole centers
1.12 (Type A)
0.72 (Type B)

J MacInnes
U of Sheffield
28 Sept 2004

0.77

0.35

Mask for Type C mixing element
(dimensions in mm)

0.175 Radius

0.385 Radius

0.2 Radius

0.21

0.75

0.375

0.4

0.56

1.4

0.105

2.24
Spacing for connecting hole centers

J MacInnes
U of Sheffield
28 Sept 2004

290
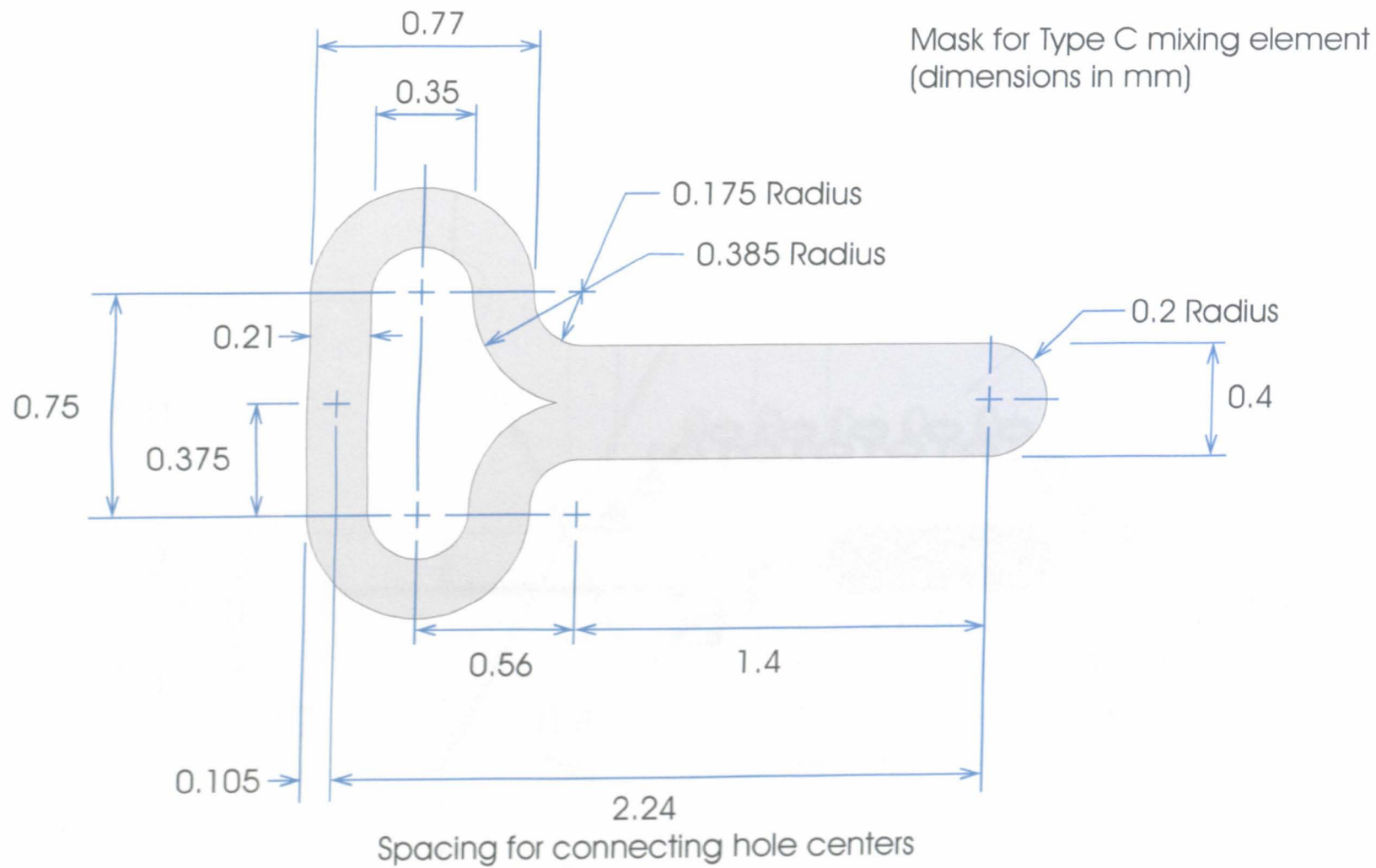
APPENDIX-3: Design Drawing of Reaction Network – Mark II

K7a,b LEFT SIDE DETAIL
J MacInnes
U of Sheffield
5 Jan 2006

2.5   1   4.33   4.77   1.4

1.5

Type A
mixing elements

5.0

0.75

1.2   0.1

0.6

0.4   0.5

3.8   2.7

0.4
Dia

0.75 Radius

2.5 Radius

4.5 Radius

All channels:
200 µm mask width
150 µm powder-blast depth

4.8

0.4
0.4   0.73   1.1

+ Connecting
hole

Dimensions in mm
(10 times actual size)

Dimension of Elements of Reaction Mixer:

0.45

0.3

0.175

0.15

0.075 Radius

0.25 Radius

0.05 Radius

0.15

0.200

0.15

0.2 Radius

0.75 connecting hole centres
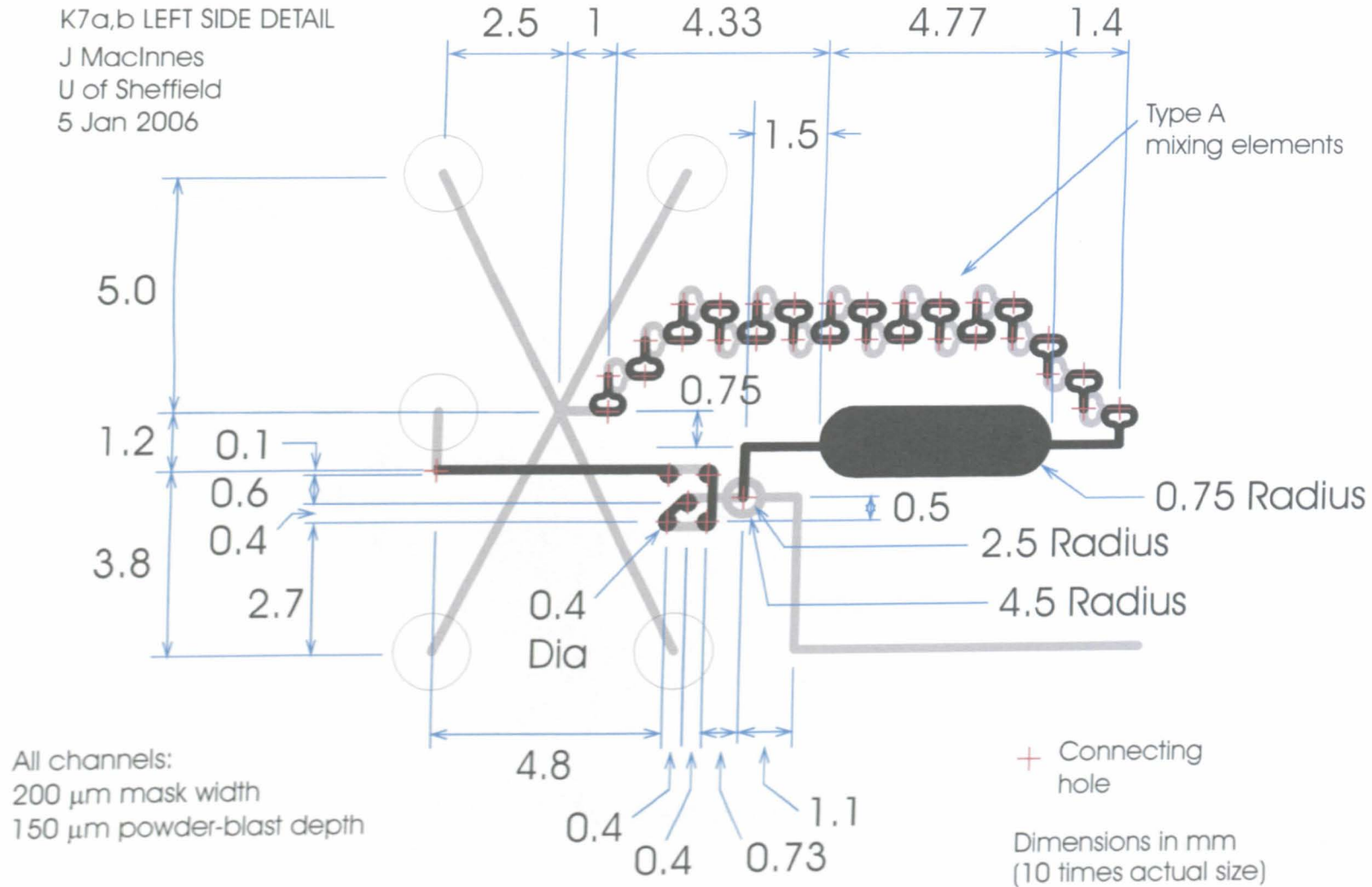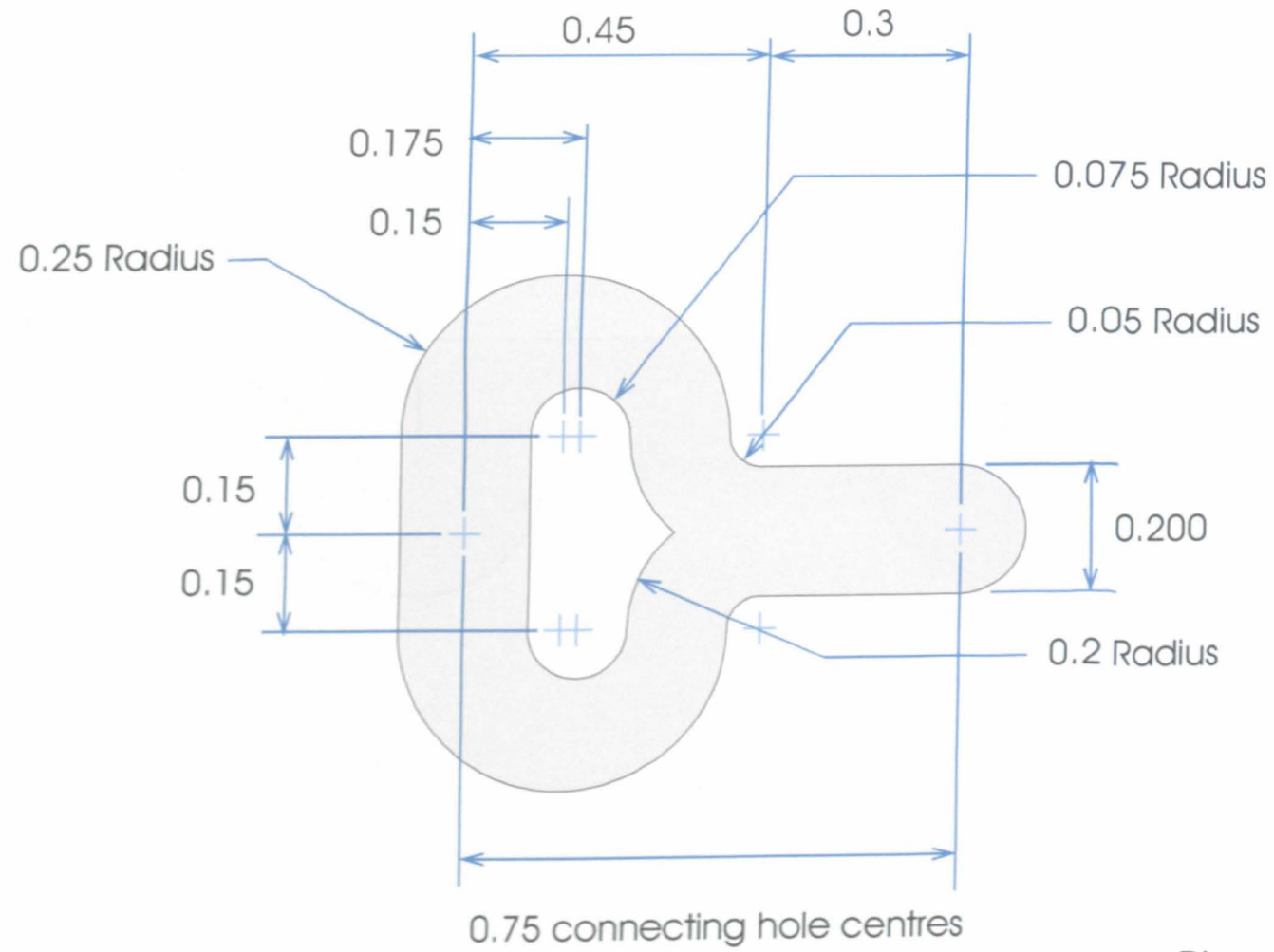
Dimensions in mm

Dimension of Elements of Dilution Mixer:

0.9 connecting hole centres

0.2 Radius

0.200

Dimensions in mm